CHARACTERIZING TSPO EXPRESSION AND RADIOLIGAND-BINDING IN THE CENTRAL NERVOUS SYSTEM AND PERIPHERAL BLOOD IN NEUROINFLAMMATORY DISEASE

Irene Nicolette Falk

St. John’s College
and
The John van Geest Centre for Brain Repair
Department of Clinical Neurosciences

January 2019
This dissertation is submitted for the degree of Doctor of Philosophy.

Preface

This dissertation is the result of my own work and includes nothing which is the outcome of work done in collaboration, except as declared in this Preface and specified in the text.

It is not substantially the same as any that I have submitted, or, is being concurrently submitted for a degree or diploma or other qualification at the University of Cambridge or any other University or similar institution except as declared in the Preface and specified in the text. I further state that no substantial part of my dissertation has already been submitted, or, is being concurrently submitted for any such degree, diploma or other qualification at the University of Cambridge or any other University or similar institution except as declared in the Preface and specified in the text.

It does not exceed the prescribed word limit for the relevant Degree Committee.

Table of Contents

Preface..i
Table of Contents iii
Index of Figures vi
Index of Tables x
List of abbreviations xii
1 Introduction: The significance of TSPO as a diagnostic and therapeutic target in inflammatory disease and potential applications in the treatment of neuroinflammation 1
  1.1 Overview 2
  1.2 Background and Significance 3
    1.2.1 The 18 kDa translocator protein (TSPO)... 3
    1.2.2 Positron-Emission Tomography (PET) Imaging 3
    1.2.3 PET imaging of TSPO expression.. 6
    1.2.4 Multiple Sclerosis 8
    1.2.5 Clinical Manifestations 8
    1.2.6 Radiological manifestations 9
    1.2.7 Genetic, environmental, and geographic risk factors 9
    1.2.8 Pathogenesis of MS 10
    1.2.9 Experimental autoimmune encephalomyelitis in the common marmoset 12
    1.2.10 Lymphocytes in MS and EAE.. 13
    1.2.11 Macrophages in MS.. 14
    1.2.12 Microglia in MS 15
    1.2.13 Astrocytes in MS 17
    1.2.14 Histopathology of MS 17
    1.2.15 TSPO in multiple sclerosis 19
    1.2.16 TSPO in microglia/macrophages.. 20
    1.2.17 TSPO in astrocytes 21
    1.2.18 TSPO in neurons 22
    1.2.19 TSPO in the periphery.. 23
    1.2.20 TSPO as a therapeutic target in MS 23
    1.2.21 Current treatment of multiple sclerosis and limitations 24
    1.2.22 Therapeutic ligation of TSPO... 25
  1.3 Summary of approach...27
  1.4 Specific Aims 27
2 Investigating the pathological significance of TSPO expression in the central nervous system of a nonhuman primate model of multiple sclerosis 31
  2.1 Introduction 32
  2.2 Methodology...35
    2.2.1 Division of responsibilities 35
    2.2.2 EAE induction and animal monitoring 35
    2.2.3 MRI scanning 36
    2.2.4 Information on the veterinary care of the animals involved....................... 36
    2.2.5 Description of the procedures for ensuring that discomfort, distress, pain, and injury will be limited to that which is unavoidable in the conduct of scientifically sound research 37
    2.2.6 Description of the use of analgesic, anesthetic, and tranquilizing drugs and/or comfortable restraining devices, where appropriate, to minimize discomfort, distress, pain, and injury 37
    2.2.7 Description of methods of euthanasia to be used and the reasons for its selection.. 38

- 2.2.8 Immunohistochemistry 39
- 2.2.9 Multiplex Immunofluorescence 40
- 2.2.10 Antibody stripping of previously stained sections 41
- 2.2.11 Multiplex immunohistochemical staining of previously stripped sections 41
- 2.2.12 Image Acquisition 42
- 2.2.13 Lesion analysis 42
- 2.2.14 Image quantification 44
- 2.2.15 Statistical Analysis 44

2.3 Results 46

- 2.3.1 TSPO is expressed in the meninges, ependyma, and vascular endothelium of control marmoset brain tissue 46
- 2.3.2 TSPO is expressed in 59% of Iba1+ microglia and macrophages in NAWM and NAGM in healthy primate brain tissue 48
- 2.3.3 TSPO is highly upregulated in demyelinated T2-hyperintense lesions in marmoset EAE, primarily in association with Iba1+ microglia and macrophages........ 52
- 2.3.4 Temporal changes in TSPO expression 56
- 2.3.5 Phenotype of TSPO+ microglia/macrophages in healthy brain 63
- 2.3.6 Phenotype of TSPO+ microglia/macrophages in acute EAE lesions 64
- 2.3.7 TSPO colocalizes with both “M1” and “M2” phenotype markers in vivo in marmoset EAE 65
- 2.3.8 Immunophenotype Changes in Chronic Lesions 67
- 2.3.9 TSPO is not expressed by astrocytes in NAWM 70
- 2.3.10 TSPO is observed in astrogliosis in the brain and spinal cord of EAE marmosets 70
- 2.3.11 Conventional immunohistochemical staining of TSPO suggests evidence of TSPO expression in neurons. 73
- 2.3.12 TSPO expression is observed in a subset of NeuN+ neurons in marmoset EAE... 75
- 2.3.13 Dim TSPO expression in seen in GLS2-expressing glutamatergic neurons but not Parvalbumin+ interneurons in marmoset EAE 78

2.4 Discussion 79

- 2.4.1 TSPO in control CNS tissue 79
- 2.4.2 TSPO in microglia and macrophages in EAE 80
- 2.4.3 TSPO immunophenotype in microglia and macrophages 80
- 2.4.4 Temporal changes in glial TSPO expression 82
- 2.4.5 TSPO in astrocytes 83
- 2.4.6 TSPO in neurons 83
- 2.4.7 Future directions 84

3 TSPO expression as a peripheral biomarker of neuroinflammation in multiple sclerosis 87

3.1 Introduction 88

3.2 Methodology 91

- 3.2.1 Division of responsibility 91
- 3.2.2 Selection of subjects 91
- 3.2.3 PBMC isolation 92
- 3.2.4 TSPO Genotyping 93
- 3.2.5 mRNA extraction 93
- 3.2.6 cDNA synthesis 94
- 3.2.7 Flow Cytometry 94
- 3.2.8 Staining with conjugated antibodies and Fixed Viability Stain 780 95
- 3.2.9 Staining marmoset PBMC with conjugated antibodies and MitoTracker Deep Red 96

3.2.10 Statistical Analysis 96
3.2.11 Protection of Human Subjects 97
3.2.12 Adequacy of Protection Against Risks 98
3.2.13 Inclusion of Women and Minorities 99
3.3 Results 100
3.3.1 Quantification of TSPO protein expression in monocytes and lymphocytes 102
3.3.2 Measuring TSPO expression as a biomarker of active disease in multiple sclerosis 109
3.3.3 TSPO expression is significantly elevated in CD14+CD16+ and CD14+CD16- monocytes in MS patients with active disease when compared to matched controls 109
3.3.4 TSPO expression patterns in marmoset PBMC are comparable to human PBMC 114
3.4 Discussion 116
3.4.1 Future directions 117
4 Comparison of TSPO protein expression and TSPO radioligand-binding in peripheral blood mononuclear cells in multiple sclerosis 121
4.1 Introduction 122
4.2 Methodology 125
4.2.1 Division of responsibility 125
4.2.2 PBMC isolation 125
4.2.3 TSPO genotyping 126
4.2.4 mRNA extraction 126
4.2.5 cDNA synthesis 127
4.2.6 KASP™ Genotyping Assays 127
4.2.7 PBMC Membrane Isolation 128
4.2.8 Bichinchoic Acid Assay 129
4.2.9 Radioligand binding assay 129
4.2.10 Statistical Analysis 130
4.3 Results 131
4.3.1 Assay Optimization 131
4.3.2 TSPO-^{3}H-PBR28 binding is lower in MS patients than in genotype-matched healthy donors 135
4.4 Discussion 138
4.4.1 Future directions 139
5 Conclusions 143
5.1 Overview 144
5.2 TSPO is expressed in both glia and neurons in marmoset EAE and is expressed predominantly by CD74+ microglia/macrophages in acute disease 144
5.3 TSPO expression is significantly elevated in multiple subsets of monocytes in the peripheral blood of MS patients and may function as a peripheral biomarker of CNS inflammation 146
5.4 PBR28-binding is decreased in the peripheral blood of MS patients with active disease, despite increases in protein expression 147
6 Concluding Summary 149
7 Appendix 151
7.1 Antibodies 151
7.2 Tables 151
7.3 Flow cytometry gating: Normal donors and MS subjects 156
7.4 R code for linear mixed effects modeling 176
8 References 187

Index of Figures

Figure 1-1 *Principles behind PET imaging. 1) Unstable parent nucleus, 2) radioactive decay with emission of positron and neutrino, 3) annihilation resulting in the formation of two 511 keV photons, 4) coincidence detection, when two detectors are simultaneously hit by the photons. Adapted from Kuzhupilly et al. 2010.* *5*

Figure 1-2. *Molecular structure of a first-generation TSPO radioligand (red) and two second-generation radioligands (blue) commonly used in the study of TSPO radioligand binding in vivo. Adapted from images provided by Dr. Bob Innis, NINDS, Bethesda, MD.* *7*

Figure 2-1*. TSPO, Iba1, and DAPI staining in the a) meninges and b) ependymal cells of a non-EAE control marmoset that died of gastrointestinal disease.* *47*

Figure 2-2. *TSPO, Iba1, and DAPI staining in the A) NAWM and B) NAGM of a non-EAE control marmoset that died of gastrointestinal disease.* *49*

Figure 2-3*. TSPO, Iba1, and DAPI staining in a region of normal appearing white matter in an untreated EAE marmoset, P1. The inset shows two TSPO+Iba1+ cells at higher resolution.* *50*

Figure 2-4*. TSPO, Iba1, and DAPI staining in a region of normal appearing gray matter in an untreated EAE marmoset, J. The inset shows two TSPO+Iba1+ cells at higher resolution.* *51*

Figure 2-5*. TSPO and Iba1 staining with DAB chromogen and hematoxylin counterstain in the region of the right thalamic nucleus of EAE marmoset A* *52*

Figure 2-6*. Top panel shows PLP, LFB, Iba1, and TSPO staining of a lesion in the left white matter tract of an EAE marmoset with antecedent HHV6B infection. Lower panel and inset show dense TSPO staining in one lesion in the right white matter tract. Iba1 and TSPO staining was visualized with DAB chromogen.* *53*

Figure 2-7*. Comparison of TSPO and Iba1 staining in three adjacent left white matter tract lesions and hyperintensities identified on postmortem PDW MRI (white arrows). Iba1 and TSPO staining was visualized with DAB chromogen and hematoxylin counterstaining.* *54*

Figure 2-8*. Comparison of PLP, LFB, Iba1, and TSPO staining with T2W spinal MRI in the A) lumbar, B) thoracic and C) cervical spinal cord of an untreated EAE marmoset. Iba1 and TSPO staining was visualized with DAB chromogen and hematoxylin counterstaining.* *55*

Figure 2-9*. T2W MRI studies performed on untreated EAE W marmoset in the 6 months prior to sacrifice indicate two lesions forming in the left optic tract. The upper lesion (blue arrow) first appeared in early September 2015 and was 5-6 months old at the time of sacrifice in February. A small circular lesion (white arrow) was first seen in mid-October and was 3-4 months old at sacrifice. Immunohistochemical stainings for TSPO and Iba1 with DAB chromogen show noticeably higher expression in the younger lesion. An ex-vivo T2*-weighted MRI also indicates multiple iron-laden lesions in the anterior commissure that appear demyelinated on LFB staining and are densely positive for TSPO.* *57*

Figure 2-10*. A section from an untreated EAE marmoset with over 10 lesions of various ages as determined by serial MRI, as well as several inflammatory nodules not seen on MRI (labeled "N/A"). Colors indicate lesion age as follows: Purple = 2-3 mo., Blue = 3-4 mo., Green = 4-5 mo., Yellow= 6-7 mo., Orange = 7-8 mo., White = Lesion age indeterminate.* *58*

Figure 2-11*. Fractions of Iba1+ cells co-expressing TSPO in lesions of different ages from A) untreated EAE animals (n=4) and B) prednisolone-treated EAE animals (n=2).* *59*

Figure 2-12*. Plot of ratio of TSPO+Iba+ cells to total Iba1+ population vs. lesion age at time of sacrifice (the number of months prior to sacrifice at which the lesion was detected).*..........61

Figure 2-13*. Multiplex staining of PLP, Iba1, and TSPO in a demyelinated optic tract lesion, showing dense infiltrates of predominantly TSPO+ macrophages and microglia in an untreated EAE marmoset.*..........65

Figure 2-14*. Multiplex staining of demyelinated optic tract lesions in animal M with dense TSPO and Iba1 staining (not shown) indicates TSPO to co-localize with both CD163 and CD74. Panel A shows distinct phagocytic cell populations identified by CD163 (purple) and CD74 (red). The colocalization of TSPO (green) and CD163 (purple) can be seen in panel B. The colocalization of TSPO (green) and CD74 (red) can be seen in panel C.*..........66

Figure 2-15. *Comparison of fractions of Iba1+ cells co-expressing TSPO and other markers of interest (CD74, CD163, Arg1, and MRP14) in a control marmoset and 3 acute lesions from two EAE marmosets. Two lesions were identified in animal M, while one lesion was identified in animal P1*..........67

Figure 2-16*. A) Percentages of Iba1+ cells that are TSPO+CD74+ (orange), TSPO+CD74- (yellow), and CD74+TSPO- in lesions of different ages (n=13) from different untreated EAE animals (M, P, B) and control marmoset P0.B) Percentages of Iba1+ cells that are TSPO+MRP14+ (orange), TSPO+MRP14- (yellow), and MRP14+TSPO- in lesions of different ages (n=13)*..........68

Figure 2-17. *Odds ratio vs. lesion age for co-expression of TSPO and A) CD74 or B) MRP14.*..........69

Figure 2-18*. Double immunohistochemical staining for GFAP (Vector blue) and TSPO (DAB) shows a large number of reactive astrocytes in the periphery of a lesion in the right white matter tract of marmoset A. However, the brown TSPO staining is predominantly restricted to GFAP- cells in the center of the lesion. The insets show the cell bodies of two representative GFAP+ astrocytes, which are negative for TSPO.*..........70

Figure 2-19*. Panel A shows a section of the cervical spinal cord with immunofluorescent staining identifying multiple bright foci distributed throughout the white matter. Panel B shows isolated GFAP and DAPI staining for this section, where the dominant color in these bright foci is found to be GFAP staining (in pink). Inset C shows a region of the white matter at higher magnification, where two dense clusters of GFAP staining are seen, indicating two distinct foci of astrogliosis. Panels D and E shows one of these gliotic lesions at higher magnification, where TSPO is observed both in an Iba1+ phagocytic cell (white arrow), and a Iba1-GFAP+ reactive astrocyte (red arrow).*..........71

Figure 2-20*. Prominent astrogliosis (GFAP staining in purple) and microglial accumulation (Iba1 staining in red) is observed in the optic chiasm of EAE marmoset A, as shown in panel A. While TSPO in the core of the nodule is predominantly associated with microglia and macrophages expressing Iba1 (red), TSPO expression lesion is also seen in reactive astrocytes, which are Iba1- but GFAP+ (as indicated by white arrows in panels B and C)*..........72

Figure 2-21*. Conventional immunohistochemical staining of TSPO with DAB and hematoxylin counterstaining on the surface of the third ventricle superior to the optic chiasm of marmoset A. Inset shows a single large cell with a large nucleus and diffuse cytoplasmic TSPO staining resembling a neuron.*..........73

Figure 2-22*. A) Section of the lumbar spinal cord of Marmoset C, an untreated EAE marmoset, stained by conventional immunohistochemistry for TSPO. Right inset shows region of lumbar gray matter with numerous stellate and crescent-shaped cells expressing TSPO, likely microglia and macrophages. B) Section of the thoracic spinal* *cord from Marmoset C, stained by conventional immunohistochemistry for TSPO, showing dense TSPO staining extending from the pial surface of the white matter. Right inset shows region of thoracic gray matter showing an extremely heterogeneous pattern of TSPO staining, including TSPO+ vascular structures and large cells resembling neurons, as well as TSPO+ glial cells.*..74

Figure 2-23. *Comparison of TSPO and NeuN staining in a region of gray matter in EAE marmoset A, which shows the absence of TSPO expression (yellow) in NeuN+ cells (pink) in a region of gray matter superior to the corpus callosum*.................................75

Figure 2-24. *Comparison of TSPO and NeuN staining in a region of cortical gray matter in EAE marmoset A, which shows diffuse cytoplasmic TSPO expression in NeuN+ cells*..76

Figure 2-25. *A) Fractions of NeuN+ cells co-expressing TSPO in the right and left cortical gray matter of control marmoset P0 and EAE marmosets P1, B, J, P2, and A. B) Mean fraction of NeuN+ cells co-expressing TSPO across all areas of interest in control marmoset P0 and EAE marmosets P1, B, J, P2, and A.* 77

Figure 2-26. *Comparison of TSPO staining with Parvalbumin and GLS2 staining after stripping and re-staining a previously stained section of brain tissue from EAE marmoset A. Diffuse cytoplasmic TSPO staining is observed in GLS2+ glutamatergic neurons (inset, white arrows) but not parvalbumin-producing interneurons (inset, red arrows).*...78

Figure 3-1. *Representative gating of fixed peripheral blood mononuclear cells (PBMC) isolated from an MS patient (n=1).* 101

Figure 3-2. *Gating strategy for isolated of CD3+ lymphocytes in human PBMC.* 102

Figure 3-3. *Comparison of MFI of TSPO staining in lymphocytes and monocytes in all donors (inclusive of both MS patients and matched normal donors). **** denotes a p-value <0.0001.*...103

Figure 3-4. *Quantification of TSPO staining intensity in monocyte subsets by flow cytometry.* 105

Figure 3-5. *Comparison of specific TSPO staining intensity vs. nonspecific isotype control staining (arrow) vs. signal intensity of unstained cells in CD3+ lymphocytes, CD14+CD16- monocytes, and CD16+CD14- monocytes in a representative MS patient and a representative normal donor. The position of the isotype control peak is indicated by the arrow in 5a-5d and 5f-5i, but in some cases, is completely overlapped by the autofluorescence peak of the unstained cells.*..107

Figure 3-6. *A) Comparison of MFI of TSPO staining in CD14+CD16+, CD14-CD16+, and CD14+CD16- monocytes in all MS patients (n=10, p<0.0001). B) Comparison of MFI of TSPO staining in CD14+CD16+, CD14-CD16+, and CD14+CD16- monocytes in all normal donors (n=10, p<0.0001). C) Comparison of MFI of TSPO staining in all subjects in CD14+CD16+, CD14-CD16+, and CD14+CD16- monocytes in all subjects (n=20, p<0.0001).* 108

Figure 3-7. *Comparison of median fluorescent intensity (MFI) of TSPO staining in distinct cell populations in MS patients with CEL and matched healthy donors.*......................109

Figure 3-8. *Comparison of MFI of TSPO staining in CD14+CD16+, CD14-16+, and CD14+CD16- monocyte subsets in MS patients (MS, red) and normal donors (ND, blue). * denotes a p-value <0.05.* 110

Figure 3-9. *Comparison of MFI of TSPO, HLA DR, CD86, and HSP60 staining in CD14+CD16+, CD14-16+, and CD14+CD16- monocyte subsets in MS patients (MS, red) and normal donors (ND, blue). * denotes a p-value <0.05.*.................................111

Figure 3-10. *TSPO vs. HLA DR, CD86, or HSP60 expression in CD14+CD16- (classical), CD14+CD16+ (intermediate), and CD14-CD16+ (non-classical) monocyte subsets in healthy controls (blue) and MS patients (pink). * denotes a p-value <0.05. B) P-values* *for TSPO vs. HLA DR, CD86, or HSP60 expression in CD14+CD16- (classical), CD14+CD16+ (intermediate), and CD14-CD16+ (non-classical) monocyte subsets. * denotes a p-value <0.05*......113

Figure 3-11. *Gating strategy for measuring TSPO and mitochondrial volume inCD3+CD14- lymphocytes and CD14+CD3- monocytes in whole live marmoset PBMC, with representative histograms of the staining intensity of TSPO and MitoTracker Deep Red in monocytes (red) and lymphocytes (blue).*......115

Figure 4-1. *Comparison of total, non-specific, and specific ^{3}H- PBR28 binding in protein homogenates isolated from PBMC and whole PBMC.*......132

Figure 4-2*. A) Comparison of total (light blue), nonspecific (gray), and calculated specific binding (dark blue) in suspensions of whole PBMC (100,000 cells per well) at ^{3}H-PBR28 concentrations of 0.1, 0.3, 1, 3, 10, 30, 100, and 300 nm. B) Comparison of total (light blue), nonspecific (gray), and calculated specific binding (dark blue) in suspensions of whole PBMC (200,000 cells per well) at ^{3}H-PBR28 concentrations of 0.1, 0.3, 1, 3, 10, 30, 100, and 300 nm.*......133

Figure 4-3. *Comparison-of-fits for one-site (red) and two-site (blue) binding curves fitted to specific binding values generated for PBMC (200,000 cells per well) from a known MAB healthy donor.*......134

Figure 4-4. *Comparison of one-site binding curves fitted to calculated specific binding values generated for a known HAB donor in wells containing A) 25,000 or B) 50,000 cells per well.*......135

Figure 4-5. *A) Comparison of ^{3}H-PBR28 specific binding curves in 4 MABS with multiple sclerosis (red) and 4 MAB normal donors (blue). B) Comparison of ^{3}H-PBR28 specific binding curves in 4 MABS with multiple sclerosis (red) normalized to one of 4 MAB normal donors (blue). C) Box plots of ^{3}H-PBR28 specific-binding values in 4 MABS with multiple sclerosis (red) and 4 MAB normal donors (blue). D) Box plots of ^{3}H-PBR28 specific-binding values in 4 MABS with multiple sclerosis (red) normalized to one of 4 MAB normal donors (blue). Curves for MS subjects were normalized to curves for normal donor subjects run on the same day.*......136

Figure 4-6. *A) Comparison of ^{3}H-PBR28 specific-binding curves in 4 HABS with multiple sclerosis (red) and 4 HAB normal donors (blue). B) Comparison of ^{3}H-PBR28 specific-binding curves in 4 HABS with multiple sclerosis (red) normalized to one of 4 HAB normal donors (blue). C) Box plots of ^{3}H-PBR28 specific-binding values in 4 HABS with multiple sclerosis (red) and 4 HAB normal donors (blue). D) Box plots of ^{3}H-PBR28 specific-binding values in 4 HABS with multiple sclerosis (red) normalized to one of 4 HAB normal donors (blue). Curves for MS subjects were normalized to values for normal donor subjects run on the same day.*......137

Index of Tables

Table 2-1. *Table summarizing gender, disease status, viral inoculation status, treatment status, age at baseline, and disease duration, of all animals examined in this study......36*

Table 2-2. *Sum-of-Squares values ("Sum Sq"), mean square values ("Mean Sq"), numerator degree of freedom (nDF), denominator degrees of freedom ("dDF"), F-statistics, and p values for the parameters of treatment (steroid-treated vs. untreated) and lesion age at time of sacrifice ("factor(MonthStop)"). * denotes a p-value <0.05. ....60*

Table 2-3. *Estimate of the fraction of Iba1+ cells expressing TSPO in a newly formed lesion ("Intercept") followed by estimates of the effects associated with steroid treatment and each time point of lesion formation relative to the time of sacrifice. * denotes a p-value <0.05. ** denotes a p-value <0.01. ....60*

Table 2-4. *Estimate of the fraction of Iba1+ cells expressing TSPO in a newly formed lesion ("Intercept"), followed by estimates of the effects associated with steroid treatment and each time point of lesion formation relative to the time of sacrifice, following alternative parameterization. * denotes a p-value <0.05. ** denotes a p-value <0.01. ....62*

Table 3-1. *Demographics (gender, ethnicity, age), MS subtype, presence of contrast-enhancing lesions (CEL) and treatment status of MS patients included in this study.....92*

Table 3-2. *Demographics (gender, ethnicity, and age) of normal donor included in this study. 92*

Table 4-1. *Genotype, demographics (gender, ethnicity, age), MS subtype, presence of contrast-enhancing lesions (CEL) and treatment status of MS patients included in this study. 125*

Table 4-2. *Genotype, demographics (gender, ethnicity, and age) of normal donor included in this study. 126*

Table 7-1*. A complete list of validated primary antibodies used for the phenotyping of microglia and macrophages expressing TSPO in inflammatory lesions in the marmoset CNS. A rabbit monoclonal antibody was used to detect TSPO, while guinea pig anti-Iba1 was used to detect activated microglia and macrophages. A mouse anti-PLP antibody was used to stain myelin and define areas of demyelinating inflammation. Anti-CD74 was used to identify microglia and macrophages with functional capacity for antigen presentation, while anti-MRP14 was used to detect phagocytes in a stage early activation. Anti-CD163 and anti-Arginase 1 were used to detect microglia and macrophages with a tolerogenic function..151*

Table 7-2*. A complete list of secondary antibodies used for the phenotyping of microglia and macrophages expressing TSPO in inflammatory lesions in the marmoset CNS. Primary antibodies are described in 152*

Table 7-3*. A complete list of validated primary antibodies used for the phenotyping of neurons and astrocytes expressing TSPO in inflammatory lesions in the marmoset CNS. A rabbit monoclonal antibody was used to detect TSPO, while guinea pig anti-NeuN and chicken anti-NFH were used to detect neuronal nuclei and axons, respectively. Mouse anti-CNPase, anti-GFP and anti-S100A antibodies were used to detect astrocyte cell bodies and processes. A rat anti-MBP antibody was used to stain myelin and define areas of demyelinating inflammation. Mouse IgG3 anti-PCNA was used to detect proliferating cells. Antibodies to lectin and collagen IV were used to detect endothelial cells and the subendothelial basement membrane, respectively..................................152*

Table 7-4. *A complete list of secondary antibodies used for the phenotyping of neurons and astrocytes expressing TSPO in inflammatory lesions in the marmoset CNS. Primary antibodies are described in* *153*

Table 7-5. *A summary of the markers used to identify and determine the immunophenotype of microglia and macrophages in healthy and EAE marmoset brain in this study, including target name, functional association, and the clone and host isotype of the antibody used to the detect the marker.* *154*

Table 7-6. *Antibodies used for the measurement of specific TSPO-antibody staining, CD86-antibody staining, HLA-antibody staining and HSP60-antibody staining in CD3+, CD14+, and CD16+ PBMC.* *155*

Table 7-7. *Antibodies used for the measurement of nonspecific staining associated with isotypes of antibodies used to detect TSPO, CD86, HLA, and HSP60 in CD3+, CD14+, and CD16+ PBMC.* *155*

List of abbreviations

MS	Multiple sclerosis
CNS	Central nervous system
RRMS	Relapsing-remitting multiple sclerosis
SPMS	Secondary progressive multiple sclerosis
PPMS	Primary progressive multiple sclerosis
NAWM	Normal-appearing white matter
NAGM	Normal-appearing gray matter
EAE	Experimental autoimmune encephalomyelitis
TSPO	Translocator protein, or the 18 kDa translocator protein (TSPO)
PBR	Peripheral benzodiazepine receptor
PET	Positron emission tomography
DVR	Distribution volume ratio
SUV	Standardized uptake value
PBR28	Acetamide, N-((2-(methoxy-11C)-phenyl)methyl)-N-(6-phenoxy-3-pyridinyl)-, a ligand for TSPO
11C-PBR28	A radioconjugate composed of TSPO ligand PBR28, conjugated to the carbon radioisotope C11
PK11195	1-(2-Chlorophenyl)-N-methyl-N-(1-methylpropyl)-3-isoquinolinecarboxamide
11C- PK11195	A radioconjugate composed of TSPO ligand PK1195, conjugated to the carbon radioisotope C11
DPA-714	N,N-diethyl-2-[4-(2-fluoroethoxy)phenyl]-5,7-dimethylpyrazolo[1,5-a]pyrimidine-3-acetamide
18F-DPA-714	A radioconjugate composed of TSPO ligand DPA-714, conjugated to the fluoride radioisotope 18F
18F-GE-180	A radioconjugate composed of TSPO ligand GE-180, conjugated to the fluoride radioisotope 18F
DAPI	4′,6-diamidino-2-phenylindole
PLP	Proteolipid protein
MOG	Myelin oligodendrocyte glycoprotein
GFAP	Glial fibrillary acidic protein
Iba1	Ionized calcium binding adaptor molecule 1
NeuN	Neuronal nuclear antigen (or hexaribonucleotide binding protein-3)
MHC	Major histocompatibility complex
HLA	Human leukocyte antigen
CD74	Cluster of differentiation 74

MRP14	Myeloid-related protein 14
CD163	Cluster of differentiation 163 (or hemoglobin-haptoglobin scavenger receptor protein)
PBMC	Peripheral blood mononuclear cells
VS780	Vital stain 780
CD14	Cluster of differentiation 14
CD16	Cluster of differentiation 16
FCγIII	Fc gamma receptor 3
CD3	Cluster of differentiation 3
HSP60	Heat shock protein 60
FSC	Forward scatter
SSC	Side scatter
FACS	Fluorescence-activated cell sorting

Acknowledgements

Many people contributed to the successful development of the projects detailed in this thesis. The collaboration described arose from a grant proposal developed between Dr. Jacobson and Dr. Matthews. Dr. Aigbirhio was subsequently identified as a collaborator and an appropriate mentor to oversee my studies in Cambridge and contribute unique perspectives on PET ligand synthesis and imaging. It was within the original grant application, which proposed to study TSPO in MS patients and EAE marmosets, that I identified questions that aligned with my own interests in neuroimaging and pathology and was given the opportunity to develop a research proposal describing specific aims and experiments that served to form the basis of my PhD.

Multiple staff scientists and associates contributed to the data presented in this thesis. Dr. Seungkwon Ha (NINDS, Bethesda, Maryland) provided significant training and expertise in conventional histology and chromogenic immunohistochemistry. He is responsible for processing whole formalin-fixed, paraffin-embedded marmoset brains and cataloguing regions of interest for comparison to MRI. These references served as a a valuable resource for trainees to identify suitable sections for our individual studies.

Dr. Pascal Sati (NINDS) oversees MRI protocol development and optimization. With Dr. Sati, I was trained to use a shared MRI database and Horos imaging software to identify and track lesions over time across multiple in vivo MRI scans. His expertise allowed me to identify archival tissue samples appropriate for study.

Dr. Dragan Maric (NINDS) trained me in the design, validation, and imaging of 10-color multiplex immunofluorescence assays. He has also provided numerous primary and secondary antibody samples for validation in formalin-fixed, paraffin embedded marmoset tissues. Every panel design is sent to him for final approval before resources are committed to staining. We met 1-2 times per week to review potential pitfalls and discuss solutions.

Dr. Yoshimi Akahata (NINDS) has been instrumental in the design of my flow cytometry studies. She has trained me in extracellular and intracellular staining, as well as data acquisition and analysis using BD FACSDiva and FlowJo 8.8.7. All experimental designs were reviewed with her prior to execution. She also reviews data analysis after acquisition to review gating strategies.

Finally, in addition to laboratory resources in Cambridge, I was granted access to resources and facilities at Imperial College London at the Hammersmith Campus in West London. Training at this location was overseen by Dr. David Owen, who also participated in this collaboration and has contributed significantly to the structure of this thesis. I also met regularly with Dr. Ruma Raha-Chowdhury, an associate director of graduate studies who reviewed my progress as a PhD student, and Dr. Susan Wan, a director in the Cambridge Clinical School that oversees the training of clinical students. Above all, I would like to thank my family for their tireless support and advice.

1 Introduction: The significance of TSPO as a diagnostic and therapeutic target in inflammatory disease and potential applications in the treatment of neuroinflammation

1.1 **Overview**

The 18-kDa Translocator Protein (TSPO), a putative cholesterol transporter that is weakly expressed in the healthy central nervous system (CNS), is strongly upregulated in CNS injury and thus of interest as a biomarker of neuroinflammation [1–3]. A transmembrane protein localized predominantly in the outer mitochondrial membrane, TSPO is abundantly expressed in activated microglia and macrophages in CNS lesions [1–4]. TSPO also binds and transports a range of PET-active radioligands [5–9], and a number of TSPO ligands are known to exert neuroprotective effects at pharmacologic doses [10–13]. Numerous studies have shown that TSPO is highly expressed in the inflammatory lesions in multiple sclerosis (MS) [4,14–16] and animal models of MS, such as experimental autoimmune encephalomyelitis (EAE) in rodents[17,18]. Together these studies suggest that TSPO may represent both a biomarker of inflammation and a therapeutic target for the treatment of MS [1,11]. However, the mechanism by which TSPO ligands exert neuroprotective effects is not completely understood. Moreover, rodent models of EAE pose numerous limitations in the modeling of MS [19–22].

Marmosets are New World monkeys of interest for their neurological similarity to humans, which renders these animals a powerful model of neuroinflammatory disease [23–25]. Most crucially, marmosets exhibit white matter/grey matter ratios similar to those of humans, which facilitate the magnetic resonance imaging (MRI) of white matter disease, providing a useful reference for PET imaging of inflammation [25]. This study seeks to compare TSPO expression in MS and marmoset EAE by characterizing the immunophenotype of TSPO-expressing cells in the central nervous system and peripheral blood. We hypothesize that TSPO is expressed at detectable levels in marmoset EAE, rendering the marmoset a useful model for the preclinical evaluation of TSPO imaging and modulation.

To test this hypothesis, we will first characterize patterns of TSPO protein expression in MS and EAE, using flow cytometry to analyze isolated human and primate peripheral blood mononuclear cells (PBMC) and immunohistochemistry to analyze CNS tissue sections from inflammatory brain lesions at various stages of progression. Next, we will compare patterns of TSPO protein expression in the peripheral blood with TSPO ligand-binding in these same tissues using autoradiography to detect binding by TSPO radioligands. Addressing these aims will help to characterize the dynamics of TSPO expression in the context of neuroinflammation and MS and potentially yield insight into avenues for therapeutic intervention and prospective investigation.

1.2 Background and Significance

1.2.1 The 18 kDa translocator protein (TSPO)

The 18-kDa translocator protein, or TSPO, is a transmembrane protein located in the outer mitochondrial membrane, where it is thought to transport cholesterol to the inner mitochondrial membrane for steroid synthesis [26,27]. TSPO contains 5 alpha-helices spanning the outer mitochondrial membrane, and a cytoplasmic C-terminal domain with tyrosine and arginine residues that are critical for cholesterol binding, as determined by site-directed mutagenesis [27]. It is closely associated with the adenosine nucleotide translocase and voltage-dependent anion channel (VDAC), with which it forms a constituent of the mitochondrial permeability transition pore (MPTP) [27].

In normal physiological conditions, the transporter is highly expressed in steroidogenic tissues, in particular, the testes, the adrenal glands, and the liver[27–31]. In addition to its role in steroidogenesis, it is implicated in a broad spectrum of biological processes, ranging from proliferation to apoptosis [32]. Increases in TSPO expression have been detected in peripheral macrophages in obesity and atherosclerosis [33–40] and tumor macrophages in malignancy [41]. In the healthy CNS, its expression is low [1,6,11]. However, TSPO become highly expressed in activated microglia and macrophages, as well as peripheral blood mononuclear cells (PBMC), and has also been observed in reactive astrocytes [12,42–44]. Consequently, TSPO expression in the CNS increases in conditions of neuroinflammation and immune cell infiltration [45–49]. It is this increase in TSPO in CNS injury that renders it a promising neuroimaging target.

1.2.2 Positron-Emission Tomography (PET) Imaging

While magnetic resonance imaging (MRI) is considered the clinical gold standard in the diagnosis and monitoring of neurological injury and disease, images obtained by MRI principally reflect structural changes in CNS tissue, for example, a decrease in fat content due to the loss of myelin lipid content in inflammatory demyelination, or an increase in water content due to tissue edema [50]. Changes detected on MRI do not directly reflect the activation of immune cells that mediate inflammatory activity, and consequently, this method of imaging is not reflective of the cellular processes that precede and likely precipitate these structural changes [51]. Positron-emission tomography (PET) is an imaging technique that detects gamma rays produced when high-energy positron particles collide and decay to a lower energy state [52–55].

Specifically, a radionuclide decays and emits an anti-electron, also called a positron, which has the same mass as an electron but is positively charged [52–55]. If the positron subsequently collides with a shell electron in an adjacent atom, it results in a process called annihilation, in which the combined mass of the electron and positron is converted to energy, most commonly producing two 511 keV gamma ray photons [56]. This process is described by the following formula, where e- represents an election, e+ represents a positron, and γ represents each of the resulting photons:

$$e- + e+ \rightarrow \gamma + \gamma$$ [57,58]

In a frame of reference in which there is no net linear momentum before collision, the resulting gamma photons travel in opposite trajectories, such that linear momentum is conserved. The photons are subsequently detected by one of many detectors arranged in a ring around the subject. Each of these detectors consists of a scintillator, which produces a burst of light upon gamma photon collision, and a photomultiplier tube or silicon avalanche photodiode, which convert photon incidence into an electrical signal [57,58]. If two photons contact separate detectors near simultaneously, it is then possible to determine a straight line of coincidence, or line or response, between the sites of photon detection, along which the origin, or site of annihilation may be localized [58].

Positron-emitting radionuclides can be attached to drug-binding ligands (radioligands), which can then be used to bind and detect specific cell markers and molecules within the body [3,29,57,59]. By localizing the site of annihilation in space, the system is able to localize the site of the radionuclide and generate a three-dimensional image showing the distribution and accumulation of the tracer within the subject [56].

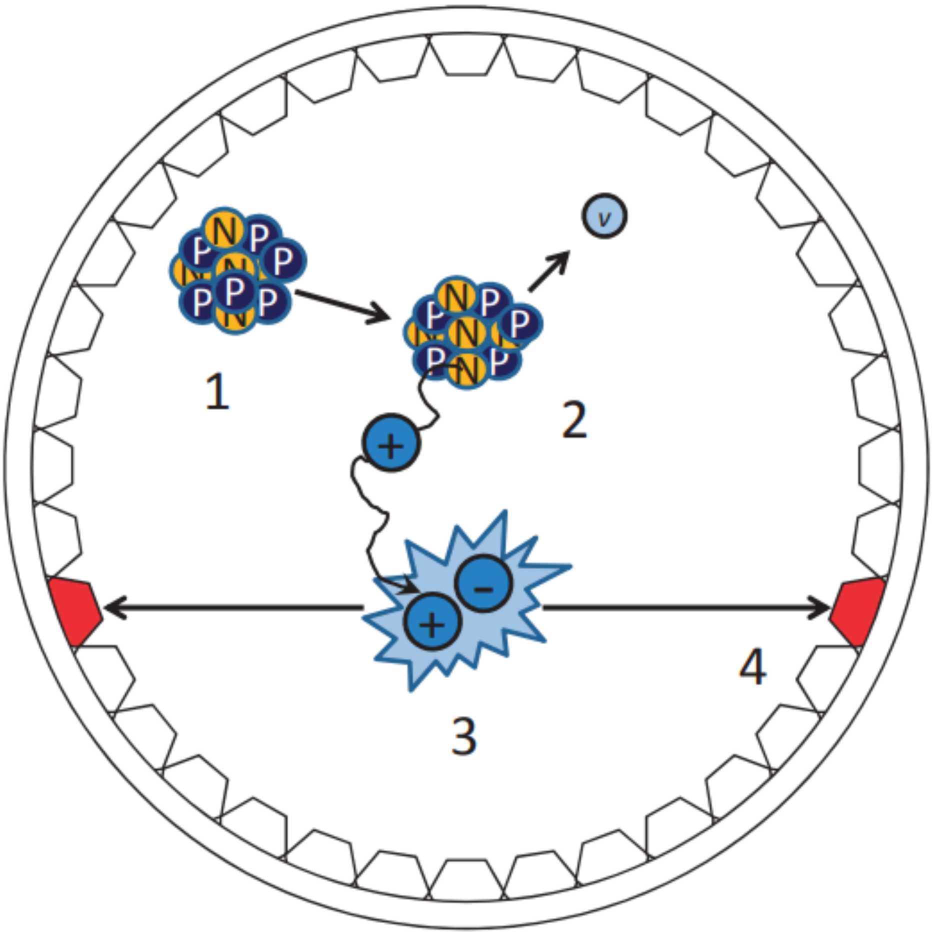

Figure 1-1 *Principles behind PET imaging. 1) Unstable parent nucleus, 2) radioactive decay with emission of positron and neutrino, 3) annihilation resulting in the formation of two 511 keV photons, 4) coincidence detection, when two detectors are simultaneously hit by the photons. Adapted from Kuzhupilly et al. 2010.*

There is particular interest in the use of PET imaging to visualize probes targeting molecular markers that are altered in neuroinflammatory environments [2,4,47,60–62]. This carries the potential of visualizing the activation of cellular mediators of inflammation and monitoring the cellular processes that lead to structural damage before further damage can occur [2,4,47,60–62]. It may provide a more sensitive means of detecting inflammatory activity for the purpose of diagnosis and initiation of disease-modifying therapy before inflammatory damage and resultant neurological deficits develop [63–66]. Alternatively, it may be used to determine how effectively a patient responds to a particular therapy – a treatment regimen may be maintained or changed on the basis of whether inflammatory processes in the brain are effectively controlled [62–66].

[11C]-MeDas is a stilbene derivation that binds specifically to myelin and can be visualized by PET for the in vitro imaging of CNS myelination and demyelination [67]. However, there is also interest in establishing markers for the early stages of inflammatory lesion progression, before significant anatomic changes have developed [63–66]. Targets for the imaging of lymphocytes have included CD20 for the imaging of B lymphocytes [68] and interleukin-2 for the imaging of T lymphocytes [69]. Other studies have examined cytokines such as cyclooxygenase 1 and 2 [70,71], matrix metalloproteinase [72], and targets specific for endothelial adhesion, such as vascular cell adhesion molecule (VCAM)-1 and vascular adhesion protein-1 [73].

Other commonly targeted processes include microglial activation and astrogliosis. In both cases, quiescent cells become activated, undergoing morphological changes and expressing a range of inflammatory markers [44,74]. One marker that is common to both a subset of activated microglia and reactive astrocytes is TSPO [1,4,16,42,75].

1.2.3 PET imaging of TSPO expression

TSPO was originally named the peripheral benzodiazepine receptor because it binds diazepam with high affinity in peripheral tissues [28,29,76]. Numerous TSPO ligands have been labeled with radionuclides for TSPO-PET imaging. One such ligand is ^{11}C-PK11195 (N-butan-2-yl-1-(2-chlorophenyl)-N-methylisoquinoline-3-carboxamide), an isoquinoline carboxamide derivative [8,77]. However, the clinical utility of this ligand has been limited by several factors, including a high nonspecific-binding, resulting in a low signal-to-noise ratio, low brain bioavailability, and the short half-life of its radioisotope, ^{11}C [61].

Other radioligands include ^{11}C-PBR28, a second-generation ligand with a significantly improved signal-to-noise ratio relative to ^{11}C-PK11195. A more recently studied ligand is [1^{8}F]DPA-714 (N,N- diethyl-2-(2-(4-(2-[18F]fluoroethoxy)phenyl)-5,7-dimethylpyrazolo[1,5-a]pyrimidin-3-yl)acetamide) as or DPA-714, which is a radioligand with a significantly higher bioavailability and signal-to-noise ratio [63,75]. Despite the advantages of these newer probes, the clinical utility of second-generation TSPO radioligands has also been limited by genetic variation in binding capacity [77,78]. Unlike first-generation ligands like ^{11}C-PK11195, second-generation TSPO ligands display a trimodal binding tendency, binding with high, “mixed”, and low affinity in different individuals, dependent upon their genotype at the single nucleotide polymorphism site rs6971[77,78]. The conversion of a cytosine nucleotide to a thymine nucleotide at this locus results in the substitution of a small, hydrophobic alanine residue with a polar threonine residue at amino acid 147, resulting in a marked reduction in the binding affinity of most TSPO radioligands [77]. Individuals carrying one copy with this substitution show reduced PET signals with PBR28. Individuals carrying two copies with the substitution showed no detectable TSPO binding to PBR28 *in vivo* or *in vitro* [77]. Approximately 50% of Caucasians carry at least one copy of the minor allele [77,78].

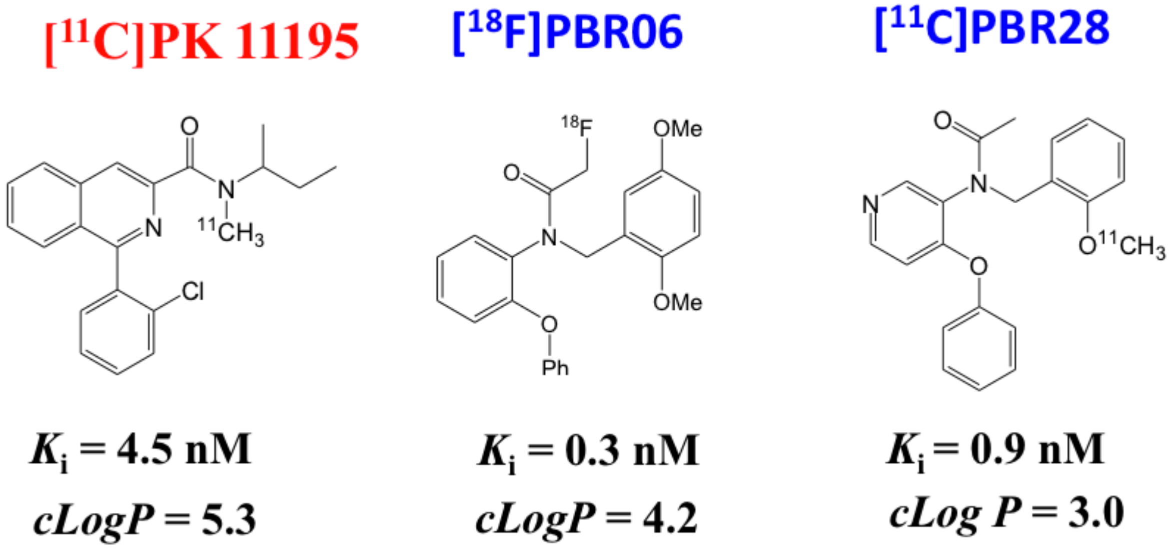
[11C]PK 11195
[18F]PBR06
[11C]PBR28
O
N
11CH3
N
Cl
18F
OMe
O
N
OMe
O
Ph
O
N
N
O
O11CH3
Ki = 4.5 nM
cLogP = 5.3
Ki = 0.3 nM
cLogP = 4.2
Ki = 0.9 nM
cLog P = 3.0

Figure 1-2. *Molecular structure of a first-generation TSPO radioligand (red) and two second-generation radioligands (blue) commonly used in the study of TSPO radioligand binding in vivo. Adapted from images provided by Dr. Bob Innis, NINDS, Bethesda, MD.*

1.2.4 Multiple Sclerosis

Multiple sclerosis is a neuroinflammatory disorder characterized by the infiltration of activated immune cells into the central nervous system, resulting in regions of focal axonal demyelination [79,80]. Radiologically, it is classically associated with the appearance of white matter lesions disseminated in time and space by magnetic resonance imaging (MRI) [81]. Clinically, it is the leading cause of non-traumatic disability in young adults [82,83], affecting approximately 250,000-350,000 people in the U.S. [84,85]. While its clinical manifestation is variable, MS most commonly exhibits a relapsing-remitting time, in which periods of disability are interspersed with periods of recovery [86,87]. However, approximately 50-60% of patients enter a secondary progressive stage (SP-MS) in the late phases of the disease[21], in which patients experience the progressive accumulation of disability without remission [88]. A small percentage of patients develop a primary progressive disease course, in which patients experience disease onset followed by the immediate and often rapid progression of disability, without ever experiencing remission [88–90].

1.2.5 Clinical Manifestations

In early relapsing-remitting MS, focal demyelination of the white matter produces similarly focal neurological deficits, typically motor deficits and visual impairments [89]. For instance, patients may perceive visual disturbances resembling flashing lights, the result of spontaneous electrical discharges following the loss of saltatory conduction [89,91]. Lesion formation is also observed in the brain stem and spinal cord [81]. Lesions of the brainstem may result in impaired swallowing and speech, while lesions of the spinal cord typically produce weakness and spasticity [89]. Lesions of the lower spinal cord are generally associated with bladder dysfunction, such as retention and incontinence, and sexual dysfunction. Urinary symptoms have also been found to be associated with pontine lesions [91], while sexual dysfunction has been found to correlate with insular lesions in female patients [92]. In later stages of the disease, motor deficits progress from focal losses to full paresis and disability[93].

MS is also observed to affect the gray matter [89,94–97]. Gray matter involvement may also be seen in the form of cortical demyelination, and is thought to be responsible for symptoms of fatigue and cognitive impairment [89,94–97]. Ultimately, irrespective of clinical course, fatigue remains the most commonly reported symptom of MS, and many patients also experience depression and cognitive symptoms, such as poor concentration and impaired executive function [89,98].

1.2.6 Radiological manifestations

Magnetic resonance imaging (MRI) is considered the most sensitive imaging technique for the detection of demyelination in the CNS [81,99] and is traditionally viewed as the gold standard imaging modality for the diagnosis and monitoring of MS [100]. The importance of MRI in MS diagnosis is indicated by the 2017 revised McDonald criteria, which requires objective detection of demyelinated CNS lesions disseminated in time and space by MRI, or lesions disseminated in space in the presence of oligoclonal bands in the CSF [101] . Radiologically, acute disease is classically characterized by T2 hyperintense or gadolinium-enhancing lesions of the CNS white matter, most frequently affecting the optic nerves, spinal cord, brain stem, and cerebellum [81,89,101] . Lesions of the cerebral hemispheres are typically periventricular, forming near the lateral ventricles and corpus callosum [89]. As lesions progress over time, a lesion may become irreversibly demyelinated, resulting in the visualization of a "black hole" lesion on T1-weighted MRI [102–105].

1.2.7 Genetic, environmental, and geographic risk factors

Like most diseases of autoimmune etiology, MS occurs predominantly in women, who constitute approximately 70% of all MS patients [106]. Primary progressive disease, in contrast, is more common in male patients and is associated with worse prognoses in men [88]. Genetic risk factors are also implicated, for example, major histocompatibility complex type II (MHC-II) haplotypes HLA-DR15 and DQ6 [107–110]. Other closely associated genotypes include DRB1*1501, DRB5*0101, DQA1*0102, and DQB2*0602 [89,111], with HLA-DRB1*1501 being the single most closely linked genotype [112,113]. Other risk factors include sunlight exposure, vitamin D deficiency, and living at high latitudes, as the incidence of MS increases with distance from the equator. Vitamin D is an immunomodulator that is crucial to the function of both innate immunity and adaptive immunity, and thus, its deficiency is thought to contribute to immune dysregulation and increased risk of autoimmune phenomena [114,115]. Its role in the pathogenesis of MS is supported by the increase in MS prevalence with distance from the equator, with increased rates of MS at higher latitudes where sunlight is less direct and vitamin D deficiency occurs more frequently [116]. At tropical latitudes, for example, the frequency of MS is only 5-6 per 100,000 [85]. In the northern hemisphere, in contrast, the frequency is 30 per 100,000 in central Europe and North America [85]. An increased frequency of 60 or more per 100,000 is seen in northern England and Scotland [85]. A similar pattern is seen in the southern hemisphere – the frequency of MS in central Australia is roughly 30 per 100,000 people [85]. In southeast Australia, in contrast, 60 or more per 100,000 people are affected [85]. It is thought that the relative lack of direct sun exposure at these latitudes results in decreased vitamin D levels, leading to immune dysregulation [85]. Because vitamin D is required for an array of immune cell functions and MHC-II is required for the presentation of endocytosed extracellular antigens by antigen-presenting cells, both associations ultimately point to the role of immune dysregulation in MS pathogenesis.

This hypothesis is further corroborated by evidence that the development of MS may be linked to immunologic exposure. Studies of MS patient blood have detected the presence of expanded clonal B cell populations upon exposure to common viruses, such as cytomegalovirus (CMV) or Epstein-Barr virus (EBV) [117,118], thus implicating these viruses as potential infectious triggers in MS pathogenesis. Epstein-Barr virus, in particular, has a marked association with MS. The virus is a human herpes virus that has been observed to demonstrate a tropism for B lymphocytes, subsequently establishing a latent infection in memory B cells that predisposes infected subjects towards lymphoproliferative disorders associated with increased risk of MS. Progression to infectious mononucleosis typically occurs in adolescence or adulthood and is associated with a several-fold increase in risk of MS [119–121]. The finding of B cell involvement coupled to the increased rates of positive EBV serology in MS patients heavily imply that environmental exposures such as antecedent viral infections may contribute to immune dysregulation, predisposing the immune system to inappropriate reactions such as those seen in autoimmunity [113].

1.2.8 Pathogenesis of MS

The pathogenesis of multiple sclerosis is not completely understood. Demographic and epidemiological studies suggest the development of MS requires the presence of one or more environmental triggers precipitating immune dysregulation in genetically susceptible individuals [21,122]. Fundamentally, the progression of disability is understood to be the product of an autoimmune process, in which the sensitization of the immune system to self-antigens, in this case, myelin antigens, leads to subsequent episodes of inflammatory demyelination. This process appears to depend on several crucial immunological processes to occur, among them:

1. the presentation of myelin antigen by dendritic cells in the spleen and lymph nodes [123,124];
2. the activation of autoreactive Th1 and Th17 lymphocytes by antigen-presenting dendritic cells in the periphery [125,126]
3. the permeabilization of the blood-brain barrier facilitating the entry of self-reactive peripheral immune cells into the brain parenchyma [123]
4. the release of pro-inflammatory cytokines and reactive oxygen species by activated immune cells, resulting in direct damage to the myelin sheath [127].

The ultimate outcome of this disease process is inflammatory damage of the CNS, involving the loss of oligodendrocytes, extensive axonal pathology, and focal neurological deficits [127]. The axonal demyelination eventually disrupts the saltatory conduction of action potentials along the length of the demyelinated nerve fiber, impeding the transmission of nerve impulses by reducing conduction velocity and increasing conduction time [128]. In the initial stages of lesion development, the loss of saltatory conduction may be compensated by the upregulation of sodium channels [129,130]. Typically localized at the nodes of Ranvier, sodium channels become increased in number and are redistributed throughout the membrane of the demyelinated axon, increasing conduction capacity [129]. This mechanism of compensation maintains the electrical transmission of nerve impulses, but is hypothesized to do so at a higher energy cost [130–133], resulting in fatigue, one of the most commonly reported symptoms among MS patients [89]. As demyelination becomes more extensive, the increase in conduction capacity no longer constitutes sufficient compensation for the loss of saltatory conduction, and electrical transmission is fully disrupted [89,134,135]. The loss of nerve impulse conduction results in a diverse and heterogeneous array of clinical manifestations, depending on the anatomical location of the lesions involved [89,93].

However, the causal relationships between these events—and the temporal sequence in which they occur—all remain controversial. Ultimately, many cell types are implicated in the initiation and maintenance of chronic neuroinflammation leading to disability in MS.

1.2.9 Experimental autoimmune encephalomyelitis in the common marmoset

Experimental autoimmune encephalomyelitis (EAE), the predominant animal model of multiple sclerosis, is most commonly induced by immunizing experimental animals with myelin-derived proteins such as myelin-oligodendrocyte glycoprotein (MOG) or proteolipid protein (PLP) in Complete Freund's Adjuvant (CFA), an oil-in-water emulsion of heat-killed mycobacteria [136]. A commonly employed model of EAE employing PLP is the C57BL6 mouse model which manifests as a chronic-acute disease progressing over several, with average onset of disease occurring within 2 weeks of immunization and peak disease severity occurring by day 21 [137].

While EAE is most commonly studied in mice, a significant challenge of this approach is the lack of murine models to recapitulate the radiological manifestations seen clinically in MS [20]. Serial MRI analysis is an especially valuable imaging modality for the non-invasive assessment of lesion load and disease progression over time, as well as the amelioration of disease in response to therapeutic intervention, but mice possess much less white matter than primates and MRI imaging of murine EAE progression is generally not informative [19]. Moreover, these predominantly chronic acute models of disease do not genuinely mirror the relapsing-remitting course of human disease [19]. Consequently, attention has turned to primate models of EAE, and the common marmoset has emerged as a useful model of EAE in addressing these limitations [19,138].

As nonhuman primates, marmosets possess a neural architecture that is functionally and structurally similar to that of humans [19,138]. Marmosets are also more immunologically similar to humans [19,21,22,24,113]. Bred in colonies, they acquire a diverse repertoire of immune exposures (in contrast to pathogen-free rodents) and their susceptibility to human herpes viruses associated with MS in humans allows the modeling of neuroinflammatory disease with antecedent viral exposure by intranasal inoculation with HHV6A, a model that was piloted in 12 animals by the Viral Immunology Section in 2015 [138]. Additionally, EAE-affected marmosets exhibit B cell involvement and infiltration of CNS lesions by CD8+ T cells [19,22]. Lesions in EAE-affected mice, in contrast, are predominantly driven by CD4+ T cell involvement [19,139,140]. Radiologically, marmosets affected with EAE have been demonstrated to manifest optic neuritis [141] and perivenular white matter lesions identifiable by MRI analysis [22], another feature of human disease typically absent in murine models [19]. Selecting the marmoset model of EAE for the study of TSPO expression would allow for the serial analysis of lesion load on MRI, which would facilitate the analysis of disease progression from a radiological standpoint as well as a clinical standpoint.

Moreover, primate studies suggest that TSPO ligand-binding with second generation ligands such as PBR28 is significantly stronger in the primate brain [142,143]. In a 2008 study of endotoxin induced injury in rhesus macaques, [^{11}C]PBR28 showed high brain uptake (300% of standard uptake values or SUV) and widespread distribution in the brain [142]. Moreover, the rs6971 polymorphism has not been reported in nonhuman primates. While high variability of TSPO-binding with second-generation ligands has been observed in baboons [143], analysis of PBR28-binding in rhesus monkeys found no outliers [142]. Therefore, the polymorphism is unlikely to be a confounding factor in the measurement of TSPO ligand binding in primates, and nonhuman primates may be considered an intriguing model for the imaging of *in vivo* TSPO binding with second-generation ligands as genotyping is not necessary to determine the binding capacity of TSPO in the animal's tissues.

However, TSPO in marmoset EAE has not yet been characterized. It is not known to what extent marmoset EAE recapitulates the patterns of TSPO expression seen in human neuroinflammatory disease or whether TSPO is expressed in cell types other than microglia. To determine if primate EAE is a useful model for the study of TSPO expression and modulation in human disease, it is necessary to determine what cell types express TSPO in marmoset EAE and whether TSPO expression correlates with changes in cell phenotype.

1.2.10 Lymphocytes in MS and EAE

In the healthy CNS, blood vessels consist of a collagenous basement membrane lined with endothelial cells, which are joined to one another by tight junctions [144,145]. These elements together constitute the blood-brain barrier, preventing the passage of cells and proteins between the blood and the brain parenchyma [144,145]. In MS, T helper cells are thought to become sensitized to pathogenic antigens at sites of antigen presentation in the peripheral blood and lymphoid tissues and subsequently become reactive to myelin antigens released by the destruction of oligodendrocytes [123–126]. An increase in blood-brain barrier permeability allows these sensitized helper Th1 and Th17 cells, as well as monocytes and macrophages, to cross from the peripheral blood and enter the parenchyma of the CNS [123,146,147]. This permeabilization is believed to be mediated by the secretion of the pro-inflammatory cytokine, Il-17, which promotes the activation of matrix metalloproteinase-3

(MMP-3), resulting in the digestion of the type IV collagen that forms the basement membrane of the cerebral capillaries [148].

Pathology in MS may be attributed not only to the action of T cells secreting proinflammatory cytokines but also loss of function in anti-inflammatory cells. T regulatory cells or T_{reg} cells are CD4+CD25+ and transcription factor forkhead box protein P3 (FoxP3+) T lymphocytes that act to downregulate autoreactive Th1 and Th17 cells [149]. Their functional impairment is implicated in many conditions of autoimmunity [150]. A particular CD39+ subset of FOXP3+ T_{reg} cells is thought to be crucial in tolerance induction, and a study of MS patient sera found MS patients to have reduced numbers of CD39+ T_{reg} cells [151]. They were also observed to have reduced capacity to suppress T cell proliferation in vitro [152]. Similar patterns have been seen in animal models of autoimmune disease, where the loss of T regulatory cells have been found to result in spontaneous autoimmune disease [149].

1.2.11 Macrophages in MS

Signs of immune dysregulation are also observed in peripheral blood monocytes in MS. Circulating blood-born monocytes from MS patients exhibit higher levels of the costimulatory molecule CD86 and higher secretion of cytokines Il-6 and Il-12 [153,154]. Moreover, while lymphocytes play a principle role in the initiation of inflammatory damage, monocyte-derived macrophages are considered among the principal effector cells of demyelination and axonal damage [155]. Upon activation, macrophages secrete inflammatory mediators such as cytokines, nitric oxide, and reactive oxygen species, as well as excitatory signaling molecules, such as glutamate [156]. In MS, activated macrophages are observed to cross through the weakened blood-brain barrier into the brain parenchyma, accumulating in lesions [156,157]. The secretion of cytokines and reactive oxygen species by these infiltrating cells in turn contributes to myelin damage [155,157]. However, macrophages have also been observed to mediate important functions in recovery and repair, such as they phagocytosis of myelin debris, which has been shown to be necessary for remyelination and axonal recovery after demyelinating injury [158].

These different functions are attributed to distinct populations of macrophages. While the many stimuli that determine macrophage phenotype in neuroinflammation in vivo cannot be replicated precisely, stimulation experiments *in vitro* have delineated several divergent populations with similarities to phenotypes observed *in vivo*. *In vitro* stimulation with lipopolysaccharide (LPS), interferon (IFN)-γ, or granulocyte-macrophage colony-stimulating factor (GM-CSF) for example, was found to produce classically activated, pro-inflammatory macrophages [159]. These macrophages express inducible nitric oxide synthase (iNOS), costimulatory markers CD80 and CD86, and MHC II molecule HLA DR, which is necessary for antigen presentation [160–162]. They also possess an enhanced ability to secrete inflammatory cytokines IL-1β, TNF, IL-12, and IL-18 [161]. Increased expression of iNOS results in increased production of nitric oxide, which facilitates the intracellular destruction of phagocytosed pathogens [160–162].

Stimulation with interleukin (IL)-4, IL-10, IL-13, TGF-β, or CSF-1 *in vitro* produces alternatively activated "M2" macrophages exhibiting tolerogenic properties associated with wound healing, tissue repair, and the resolution on inflammation [156,162–164]. These M2 macrophages have been reported to express phagocytic markers such as mannose receptor CD206 and hemoglobin-haptoglobin receptor CD163 but neither has been confirmed as a specific independent marker of M2 phenotype [162]. This class was subsequently subdivided by Mantovani et al. into four subclasses: M2a, or alternatively activated macrophages, which are produced by stimulation with IL-4 or IL-13; M2b macrophages, which are produced by stimulation with IL-1 receptor ligands, immune complexes and LPS; M2c macrophages, also called deactivated macrophages, which are elicited by treatment with IL-10, TGF-β and glucocorticoids; and M2d macrophages, which are produced by treatment with IL-6 and adenosine [165–167].

In vivo macrophages are understood to occupy a spectrum, ranging from conventional M1 and M2 phenotypes to mixed phenotypes with properties of both [158]. Inflammatory MS lesions have been found to be predominantly populated by macrophages exhibiting M1-like properties, such as iNOS expression [168]. However, many active and chronic lesions contain macrophages with a "foamy" appearance, likely resulting from the phagocytosis of lipid content in myelin debris [16]. In addition to their capacity for phagocytosis, these macrophages have been found to secrete anti-inflammatory cytokines, suggesting a tolerogenic influence similar to that of M2 macrophages [16].

1.2.12 Microglia in MS

Microglia play an important role in the pathogenesis of MS. Derived from erythromyeloid precursor cells in the embryonic yolk sac, myeloid microglial progenitors migrate into the neuroepithelium that forms the primitive nervous system in early embryonic development, where they develop into resident microglia, ultimately constituting approximately 5-20% of the total cell population of the brain [169,170]. Their major immunological functions include surveillance of the CNS microenvironment, phagocytosis of extracellular debris for antigen presentation, and the secretion of cytokines and other inflammatory mediators [76,171–173]. As phagocytic cells capable of antigen presentation and cytokine secretion, microglia are implicated both in the recruitment of peripherally sensitized myelin-reactive T cells in the early acute phases of MS and also in the reactivation of autoreactive memory T cells, which is thought to be crucial in the maintenance of chronic neuroinflammation [76,171–173].

However, microglia remain extremely heterogeneous in function and phenotype, both at baseline and in response to inflammatory injury. Like macrophages, microglia can be stimulated in vitro with LPS to generate an "M1" pro-inflammatory phenotype associated with the increased expression of co-stimulatory marker CD86, antigen presentation molecule MHC class II, and HLA chaperone protein CD74 [174–176]. Alternatively, they may be stimulated with IL-4 to generate "M2" pro-tolerogenic microglia expressing increased levels of phagocytic receptors. These IL-4-stimulated microglia are observed to facilitate oligodendrocyte differentiation and neurogenesis in tissue repair [158], suggesting they may aid the process of remyelination, in which oligodendrocyte precursor cells (OPC) migrate to the site of demyelinating injury, proliferate, and differentiate into mature oligodendrocytes. Studies of oligodendrocyte lineage have traced this proliferating cell population to a specific subpopulation expressing nerve and glial antigen-2 (NG-2) and platelet derived growth factor-α (PDGFR-α) [177,178], called NG-2 glia. However, the capacity for remyelination has been observed to decline in aging and inflammation, and this decline has been attributed to changes in the surrounding cellular microenvironment [158,179].

As with macrophages, the M1/M2 paradigm is considered too simplistic to fully represent all microglial phenotypes present in the healthy and diseased brain. Like macrophages *in vivo*, endogenous microglia are thought to occupy a spectrum encompassing mixed phenotypes that do not fully conform to a prototypic M1 or M2 phenotype. Nonetheless, it has been found that remyelinating MS lesions typically exhibit a high density of M2-like microglia [158,180]. In contrast, high levels of M1 microglia have been implicated in the progression of autoimmune disease [181]. Similar trends are seen in animal models of multiple sclerosis, where peak clinical scores are associated with high M1:M2 ratios [158]. This suggests that the progression and persistence of demyelinating lesions in MS stem not only the extent of the initiating demyelinating injury but also from defects in the process of healing and regeneration, particularly defects in remyelination [158,180].

1.2.13 Astrocytes in MS

In the healthy CNS, astrocytes are critical in the maintenance of blood-brain barrier, where they extend processes directly to the endothelial cells of the CNS vasculature, restricting the movement of cells and inflammatory mediators between the blood and the CNS parenchyma [182]. Astrocytes also interact with neurons, contacting synapses between neurons and neuronal axons at the nodes of Ranvier, forming what is called a tripartite synapse, in which glial cells are active components of synaptic transmission. Astrocytes are known to both release and express receptors for neurotransmitters and neuromodulators, enabling recognition and even modulation of adjacent synaptic events [183].

In inflammatory CNS injury, astrocytes become reactive, undergoing considerable morphological changes [74,184]. Many become hypertrophic, which is coupled to increased expression of intermediate filament, particularly glial fibrillary acidic protein (GFAP), which facilitates glial scar formation [43,185]. Reactive astrocytes are also observed to release pro-inflammatory cytokines [182]. Reactive astrogliosis is most pronounced in later stages of lesion developments, in both MS and animal models of neuroinflammatory disease [157].

1.2.14 Histopathology of MS

MS lesions, clinically described as plaques, are histologically characterized by demyelination, axonal damage, and extensive accumulation of immune cells, consisting of both endogenous microglia and perivenular infiltrates of peripheral blood mononuclear cells, in particular, CD8+ T lymphocytes, macrophages, B lymphocytes, and plasma cells [157,186–188]. The inflammatory injury mediated by these infiltrating and resident immune cells results in the separation of the outer lamellae of the oligodendrocyte processes surrounding each axon, which disrupts the integrity of the myelin sheath [93]. Transected axons have also been found to be a common histological feature of MS lesions [189]. A 1998 study by Trapp et al. found acute axonal injury occurred early in disease development and is most prominent in the first year [189]. As amyloid precursor protein (APP) is transported anterograde through the axon, transection results in accumulation of APP in the proximal axons, which appear as APP+ spheroids – these occur most frequently in the first year after diagnosis [189].

A recently proposed classification by Kuhlmann et al. categorizes newly formed lesions as active lesions – demyelinated lesions which are hypercellular due to infiltration by monocyte-derived macrophages and lymphocytes and the accumulation of microglia [190]. Active lesions may be further divided into early and late demyelinating active lesions, in which myelin break-down products such as PLP and MBP can be visualized in the cytoplasm of microglia and macrophages, or post-demyelination active lesions, in which macrophages may appear "foamy" due to lipid accumulation but lack distinct breakdown products [190,191]. Early active demyelinating lesions are defined by the presence of minor myelin proteins, such as MOG, CNP, or MAG, in addition to major proteins MBP and PLP, while late active lesions are defined by the presence of major proteins in the absence of these minor proteins [190,191]. Inactive lesions, in contrast, are hypocellular, with very few microglia, macrophages or lymphocytes, and a complete absence of mature oligodendrocytes [190].

As lesion development progresses over time, inflammatory cell infiltrates become less pronounced, and reactive gliosis becomes the more prominent histological feature [157,186]. Mixed active/inactive lesions are defined by a rim of active microglia/macrophages surrounding a hypocellular core that is almost completely devoid of microglia/macrophages but may contain hypertrophied astrocytes [186,190]. Like active lesions, these mixed lesions may be further divided into demyelinating and post-demyelination lesions, depending on the presence of cytoplasmic myelin breakdown products in phagocytic cells [190].

According to a classifications described by Lucchinetti et al, lesions may be further divided into: pattern I lesions, which contain demyelination in the presence of macrophages and microglia; pattern II lesions, which show complement activation suggestive of antibody deposition; pattern III lesions, which show oligodendrocytes with nuclear consolidation; and pattern IV lesions, which are very rare and may show evidence of repair e.g. non-apoptotic oligodendrocyte cells [190]. It is unknown whether these distinct patterns represent different etiologies of lesion development or different stages of a single etiology of lesion development[190].

Gray matter lesions in MS are predominantly seen in the cortex and cerebral nuclei[192,193], and the majority of cortical demyelinated plaques in the gray matter are contiguous with subcortical demyelinated plaques in the white matter, suggesting gray matter pathology may develop as a result of white matter pathology [194]. Histologically, cortical lesions are characterized by the presence of apoptotic neurons and the infiltration of the lesion by ramified microglia [195].

1.2.15 TSPO in multiple sclerosis

Studies of TSPO expression in vivo in MS have predominantly measured the signal of first-generation ligand ^{11}C-PK11195. One of the earliest studies of TSPO expression in MS found ^{11}C-PK11195 binding was significantly increased in acute MS lesions but was diminished in chronic lesions. A 2014 study similarly found increased ^{11}C-PK11195 binding in contrast-enhancing lesions identified on gadolinium enhanced T1-weighted MRI [29]. Additionally, in comparing the normal appearing white and gray matter of MS patients and normal donors, a 2000 study by Banati et al. found that ^{11}C-PK11195 signal was also diffusely elevated in the normal appearing white matter and grey matter of MS patients [196,197].

Subsequently comparing non-enhancing lesions in patients experiencing clinical relapse against non-enhancing lesions in patients in remission, it was found that ^{11}C-PK11195 binding was elevated in the non-enhancing lesions of patients experiencing relapse [196]. In fact, it was observed that ^{11}C-(*R*)-PK11195 binding in "black hole" lesions more than doubled during periods of clinical relapse, suggesting that activated microglia and macrophages may infiltrate these structurally damaged lesions during periods of increased disease activity. As in previous studies, ^{11}C-PK11195 binding was also found to be significantly increased in contrast-enhancing lesions [196].

More recent studies examining the binding of second-generation ligands such as PBR28 have also found increased TSPO signal in MS lesions. A 2017 by Datta et al. found TSPO radioligand uptake of second-generation ligands ^{11}C-PBR28 and ^{18}F-PBR111 was increased in the brains of MS patients when compared to health controls [198]. Furthermore, enhanced radioligand uptake was observed in the brain lesions of both RR-MS and SP-MS patients, facilitating the classification of lesions as “active,” “peripherally inactive,” or inactive in accordance with the distribution of ligand uptake within the lesion [198].

Moreover, there is increasing evidence that the TSPO-PET imaging may have a prognostic value and that increased TSPO expression may be predictive of poorer radiological and clinical outcomes [14,198]. A 2016 study by Colasanti et al. showed that patients with higher BDI depression scores also have an increased burden of hippocampal microglial activation as determined by TSPO-PET imaging with 18F-PBR111 [14]. In their 2017 study, Datta et al. also found that patients with a higher DVR signal at baseline demonstrated higher rates of T2 lesion development and lesion growth over the course of the following year [198].

1.2.16 TSPO in microglia/macrophages

The finding of increased PK11195 binding in MS lesions was additionally corroborated by comparative studies of histopathology and autoradiography in postmortem MS tissues [196]. Micro-autoradiography studies using ^{3}H-PK11195 found minimal binding in control tissue and maximal binding in MS plaques [196]. The highest binding signal was detected in in gadolinium-enhancing lesions, while lower levels of binding were detected in "black hole" lesions with structural damage, which is consistent with clinical studies of ^{11}C-PK11195 in vivo [196]. Immunohistochemical studies confirmed the accumulations of ramified microglia and macrophages in MS plaques that showed high ^{3}H-PK11195 binding. Moreover, it was found that patients with higher disability scores exhibited higher ^{11}C-(*R)*-PK11195 binding overall [196]. However, the degree of binding did not correlate strongly with standard measures of disability, such as EDSS scores [196]. The apparently correlation between clinical relapse and increased binding in lesions, even irreversibly demyelinated lesions, suggested TSPO expression may be more representative of active inflammation than previous damage and may have value as a prognostic indicator [196].

A 2014 study by Wang et al. examined the effect of TSPO knockdown in retinal microglia in a mouse model of retinal injury using lentiviral small hairpin RNA (shRNA) [199]. The study found that the administration of shRNA to BV2 microglia in vitro resulted in the increased production of reactive oxygen species and increased levels of TNF-a mRNA, as well as increased TNF-a protein secretion when challenged with LPS [199]. The LPS-challenged BV2 cells also exhibited increased proliferation after TSPO knockdown with shRNA [199]. These results suggest that TSPO may play a role in the downregulation of the pro-inflammatory response induced by LPS. This finding was corroborated by another 2014 study by Bae et al., which similarly found TSPO knockdown to increase pro-inflammatory cytokine release in BV2 microglia stimulated with LPS [200]. Additionally, the study found

TSPO overexpression to reduce pro-inflammatory cytokine release after LPS challenge while increasing the expression of markers of alternative activation, such as Arg1 and IL10 [200].

While these studies were limited to mice, clinical studies have similarly suggested that TSPO may be beneficial and that the loss of TSPO may contribute to clinical neurological pathologies. For example, reduced levels of TSPO mRNA have been found in psychiatric disorders, such as high anxiety [201], and TSPO ligand XBD173 was found to produce rapid anxiolytic effects in healthy volunteers [202]. Another ligand, etifoxine, was similarly found to reduce anxiety in human subjects [203].

Other studies suggest that TSPO expression promotes and enhances M2 (tolerogenic) polarization [200,204], which may have therapeutic application in demyelination. The process of remyelination in inflammatory CNS lesions is known to be strongly linked to the surrounding milieu of immune cells [158,180]. A recent study by Miron et al. showed that M2 macrophage-conditioned media enhanced oligodendrocyte differentiation in vitro and that M2 cell density is increased in remyelinating MS lesions, suggesting that remyelination is favored by the replacement of macrophages and microglia of an M1 phenotype with M2-biased cells [158,180].

However, the pathophysiological significance of TSPO expression in this context is not well understood. A 2018 study by Beckers et al. in mice found that TSPO mRNA levels were increased in M1 (LPS-stimulated) microglia in culture, but not in M2 microglia stimulated with IL4 [205]. Subsequent studies of TSPO expression in multifunctional protein-2 (Mf2) deficiency, a chronic model of neuroinflammation, found that TSPO protein and mRNA levels were increased in the inflamed brain tissue of Mf2-knockout mice [205]. A recent study by Vogel et al. found TSPO is expressed by both M1- and M2-biased microglia in MS brain tissue [16]. In macrophages, in contrast, LPS-stimulation has been found to downregulate TSPO expression [204].

1.2.17 TSPO in astrocytes

While studies by Banati et al. have found areas of increased ^{11}C-PK11195-binding to correspond to regions with increased density of activated microglia and macrophages [196], the increased density of TSPO in MS lesions has not been definitively co-localized to activated macrophages and microglia alone. TSPO expression has also been observed in other cell types, particularly astrocytes [42] and in some cases, neurons [206].

TSPO expression has been found to increase significantly in reactive astrogliosis after CNS injury [42], but the presence and extent of this upregulation appears to vary according to the model of neuroinflammation studied. Astrocytic TSPO expression is observed in MS and many mouse models of EAE, but certain rat models of EAE appear to lack this astrocytic component of TSPO expression [1]. In those models in which it is observed, astrocytic TSPO expression appears to play a significant role in neurodegeneration [18,43]. A 2016 study by Daugherty et al. created a conditional TSPO mouse knockout model to selectively block TSPO expressive in reactive astrocytes expressing GFAP [18]. Blocking TSPO expression in these reactive astrocytes appears to aid recovery after neuroinflammatory injury, with knockout mice exhibiting lower clinical scores at peak disease [18]. Interestingly, TSPO-/- astrocytes ultimately expressed less GFAP as well, suggesting the expression of TSPO may be necessary for the upregulation of GFAP in glial scar formation [18,43]. TSPO knockout in these animals was also associated with reduced TNF-a mRNA levels [18]. Other theories hypothesize that astrocytic TSPO expression may facilitate recovery by facilitating the transport of cholesterol for the synthesis of neuroprotective steroids, such as allopregnenalone, and increased TSPO expression in astrocytes has also been found to correlate with reduced neuronal damage in a mouse model of Alzheimer's disease [207].

Astrocytes are also hypothesized to play an important role in remyelination after inflammatory injury. In the course of neuroinflammatory injury in mice, TSPO expression appear to shift from activated microglia to hypertrophic reactive astrocytes [1,2]. In remyelinating lesions, microglial TSPO expression rapidly decreases while astrocytic TSPO expression becomes dominant [2]. Astrocytes are hypothesized to support oligodendrocyte progenitor cells (OPCs) in remyelination, and the coincident upregulation of TSPO in remyelination suggests that astrocytes may promote OPC proliferation through increases in steroid synthesis and increased secretion of steroidal trophic factors [208].

1.2.18 TSPO in neurons

Studies of cultured neurons in vitro have reported TSPO expression in neuroblastoma and glioblastoma cell lines, primary cortical neurons in mammals, and dorsal root ganglia sensory neurons in rats [209–211]. A 2009 study of a murine neural stem cell line detected TSPO protein expression and increased mRNA levels in differentiating and regenerating neuronal precursor cells at an intermediate stage of maturation, but not in mature neurons themselves

[209]. A recent immunopathological study of the healthy mouse brain found colocalization of TSPO with calbindin in Purkinje neurons [206]. Studies of TSPO in neuropathology have found increased TSPO expression in peripheral nerves after axonal resection, suggesting TSPO may play a role in neuronal pathology as well [209,212].

1.2.19 TSPO in the periphery

While TSPO is highly upregulated in CNS lesions, a 2012 study of PBR28 binding in isolated PBMC unexpectedly showed reduced TSPO binding in 25 MS patients when compared with 32 healthy donors [213]. Moreover, multiple studies have found decreased TSPO levels in platelets in neuropsychiatric disease [214–218]. More recent structural studies show that ligands thought to bind different regions of the TSPO molecule show different patterns of binding in neuroinflammation [4,28]. This suggests that neuroinflammatory changes may induce conformational changes that hide certain regions while leaving others exposed.

A 2017 study by Narayan et al. characterized TSPO expression in macrophages derived from peripheral blood monocytes and synovial monocytes harvested from healthy donors and rheumatoid arthritis patients [204]. The study detected relatively little TSPO mRNA in these monocytes but saw a considerable increase in TSPO mRNA levels in monocyte-derived macrophages. TSPO protein levels were also much higher in these cultured macrophages than in the monocytes from which they were derived. Surprisingly, TSPO expression was significantly decreased in LPS-treated M1 macrophages but was upregulated in IL-4-treated M2 macrophages [204]. This study suggests peripheral blood mononuclear cells may be a useful model for probing the relationship between TSPO expression and immunophenotype in phagocytic cells.

1.2.20 TSPO as a therapeutic target in MS

Current strategies of MS treatment are predominantly immunomodulatory, ranging from systemic immunosuppression with glucocorticoids for acute exacerbations to T and B lymphocyte-specific modulatory therapies for long-term maintenance [82,219–221]. However, despite the wide range of immunomodulatory treatments used for MS, few have shown a reduction in cumulative disability [221]. Moreover, widely immunosuppressive therapies are associated with significant risk of adverse events and morbidities [82,219–221].

Studies of TSPO ligands in the treatment of anxiety indicate TSPO may be not only be an imaging target but also a therapeutic target as a result of its action on cholesterol transport and subsequent neurosteroid synthesis in neuronal and glial cells [10,12,13]. The following section examines the efficacy and limitations of current immunomodulatory treatments as well as the risk of adverse events associated with mainstays of pharmacological therapy in MS. Subsequently, I will discuss the potential of TSPO modulation as a possible strategy of immune modulation in MS and its relative benefits.

1.2.21 Current treatment of multiple sclerosis and limitations

The majority of currently available therapies for MS are immunosuppressive agents, which aim to prevent the progression of inflammatory damage by inhibiting the cellular and molecular actors that mediate inflammatory activity. These include glucocorticoid treatments, such as intravenous prednisolone and methylprednisolone, which are broadly immunosuppressive, inhibiting the proliferation of lymphocytes, monocytes, and neutrophils[221]. While these treatments are observed to improve recovery time and are preferred in the treatment of acute exacerbations, they have not been shown to improve the outcome or degree of recovery [221] and are also associated with wide array of undesirable systemic effects. Patients are also at risk of developing osteoporosis if steroid therapy is maintained for long periods of time [222]. More specific antibody-mediated therapies are generally used for the depletion of specific subsets of T cells and B cells [223], such as Alemtuzumab, or Campath, which is a human anti-CD52 monoclonal antibody for the depletion of T lymphocytes and monocytes, and rituximab, a [220,224] While a systematic review of clinical studies found a decrease in the rate of acute exacerbations in interferon-treated patients [225], a 2014 study found that interferon treatment failed to reduce the extent of disability in MS patients [226]. Glatiramer acetate (GA) is an acetate salt of a synthetic 4-amino acid polypeptide consisting of L-alanine, L- lysine, L-glutamic acid and L-tyrosine, an peptide found in myelin basic protein (MBP)[227], which has been shown to promote self-tolerance of myelin proteins by inducing T regulatory cells to recognize MBP as a self-antigen. However, while GA has little risk of significant adverse side effects relative to other immunosuppressive therapies, a multi-center, placebo-controlled trial of GA in MS patients failed to slow the rate of disease progression [228].

Ultimately, currently available treatments are predominantly used for the treatment of relapsing-remitting MS, in which demyelinating injury is relatively limited and the patient is less likely to have developing permanent deficits [89,221]. The majority of these agents are immunosuppressive pharmaceuticals, which exert their therapeutic effects through the depletion and downregulation of immune cells [89,219,221,229]. Thus, many are associated with adverse side effects where the immune system is inappropriately suppressed, leaving the patient predisposed to infection, or inappropriately activated, leading to autoimmunity [229]. Moreover, there are currently no accepted drugs showing clinical efficacy in the treatment of secondary progression, in which inflammatory damage is more extensive and potentially irreversible. While many current therapies are believed to exert some neuroprotective effects promoting repair and remyelination, few therapies have demonstrated clinical efficacy [230]. This points to a need for better regenerative therapies for MS, particularly for secondary progressive MS [229].

1.2.22 Therapeutic ligation of TSPO

A variety of TSPO ligands have demonstrated neuroprotective effects in the treatment of inflammatory CNS injury and systemic autoimmune disease. It has been hypothesized that TSPO activation facilitates cholesterol transport and steroid synthesis, which in turn promotes the secretion of neurosteroids that enhance protective GABAminergic transmission following CNS injury [12]. Thus, activating TSPO ligands, such as 4′-chlorodiazepam (Ro5-4864) PK11195, may enhance GABAminergic signaling [231].

Etifoxine is an anxiolytic anticonvulsant medication currently under investigation for application in pain management. It is structurally distinct from benzodiazepines and does not bind the diazepine receptor but does bind TSPO. In a mouse model of EAE, etifoxine treatment at peak symptom onset was associated with decreased TSPO expression, fewer activated microglia, and increased myelin staining on Luxol Fast Blue staining [18]. It has also been found to increase the production of allopregnenalone, a neurosteroid shown to augment oligodendrocyte proliferation. The same neurosteroid has been found to decrease inflammatory cytokine secretion [18]. N-benzyl-N-ethyl-2-(7,8-dihydro-7-benzyl-8-oxo-2-phenyl-9H-purin-9-yl) acetamide, or ZBD-2, is a second generation TSPO ligand with demonstrated anxiolytic effects also under investigation for use in chronic pain, that has also been demonstrated to attenuate excitotoxicity in focal cerebral ischemia. In a mouse model of chronic pain, ZBD-2 treatment was found to attenuate glutamate excitotoxicity while augmenting GABAminergic activity [232]. XBD173 is a phenylpurine TSPO ligand which was previously investigated for the treatment of anxiety but failed to pass Phase II trials. A highly specific activating ligand, it is associated with increased allopregnenalone levels in the brains of healthy and panic-prone rats [1]. Similarly, treatment with XBD173 abrogated microglial activation in LPS-treated cultures [231]. Significantly, despite its binding site, it lacks the sedating side effects of benzodiazepines [202].

1.3 Summary of approach

PET imaging of TSPO in MS represents the potential to directly monitor the activation of immune cells in the course of disease progression. However, there is a significant variation in the affinity and specificity with which different TSPO radioligands bind TSPO. These differences may be due to quaternary changes in TSPO structure, which may differentially affect the binding sites of different ligands[4,28]. To directly probe the relationship between binding and expression, we propose to first characterize the immunological significance of TSPO expression in a relevant primate EAE model and then directly compare TSPO expression with radioligand-binding using second-generation radioligand PBR28. The relationship between protein expression and radioligand-binding will be examined peripherally in PBMC isolated from MS patients and healthy donors.

1.4 Specific Aims

The project aims to 1) identify and immunophenotype TSPO-expressing cells in the CNS and peripheral blood in primate EAE and MS, and 2) compare patterns of TSPO expression with patterns of TSPO ligand-binding in the peripheral blood of MS patients using a second-generation TSPO radioligand. Together, these experiments will provide critical insight into the pathological significance of TSPO expression in neuroinflammation and variations in the relationship between TSPO expression and radioligand-binding in response to a pro-inflammatory milieu. Better understanding of this correlation is crucial to understanding the clinical significance of TSPO radioligand-binding in multiple sclerosis and its implications for patient management and prognosis.

Summary of Aim 1

Questions: A) In what cells is TSPO expressed in healthy primate brain tissue? In what cells is TSPO expressed in marmoset EAE? Does marmoset EAE recapitulate aspects of TSPO expression observed in human disease? B) Do changes in TSPO expression reflect changes in lesion age or inflammatory cell milieu? Can these changes shed light on the functional associations of TSPO expression in neuroinflammation and its potential as a therapeutic target?

Aim: I aim to identify and phenotype cells expressing TSPO in EAE and non-EAE control tissue. Furthermore, I aim to measure changes in TSPO expression in microglia and macrophages over time in EAE lesions of different ages.

Hypothesis: I hypothesize that TSPO is expressed rarely in Iba1+ cells in healthy CNS tissue. In EAE lesions, I hypothesize that TSPO levels increase and that the principal contributors of TSPO expression are Iba1+ microglia and macrophages with M1-biased phenotype. I also hypothesize that TSPO expression in microglia and macrophages is stable over time in lesions of different ages.

Summary of Aim 2

Question: What cells express TSPO in the peripheral blood of MS patients and healthy donors? Is TSPO expression in monocytes associated with the expression of other markers of immunophenotype (e.g. HLA expression)?

Aim: I aim to measure TSPO expression in classical, non-classical (atypical) and intermediate monocytes in MS patients and determine whether increases in TSPO expression correlated increases in mitochondrial volume and expression of HLA-DR and CD86.

Hypothesis: I hypothesize that TSPO expression is increased in all subsets of PBMC in multiple sclerosis patients. I further hypothesize that TSPO expression is higher in non-classical and intermediate monocytes with pro-inflammatory characteristics than in classical monocytes.

Summary of Aim 3

Question: Do changes in TSPO expression in PBMC in MS correlate directly to changes in ligand-binding with second-generation TSPO ligands?

Aim: I aim to measure TSPO-ligand binding with second-generation ligand PBR28 in MS patients and matched healthy donors and compare levels of TSPO-radioligand-binding with levels of TSPO protein expression measured in Aim 2.

Hypothesis: I hypothesize that TSPO expression is correlated directly to ligand-binding in human PBMC from MS patients and matched healthy controls.

2 Investigating the pathological significance of TSPO expression in the central nervous system of a nonhuman primate model of multiple sclerosis

2.1 Introduction

Understanding of the cell types responsible for TSPO expression is necessary to interpret not only baseline TSPO-PET signal in healthy individuals, but also TSPO signal in disease and in response to treatment [233]. Studies of healthy rodent brain tissue have reported TSPO expression in the vascular endothelium, choroid plexus, and ependyma [137,206,234]. Neuronal TSPO was detected in areas of neurogenesis in the subventricular zone, the subgranular zone of the dentate gyrus, and the Purkinje cells of the cerebellum in the mouse brain [206]. While studies of CNS injury have identified microglia as the primary cellular source of TSPO in neuroinflammation [4,13,235,236], TSPO has also been detected in astrocytes and neurons in various models of CNS injury [42,75,206].

Ultimately, correlation of imaging findings with pathology is necessary to understand the cell types contributing to TSPO signal, as well as the immunological functions associated with TSPO expression. This is currently controversial. A 2018 study by Beckers et al. in mice found that TSPO mRNA levels were increased in M1 (LPS-stimulated) microglia in culture, but not in M2 microglia stimulated with IL4 [236]. Subsequent studies of TSPO expression in multifunctional protein-2 (Mf2) deficiency, a chronic model of neuroinflammation, found that TSPO protein and mRNA levels were increased in the inflamed brain tissue of Mf2-knockout mice. A 2017 study by Narayan et al, conversely, found that TSPO protein and mRNA levels were reduced in LPS-stimulated M1 macrophages. A recent study by Nutma et al. found TSPO is expressed by both M1- and M2-biased microglia in MS brain tissue [4].

The correlation of PET signal to pathology in MS is limited, as biopsies in MS subjects are relatively rare – studies of pathology in MS may be obtained from autopsy in patients with advanced disease or patients who died of other causes, but biopsies from earlier stages of disease are generally obtained due to an atypical presentation, in which infection or malignancy is suspected and tissue sampling is necessary to obtain a definitive diagnosis [81,237]. Ultimately, animal models are necessary for direct correlation of imaging and pathology.

However, rodent models of neuroinflammatory disease generally lack sufficient white matter for adequate MRI imaging of white matter lesions [19,21]. The marmoset EAE model, in contrast, is advantageous for the serial monitoring of lesions on MRI as a result of its comparatively high white matter-gray matter ratios, which are more similar to those of humans [23]. It is also a valuable model for neuroinflammation for its neuroanatomical and immunological similarity to humans [19,21]. Previous PET experiments have been performed on marmosets with and without anesthesia in various contexts of neurological disease [238].

If TSPO expression is detectable in marmoset EAE, the animal would represent an ideal model to monitor changes in TSPO expression in neuroinflammation by PET and correlate PET changes to pathology. The availability of MRI images would facilitate the comparison of PET and MRI imaging, allowing researchers to determine the accuracy with which PET imaging of TSPO radioligands detects inflammatory activity in known MRI lesions as well as the extent to which it detects inflammatory activity preceding the development of lesions later detected on MRI. Conceivably, PET visualization of inflammatory activity could be used to corroborate MRI detection of pre-lesional changes, such as changes in T1 signal associated with increased blood-brain barrier permeability [239]. Furthermore, PET imaging of TSPO could potentially be used to visualize chronic inflammatory activity in lesions where structural damage has already occurred, for example, the infiltration of activated microglia and macrophages into an existing demyelinated lesion, which may have prognostic value [240]. Serial PET imaging might allow us to chart the time course of inflammatory cellular processes and better understand the influence of immunomodulatory treatments in the context of chronic neuroinflammation. Finally, the correlation of PET imaging and pathology would enable the more definitive identification of cell-types contributing to TSPO-PET signal in this model.

To assess the suitability of the marmoset for the study of TSPO in neuroinflammation, it is first necessary to establish whether TSPO is expressed at detectable levels in marmoset EAE lesions and in what cell types it is expressed. Furthermore, it is necessary to understand the functional significance of TSPO expression in this context and the extent to which TSPO expression varies with lesion type and stages of lesion development. We will measure TSPO by conventional immunohistochemistry and multiplex immunofluorescence in acute and chronic EAE lesions of different ages as determined by serial MRI and compare TSPO expression with markers of immunophenotype to gain insight into the function of TSPO in neuroinflammation.

Summary of Aim 1

Questions: A) In what cells is TSPO expressed in healthy primate brain tissue? In what cells is TSPO expressed in marmoset EAE? Does marmoset EAE recapitulate aspects of TSPO expression observed in the human disease? B) Do changes in TSPO expression reflect changes in lesion age or inflammatory cell milieu? Can these changes shed light on the functional associations of TSPO expression in neuroinflammation and its potential as a therapeutic target?

Aim: I aim to identify and phenotype cells expressing TSPO in fixed EAE marmoset and non-EAE marmoset control tissue. Furthermore, I aim to measure changes in TSPO expression in microglia and macrophages over time in EAE lesions of different ages.

To achieve this aim, I will:

i) compare % of Iba1+ microglia expressing TSPO in NAWM, NAGM, lesions of different ages, and healthy control white matter and gray matter

ii) quantify % of Iba1+TSPO+ microglia co-expression M1 and/or M2 markers (MHCII, MRP14, Arg1, CD163)

iii) visualize TSPO expression in neurons and astrocytes by co-staining with NeuN or GFAP, respectively.

Hypothesis: I hypothesize that TSPO is expressed rarely in Iba1+ cells in healthy CNS tissue. In EAE lesions, I hypothesize that TSPO levels increase and that the principal contributors of TSPO expression are Iba1+ microglia and macrophages with M1-biased phenotype. I also hypothesize that TSPO expression in microglia and macrophages is stable over time in lesions of different ages.

2.2 Methodology

2.2.1 Division of responsibilities

As a PhD student, I performed animal handling, catching, sedation, intubation, positioning for MRI, anesthesia administration, and animal monitoring. MRI protocols were run by members of the Translation Neuroradiology Section. Clinical scoring was performed by clinic fellows in neurology. EAE induction, terminal scanning and euthanasia were performed a team consisting of members of the Viral Immunology Section and the Translational Neuroradiology Section. Harvesting of CNS tissues was performed by Drs. Afonso Silva and Seung-kwon Ha. Tissue sectioning was performed by Dr. Ha and myself. I performed all immunohistochemical stainings and imaging of all single or two- or three-color stains.

I also designed all multiplex panels and validated all antibodies individually, with the exception of GLS2 and Parvalbumin, which were validated by Dr. Dragan Maric. Multiplex immunofluorescence stainings were performed by myself or a member of the FACS core facility (NINDS, Bethesda, MD). Sections stained with more than 4 colors were imaged by Dr. Maric. I performed all subsequent lesion and cell counting analyses.

2.2.2 EAE induction and animal monitoring

EAE was induced by subcutaneous immunization with 0.2 g of white matter homogenate emulsified in Complete Freund’s Adjuvant (CFA) in 9 adult marmosets at 4 dorsal sites adjacent to the inguinal and axillary lymph nodes. Animals were monitored daily for clinical symptoms of EAE progression and assigned clinical EAE scores weekly based on extent of disability. Marmosets were scored on neurological exam as performed by a clinical neurologist prior to each MRI scan. The scoring system is described as follows: 0, no clinical signs; 0.5, apathy or altered ambulation without ataxia; 1, lethargy or tremor; 2, ataxia or optic disease; 2.25, monoparesis; 2.5, paraparesis or sensory loss; 3, paraplegia or hemiplegia. Body weights were recorded 3 times per week. Blood was drawn prior to each MRI scan. All animals discussed in this study are shown in **Table 2-1**.

Animal ID	Gender	Disease Status	Viral exposure	Treatment	Age at EAE induction (years)	Disease duration (days)
A	M	EAE	HHV6B	None	3.9	71
B	M	EAE	None	None	2.6	384
C	F	EAE	None	None	1.5	89
D	M	EAE	HHV6B	None	4.6	51
M	F	EAE	None	None	4.6	32
J	M	EAE	None	None	5.6	422
P1	F	EAE	None	None	2.9	105
P2	F	EAE	None	Steroids	2.9	123
W	M	EAE	None	Steroids	2.6	282
P0	M	Control	None	None	N/A	N/A

Table 2-1. *Table summarizing gender, disease status, viral inoculation status, treatment status, age at baseline, and disease duration, of all animals examined in this study.*

EAE marmoset A was previously inoculated with HHV-6B as part of trial studying the effects of viral exposure on neuroinflammatory response. Animals M2 and P2 received steroid treatment as part of another study.

2.2.3 MRI scanning

MRI analyses are performed according to established marmoset imaging protocols using T1, T2, T2*, and PD-weighted sequences on a Bruker 7T animal magnet. In tracking lesion load and disease progression, we are collaborating with the Reich laboratory, which is developing image analysis protocols for the quantitative determination of lesion volume. Marmosets were scanned biweekly over the course of the EAE study. Following the completion of EAE studies, the brains, spinal cords, and optic nerves excised from euthanized animals were scanned by MRI for postmortem characterization of brain lesions and previously uncharacterized spinal lesions and optic lesions.

2.2.4 Information on the veterinary care of the animals involved

Prior to EAE induction, marmosets are housed as twin pairs in enriched environments where they receive two meals a day. In addition to daily monitoring by veterinary staff seven days per week, they received physical exams and were tested for tuberculosis twice annually.

Additionally, they were vaccinated against measles and Klebsiellae. Tuberculosis testing was discontinued in EAE marmosets, as exposure to heat-killed emulsified tuberculin toxin in the adjuvant during EAE induction would result in a positive reaction regardless of infectious status.

2.2.5 Description of the procedures for ensuring that discomfort, distress, pain, and injury will be limited to that which is unavoidable in the conduct of scientifically sound research

Marmosets received regular veterinary care and receive daily neurological exams over the course of EAE progression to detect signs of distress and symptoms of disability. They are weighed three times each week. The site of adjuvant injection is carefully treated and dressed to prevent infection and discourage the animal from touching or scratching the site if local inflammation occurs. Animals are also monitored for behavioral changes and animals sharing cages are separated if they display aggression or violence towards one another.

2.2.6 Description of the use of analgesic, anesthetic, and tranquilizing drugs and/or comfortable restraining devices, where appropriate, to minimize discomfort, distress, pain, and injury

Prior to each MRI scan, marmosets were identified by an ID tattoo on the inner thigh and captured using a standard catch cage. They were weighed in this catch cage, loaded into a covered animal crate lined with soft absorbent fabric, and transported in this carrier from the veterinary facility to the scanner room through a secure elevator directly connecting the two areas. In the scanner room, the animals are carefully removed from their cages using thick leather gloves, sedated with ketamine (10 mg/kg, intramuscular), anesthetized with inhaled isoflurane, and intubated with a small lidocaine-coated non-rebreathing tube delivering 40% oxygen and 60% nitrogen. Following intubation, the marmoset's foot was shaved and a pulse oximeter is placed to measure heart rate, oxygen levels, and carbon dioxide levels. An IV access line for the injection of MRI contrast is placed in the tail vein and stabilized with surgical tape. Once the marmoset's heart rate has decreased to approximately 200 beats/minute and blood oxygen levels are observed to be stable, the marmoset is wrapped in a warming blanket and placed in the scanning cradle in the sphinx position. Lidocaine-coated ear bars are placed in the animal’s ears to maintain the position of the animal's head. A lubricant is place in the eyes to prevent dehydration and discomfort. A rectal probe is placed to monitor body temperature. Over the course of the scan, vital signs are monitored continuously and recorded every 15 min.

For the induction of EAE, animals were transported, sedated, and anesthetized as described above. White matter homogenates are injected at four sites as described in the study description. Topical antibiotics and dressings are used to treat and cover the injection sites of EAE animals. Animals are inspected regularly by veterinary staff for signs of irritation or distress.

2.2.7 Description of methods of euthanasia to be used and the reasons for its selection

Marmosets are monitored closely for signs of disability and cognitive change after the induction of disease. Animals that develop hemiplegia or paraplegia are euthanized in accordance with the recommendations of the American Veterinary Association's Guidelines on Euthanasia and NIH IACUC protocols. Briefly, animals are weighed and transported to the Building 49 MRI facility and anesthetized with inhaled isoflurane as previously described to undergo a terminal MRI scan. Following the completion of the scan, they are maintained on inhaled isoflurane and transported to a fume hood in an adjacent veterinary facility for cardiac perfusion. 100 mg/kg of sodium pentobarbital are administered intravenously. Once the animal is fully anesthetized and confirmed to be unresponsive to painful stimuli, the chest is opened to expose the left wall of heart and a sterile catheter is positioned in the left ventricle. Warm heparinized saline in injected into the catheter to thin the animal's blood and facilitate the flow of blood from the right atrium which is cut to permit drainage. Following the heparinized saline, 4% paraformaldehyde is injected into the catheter. Once the animal is adequately perfused with paraformaldehyde, the skull and stomach are opened to harvest the brain, spinal cord, and lymphoid tissues.

To facilitate the correlation of lesions visualized on MRI with lesions seen on histopathology, 3-D modeling of brain scans was used to develop individualized cradles holding brain specimens in alignment with their position during scanning. These cradles are currently used by our imaging partner group and will ensure that sections cut for histology align with MRI sections [138,241]. Briefly, a 3D model of each brain was subtracted from a scaffold block template to produce a cradle for sectioning. Cradles were printed using an

Airwolf 3D printer with notches for cutting blades strategically placed 100 µm anterior to lesions identified on MRI. Using this approach to section the brain, we were able to efficiently obtain sections containing the same landmarks and confirm these lesions by conventional immunohistochemistry techniques.

2.2.8 Immunohistochemistry

Pathological brain specimens from EAE marmosets have been provided by the Neuroimmunology Branch (NIB) of NINDS.

To determine TSPO expression by microglia and infiltrating macrophages in inflammatory MS and EAE lesions, marmoset CNS tissues from healthy or EAE-affected animals have been formalin-fixed and paraffin-embedded for staining. Marmoset tissues are provided by VIS. Proteolipid protein (PLP) staining was used to visualize loss of myelin protein, while Luxol Fast Blue staining was used to detect loss of lipid content in demyelinated lesions. GFAP was used to detect reactive astrocytes. Ionized calcium binding adaptor molecule 1 (Iba1) was used to detect activated macrophages and microglia. NeuN was used to detect neuronal nuclei, while NFH was used to detect axons and MAP2A was used to label dendrites. S-100-β was used to detect astrocyte cell bodies while GFAP was used to detect reactive astrocyte processes and cell bodies. The combination of Iba1 and lectin was also used to visualize endothelial cells, which express lectin alone, and differentiate them from activated microglia, which express both lectin and Iba1.

For immunohistochemistry, paraffin-embedded sections were deparaffinized in three changes of xylene, rehydrated in three changes of graded ethanol, and washed in ultrapure water. Antigen retrieval was performed by steaming the slide in 10 mM citrate buffer (pH 6) for 20 minutes. Sections were washed with tris-buffered saline (TBS), blocked for 20 minutes in 10% non-fat dairy protein in TBS, and again washed with TBS.

For DAB staining, sections were washed three times in TBS and incubated with a horseradish peroxidase-conjugated secondary antibody diluted 1:2000 in TBS for 15 minutes at room temperature. The section was then incubated with DAB chromogen substrate, which was prepared according to the manufacturer's instructions using a DAB Peroxidase Substrate kit (Vector Laboratories, Maravai Life Sciences, San Diego, CA). For Vector Blue staining, sections were washed three times in TBS and incubated with an alkaline phosphatase-conjugated secondary antibody diluted 1:2000 in TBS. The section was then washed three times in TBS and incubated with Vector Blue substrate, which was prepared according to the manufacturer's instructions using a Vector Blue substrate kit (Vector Laboratories, Maravai Life Sciences, San Diego, CA). DAB-stained sections were differentiated in Blue Buffer (Leica Biosystems, Wetzlar, Germany) and counterstained with hematoxylin (Leica Biosystems, Wetzlar, Germany), while Vector Blue-stained sections were counterstained with Methyl Green or Fast Red (Vector Laboratories, Maravai Life Sciences, San Diego, CA). For Luxol Fast Blue (LFB) staining, sections were incubated overnight in NovaUltra LFB Solution (IHC World, Ellicott City, MD, USA) at 56C, differentiated with lithium carbonate, and counterstained with periodic acid-Schiff (PAS) (IHC World, Ellicott City, MD, USA). Following substrate visualization, sections were washed in TBS and coated with Immu-Mount (Fisher, 99-904-02), after which each section was sealed with a 22 x 50 mm coverslip. Secondary antibodies are described in the Appendix.

2.2.9 Multiplex Immunofluorescence

To immunophenotype macrophages and microglia expressing high levels of TSPO in the CNS, I worked with the NINDS FACS Core Facility to design a 10-color multiplex immunofluorescence panel staining for Iba1, TSPO, early activation markers MRP14, MHC-II molecule HLA-DR, phagocytic receptor CD163, and canonical M2 marker Arg1. All markers were validated to work in both marmoset and human tissues that were formalin-fixed and paraffin-embedded. To further probe the expression of TSPO in reactive astrocytes and neurons, selected sections were stripped and re-stained with a second panel staining to Iba1, GFAP, calcium binding astrocytic marker S-100-B, neuronal nuclear marker NeuN, dendritic marker MAP2a, and axonal filament NFH.

For multiplex immunofluorescent staining, paraffin-embedded sections were deparaffinized in three changes of xylene, rehydrated in three changes of graded ethanol, and washed in ultrapure water. Prior to staining, sections were washed twice in NPM, followed by two washes in distilled water. Antigen retrieval was performed by boiling the slide in 10 mM citrate buffer (pH 6) for 10 minutes in a 1.2 kW microwave at maximum power, after which the sections were allowed to cool for 30 minutes to room temperature and washed twice in distilled water. To reduce nonspecific Fc receptor binding, Fc receptor blocking was performed by coating the section in 250 µl FcR blocker (Innovex Biosciences, NB309) for 15 minutes at room temperature, after which the section was washed twice in distilled water. To further reduce background, sections were then coated with 250 µl Background Buster (Innovex Biosciences, NB306) for 15 minutes at room temperature and washed twice in distilled water. Sections were then covered with a primary antibody cocktail containing the following antibodies diluted as specified in NPM in **Table 7-1**. Sections were incubated in the primary antibody cocktail for 45 minutes at room temperature and washed in NPM followed by three changes of distilled water, after which they were covered in a secondary antibody cocktail composed of the following secondary antibodies diluted as specified in NPM containing DAPI (Invitrogen, D1306, 100 ng/ml) in **Table 7-2**. The sections were incubated in the secondary antibody cocktail for 45 minutes at room temperature, washed once in NPM, and twice in distilled water. To facilitate mounting, the sections were air-dried for 15 minutes at room and coated with Immu-Mount (Fisher, 99-904-02), after which each section was sealed with 22 x 50 mm coverslip and allowed to dry overnight prior to image acquisition.

2.2.10 Antibody stripping of previously stained sections

To facilitate the re-staining of previously stained sections, coverslips were removed carefully from mounted sections and the uncovered sections were incubated for 10 minutes at room temperature in 250 µl of NewBlot Nitro 5X Stripping Buffer (Li-Cor, 928-40030). The stripped sections were washed once in NPM, followed by two washes in distilled water.

2.2.11 Multiplex immunohistochemical staining of previously stripped sections

To detect antigens not restored by prior antigen retrieval, sections were boiled for an additional two minutes in citrate buffer (pH 6.0) in a 1.2 kW microwave at 100% power, after which the sections were allowed to cool for 30 minutes to room temperature and washed twice in distilled water. The sections were covered 250 µl FcR blocker (cat. no. Innovex Biosciences, NB309) for 15 minutes at room temperature, after which the section was washed twice in distilled water. Sections were then blocked for 15 minutes at room temperature in 250 µl Background Buster (Innovex Biosciences, cat. no. NB306) and washed twice in distilled water. Sections were then covered with the R2 primary antibody cocktail, which consists of the following antibodies diluted in NPM as described in **Table 7-3**. Sections were incubated in the R2 primary antibody cocktail for 45 minutes at room temperature and washed in NPM followed by three changes of distilled water, after which they were covered in the R2 secondary antibody cocktail composed of the following secondary antibodies diluted as specified in NPM containing DAPI (Invitrogen, cat. no. D1306, 100 ng/ml) as specified in **Table 7-4.**

The sections were incubated in the secondary antibody cocktail for 45 minutes at room temperature, washed once in NPM, and twice in distilled water. To facilitate mounting, the sections were air-dried for 15 minutes at room and coated with Immu-Mount (Fisher, cat. no. 99-904-02), after which each section was sealed with a 22 x 50 mm coverslip and allowed to dry overnight prior to image acquisition.

2.2.12 Image Acquisition

Sections stained with more than 4 markers were imaged using a 20x/0.8NA/Phase2 Plan-Apochromat Zeiss objective mounted on an AxioImager.Z2 widefield scanning fluorescence microscope with a 600 μm x 600 μm field of view and 5% overlap between each imaged tile. To detect the additional markers, the microscope is outfitted with 10 distinct narrow band-pass filters. The scanner moves the stage with precision and acquires an image at each tile location from each color channel. Each image is a 16-bit monochrome image of the fluorescence intensity. A dataset from a fully scanned slide is typically comprised of 800-1200 image tiles, which are each 2048 x 2048 pixels.

2.2.13 Lesion analysis

After matching sections of interest to their corresponding slice on MRI, preliminary ROI were defined by pathology, using PLP and Iba1 staining to detect demyelination and microglial clustering. Serial MRI studies were used to classify hyper-intensities by time of appearance and mark changes in size or shape. The MRI scan showing highest level of activity was used to draw ROI encompassing each hyperintensity at its largest. I then superimposed ROI identified on MRI over ROI identified by pathology in corresponding tissue section. Where there was a discrepancy between the size of the ROI observed on MRI and the corresponding ROI identified by histopathology, the larger ROI was chosen. Lesions were color-coded by time of appearance as follows:

Purple = 2-3 mo.
Blue = 3-4 mo.
Green = 4-5 mo.
Yellow= 6-7 mo.
Orange - 7-8 mo.
White= lesion age indeterminate.

2.2.14 Image quantification

To quantify TSPO in Iba1+ cells in primate brain, we chose to limit our analysis to Iba1+ cells with visible DAPI+ nuclei, thereby restricting or analysis to macrophages and microglia with a nucleus in the plane of the section. An erosion/dilation algorithm coded in C++ was used to segment DAPI+ signal and identify nuclei. Each DAPI+ region was then for contiguous Iba1+ pixels to identify microglial nuclei. This was done to exclude Iba1+ fragments not associated with DAPI+ nuclei and exclude DAPI+ nuclei not associated with Iba1. After identifying microglial nuclei, all pixels within a 15-pixel radius of each nuclei were scanned for Iba1+ signal above a certain threshold, which was defined for each section by visual inspection. If a pixel had an intensity of Iba1 staining above threshold and was contiguous with the nucleus or other Iba1+ pixels that were contiguous with the nucleus, this pixel was identified as containing cytoplasm. The pixels constituting the cytoplasm and the nucleus were added to one another to form a cell mask, which was then assigned a number and scanned for expression of other markers, e.g. TSPO, Arg1, CD74.

To count neurons, a 500 μm x 500 μm region of interest was selected in the right and left cortical gray matter and NeuN+ and NeuN+TSPO+ cells were counted manually.

2.2.15 Statistical Analysis

To study changes in TSPO expression over time in lesions of different ages, in which a subset of lesions of different ages were found in the same animal, a linear mixed effects model was used to account for the non-independence of these data points [242,243]. Changes in the fraction of Iba1+ cells expressing TSPO were modeled as a function of lesion age at time of sacrifice, animal identity, and animal treatment status.

Specifically, the fraction of Iba1+ cells expressing TSPO ("TSPO Ratio") in each lesion is modeled as a dependent variable that varies as a function of treatment status (i.e. "steroid-treated" or "untreated") and lesion age at time of sacrifice ("Month.Stop"), which is treated conditionally as a fixed effect. Secondly, to account for multiple levels of random variation, random variation associated with animal identity ("Error(Monkey)") is differentiated from random variation between lesions within individual animals ("PureError(Lesion|Monkey)"), which represents the standard residual variation due to factors not taken into account by the model.

The relationship between TSPO expression and treatment status and lesion age can thus be modeled via additive offsets from a reference state at time of lesion onset (e.g. Month.Stop = 0) in the absence of the steroid treatment. This model may be represented by the following equation, where the y-intercept of the function ("Intercept") is implicitly defined primarily by fixed effects but also in part by random effects:

TSPO Ratio ~ Intercept + Steroid*[Treatment=Steroid]
+ Sum(MonthEffect@month*[Month=month]; month in the Set{1:7})
+ Error(Monkey) + PureError(Lesion|Monkey)

An alternative parameterization estimates the intercept as the fraction of Iba1+ cells that are TSPO+ in the absence of steroid treatment over all months before sacrifice and incorporates dependence on months before sacrifice as a sequence of successive differences from the cumulative average of the preceding values up to that time e.g. subtracting the TSPO+ ratio three months prior to sacrifice from the average of the TSPO+ ratios at one and two months prior to sacrifice. Thus, for this model, the intercept estimates an overall "TSPO Ratio" across months before sacrifice in the absence of steroid treatment.

A table summarizing animal identity, treatment status, and lesion age for each lesion is included in the appendix. Analysis was performed in R (R Foundation for Statistical Computing, Vienna, Austria). A p-value of less than 0.05 was considered significant. The R code used to perform this analysis was derived from analyses by Kusnetsova et al. [243,244] and is included in the appendix.

To assess for dependence between TSPO and other markers of immunophenotype, joint responses to multiple markers have been represented by determining the odds ratio statistic for each individual lesion, which are calculated as followed, for MRP14 as an example:

$$\text{OddsRatio(TSPO,MRP14)} = \frac{(\text{TSPO+MRP14+}) * (\text{TSPO-MRP14-})}{(\text{TSPO+MRP14-}) * (\text{TSPO-MRP14+})}$$

2.3 **Results**

2.3.1 TSPO is expressed in the meninges, ependyma, and vascular endothelium of control marmoset brain tissue

To detect and determine the identity of TSPO-expressing cells in healthy and EAE marmoset CNS tissue, we applied a multiplex immunofluorescence panel described in **Table 7-1** and **Table 7-2** to sections of brain and spinal cord tissue from EAE marmosets and a non-EAE control marmoset that died of non-neurological disease. Figure 1 shows representative multiplex immunofluorescence images of TSPO, Iba1, and DAPI staining in regions of NAWM and NAGM from the brain from this control animal, a neurologically healthy primate that died of gastrointestinal disease. As shown in ***Figure 2-1***, there is dense TSPO staining in the meninges (**2-1A**) and ependymal cells (**2-1B**) of the non-EAE control marmoset that does not colocalize with Iba1.

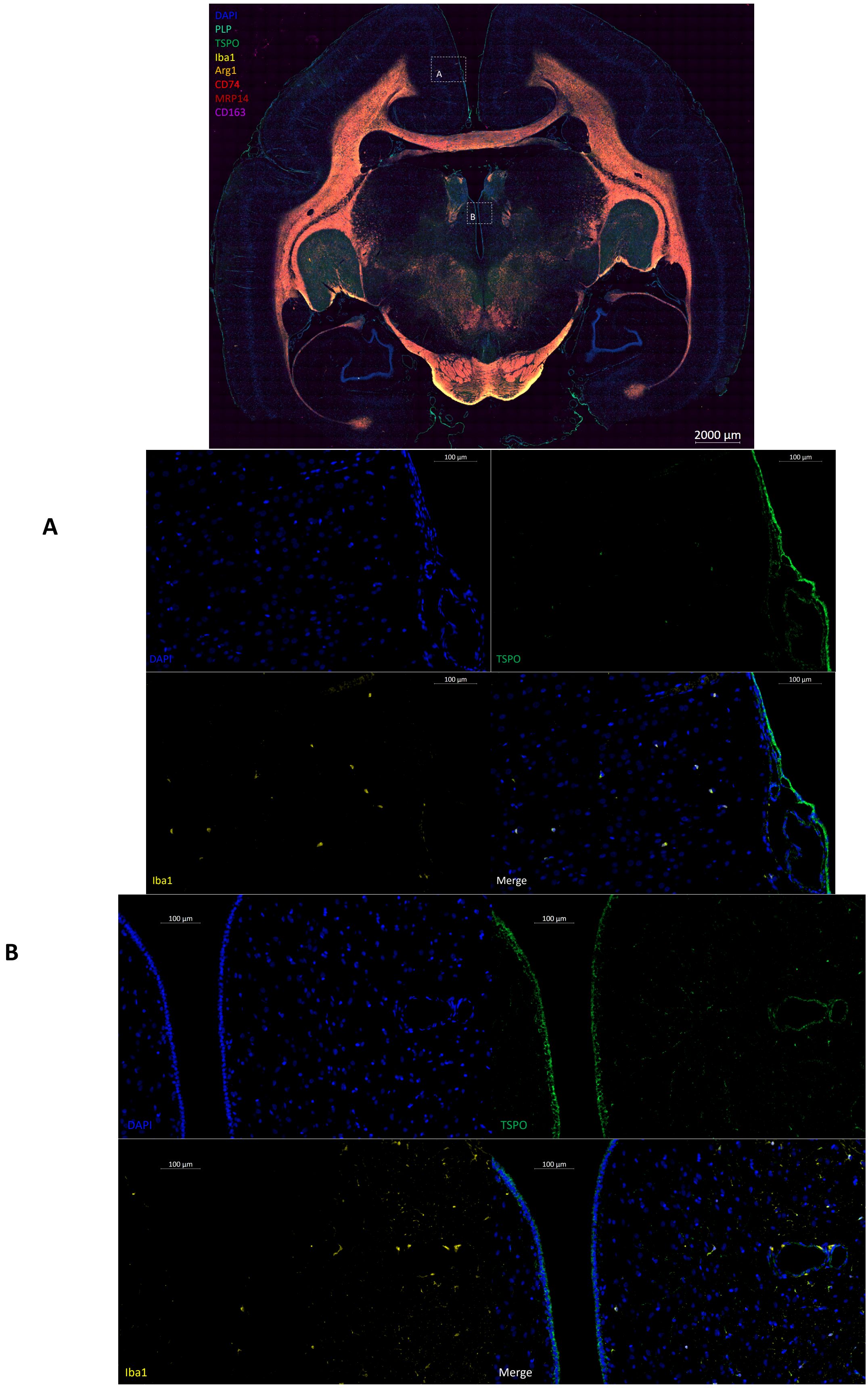
DAPI
PLP
TSPO
Iba1
Arg1
CD74
MRP14
CD163
A
B
2000 µm
A
100 µm
DAPI
TSPO
Iba1
Merge
B
100 µm
DAPI
TSPO
Iba1
Merge

Figure 2-1. *TSPO, Iba1, and DAPI staining in the a) meninges and b) ependymal cells of a non-EAE control marmoset that died of gastrointestinal disease.*

2.3.2 TSPO is expressed in 59% of Iba1+ microglia and macrophages in NAWM and NAGM in healthy primate brain tissue

TSPO expression was observed in Iba1+ cells in both normal-appearing white matter and normal-appearing grey matter in both healthy and diseased primate tissue. ***Figure 2-1*** shows multiplex immunofluorescence images of TSPO, Iba1, and DAPI staining in regions of NAWM and NAGM from the brain of P0, the control primate that died of non-neurological disease. Segmentation of Iba1+ cells with visible DAPI-stained nuclei identified 34,345 activated microglia and macrophages within the section. As there was no evidence of blood-brain barrier compromise in this animal, the vast majority of Iba1+ cells in this animal are presumed to be resident microglia. A small quantity of Iba1+ cells were observed within the intravascular space of cerebral blood vessels and are thought to be peripheral blood macrophages. Quantification of TSPO+ pixels with an intensity above 2300 indicated TSPO expression above threshold of in 58.65% of Iba1+ cells in this section of the brain.

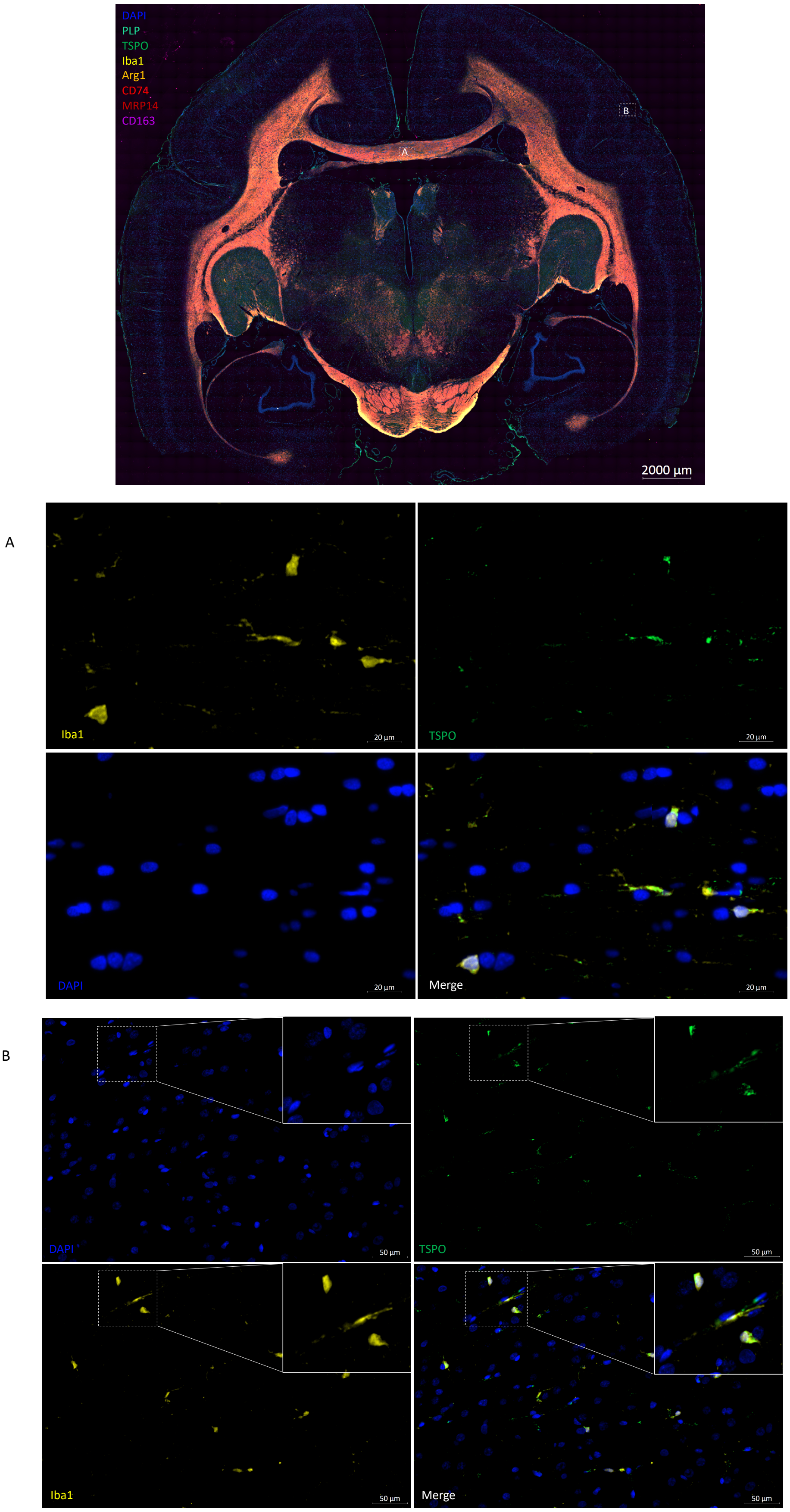
DAPI
PLP
TSPO
Iba1
Arg1
CD74
MRP14
CD163
A
B
2000 µm
A
Iba1
20 µm
TSPO
20 µm
DAPI
20 µm
Merge
20 µm
B
DAPI
50 µm
TSPO
50 µm
Iba1
50 µm
Merge
50 µm

Figure 2-2. *TSPO, Iba1, and DAPI staining in the A) NAWM and B) NAGM of a non-EAE control marmoset that died of gastrointestinal disease.*

TSPO expression was also observed in Iba1+ microglia/macrophages in the NAWM and NAGM of EAE animals. **Figure 2-3** shows multiplex immunofluorescence images of TSPO, Iba1, and DAPI staining in regions of NAWM of Marmoset P1, an EAE marmoset. **Figure 2-4** shows multiplex immunofluorescence images of TSPO, Iba1, and DAPI staining in regions of NAGM from Marmoset J, another untreated EAE marmoset.

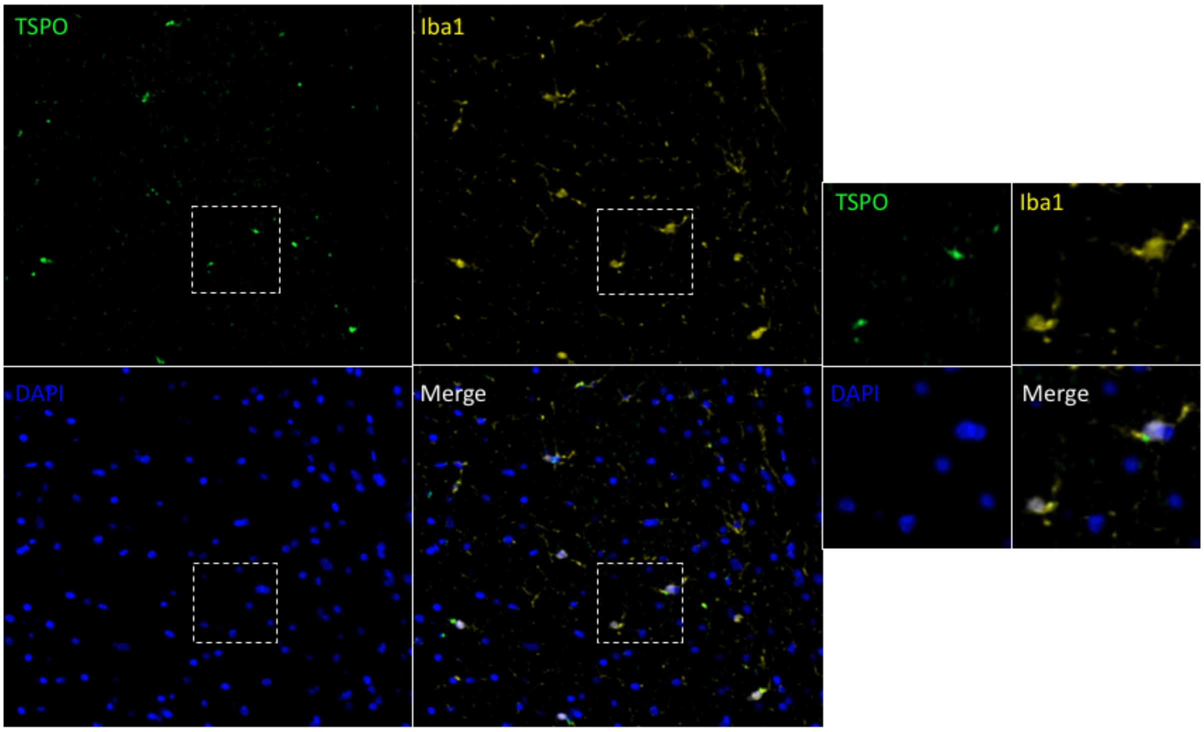

Figure 2-3. *TSPO, Iba1, and DAPI staining in a region of normal appearing white matter in an untreated EAE marmoset, P1. The inset shows two TSPO+Iba1+ cells at higher resolution.*

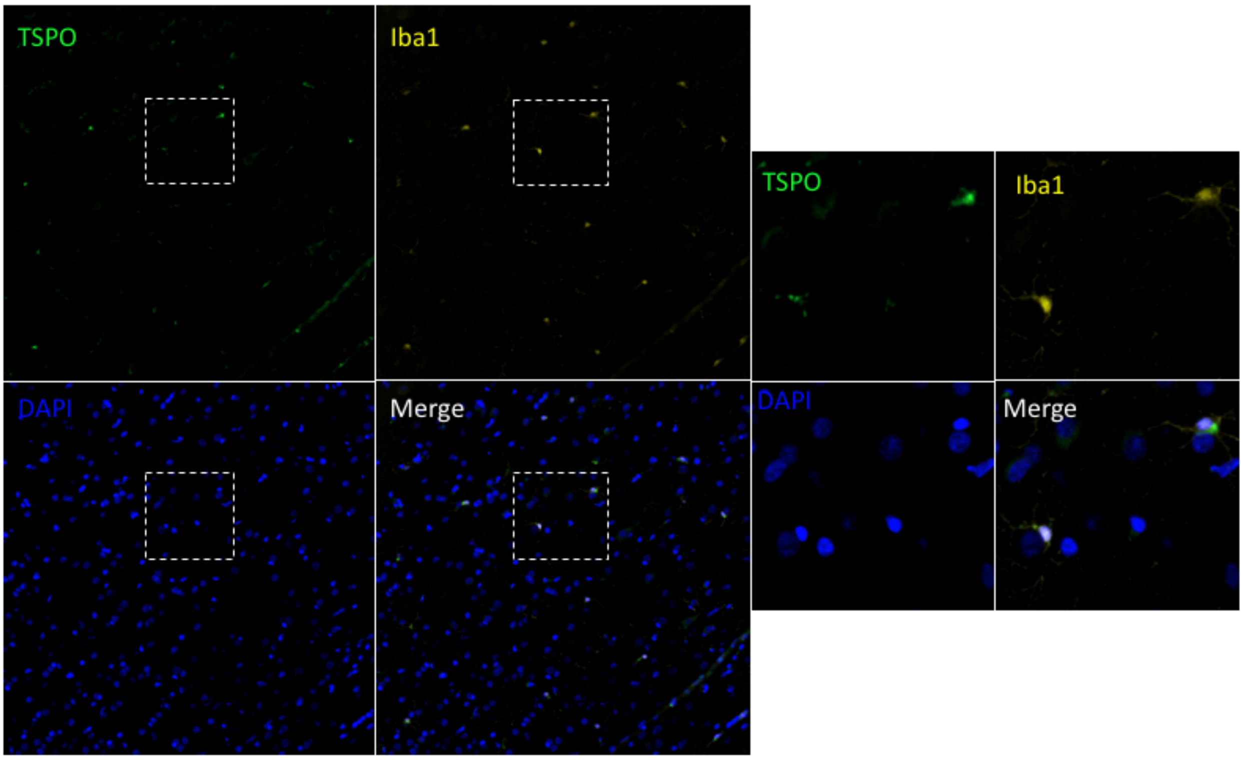

Figure 2-4. *TSPO, Iba1, and DAPI staining in a region of normal appearing gray matter in an untreated EAE marmoset, J. The inset shows two TSPO+Iba1+ cells at higher resolution.*

While conventional MRI does not allow the effective imaging of demyelination in the gray matter in these animals, Iba1 staining facilitated the identification of regions of phagocytic activation in the vicinity of the right thalamic nucleus of marmoset A, an EAE marmoset with antecedent HHV-6B infection included through a trial studying the effects of viral exposure on neuroinflammatory response. A subtle increase in TSPO positivity is seen in this same region, suggesting TSPO could be used to detect areas of inflammatory activity that are not yet detectable on MRI.

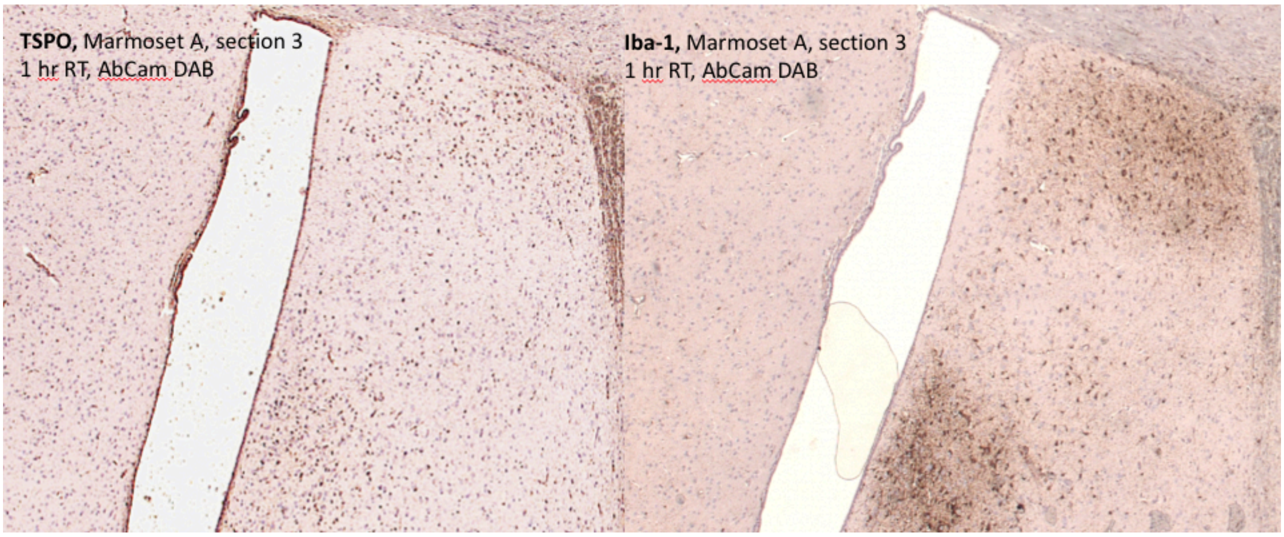

Figure 2-5. *TSPO and Iba1 staining with DAB chromogen and hematoxylin counterstain in the region of the right thalamic nucleus of EAE marmoset A.*

2.3.3 TSPO is highly upregulated in demyelinated T2-hyperintense lesions in marmoset EAE, primarily in association with Iba1+ microglia and macrophages

Fixed sections of brain and spinal cord tissue from EAE marmosets A and C were stained by conventional immunohistochemistry for TSPO and counterstained with hematoxylin and eosin to visualize cellular structures and nuclei. Contiguous serial sections were stained for Iba1 to visualized activated macrophages and microglia and PLP to visualize demyelination in gray and white matter. Luxol Fast Blue staining was performed to visualize demyelinated lesions in the white matter. PLP and LFB staining revealed clusters of demyelinated lesions, while Iba-1 staining shown dense phagocytic activation within the lesions. These lesions were found to be highly positive for TSPO. Images taken at higher magnification (10x) shows many ramified crescent-shaped cells consistent with microglial morphology (***Figure 2-6***).

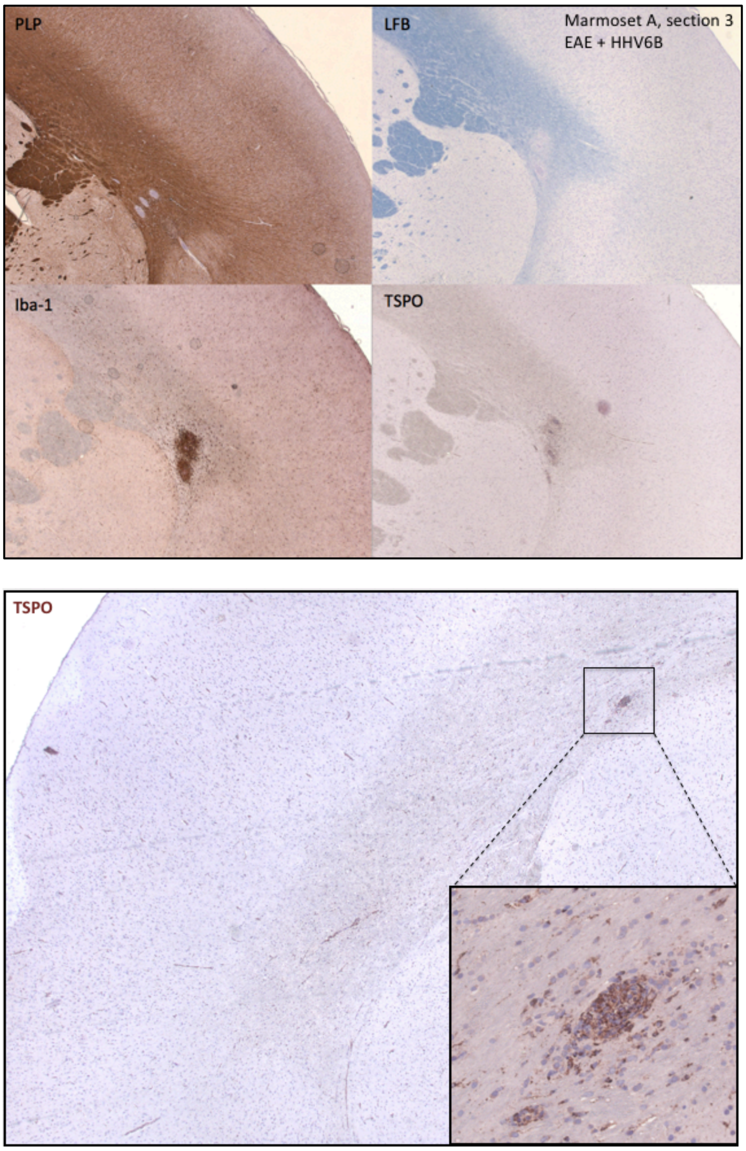

Figure 2-6. *Top panel shows PLP, LFB, Iba1, and TSPO staining of a lesion in the left white matter tract of an EAE marmoset with antecedent HHV6B infection. Lower panel and inset show dense TSPO staining in one lesion in the right white matter tract. Iba1 and TSPO staining was visualized with DAB chromogen.*

Moreover, these lesions were found to correlate with hyperintensities identified on serial T2W and postmortem PD-weighted MRI. A comparison of TSPO and Iba1 staining with T2W hyperintense demyelination in a cluster of lesions in the left white matter tract of an EAE marmoset with antecedent HHV6B infection is shown in **Figure 2-7**.

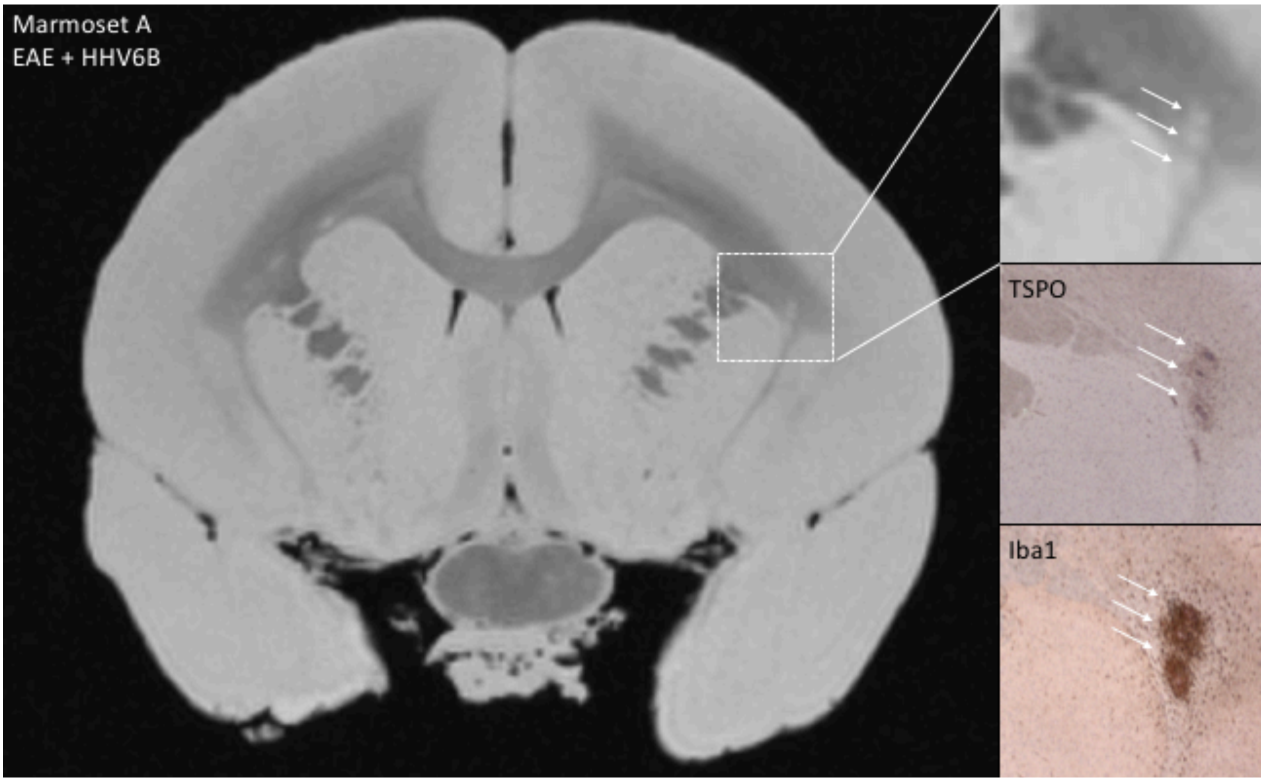

Figure 2-7. Comparison of TSPO and Iba1 staining in three adjacent left white matter tract lesions and hyperintensities identified on postmortem PDW MRI (white arrows). Iba1 and TSPO staining was visualized with DAB chromogen and hematoxylin counterstaining.

This pattern was found to persist in the spinal cord of an EAE marmoset, Marmoset C (**Figure 2-8**). White matter demyelination was detected by LFB and conventional immunohistochemical staining for PLP staining and was observed to extend from the pial surface of the spinal cord at the cervical, thoracic, and lumbar levels. This white matter demyelination was observed to correlate with increased densities of Iba1+ microglia and macrophages in all three sections. Gray matter demyelination is less apparent, but some areas of patchy demyelination can be correlated to Iba-1 staining on higher magnification. These were also found to correlate with demyelinated lesions identified by T2W MRI [138]. TSPO staining was found to correspond spatially with Iba1 staining and demyelination of the rim of the spinal cord at all levels.

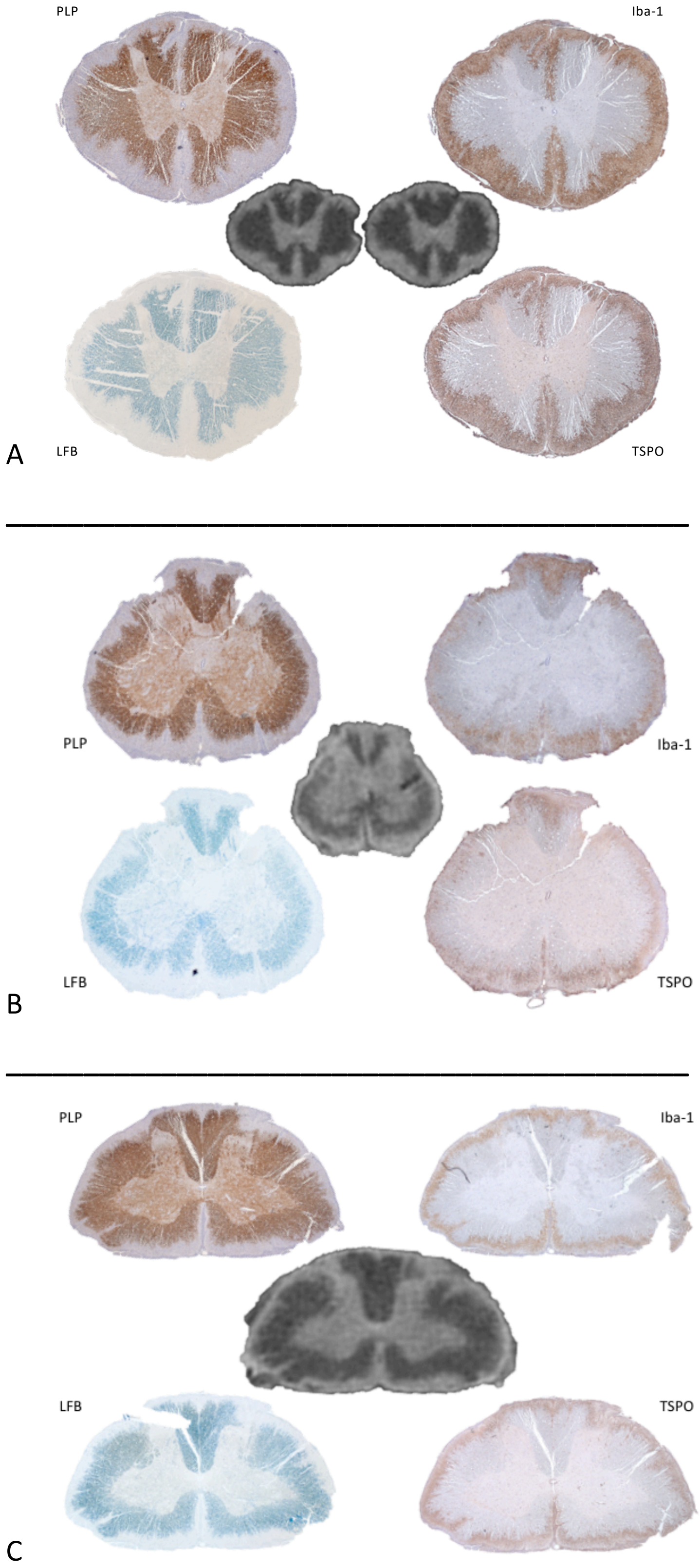
PLP
Iba-1
LFB
TSPO
A
PLP
Iba-1
LFB
TSPO
B
PLP
Iba-1
LFB
TSPO
C

Figure 2-8. *Comparison of PLP, LFB, Iba1, and TSPO staining with T2W spinal MRI in the A) lumbar, B) thoracic and C) cervical spinal cord of an untreated EAE marmoset. Iba1 and TSPO staining was visualized with DAB chromogen and hematoxylin counterstaining.*

2.3.4 Temporal changes in TSPO expression

Evidence of temporal changes in TSPO expression in marmoset EAE were first observed in tissue from a male EAE marmoset, W, that had received steroids intermittently over the course of its disease and had developed an afferent pupillary defect, indicating pathology of the optic nerves and tracts. A coronal ex-vivo T2* MRI confirmed two large lesions in the left optic tract, which were determined to be between 4 and 7 months old by review of serial biweekly MRIs over the course of disease, as well as many iron-containing lesions in the anterior commissure, which were visible but too small to be effectively aged. TSPO staining was significantly improved in these lesions with antigen retrieval using citrate buffer at pH 6 with high heat (boiling) and correlated to demyelination and phagocytic activation by LFB and Iba-1 staining in both the optic nerve and anterior commissure (Iba-1 not shown). Interestingly, a distinct difference in the intensity of TSPO staining was observed between the two lesions in the left optic tract. An analysis of serial MRI studies over the 6 months prior to the animal's death in February 2016 found that the upper lesion (***Figure 2-9***, blue arrow) had developed in early September 2015 and was approximately 5-6 months old at the time of the animal's death. The lower lesion (***Figure 2-9***, white arrow) did not develop until mid-October and was approximately 3-4 months old at the animal's time of death.

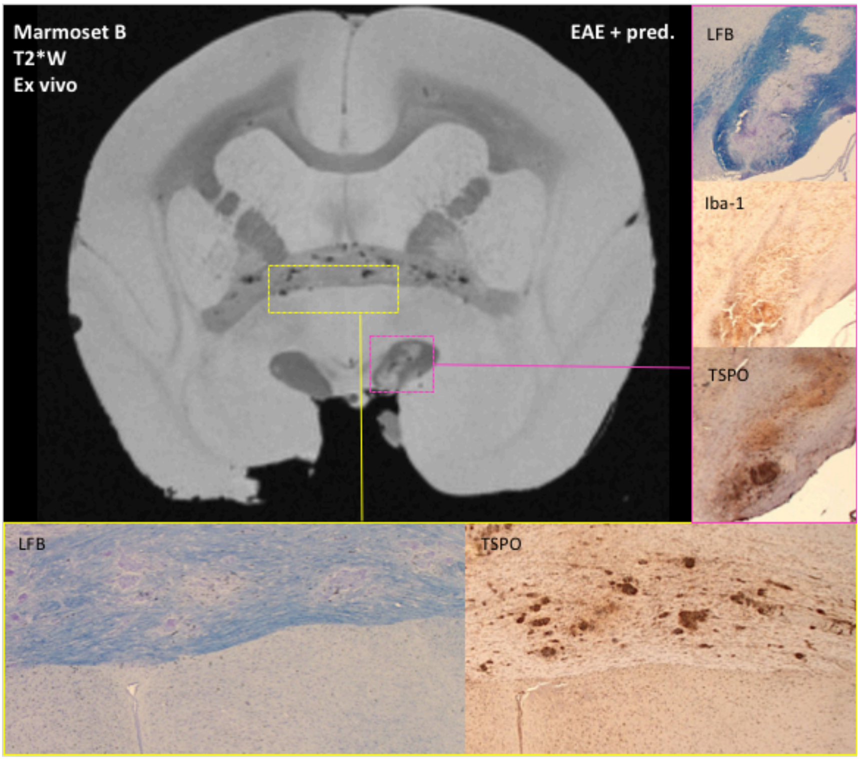

***Figure 2-9**. T2W MRI studies performed on untreated EAE W marmoset in the 6 months prior to sacrifice indicate two lesions forming in the left optic tract. The upper lesion (blue arrow) first appeared in early September 2015 and was 5-6 months old at the time of sacrifice in February. A small circular lesion (white arrow) was first seen in mid-October and was 3-4 months old at sacrifice. Immunohistochemical stainings for TSPO and Iba1 with DAB chromogen show noticeably higher expression in the younger lesion. An ex-vivo T2*-weighted MRI also indicates multiple iron-laden lesions in the anterior commissure that appear demyelinated on LFB staining and are densely positive for TSPO.*

On histopathology, the younger lesion was found to contain a higher density of Iba1+ cells and a much higher density of TSPO staining when compared to the older lesion, suggesting it may be useful to gain insight into the time course of TSPO regulation.

To further probe the time course of marmoset EAE, a multiplex immunofluorescence measuring TSPO, Iba1, CD74, and MRP14 was applied to sections of brain tissue from four untreated EAE marmosets (animals M, B, J, and P1) and two steroid-treated marmosets (animals W and P2). ***Figure 2-10*** shows a section from animal B, an untreated male EAE animal whose disease developed over the course of 10 months. This animal was monitored monthly by MRI, which facilitated the identification of many lesions of different ages at the time of the animal's death. The section shown was selected because it was found to contain lesions ranging from 2-3 months to 7-8 months of age. The section was stained with an antibody cocktail targeting TSPO, PLP, Iba1, and multiple immunophenotype markers observed to correlated to M1 and M2 phenotype induction in vitro.

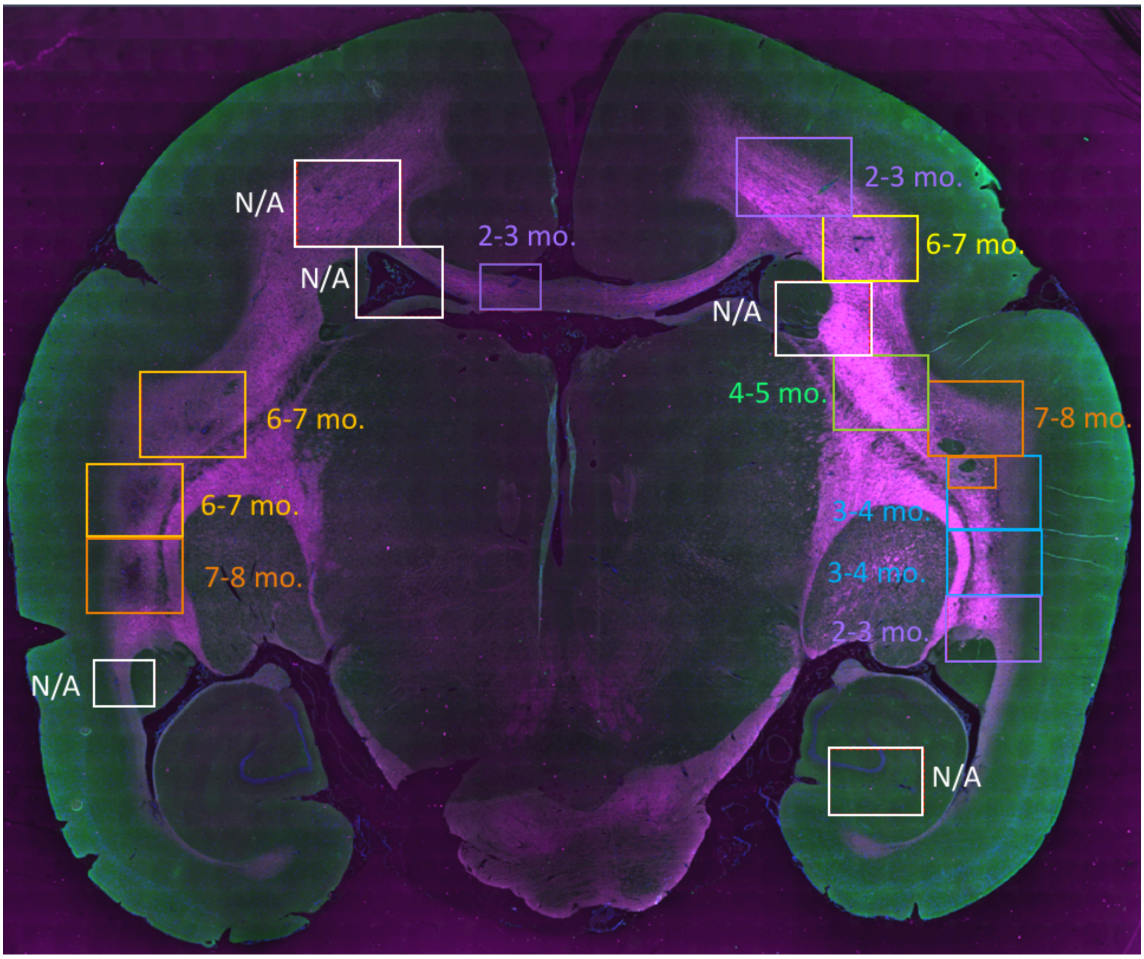

Figure 2-10*. A section from an untreated EAE marmoset with over 10 lesions of various ages as determined by serial MRI, as well as several inflammatory nodules not seen on MRI (labeled "N/A"). Colors indicate lesion age as follows: Purple = 2-3 mo., Blue = 3-4 mo., Green = 4-5 mo., Yellow= 6-7 mo., Orange = 7-8 mo., White = Lesion age indeterminate.*

Quantification of TSPO within Iba1+ cells indicated that the percentage of Iba1+ cells that were also TSPO+ was highest in younger lesions. To test if this trend was observed in other animals, the percentage of Iba1+ cells expressing TSPO was quantified in lesions of different ages in the other EAE marmosets. The results are shown in ***Figure 2-11***.

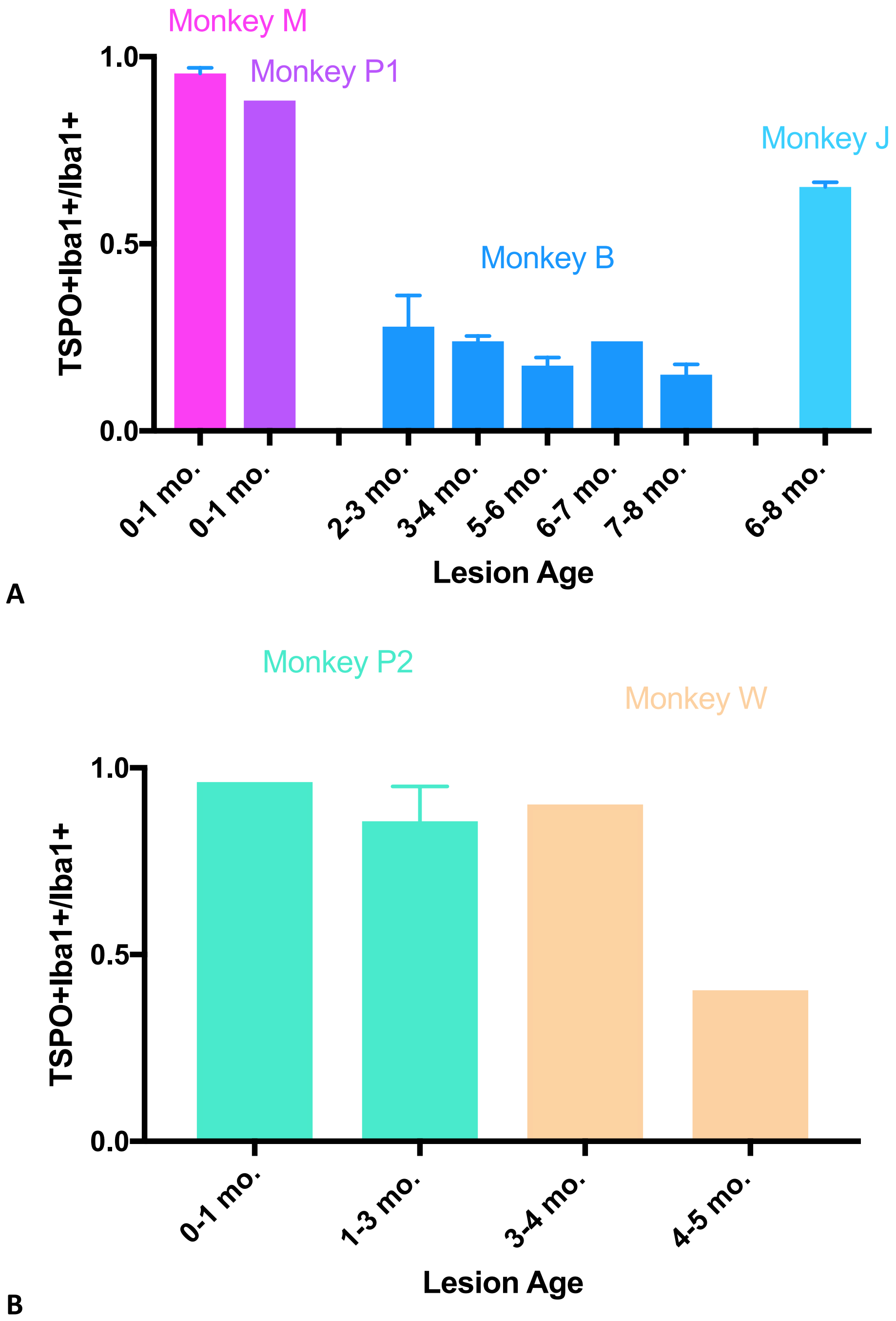

Figure 2-11. *Fractions of Iba1+ cells co-expressing TSPO in lesions of different ages from A) untreated EAE animals (n=4) and B) prednisolone-treated EAE animals (n=2).*

An overall ANOVA (with Satterthwaite-corrected degrees of freedom) indicates a statistically significant effect for lesion age at time of sacrifice ("MonthStop") (p=0.01041, F(7.0, 5.3091)=9.46), but no significance was associated with steroid treatment status (p=0.28152, F(1.0, 3.15)=1.68) after adjustment for other fixed effects via a Type III Sum-of-Squares. These are summarized in **Table 2-2**.

Parameter	Sum Sq	Mean Sq	nDF	dDF	F-stat	p-value
Treatment	0.004168	0.004168	1	3.1515	1.6814	0.28152
factor(-MonthStop)	0.164179	0.023454	7	5.3091	9.4616	0.01041 *

Table 2-2. *Sum-of-Squares values ("Sum Sq"), mean square values ("Mean Sq"), numerator degree of freedom (nDF), denominator degrees of freedom ("dDF"), F-statistics, and p values for the parameters of treatment (steroid-treated vs. untreated) and lesion age at time of sacrifice ("factor(MonthStop)"). * denotes a p-value <0.05.*

The fixed effects in this model, summarized in ***Table 2-3*** estimate the fraction of Iba1+ cells expressing TSPO ("TSPO Ratio") at lesion onset (i.e. "Month-to-Sacrifice"=0) to be 0.85 (SEM=0.14; p<0.009). The individual effects observed at each time point prior to time of sacrifice are summarized in the table below, with the largest change in TSPO expression observed with a lesion age of 4-5 months at time of sacrifice ("Month.Stop.4"). The estimated effect associated with this timepoint is -0.83, indicating a decrease in TSPO expression from 0.85 to 0.02, which is statistically significant (SEM=0.19; p=0.01398). The effect of steroid treatment is estimated to be 0.25 and is not significant (SEM=0.19; p=0.28152). A plot of lesion age vs. fraction of Iba1+ cells expressing TSPO for all subjects is shown in **Figure 2-12.**

Parameter	Estimate	Std. Error	dF	t-stat	p-value	
Intercept	0.85050	0.14353	3.07113	5.925	0.00899	**
Steroid treatment effect	0.25136	0.19384	3.15145	1.297	0.28152	
factor(-MonthStop)1	-0.11178	0.06064	7.23654	-1.843	0.10644	
factor(-MonthStop)2	-0.30431	0.18535	3.32704	-1.642	0.19017	
factor(-MonthStop)3	-0.33983	0.18311	3.17421	-1.856	0.15542	
factor(-MonthStop)4	-0.83048	0.19179	3.77872	-4.330	0.01398	*
factor(-MonthStop)5	-0.40831	0.18535	3.32704	-2.203	0.10604	
factor(-MonthStop)6	-0.33629	0.18417	3.24118	-1.826	0.15844	
factor(-MonthStop)7	-0.43331	0.18535	3.32704	-2.338	0.09283	

Table 2-3. *Estimate of the fraction of Iba1+ cells expressing TSPO in a newly formed lesion ("Intercept") followed by estimates of the effects associated with steroid treatment and each time point of lesion formation relative to the time of sacrifice. * denotes a p-value <0.05. ** denotes a p-value <0.01. here, the Intercept captures lesion formation proximal to the time of sacrifice, denoted 0-1 or <1 months; for the factor level offsets for the lesion formation intervals, 1=1-2 or >1 (coded as 1-3) months, 2=2-3, 3=3-4, 4=4-5, 5=5-6, 6=6-7 or 6-8, and 7=7-8 months. * denotes a p-value <0.05. ** denotes a p-value <0.01.*

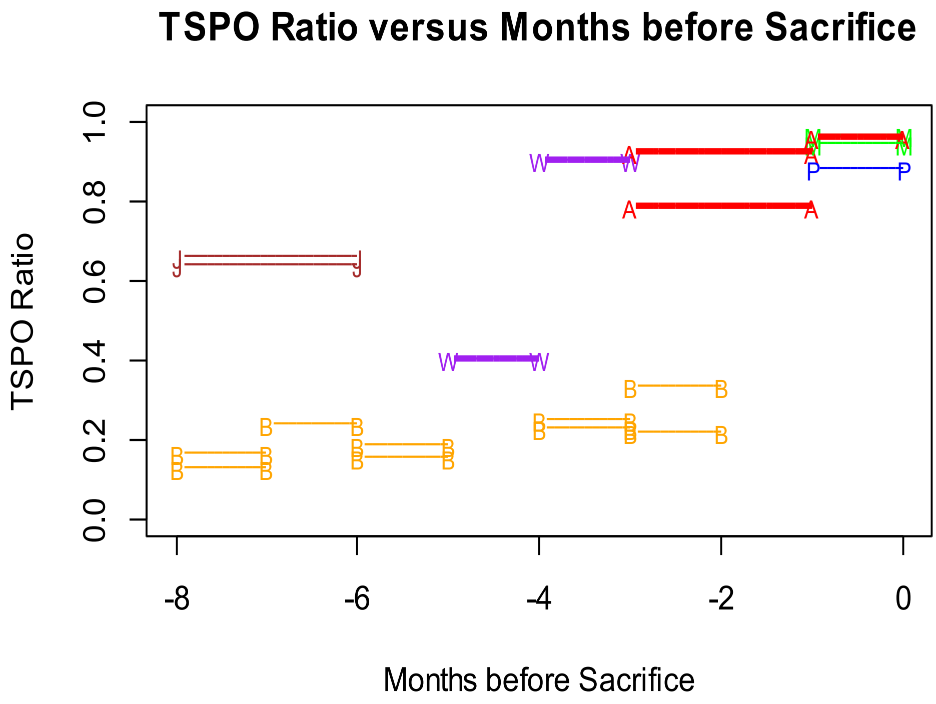

Figure 2-12. *Plot of ratio of TSPO+Iba+ cells to total Iba1+ population vs. lesion age at time of sacrifice (the number of months prior to sacrifice at which the lesion was detected).*

An alternative parameterization was then used to estimate the intercept as the fraction of Iba1+ cells that are TSPO+ in the absence of steroid treatment over all months before sacrifice and compare the TSPO+ ratio at each lesion age to the cumulative average of the preceding values up to that time e.g. calculating successive differences by subtracting the TSPO+ ratio two months prior to sacrifice from the average of the TSPO+ ratios at zero and one months prior to sacrifice, etc. These estimates are shown in **Table 2-4**. With Bonferroni correction, the minimum two-sided p-value is 0.00105 for lesions 4-5 months old at time of sacrifice, which indicates a statistically significant change-point across the 7 time points (p = 0.00735, two-sided).

Parameter	Estimate	Std. Error	dF	t-stat	p value	
Intercept	0.50496	0.12015	3.07474	4.203	0.02342	*
Steroid treatment effect	0.25136	0.19385	3.15133	1.297	0.28152	
factor(-MonthStop)1	-0.05589	0.03032	7.23657	-1.843	0.10644	
factor(-MonthStop)2	-0.08281	0.06188	3.34786	-1.338	0.26447	
factor(-MonthStop)3	-0.05028	0.03120	3.45232	-1.612	0.19348	
factor(-MonthStop)4	-0.12830	0.02264	6.39094	-5.667	0.00105	**
factor(-MonthStop)5	-0.01517	0.01420	5.42998	-1.068	0.33058	
factor(-MonthStop)6	-0.00055	0.01114	6.88651	-0.049	0.96208	
factor(-MonthStop)7	-0.01254	0.00834	6.98560	-1.503	0.17656	

Table 2-4. *Estimate of the fraction of Iba1+ cells expressing TSPO in a newly formed lesion ("Intercept"), followed by estimates of the effects associated with steroid treatment and each time point of lesion formation relative to the time of sacrifice, following alternative parameterization. * denotes a p-value <0.05. ** denotes a p-value <0.01.*

2.3.5 Phenotype of TSPO+ microglia/macrophages in healthy brain

To determine the immunophenotype of TSPO-expressing cells in the healthy marmoset brain, we applied the immunophenotyping antibody panel in **Table 7-1** and **Table 7-2** to a section of brain tissue from control marmoset P0. Conventional "M1" markers included early activation marker MRP14 and HLA DR chaperone protein, CD74, while conventional "M2" markers included canonical tolerogenic marker Arg1 and the hemoglobin-haptoglobin scavenger receptor, CD163. All markers detected in this panel are listed in **Table 7-1**. With the exception of a small number of cells observed within blood vessels in the brain parenchyma, the vast majority of these Iba1+ cells are located within the parenchyma itself and are presumed to be more representative of microglia than peripheral macrophages, as there was no evidence of blood-brain barrier compromise in this animal. However, hemoglobin-haptoglobin scavenger receptor CD163 was only observed within blood vessels in the healthy primate brain. Thus, CD163 in the healthy primate brain appears to be a marker exclusively associated with peripheral macrophages still located in the intravascular space. This is consistent with our studies of normal appearing white matter in EAE brains, where CD163 expression is observed in the parenchyma of white matter lesions, but CD163 in the normal-appearing white matter is restricted to intravascular cells.

Of the established immunophenotype markers monitored in this panel, Arg1 was the most frequently expressed in activated phagocytic cells, occurring in 25% of Iba1+ cells. Arg1 was also the marker most frequently co-expressed with TSPO, as 16.5% of Iba1+ cells were TSPO+Arg1+ (***Figure 2-15***). While TSPO is expressed in approximately 58.65% % of Iba1+ cells in the healthy brain, it was expressed in 87% of Arg1+Iba1+ cells.

This pronounced association between TSPO and Arg1 in the healthy brain is consistent with studies of immunophenotype in vitro, which associate TSPO with an M2 phenotype [204]. However, TSPO is also closely associated with CD74, which is typically considered an M1 marker. This finding illustrates the complexity of characterizing immunophenotype in vivo, where cells are exposed to wide variety of known and unknown stimuli and therefore may not conform to the strictly delineated "M1" and "M2" phenotypes observed in vitro. Ultimately TSPO appears to be expressed in both "M2"- and "M1"-like phagocytes in control CNS tissue.

2.3.6 Phenotype of TSPO+ microglia/macrophages in acute EAE lesions

Of the 9 EAE animals examined in this study, 2 were found to have acute lesions at the time of sacrifice. In these acute EAE lesions, there is a massive increase in both the density of microglia and the density of TSPO relative to levels observed in the non-EAE control brain. In fact, TSPO was found in over 90% of Iba1+ microglia/macrophages in these acute lesions. While conventional immunohistochemical stains established a correlation between the density of TSPO and Iba1 in demyelinated lesions, multiplex staining was ultimately necessary to establish the colocalization of TSPO in Iba1+ microglia/macrophages and illuminate the specificity of this correlation. **Figure 2-13** shows images of TSPO, Iba1, and PLP in acute demyelinated lesions (<4 weeks old) in the optic nerve of EAE marmoset M. While these images highlight the concordance of TSPO and Iba1 on a gross scale, they also reveal subtle differences. Whereas Iba1 is distributed fairly evenly throughout the demyelinated region, TSPO appears most concentrated in the center of each focal lesion, where demyelination is most extensive, typically arranged in patterns suggestive of vascular structures.

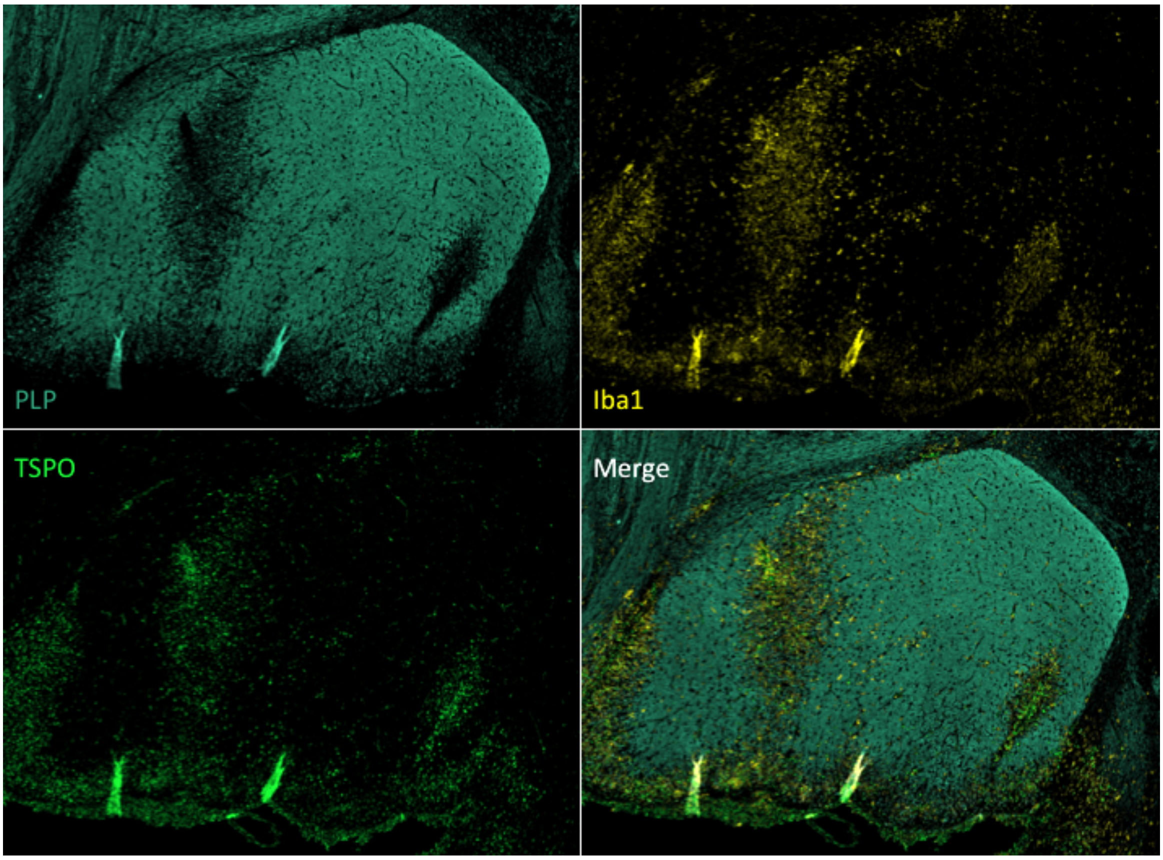

***Figure 2-13**. Multiplex staining of PLP, Iba1, and TSPO in a demyelinated optic tract lesion, showing dense infiltrates of predominantly TSPO+ macrophages and microglia in an untreated EAE marmoset.*

2.3.7 TSPO colocalizes with both "M1" and "M2" phenotype markers in vivo in marmoset EAE

To determine the phenotypic associations of TSPO in marmoset EAE, we examined the expression of TSPO and various markers of immunophenotype in acute EAE lesions (n=3) from EAE animals M and P1. The tissue section obtained from animal M contained 2 lesions <4 weeks old, while the section obtained from P1 contained 1 lesions < 4 weeks old. None of the other animals were found to have acute lesions at time of sacrifice. Immediately evident from this study was a striking increase in not only the expression of Iba1 and TSPO but also the M1 marker CD74, which is an HLA DR chaperone protein associated with antigen presentation, and CD163, which is a hemoglobin-haptoglobin receptor and conventional M2 marker associated with phagocytosis. While these markers appear to label distinct populations of phagocytes in the brain, multiplex staining confirmed that TSPO was co-expressed in both CD74+ and CD163+ phagocyte populations (**Figure 2-14**).

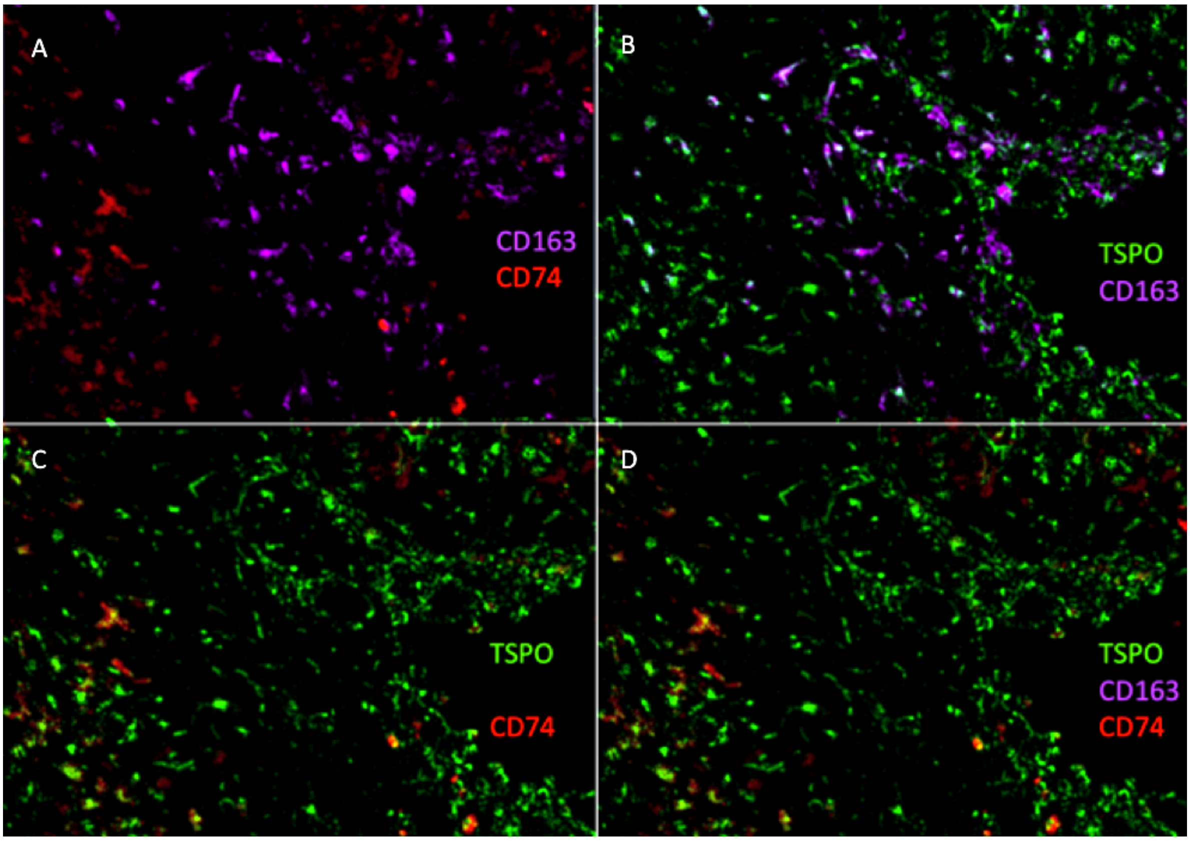

Figure 2-14. *Multiplex staining of demyelinated optic tract lesions in animal M with dense TSPO and Iba1 staining (not shown) indicates TSPO to co-localize with both CD163 and CD74. Panel A shows distinct phagocytic cell populations identified by CD163 (purple) and CD74 (red). The colocalization of TSPO (green) and CD163 (purple) can be seen in panel B. The colocalization of TSPO (green) and CD74 (red) can be seen in panel C.*

To quantify the extent to which TSPO is co-expressed with these distinct markers of microglial activation, a segmentation algorithm was developed to analyze high-resolution immunofluorescence images and identify DAPI+ nuclei with an Iba1+ cytoplasm within a 15-pixel radius. The addition of the nuclei and surrounding Iba1-defined cytoplasm yielded a mask defining the shape and location of each Iba1+ cell. The area defined by the mask was then scanned for TSPO+ pixels, CD74+ pixels, CD163+ pixels, and MRP14+ pixels. The percentages of total Iba1+ microglia and macrophages expressing TSPO and other markers in healthy brain and acute lesions are shown in **Figure 2-15**.

While CD74 was co-expressed with TSPO in only 8.7% of Iba1+ microglia in the healthy brain, over 50% of Iba1+ cells in acute lesions co-expressed TSPO with CD74. There are also marked increases in both the absolute number of CD163+ microglia/macrophages and the percentage of TSPO+ microglia/macrophages co-expressing CD163, which constitute less than 2% of Iba1+ cells in healthy brain parenchyma but over 20% in acute lesions. This is consistent with the expectation that compromise of the blood-brain barrier would lead to increased expression of the haptoglobin-hemoglobin receptor CD163 in the brain parenchyma, whether due to the infiltration of macrophages from the peripheral blood or induced CD163 expression in resident microglia exposed to blood and plasma proteins. Likewise, MRP14, which was expressed in less than 1% of Iba1+ cells in healthy brain tissue, was found in nearly 14% of Iba1+ cells in the right optic tract and 20% of Iba1+ cells in the left optic tract. In both healthy and diseased tissue, these MRP14+Iba1+ cells are 99.5% positive for TSPO.

Surprisingly, while Arg1 was the most commonly detected immunophenotypic marker in our panel in control brain tissue, its expression does not appear to increase to the same degree as that of the CD74, MRP14 or CD163. In these acute lesions, it was co-expressed with TSPO in, on average, 23% of Iba1+ cells, vs. 16.5% of Iba1+ cells in healthy brain tissue.

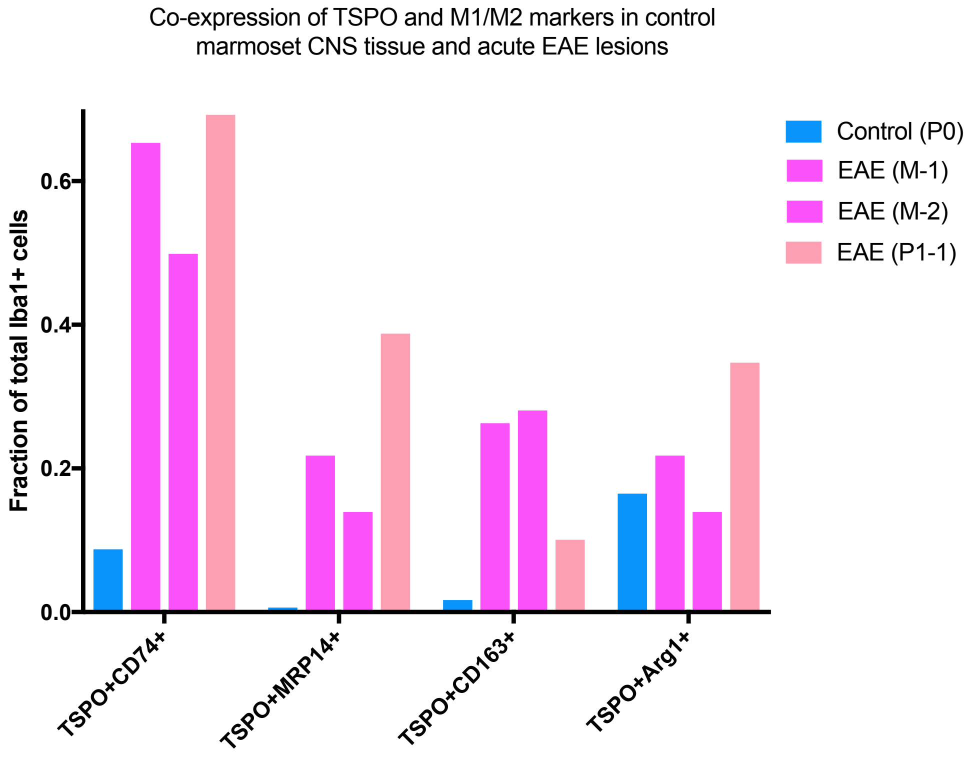

Co-expression of TSPO and M1/M2 markers in control marmoset CNS tissue and acute EAE lesions

Figure 2-15. Comparison *of fractions of Iba1+ cells co-expressing TSPO and other markers of interest (CD74, CD163, Arg1, and MRP14) in a control marmoset and 3 acute lesions from two EAE marmosets. Two lesions were identified in animal M, while one lesion was identified in animal P1.*

2.3.8 Immunophenotype Changes in Chronic Lesions

While TSPO expression decreased significantly over time and M2 markers were generally not detected in chronic lesions due to high level of autofluorescence after fixation in these tissues, M1 markers did not decrease to the same degree. The fraction of cells co-expressing CD74 and TSPO (orange) peaks at approximately 50% in lesions < 1 month old and decreased to less than 10% in lesions over 4 months old. However, CD74 expression in the absence of TSPO (red) persisted to a much greater degree in chronic lesions, even as TSPO decreased. MRP14 expression decreased more rapidly than CD74, and there were very few MRP14+TSPO- cells (red). The percentage of total Iba1+ cells expressing TSPO with either CD74 or MRP14 and the percentages of cells expressing MRP14, CD74, or TSPO alone are shown **Figure 2-16**.

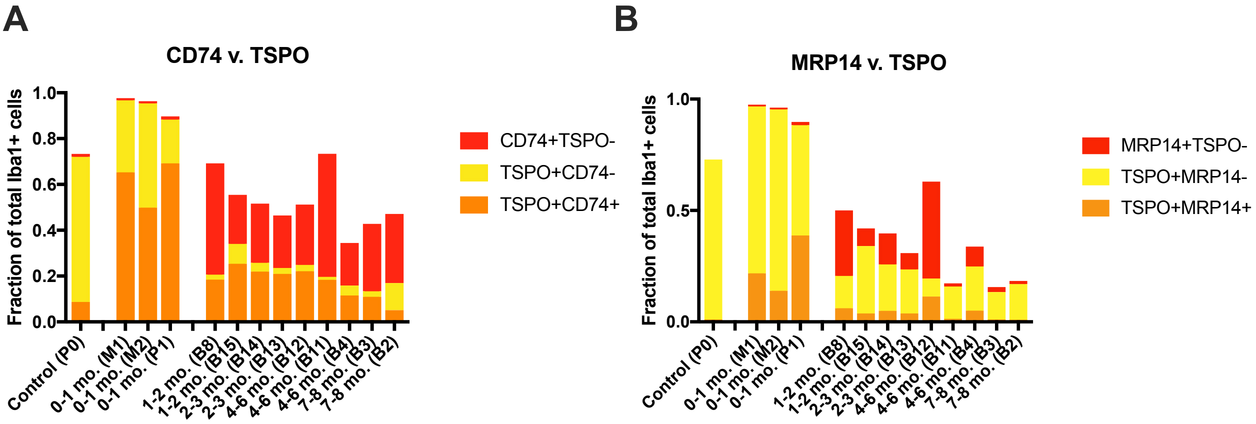

***Figure 2-16**. A) Percentages of Iba1+ cells that are TSPO+CD74+ (orange), TSPO+CD74- (yellow), and CD74+TSPO- in lesions of different ages (n=13) from different untreated EAE animals (M, P, B) and control marmoset P0.B) Percentages of Iba1+ cells that are TSPO+MRP14+ (orange), TSPO+MRP14- (yellow), and MRP14+TSPO- in lesions of different ages (n=13)*

To assess for dependence between TSPO and these other phenotypic markers, the odds ratio was calculated for the co-expression of TSPO with MRP14 and CD74. Furthermore, the relationship between TSPO and MRP14 and CD74 was analysed over time for a potential change-point using the same linear mixed effects model used to analyse TSPO expression over time. There were no statistically significant features among the diseased monkeys among the various markers. For the single healthy monkey (P0, denoted as "Q" in the display), the observed odds ratio was 27.70907 and was tested against the independent sample estimate.

For model parameterizations representing lesion age at sacrifice as contrasts, the intercept of the model was taken to be the overall mean, which was estimated to be 3.0912720 (SEM=4.0431817, dF=0.7173073). The odds ratio was calculated to be 27.70907, which was non-significant (0.169282, two-sided). Plots of odds ratio vs. lesion age are shown in ***Figure 2-17***. Identical analysis of TSPO in relation to CD74 showed no visible effect and no statistical significance. Plots of odds ratio vs. lesion age are shown in ***Figure 2-17***.

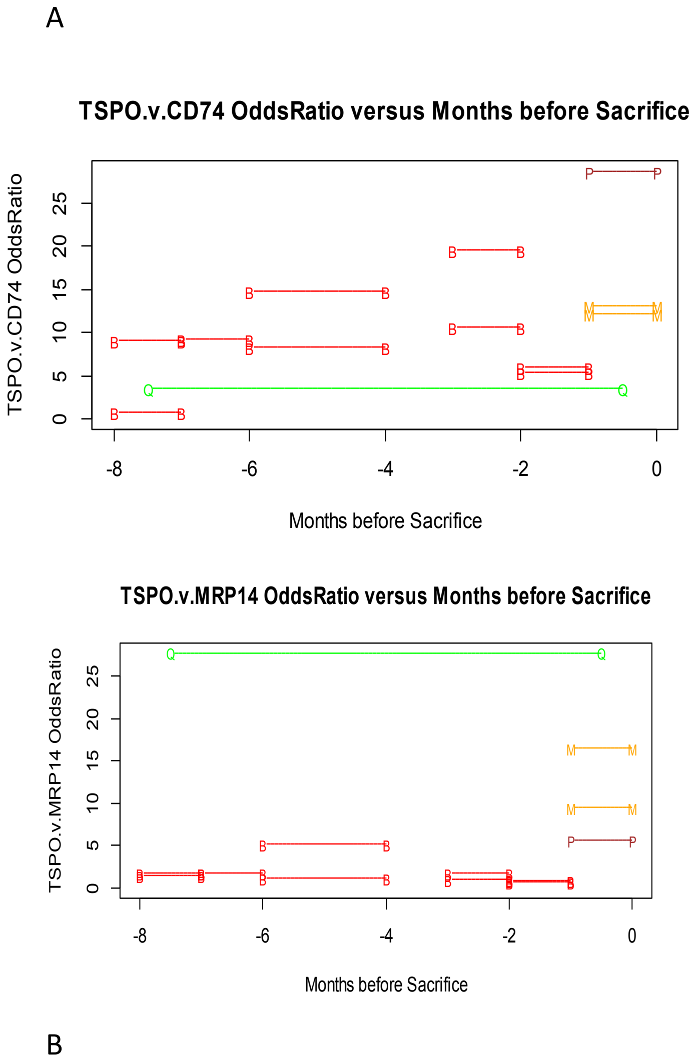

Figure 2-17. *Odds ratio vs. lesion age for co-expression of TSPO and A) CD74 or B) MRP14.*

2.3.9 TSPO is not expressed by astrocytes in NAWM

In conjunction with a pilot study on the effects of HHV6 viral exposure on the clinical course and pathophysiology of neuroinflammatory disease, astrocytic TSPO expression was initially assessed in EAE marmosets with and without antecedent HHV6B infection by conventional immunohistochemistry. Reactive GFAP+ astrocytes in normal appearing white matter (NAWM) were found to be virtually devoid of TSPO. A representative staining of astrocytes in NAWM adjacent to an EAE lesion is shown in **Figure 2-18**.

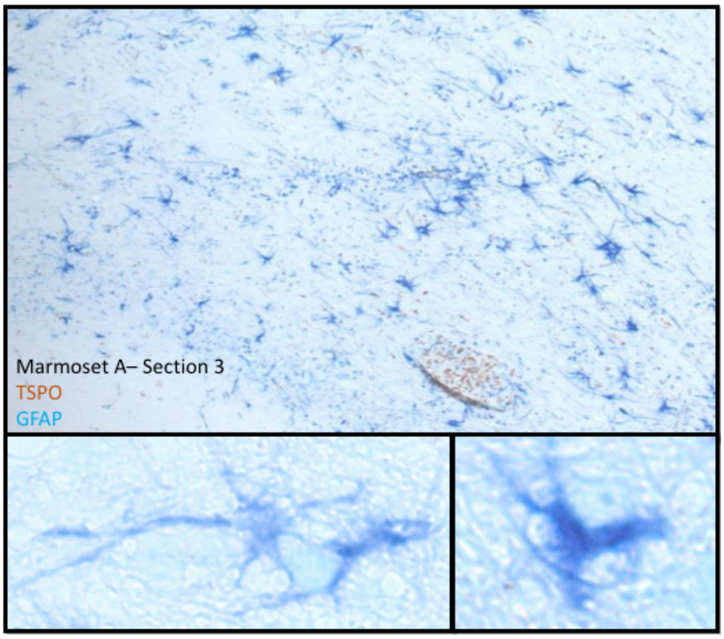

Figure 2-18. *Double immunohistochemical staining for GFAP (Vector blue) and TSPO (DAB) shows a large number of reactive astrocytes in the periphery of a lesion in the right white matter tract of marmoset A. However, the brown TSPO staining is predominantly restricted to GFAP- cells in the center of the lesion. The insets show the cell bodies of two representative GFAP+ astrocytes, which are negative for TSPO.*

2.3.10 TSPO is observed in astrogliosis in the brain and spinal cord of EAE marmosets

Sections of spinal cord from marmoset C and sections of brain tissue from P0 and multiple EAE marmosets (B, J, M, P1, and P2) were stained for TSPO, Iba1, DAPI, and GFAP to differentiate TSPO expression in microglia and macrophages from TSPO expression in astrocytes (***Figure 2-19***). Multiple foci of astrogliosis were seen in the cervical spinal cord of marmoset C. On closer examination of one lesion (green inset), TSPO is seen both in the microglia (white arrow) and in the reactive astrocyte (red arrow).

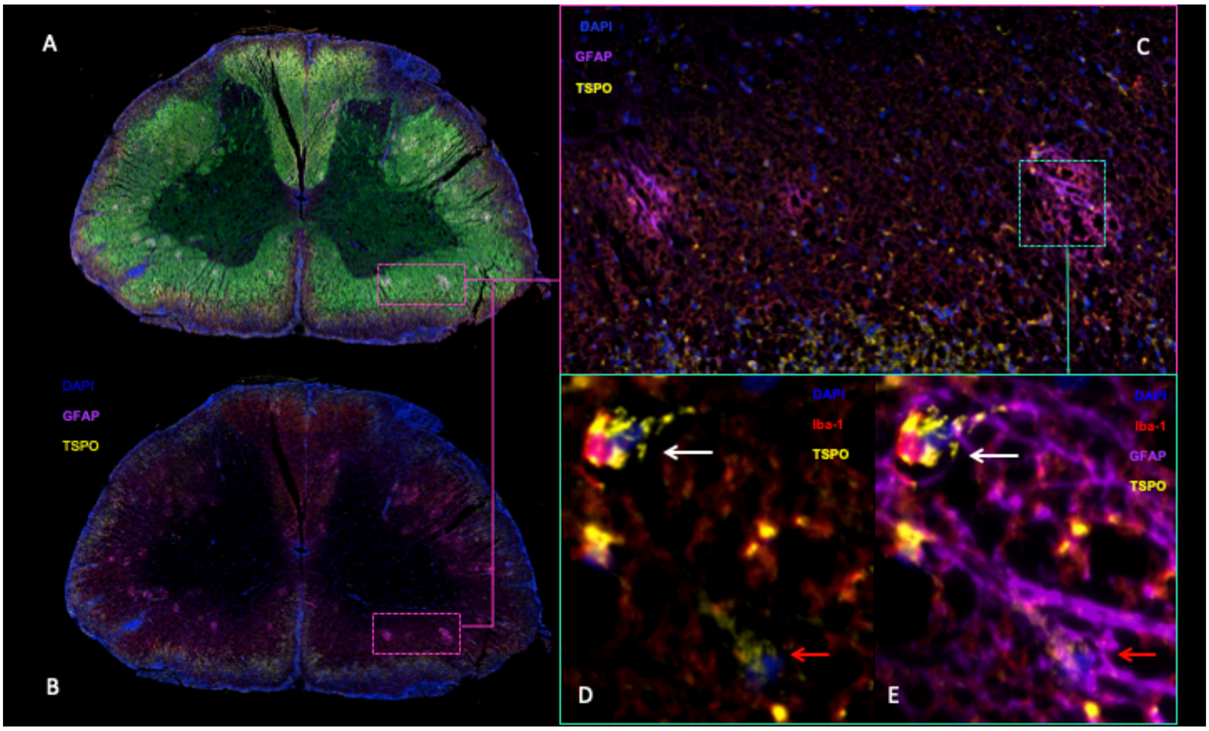

Figure 2-19*. Panel A shows a section of the cervical spinal cord with immunofluorescent staining identifying multiple bright foci distributed throughout the white matter. Panel B shows isolated GFAP and DAPI staining for this section, where the dominant color in these bright foci is found to be GFAP staining (in pink). Inset C shows a region of the white matter at higher magnification, where two dense clusters of GFAP staining are seen, indicating two distinct foci of astrogliosis. Panels D and E shows one of these gliotic lesions at higher magnification, where TSPO is observed both in an Iba1+ phagocytic cell (white arrow), and a Iba1-GFAP+ reactive astrocyte (red arrow).*

A similar pattern of expression was seen in marmoset A, an animal that had been exposed to HHV6B prior to EAE induction and eventually developed an afferent pupillary defect suggesting damage of the optic nerves. While astrocytes in small lesions and NAWM in this same animal exhibited no TSPO expression, extensive non-microglial TSPO expression was seen in lesions bearing signs of chronicity, particularly, those with significant astrogliosis. **Figure 2-20** shows one such lesion in the optic chiasm of marmoset A with dense GFAP staining suggestive of reactive astrogliosis. While the majority of TSPO staining in this lesion colocalized with Iba1 staining indicating active microglia and macrophages, there are several cells with large cell bodies defined by patchy, diffusely distributed TSPO staining (yellow) that is not associated with Iba1 (red), which are indicated by white arrows. The cell bodies were found to be densely positive for GFAP and morphologically resembled hypertrophic astrocytes.

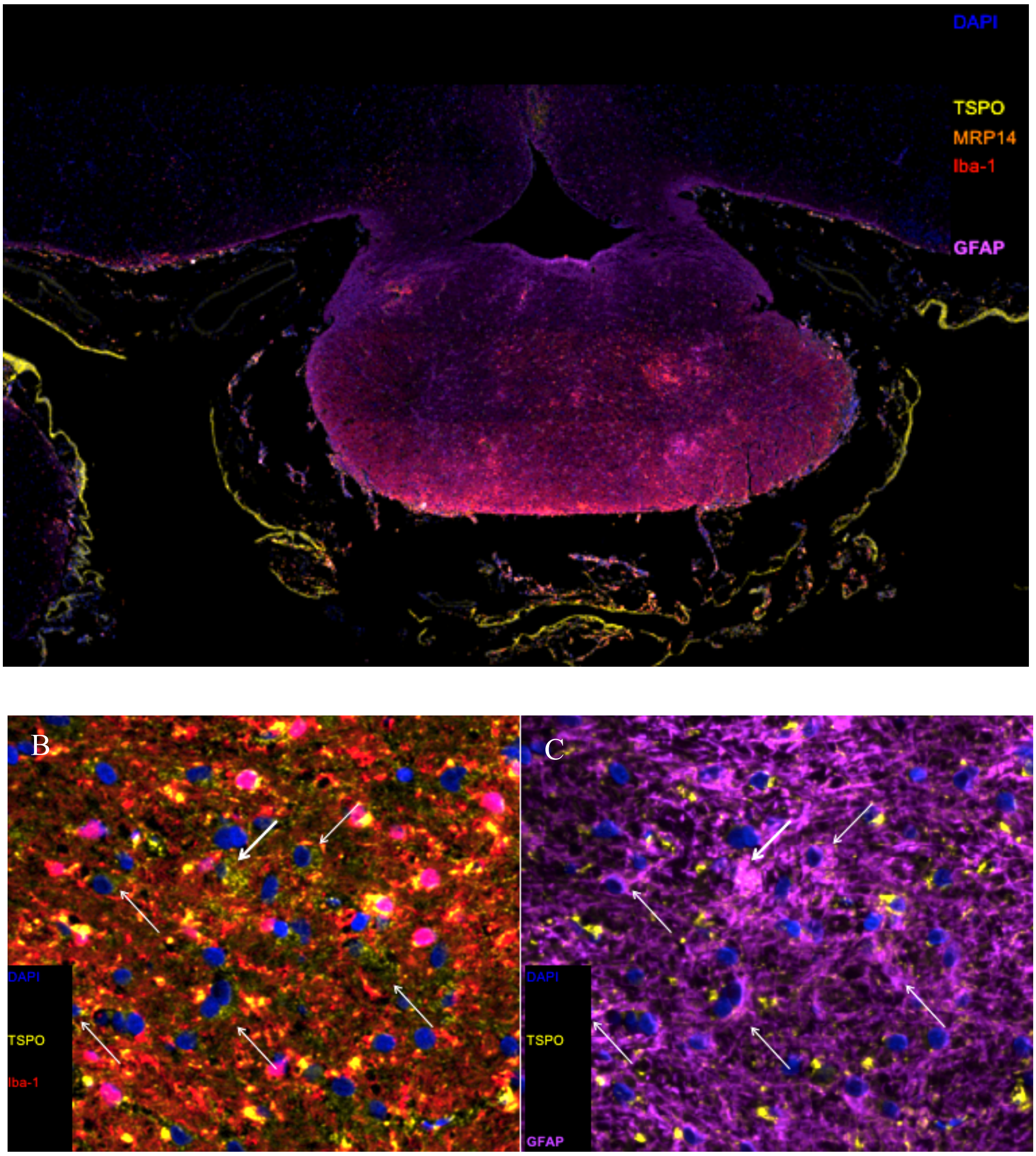
DAPI
TSPO
MRP14
Iba-1
GFAP
B
DAPI
TSPO
Iba-1
C
DAPI
TSPO
GFAP

Figure 2-20*. Prominent astrogliosis (GFAP staining in purple) and microglial accumulation (Iba1 staining in red) is observed in the optic chiasm of EAE marmoset A, as shown in panel A. While TSPO in the core of the nodule is predominantly associated with microglia and macrophages expressing Iba1 (red), TSPO expression lesion is also seen in reactive astrocytes, which are Iba1- but GFAP+ (as indicated by white arrows in panels B and C).*

2.3.11 Conventional immunohistochemical staining of TSPO suggests evidence of TSPO expression in neurons.

TSPO staining suggestive of neuronal expression was observed in marmoset EAE tissue, particularly in the vicinity of large, chronic lesions. **Figure 2-21** shows a region adjacent to the surface of the third ventricle of an EAE animal with HHV6B infection. There are numerous small, crescent-shaped TSPO+ cells clustering along the surface of the ventricle, suggesting localized inflammation mediated by the infiltration and activation of phagocytic cells in the brain parenchyma. In the midst of these small cells, we observe a single cell with a large nucleus and granular TSPO staining distributed evenly throughout the cytoplasm, likely a neuron.

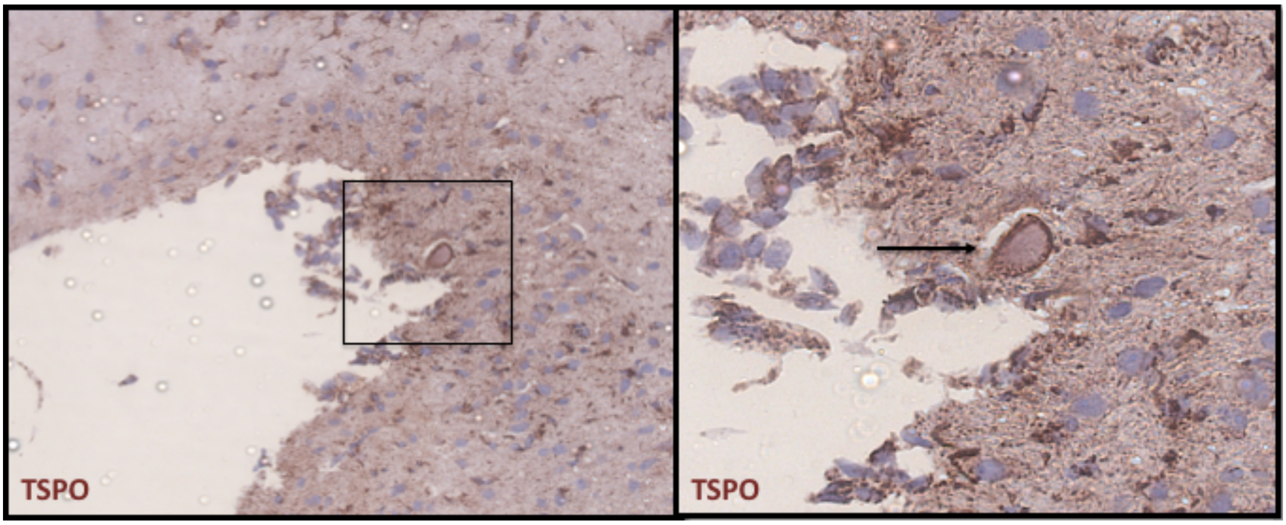

***Figure 2-21**. Conventional immunohistochemical staining of TSPO with DAB and hematoxylin counterstaining on the surface of the third ventricle superior to the optic chiasm of marmoset A. Inset shows a single large cell with a large nucleus and diffuse cytoplasmic TSPO staining resembling a neuron.*

A similar observation was made in the spinal cord, shown in Figure 2-22. In the gray matter of the lumbar spinal cord of marmoset C, an untreated virus-naïve EAE marmoset, TSPO expression is restricted to small crescent shaped cells resembling microglia and a few stellate cells, potentially microglia or astrocytes. In the thoracic spinal cord, however, not only is the white matter lesion thicker and more densely positive for TSPO, but TSPO expression in the gray matter is also elevated, and a greater heterogeneity is seen in the distribution and type of TSPO+ cells. Dense TSPO staining is still seen in crescent-shaped and stellate cells as in the lumbar spinal cord. However, dark TSPO staining is also observed in the blood vessels, appearing to outline the outer laminae of the dilated vessel. Moreover, moderate TSPO expression is seen in larger cell bodies that appear to be shrunken, possibly degenerating or apoptotic neurons. In contrast to the dense, vesicular TSPO staining observed in microglia/macrophages and vascular structures, the staining in these larger cells is lighter and more diffusely distributed throughout the cytoplasm. The contrast between these two areas of the spinal cord illustrates the wide potential for variation in TSPO expression. Collectively, these images allude to the putative functional significance of neuronal TSPO expression. In light of the presence of this likely neuronal TSPO expression in the heavily inflamed thoracic spinal cord, the absence of any evidence of neuronal TSPO in the moderately inflamed lumbar spinal cord suggests neuronal TSPO expression is induced only in specific conditions, perhaps dependent on the density of activated phagocytic cells.

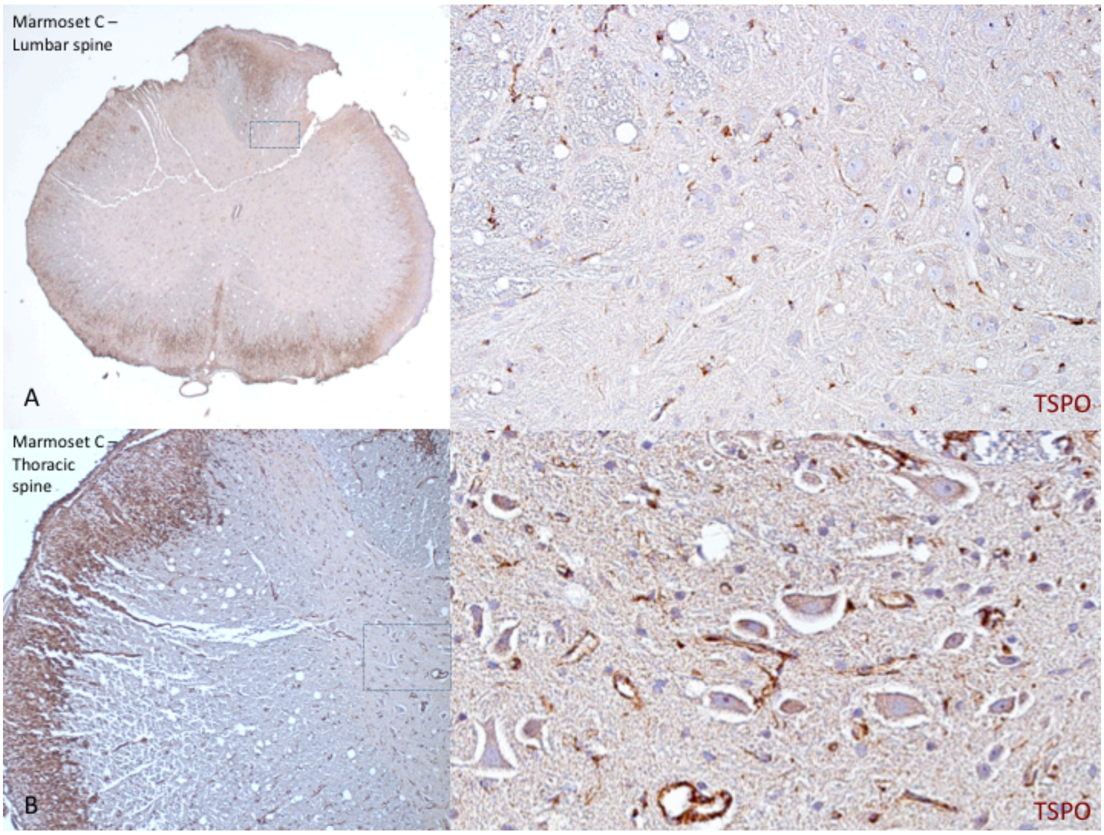

Figure 2-22. *A) Section of the lumbar spinal cord of Marmoset C, an untreated EAE marmoset, stained by conventional immunohistochemistry for TSPO. Right inset shows region of lumbar gray matter with numerous stellate and crescent-shaped cells expressing TSPO, likely microglia and macrophages. B) Section of the thoracic spinal cord from Marmoset C, stained by conventional immunohistochemistry for TSPO, showing dense TSPO staining extending from the pial surface of the white matter. Right inset shows region of thoracic gray matter showing an extremely heterogeneous pattern of TSPO staining, including TSPO+ vascular structures and large cells resembling neurons, as well as TSPO+ glial cells.*

2.3.12 TSPO expression is observed in a subset of NeuN+ neurons in marmoset EAE

Sections of brain tissue from a healthy primate and an EAE primate with an antecedent HHV-6B infection were stained with TSPO, Iba1, NeuN and DAPI. In the healthy primate brain, less than 1% of NeuN+ cells were observed to express TSPO. Even in the EAE marmoset, the majority of neurons were also TSPO- (**Figure 2-23).** However, in the cortex (**Figure 2-24**), TSPO was observed in the cell bodies of a subset of NeuN+ neurons. In contrast to the dense perinuclear vesicular pattern of TSPO staining observed in microglia and macrophages, TSPO staining in these neurons was much less intense but appeared to be distributed diffusely throughout the cytoplasm of the neuronal cell body (indicated by white arrows).

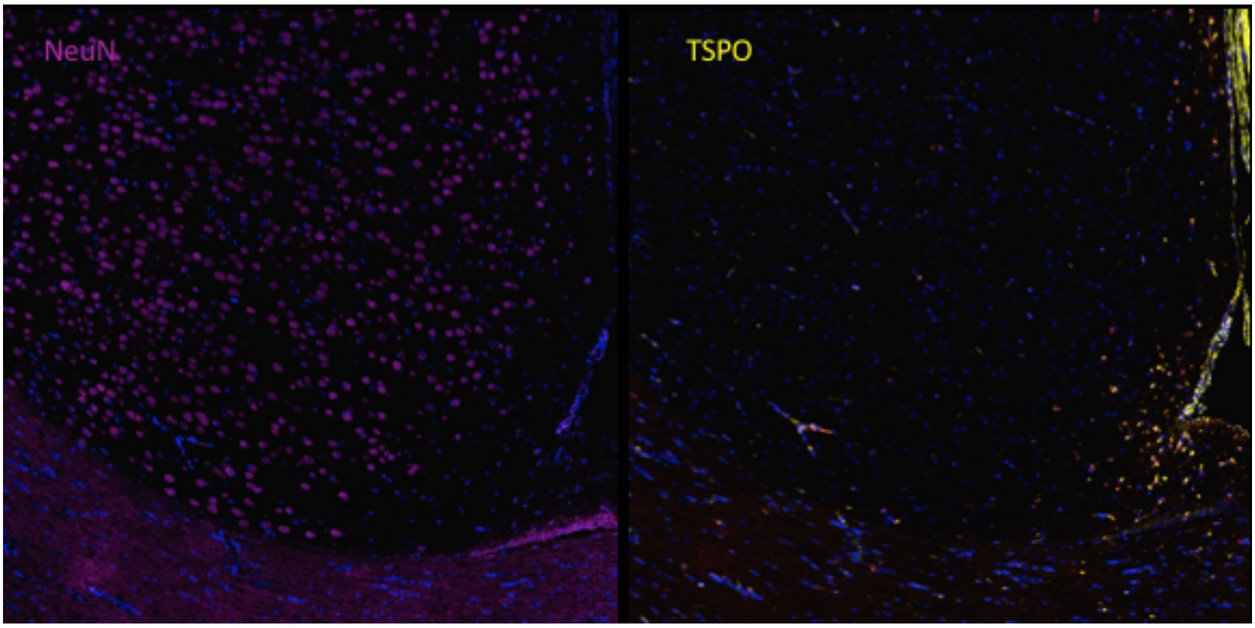

Figure 2-23*. Comparison of TSPO and NeuN staining in a region of gray matter in EAE marmoset A, which shows the absence of TSPO expression (yellow) in NeuN+ cells (pink) in a region of gray matter superior to the corpus callosum.*

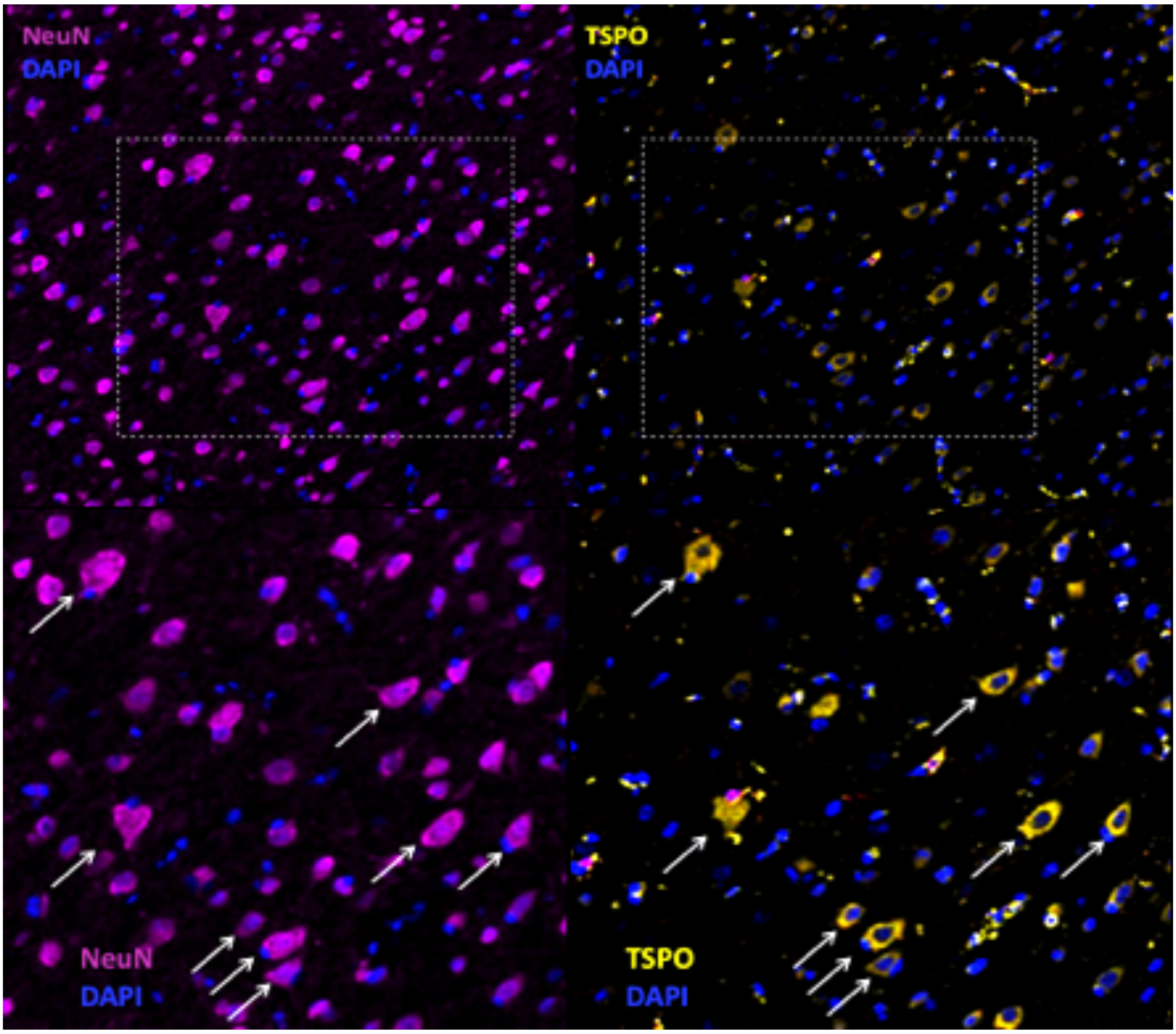

Figure 2-24. *Comparison of TSPO and NeuN staining in a region of cortical gray matter in EAE marmoset A, which shows diffuse cytoplasmic TSPO expression in NeuN+ cells.*

To quantify the percentage of neurons expressing TSPO, two 500 x 500 mm regions of interest were selected in the right and left cortical gray matter of the control animal and 4 EAE marmosets. NeuN+ cells and the number of NeuN+ cells co-expressing TSPO were counted manually. The fraction of NeuN+ cells expressing TSPO in the right and left cortical gray matter of each animal are shown in **Figure 2-25**. In P0, the control marmoset, the percentage of neurons expressing TSPO across both regions of interest was 0.6%. In the 5 EAE marmosets assessed in this study, the mean percentage of TSPO+ neurons was 12.1% with an SEM of 5.0% and a 95% CI of 1.9 to 26.1%.

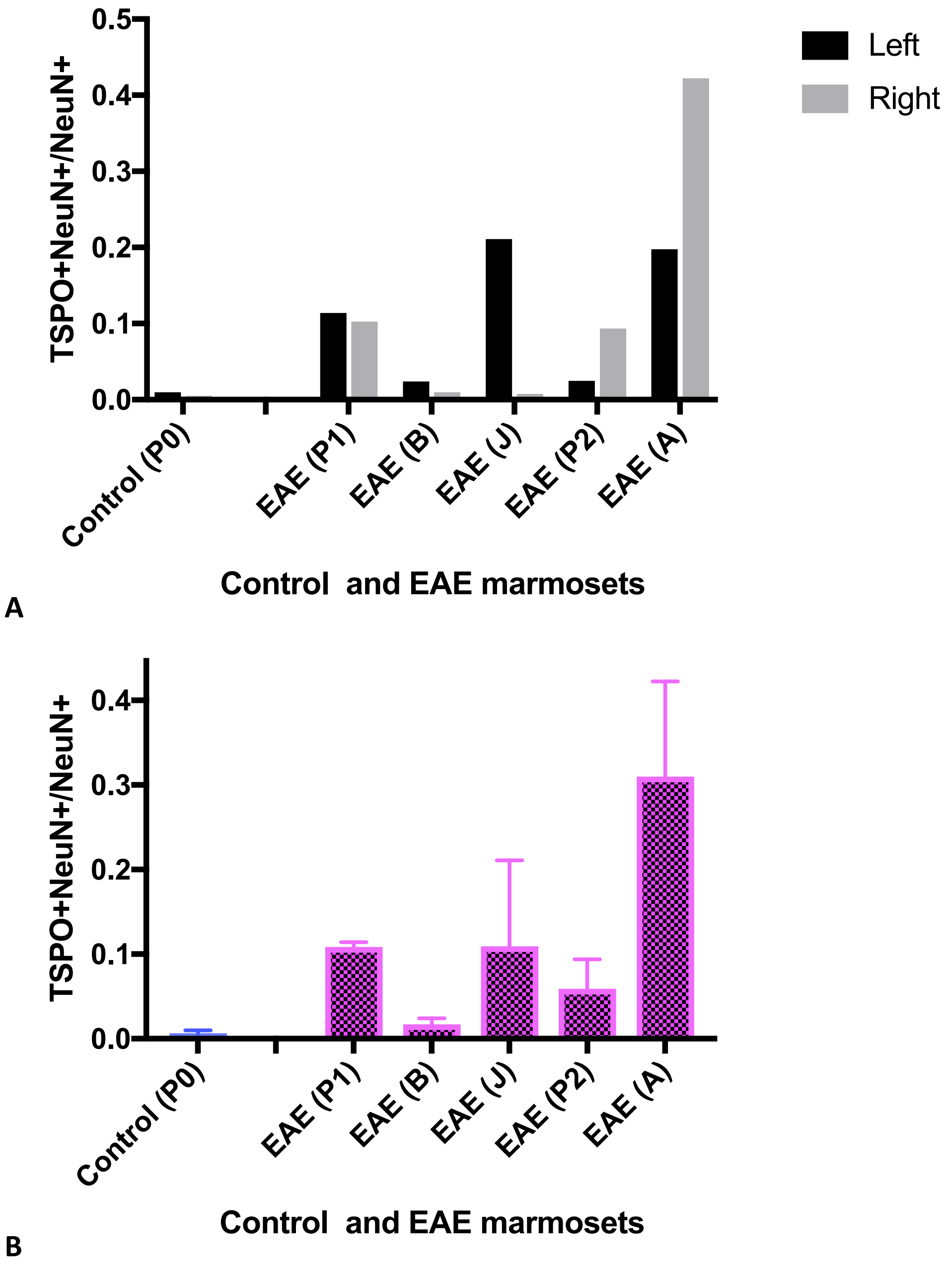

Figure 2-25. *A) Fractions of NeuN+ cells co-expressing TSPO in the right and left cortical gray matter of control marmoset P0 and EAE marmosets P1, B, J, P2, and A. B) Mean fraction of NeuN+ cells co-expressing TSPO across all areas of interest in control marmoset P0 and EAE marmosets P1, B, J, P2, and A.*

2.3.13 Dim TSPO expression in seen in GLS2-expressing glutamatergic neurons but not Parvalbumin+ interneurons in marmoset EAE

To determine the phenotype of TSPO+ neurons in EAE, an antibody stripping protocol was applied to the TSPO-stained tissue section from the HHV6B-infected EAE marmoset A, and the tissue section was re-stained with antibodies against neuronal phenotypic markers GLS2, a glutaminase expressed in excitatory glutamatergic neurons, and parvalbumin, a calcium binding albumin protein expressed by inhibitory GABAminergic interneurons. Examples of GLS2+ and parvalbumin+ cells are e shown in **Figure 2-26.** In the green inset, three parvalbumin+ interneurons (red arrows) and multiple GLS2+ neurons (white arrows) are visible; however, only the GLS2+ neurons are observed to express TSPO.

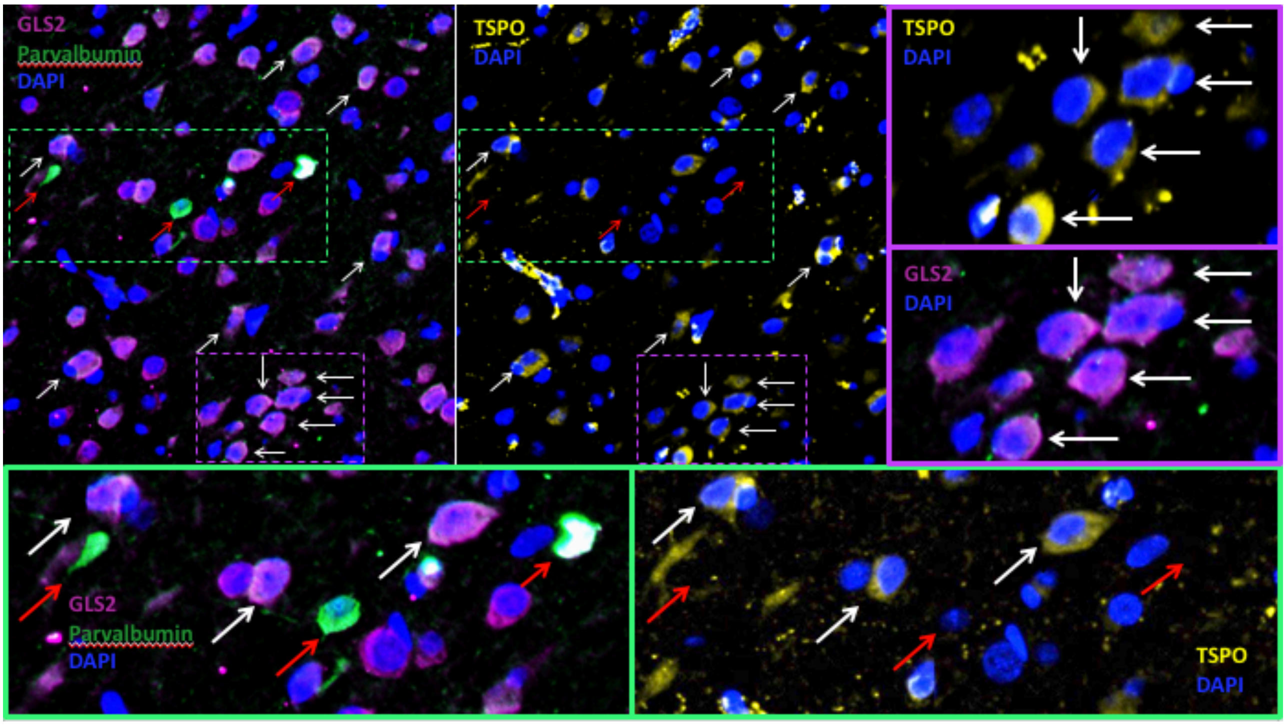

Figure 2-26*. Comparison of TSPO staining with Parvalbumin and GLS2 staining after stripping and re-staining a previously stained section of brain tissue from EAE marmoset A. Diffuse cytoplasmic TSPO staining is observed in GLS2+ glutamatergic neurons (inset, white arrows) but not parvalbumin-producing interneurons (inset, red arrows).*

2.4 **Discussion**

From this study, we conclude that the common marmoset is a relevant model and proxy for the study of TSPO in multiple sclerosis. This study is the first to our knowledge to have characterized TSPO expression in the CNS of the common marmoset and the first to have established its expression in neuroinflammatory disease in microglia/macrophages, astrocytes, and neurons. This model of EAE recapitulates the expression of TSPO in both astrocytes and microglia that is observed in multiple sclerosis, rendering it a valuable model for the study of TSPO-based PET imaging of neuroinflammatory disease, one that would give significant insight into the clinical utility of novel PET ligands in the imaging of multiple sclerosis. Furthermore, this study is the first to have characterized the time course of TSPO expression in marmoset EAE, which peaks in the first month of lesion development and declines gradually over a period of 6 months or more, depending on disease duration.

2.4.1 TSPO in control CNS tissue

As in prior mice and human studies [4,206], TSPO in the healthy marmoset brain is expressed by meningeal arachnoid tissue, vascular endothelium, and ependymal cells, but not astrocytes or neurons. In contrast to prior studies in mice [206], which found no TSPO expression in the microglia of healthy animals, I found TSPO expression in a subset of Iba1+ cells. With the exception of a small number of Iba1+ cells observed within the lumina of cerebral blood vessels, the vast majority of these Iba1+ cells are located within the parenchyma itself. As peripheral hemoglobin-haptoglobin scavenger receptor CD163 was only observed in Iba1+ cells confined within blood vessels, and not in Iba1+ cells in the brain parenchyma, the marker appears to be exclusively associated with peripheral macrophages still located in the intravascular space, supporting the absence of BBB compromise. All parenchymal Iba1+ cells in this control animal are therefore presumed to be resident microglia, rather than peripheral macrophages,

Within this control brain tissue, TSPO was expressed in approximately half (58.65%) of all Iba1+ microglia and was found to be more closely associated with the pro-tolerogenic markers, Arg1, which is expressed by 25% of TSPO+ microglia. This finding is consistent with studies of M2 human macrophages in vitro that associate TSPO with an M2 phenotype [146]. MRP14 and CD163, in contrast, were observed in only 1% and 0.5% of Iba1+ cells, respectively. However, approximately 14% of TSPO+ microglia also express HLA-DR component CD74, which is conventionally considered an M1 marker due to its association with antigen presentation. Thus, despite a predominance of Arg1+/”M2”-biased TSPO+ microglia, TSPO is ultimately expressed in both “M2”- and “M1”-biased microglia in healthy brain tissue.

2.4.2 TSPO in microglia and macrophages in EAE

In marmoset EAE, TSPO is highly expressed by activated microglia and macrophages in both demyelinated lesions and normal-appearing white and grey matter, a pattern that is consistent with patterns of expression reported in human disease [5,245–247]. In fact, even some areas of radiologically normal-appearing white and gray matter were found to contain a moderately increased density of Iba1+ activated microglia and macrophages, where TSPO density increased in proportion with Iba1 density. This proportional increase in TSPO suggests that the PET imaging of TSPO radioligands may facilitate the detection of phagocytic activation in pre-lesional areas, before the onset of the structural damage that is ultimately detected by MRI [5].

2.4.3 TSPO immunophenotype in microglia and macrophages

The immunophenotypic significance of TSPO expression in macrophages and microglia is controversial. A 2018 study by Beckers et al. in mice found that TSPO mRNA levels were increased in LPS-stimulated M1 microglia in culture, but not in M2 microglia stimulated with IL-4 [205]. Moreover, in the brains of mice with chronic neuroinflammation secondary to multifunctional protein-2 (Mf2)-deficiency, both TSPO and mRNA levels were found to be increased, suggesting TSPO levels to correlate with a pro-inflammatory environment *in vivo* [205]. A 2017 study by Narayan et al., conversely, found that TSPO protein and mRNA levels were reduced in LPS-stimulated human macrophages [204]. Recent studies by Vogel et al. and Nutma et al. have found TSPO expression in both M1- and M2-biased microglia in MS brain tissue [4,16].

While my experiments confirm the presence of TSPO in Iba1+ microglia and macrophages, not all Iba1+ microglia/macrophages were found to express TSPO. Ultimately, TSPO was expressed in only a subset of Iba1+ microglia in healthy primate brain tissue and was found to be more closely associated with pro-tolerogenic markers such as Arg1, a feature that is consistent with studies of M2 human macrophages in vitro [204]. Additionally, while the phagocytic "M2" marker, hemoglobin-haptoglobin receptor scavenger receptor CD163, is not expressed in healthy brain parenchyma, the receptor is expressed by phagocytic cells in EAE lesions in the context of blood-brain barrier compromise, and many Iba1+CD163+ cells were found to co-express TSPO. However, multiplex immunofluorescence staining also confirmed the colocalization of TSPO and HLA-DR chaperone protein, CD74. This colocalization was seen in Iba1+ cells in both healthy primate brain and EAE lesions and is consistent with work by Vogel et al. demonstrating the association of TSPO with HLA DR expression in human MS lesions [16]. While Iba1+ cells expressing M1 early activation marker MRP14 were relatively rare, over 90% of Iba1+MRP14+ also expressed TSPO, indicating that TSPO is often present in early activation.

The concurrent co-expression of TSPO with both conventional "M1"- and "M2"-associated markers ultimately demonstrates the complexity of immunophenotypes observed *in vivo* in neurological disease, which are the product of multiple known and unknown stimuli and understood to exist on a continuum, rather than a binary consisting of distinct M1 and M2 phenotypes. This is consistent with studies of TSPO in other forms of neurological injury, such as hemorrhagic stroke, where TSPO was found to co-localize with both M1 markers such as CD16/32 and M2 markers such as mannose receptor CD206 in a mouse model, as well as the observations of Nutma et al. in MS lesions [4,248].

While we cannot definitively link TSPO to a conventionally defined M1 or M2 immunophenotype in vivo, changes in the immunophenotypic association of TSPO become clearer through the comparison of diseased and healthy brain. As previously discussed, in the control primate brain, TSPO is expressed in only 58.65% of Iba1+ microglia and is more frequently co-expressed with Arg1 than with CD74 or MRP4, suggesting an association with an M2-biased immunophenotype. In acute lesions, however, TSPO expression is observed in over 90% of Iba1+ cells, yet the percentage of TSPO+Iba1+ cells co-expressing Arg1 does not increase significantly. The most drastic change in marker expression between healthy and diseased brain is instead seen in the expression of CD74, which is rarely expressed in healthy brain tissue but is expressed in over 50% of Iba1+ microglia/macrophages in acute lesions. In essence, in acute lesions, TSPO becomes more frequently associated with CD74, a marker of antigen-presentation and M1 phenotype. The shift from an association with predominantly Arg1+/"M2"-like phagocytes in healthy brain tissue to an association with predominantly CD74+/"M1" phagocytes in acute inflammatory lesions may indicate dysregulation of TSPO expression occurring in acute inflammation.

Alternatively, this shift could represent not only a change in the phenotype of resident microglia but rather a change in the proportion of resident microglia relative to infiltrating peripheral macrophages. In future experiments, markers such as TMEM119 may be used to distinguish resident microglia from infiltrating macrophages [137,249]. While we were not able to validate an existing TMEM119 antibody for staining in fixed marmoset tissue at the time of the stainings performed for this thesis, an anti-human TMEM119 antibody was subsequently validated by Lee et al. [250]

2.4.4 Temporal changes in glial TSPO expression

Interestingly, the percentage of Iba1+ cells co-expressing TSPO in a given lesion was found to decrease with lesion age, as determined by serial biweekly or monthly MRI studies. While over 85% of Iba1+ cells expressed TSPO in acute lesions less than 4 weeks old, the percentage expressing TSPO was as low as 13% in lesions in lesions 7-8 months old at the time of sacrifice. Modeling this relationship with a linear mixed effects model to account for random and non-random sources of variation, lesion age at time of sacrifice was demonstrated to have a significant effect upon the fraction of Iba1+ cells expressing TSPO, with a statistically significant decrease occurring at 4-5 months. This finding has significant implications for the clinical use of PET TSPO imaging for the monitoring of microglia and macrophages. Essentially, it implies that while TSPO may be a sensitive marker of microglia and macrophages in acute lesions, it becomes a significantly less sensitive marker in chronic disease; in lesions older than one month of age, at least a third of Iba1+ microglia/macrophages do not express TSPO and would not be detected by TSPO-PET imaging.

This runs counter to our hypothesis that TSPO levels would persist over the full course of EAE progression and may point to a potential limitation of the primate EAE model, which is that, while it is a relapsing-remitting disease, it progresses over the course of months and is difficult to compare to the time course of a multi-decade disease process. Therefore, it is not clear whether the discordance between TSPO expression and microglial cell content in EAE is an accurate reflection of the time course of TSPO expression in MS.

2.4.5 TSPO in astrocytes

Marmoset EAE was also found to recapitulate the astrocytic expression of TSPO in gliotic lesions that is observed in multiple sclerosis. TSPO expression was seen in hypertrophic GFAP+ reactive astrocytes in lesions where extensive astrogliosis is present, but not in GFAP+ astrocytes in NAWM or lesions without astrogliosis. Thus, it cannot be assumed that diminished TSPO signal in a lesion corresponds directly to a reduction in the population of macrophages and microglia in the lesion – in marmoset EAE, it is evident that TSPO is expressed by only a subset of macrophages and microglia in chronic lesions and that the percentage of Iba1+ cells expressing TSPO declines with lesion age. Moreover, it cannot be assumed that a subsequent increase in TSPO signal corresponds to an influx of macrophages, as TSPO signal may also be contributed by astrocytes in glial scar formation.

This feature distinguishes marmoset EAE from many rodent models of EAE, where astrocytic TSPO expression is absent or inconsistently observed [42,245,251]. Furthermore, the finding of decreasing microglial TSPO expression and increasing astrocytic TSPO expression with time is consistent with temporal patterns of TSPO expression observed in MS, as well as rodent models where astrocytic TSPO expression is present [42,245,251].

2.4.6 TSPO in neurons

Finally, this model of marmoset EAE also features neuronal TSPO expression, a characteristic that has been observed in mice [206,252] and cultured neurons *in vitro* [253] but is less frequently studied and has not yet been confirmed in many other models. TSPO expression was observed in a subset of NeuN+ neurons in some regions of normal appearing gray matter but not others. The percentage of neurons expressing TSPO ranged from 1% to 42%, with an average of 12%. This is in contrast to the control CNS tissue, where less than 1% of neurons were found to express TSPO. While further studies are needed to confirm the phenotype of TSPO+ neurons in marmoset EAE, a multiplex study of neuronal phenotype markers in an HHV6B+ EAE marmoset revealed TSPO expression in neurons expressing GLS2, a glutaminase found in excitatory glutamatergic neurons, but not in interneurons expressing parvalbumin. This is consistent with recent RNAseq studies profiling TSPO in single cells obtained from human brain homogenates, which found neuronal TSPO to be moderately expressed in pyramidal neurons but comparatively low in interneurons [254–256].

2.4.7 Future directions

These features render EAE in the common marmoset a relevant and suitable model for the study of TSPO expression in neuroinflammatory disease. Additionally, primates are not known to carry the rs6971 polymorphism, which is observed to abrogate the binding of second-generation ligands in vivo. We would therefore expect all marmosets to be high-affinity ligand binders with respect to second-generation ligands, such as PBR28. We may therefore envision informative PET imaging experiments in EAE marmosets comparing TSPO-radioligand binding by first- and second-generation ligands with multiple parameters of disease progression, principally, MRI lesion burden, clinical disability, and weight loss. We may also perform direct spatial comparisons of changes in TSPO-radioligand binding on PET imaging with T2W hyperintense lesions on MRI and T1W signal changes associated with changes in blood-brain barrier permeability. Finally, these experiments would facilitate the comparison of terminal PET imaging studies with postmortem pathology. If PET imaging of TSPO radioligand-binding were to reveal regions of increased microglial activation before MRI lesions were detected, the finding may provide the rationale for the initiation or modification of disease-modifying treatments to prevent the development of MRI lesions before they form.

However, there are several limitations to these studies. Most crucial is our limited access to control tissue. Our ability to assess Our analysis of TSPO in astrocytes and neurons, for example, is limited for several reasons. Due to the irregular cell shape of hypertrophic astrocytes, it is not possible to identify GFAP+ cell bodies with conventional cell-segmentation algorithms. Moreover, as TSPO staining was stripped from studied sections prior to staining for GFAP and NeuN, the resulting images of GFAP and NeunN staining are not aligned with the images of TSPO staining taken prior to re-staining. Alignment of these images for analysis of co-localization of GFAP and TSPO would require both translation and rotation of the image, which is not possible with our existing analysis software. While studies of neuronal phenotype in marmoset A were informative, these were not repeated in other animals due to limited tissue availability for phenotyping.

Another limitation of this study is that localization of TSPO protein expression with immunofluorescence has not been correlated with radioligand-binding. Radioligand-binding assays, such as autoradiography, are typically performed on fresh frozen tissues that have not undergone fixation. Due to the scanning protocol for EAE animals at our institution, EAE marmoset tissue is highly fixed at the time of pathological analysis. Under this protocol, animals undergo a terminal MRI scan prior to cardiac perfusion, followed by autopsy for tissue collection and harvesting of the brain and spinal cord for high-resolution ex-vivo imaging. These scans may last as long as 36 hours. The requirement for immediate ex vivo MRI in fixative after cardiac perfusion leads to significant tissue fixation before tissue can be obtained for pathology and other studies. Not only does this tissue often require intensive antigen retrieval methods, such as boiling in citrate buffer to expose antigens for subsequent immunohistochemical detection, but it is unknown how this level of fixation would affect radioligand-binding. Due to limited tissue availability, autoradiography with TSPO-radioligands was not attempted on marmoset CNS tissue.

3 TSPO expression as a peripheral biomarker of neuroinflammation in multiple sclerosis

3.1 **Introduction**

Currently, there is growing interest in identifying peripheral biomarkers of central nervous system disease both as a means of diagnosing neurological disease and monitoring prognosis, as clinical limitations represent a barrier to CNS imaging and CSF analysis. CSF analysis, for example, requires an invasive and potentially distressing patient procedure called a lumbar puncture, in which a needle is inserted through the intervertebral spaces of the lumbar spine to draw CSF from the intrathecal space below the spinal cord [89]. MRI and PET imaging studies are costly, and PET studies of the brain ultimately require the injection of radioisotopes for imaging, exposing patients to radiation [257]. Blood-based detection of peripheral biomarkers represents a significant opportunity for non-invasive testing that is both informative and cost-effective.

While TSPO expression in the central nervous system has been extensively studied in human neurodegenerative disease, studies of TSPO in the periphery remain comparatively limited. Studies in peripheral immune cells such as macrophages has been predominantly examined TSPO in cardiovascular diseases, such as atherosclerosis [40] and myocarditis [6,258], or other diseases of systemic inflammation, such as cancers [32,41,259]. A recent study by Narayan et al., for example, examined TSPO expression in macrophages derived from peripheral blood monocytes and synovial monocytes isolated from patients with rheumatoid arthritis after treatment with pro-inflammatory and anti-inflammatory stimuli [204]. The study found that macrophages derived from synovial and peripheral blood monocytes produced significantly higher levels of TSPO mRNA and protein than the monocytes themselves. However, when challenged with LPS, these macrophages downregulated their TSPO expression, such that qPCR and Western blot studies showed lower levels of TSPO mRNA and protein in the LPS-treated macrophages than in untreated macrophages [204]. Densitometry measurement on western blotting demonstrated significant decreases in TSPO band density as early as 2 hours after stimulation with LPS and IFN-γ [204].

M2 macrophages derived by IL-4, dexamethasone, or TGF-β treatment, in contrast, showed no difference in TSPO protein or mRNA levels when compared to untreated macrophages [204]. This was true of M2-polarized THP1 MDM, macrophages derived from human PBMC, and synovial macrophages [204]. This study demonstrates how peripheral blood mononuclear cells may be used to probe the relationship between TSPO expression and immunophenotype in phagocytic cells, ultimately giving insight into the function of TSPO in macrophage biology.

However, this study was concentrated on TSPO modulation in the context of systemic inflammatory disease i.e. rheumatoid arthritis. Studies of peripheral TSPO expression in the context of central neuroinflammation have predominantly examined TSPO in platelets [201,214,215,217,218]. Interestingly, Nudmamud et al. reported in 2000 that TSPO mRNA levels and radioligand binding signals are reduced in the peripheral blood of patients with psychiatric disorders, such as high anxiety [201]. A 2012 study of TSPO in the peripheral blood of MS patients likewise found a reduction in TSPO binding with second-generation ligand PBR28 in isolated PBMC when compared to healthy controls [213]. However, this study did not directly measure TSPO protein expression in the same subjects in which radioligand-binding was measured. It is unknown whether the TSPO radioligand-binding measured in Harberts's study directly reflects TSPO protein levels in the peripheral blood and therefore, it is not certain that TSPO protein levels are truly decreased in MS patient PBMC. While differences in cytokine secretion and immune cell phenotype have been observed between MS patients and normal donors, it is not known whether these differences correlate to changes in TSPO expression. Nonetheless, these studies have shown the potential of using peripheral immune cells to model the modulation of TSPO expression in diverse disease contexts, raising the possibility of using PBMC to monitor correlation of TSPO with other markers of inflammation.

Flow cytometry is a useful technique to monitor changes in multiple parameters in multiple cell populations in suspension, for example, isolated PBMC [260–262]. Classical monocytes are identified by high surface expression of CD14 without expression of CD16 and represent approximately 80-90% of all monocytes in healthy individuals [263,264]. Atypical or "nonclassical monocytes exhibit high surface expression of CD16 and low expression of CD14 [263,264]. Intermediate monocytes express high levels of both CD14 and CD16, and were found to secrete high levels of TNF-α in response to LPS stimulation [265]. Together, atypical and intermediate monocytes constitute approximately 10-20% of the total monocyte population in humans, with atypical monocytes being the more abundant of the two populations [263,264]. A 2015 study by Mukherjee et al. found classical monocytes to possess a phagocytic phenotype with pro-inflammatory characteristics, while non-classical monocytes exhibited pro-inflammatory features associated with antigen presentation [266]. Specifically, non-classical monocytes were found to express high levels of pro-inflammatory markers such as costimulatory molecules CD80 and CD86, as well as toll-like receptors (TLRs) and HLA-DR, which are involved in antigen recognition and presentation, respectively [266]. Classical monocytes were found to express high levels of phagocytic markers CD163 and CD36 but expressed significantly lower levels of the pro-inflammatory markers found in non-classical monocytes [266]. Intermediate monocytes were found to exhibit characteristics associated with both phagocytosis and antigen presentation and are hypothesized to represent a transitional state between the other two classes [266].

If TSPO were established as a peripheral biomarker of central neuroinflammation, the detection of TSPO in the peripheral blood may facilitate disease monitoring in the future and potentially guide treatment decisions. To determine differences in TSPO protein expression in MS patients, my aim is to characterize TSPO expression in peripheral blood mononuclear cells from MS patients and age- and gender-matched healthy controls using flow cytometry.

Summary of Aim 2

Questions: What cells express TSPO in the peripheral blood of MS patients and healthy donors? Is TSPO expression in monocytes associated with the expression of other markers of immunophenotype (e.g. HLA or CD86 expression) or increases in mitochondrial volume?

Specific Aim: I aim to measure TSPO expression in classical, non-classical (atypical) and intermediate monocytes in MS patients (N=10) and matched healthy donors (N=10). I will use a student's T-test to determine there are differences in TSPO expression between these cohorts. I will use linear regression to determine whether increases in TSPO expression correlate with increases in mitochondrial volume and expression of HLA-DR and CD86.

Specifically, I aim to:

i) quantify mean fluorescent intensity (MFI) of TSPO, HLA DR, CD86, and HSP60 staining in CD14+CD16-, CD16+CD14-, and CD14+CD16+ monocytes

ii) quantify MFI of TSPO and HSP60 staining in CD3+CD16- lymphocytes, CD16+ CD3- NK cells, and CD16+CD3+ NKT cells.

Hypothesis: I hypothesize that TSPO protein expression is elevated in both lymphocytes and monocytes subsets in MS patients. I further hypothesize that TSPO expression will be higher in non-classical and intermediate monocytes expressing CD16 than in classical monocytes expressing CD14 and not CD16 and that increased in TSPO will correlate to increases in mitochondrial volume and expression of inflammatory markers.

3.2 **Methodology**

3.2.1 Division of responsibility

Blood draws were performed by clinical staff at the NIH Blood Bank and the Neuroimmunology Branch Clinic (Bethesda, Maryland). Accession of patient data to determine treatment status and MS subtype was performed by clinical fellows in Neurology. I performed all subsequent patient selection, matching, cell staining, flow cytometry, and data analysis, as well as mRNA extraction and cDNA synthesis for subsequent genotyping (described in Chapter 4).

3.2.2 Selection of subjects

Whole blood or lymphocyte aphereses were obtained from the NIH Blood Bank. All subjects provided informed written consent under a research protocol approved by the Institutional Review Board of the National Institutes of Health Clinical Center. The demographics of selected patients and normal donors and the process of selection are shown below. MS patients are shown in **Table 3-1**. Gender-, race-, and age-matched ND subjects are shown in **Table 3-2**. MS patients selected for study were primarily either untreated or on first-line therapies such as interferon-ß (Rebif), glatiramer acetate, or dimethyl fumarate. Patients treated with fingolimod (Gilenya) or natalizumab (Tysabri) were excluded, as these medications are considered more potent [267,268] and more likely to modulate the inflammatory response being studied in these patients with actively enhancing lesions. The demographics and treatment statuses of MS patients and the demographics of healthy donors are discussed in the section 3.2.14. Inclusion and exclusion criteria are described further in sections 3.2.10-3.2.12.

Subject	Gender	Ethnicity	Age	MS subtype	CEL	Treatment
1	F	White	40	RRMS	present	None
2	F	AA	45	SPMS	present	None
3	F	white	26	RRMS	present	None
4	F	white	29	RRMS	present	Copaxone
5	F	white	38	RRMS	present	None
6	F	AA	42	RRMS	present	None
7	M	Latino	42	RRMS	present	None
8	F	white	39	RRMS	present	None
9	F	AA	44	*RRMS*	present	Copaxone
10	F	AA	45	RRMS	present	Tecfidera

***Table 3-1.** Demographics (gender, ethnicity, age), MS subtype, presence of contrast-enhancing lesions (CEL) and treatment status of MS patients included in this study.*

Subject	Gender	Ethnicity	Age
1	F	white	43
2	F	AA	50
3	F	white	51
4	F	white	22
5	F	white	32
6	F	white	44
7	M	Latino	42
8	F	white	32
9	F	AA	45
10	F	white	50

***Table 3-2.** Demographics (gender, ethnicity, and age) of normal donor included in this study.*

3.2.3 PBMC isolation

The peripheral blood mononuclear cells (PBMC) were isolated by Ficoll-gradient separation, in which blood is layered on Ficoll for centrifugation, and the buffy coat is isolated using a syringe. The isolated buffy coats were treated with erythrocyte lysis buffer to remove residual erythrocytes and the lysis was quenched with the addition of DMEM, after which the suspension was centrifuged and washed with PBS.

Following separation, isolated PBMC were cryofrozen in RPMI-1640 media containing 10% DMSO and 10% FBS. MS subjects (n=10) and normal donors (n=10) were matched in terms of age, race, and gender. Demographic information is shown in Table 1.

Peripheral blood was also collected from healthy and EAE marmosets 1-2 times per month as described under Animal Use. Mononuclear cells were isolated from peripheral blood by Ficoll-gradient separation, as described above.

3.2.4 TSPO Genotyping

De-identified patient and normal donor PBMC samples from 25 patients and 25 normal donors were assigned alphanumerical IDs and genotyped to detect the rs6971 polymorphism. 1 x 10^6 thawed PBMC were washed in PBS and reserved for mRNA extraction and cDNA synthesis. Subjects were categorized as high-, low-, or non-binders on the basis of genotype, so that patients and normal donors could be matched in terms of genotype, gender, and age.

3.2.5 mRNA extraction

mRNA extraction was performed using a Qiagen RNAeasy Kit (Qiagen, Germantown, PA). 1 x 10^6 thawed PBMC were washed in FACS buffer (1% heat-inactivated fetal bovine serum, 0.1% sodium azide in PBS) and lysed in 350 µl RLT buffer (Qiagen, Germantown, PA). The lysate was centrifuged at 20835 x G for 3 minutes, and the supernatant was collected and combined with an equal volume of 70% molecular-biology grade ethanol. The combined volume was transferred to an RNA microcentrifuge column, which was centrifuged at 8000 x G for 30 seconds, after which the flow-through was discarded and the column was rinsed with 350 µl RW1 buffer (Qiagen, Germantown, PA). After the first wash, 80 µl DNAse I in RDD buffer (Qiagen, Germantown, PA) was added to the column and incubated for 15 minutes at room temperature. The column was washed twice with 500 µl RPE buffer (Qiagen, Germantown, PA) and centrifuged at 8000 x G for 30 seconds on the first wash and 2 minutes on the second wash. The column membrane was dried by centrifuging for 1 minute in an empty collection tube. mRNA was eluted in 40 µl RNase free water into a collection tube by centrifugation at 8000 x G for 1 minute. The mRNA concentration of the resulting eluent was quantified using a Nanodrop 2000c spectrophotometer (Thermo Scientific, Waltham, MA). Isolated mRNA samples were stored at -80C for subsequent cDNA synthesis and genotyping.

3.2.6 cDNA synthesis

To reduce mRNA secondary structures and facilitate primer annealing, 75 or 150 µg of purified mRNA was incubated with an equivalent quantity of RT Random Primer mix (Promega, Madison, WI) and RNase-free water in a total reaction volume of 15 µl at 70°C for 10 minutes, after which the samples were immediately cooled on ice. The following were added to the annealed sample: 5 µl 5x Reaction Buffer (250mM Tris-HCl, pH 8.3 at 25°C), 375mM KCl, 15mM $MgCl_2$, 50mM DTT), 1 µl Reverse Transcriptase, and 1 µl dNTP. RNase-free water was added to bring the total reaction volume to 40 µl. The samples were incubated for 1 hour at 37C in a C1000 Touch ThermoCycler (Bio-Rad, Deeside, UK). The resulting cDNA was stored at -20C for subsequent genotyping.

3.2.7 Flow Cytometry

To quantitatively characterize TSPO expression in human PBMC, human PBMC fixed for 30 minutes, permeabilized, and stained with directly-conjugated fluorescent antibodies to CD14, CD3, CD16, TSPO, HLA-DR, and CD86. The isolated PBMC were stained simultaneously with a fixable viability dye to distinguish live cells from dead and apoptotic cells, population surface markers to distinguish lymphocyte and monocyte subsets, and immunophenotype surface markers indicating immune activation. Population markers included CD3 to identify lymphocytes and CD14 and CD16 to identify monocyte subsets. To measure immune activation, cells were stained with either specific antibodies to CD86 and HLA DR or nonspecific isotype controls conjugated to identical fluorophores. Following surface marker staining, the PBMC were fixed, permeabilized and stained with either antibodies specific to TSPO and HSP60, a mitochondrial chaperonin, or isotype controls conjugated to the same fluorophores. Antibodies and isotypes used for these experiments are listed in the Appendix (***Table** 7-6*-**Table 7-7**).

In marmoset PBMC studies, CD86, HLA-DR, HSP60, and CD16 are omitted due to lack of cross-reactive commercial antibodies. Instead, previously validated cross-reactive antibodies to TSPO, CD3 and CD14 were used to study TSPO expression in monocytes and lymphocytes; a validated antibody to activation marker MRP14 and HLA-DR invariant chain

CD74 will be used to detect activation. Isolated PBMC were thawed and diluted in RPMI and resuspended in FACS buffer to a concentration of 1 x 10^6 cells per 50 µl.

3.2.8 Staining with conjugated antibodies and Fixed Viability Stain 780

Isolated human PBMC were thawed and diluted in complete RPMI (containing 10% heat-inactivated FBS) and washed twice in FACS buffer. 5 x 10^5 cells were stained for 15 minutes in 50 µl FACS buffer containing Fixable Viability Stain 780 (1:1000) at 4C while protected from light in a 96-well plate. Three wells were prepared for each subject: well A, B, and C. After incubation, cells were washed in 200 µl cold FACS buffer and centrifuged at 400 x G for 5 minutes. The stained cells were re-suspended 100 µl IC Fixation Buffer (eBiosciences, San Diego, CA) and incubated for 30 minutes in the dark at 4C. After fixation, cells were washed twice in 200 µl cold FACS buffer, centrifuged at 400 x G for 5 minutes, and re-suspended in cold FACS buffer. cells were centrifuged at 400 x G and resuspended in 200 µl IC permeabilization buffer (eBiosciences, San Diego, CA) diluted to a 1x concentration in sterile water. Cells were incubated in permeabilization buffer for 5 minutes and centrifuged at 400 x G for 5 minutes. 150 µl permeabilization buffer was removed from each well and cells were re-suspended in the 50 µl remaining. For each subject, one well received an antibody cocktail A (antibodies listed in ***Table 7-6***), while the second well received cocktail B (antibodies listed in **Table 7-7**). A third well was left unstained. After 15 minutes incubation at 4C while protected from light, the staining was quenched by the addition of 200 µl cold FACS buffer and the plate was centrifuged at 400 x G for 5 minutes. The supernatant was removed, and the cells were washed a second time in 200 µl cold FACS buffer. Following the second wash, wells A and B were re-suspended in FACS buffer containing DAPI (1 µg/ml) and well C was re-suspended in FACS buffer without nuclear dye. Following staining, cells were transported on ice to a second facility, where they were strained through a 100-um filter for analysis. Strained cell samples were subsequently analyzed using a Fortessa A at a flow rate of 1-3 µl per second. 50,000-150,000 cells were acquired per sample. Data was analyzed using FlowJo 10 (Tree Star, Ashland, OR).

3.2.9 Staining marmoset PBMC with conjugated antibodies and MitoTracker Deep Red

Three wells were prepared for each subject in a 96-well plate: wells A, B, and C. MitoTracker Deep Red was added to wells A and B, and the samples were shielded from light and incubated for 10 minutes at 37C. Following incubation, cells were centrifuged at 395 x G for 5 minutes and washed twice with 200 µl cold FACS buffer. 100 µl Fixation Buffer (BD Biosciences, San Jose, CA) was added to each well and samples were incubated for 30 minutes in the dark at 4C. After fixation, cells were centrifuged at 395 x G for 5 minutes and washed twice in 200 µl IC permeabilization buffer (BD Biosciences, San Jose, CA) diluted to 1x concentration in sterile water. 150 µl permeabilization buffer was removed from each well and cells were re-suspended in the remaining 50 µl. For each subject, well received an antibody cocktail containing CD14, CD3, and TSPO antibodies (***Table 7-6***), while the second well received antibodies for CD14 and CD3, and the corresponding isotype control for TSPO (***Table 7-6***, **Table 7-7**). A third well was left unstained. After 15 minutes incubation at 4C while protected from light, the staining was quenched by the addition of 200 µl cold FACS buffer and the plate was centrifuged at 400 x G for 5 minutes. The supernatant was removed, and the cells were washed a second time in 200 µl cold FACS buffer. Following the second wash, wells A and B were re-suspended in FACS buffer containing DAPI (1 µg/ml) and well C was resuspended in FACS buffer without DAPI.

Data acquisition was performed using a LSRII and data was analyzed using BD FACSDiva.

3.2.10 Statistical Analysis

Data are expressed as a mean ± SEM of (n) independent experiments. Two-tailed students t-tests were used to assess significance between MS patients and normal donors. T-tests were also used to analyze differences between the MS patient cohort and the healthy control cohort in terms of demographic composition. ANOVA was used to analyse differences between classical, non-classical, and intermediate monocytes. A p-value of less than or equal to 0.05 was considered significant. There were no significant differences in terms of age, race, or sex.

3.2.11 Protection of Human Subjects

While blood collected from patients was not specified for a specific study and patients consented at the time of collection that their blood and saliva may be used for a variety of immunological studies, their blood samples are labeled with their medical record number and are therefore identifiable to members of our branch. The risk to subjects from blood collection are minimal discomfort and have no impact on the course of their clinical care. Patients do not pay or receive compensation to be treated in our branch, nor do they benefit directly from the proposed study.

Patients were recommended for consideration in this study by clinical fellows and nursing staff on the basis of disease activity. To ensure that only relevant information is shared with research staff, clinical fellows in our lab use the National Institutes of Health's Clinical Research Information System (CRIS) to access patient records and report only relevant criteria in a private shared document. In this private document, patients selected by NIH clinical staff are identified and linked to the following information:

- Name
- Birthdate and age
- Race
- MS subtype (if applicable)
- Date of disease onset (if applicable)
- Date of blood draw
- Current disease-modifying medications (if applicable)
- Presence or absence of contrast-enhancing lesions on most recent MRI
- Presence or absence of leptomeningeal enhancement of most recent MRI
- Use of disease-modifying medication in the previous 6 months (if applicable)
- HLA subtype

Analysis was principally conducted at a research laboratory on the NIH main campus in Bethesda, MD. However, this group does not have access to the radioligands or equipment necessary to monitor TSPO levels by PET imaging. Therefore, ligand-binding experiments were conducted with collaborators in PET imaging at one of two sites:

1. Molecular Imaging Chemistry Laboratory
   West Forvie Site
   Addenbrooke's Hospital
   Cambridge, UK, CB2 5QQ
2. Division of Brain Sciences
   Burlington Danes Building
   Hammersmith Hospital
   London, UK, W12, OUA

3.2.12 Adequacy of Protection Against Risks

This study involves adult patients seen at the NIB outpatient clinic and consent was obtained from all patients by clinical staff upon intake to the clinic. Clinicians explained that blood samples are taken for both clinical and research purposes and that research blood samples may be used for a variety of studies. The patients then signed relevant consent forms. Research blood samples drawn from patients are then processed by trained laboratory technicians.

After establishing a secure VPN connection and identifying patients that meet the inclusion criteria on a given visit by logging in to a secure shared drive for members of our section, I then mark the patient visit and login to our patient sample database, STAMS, to record the number of blood vials stored from the visit of interest. In a separate document in our secure shared drive, I listed the patient medical record number, clinical ID, the date of the visit, and the location of available vials from this visit in our section's liquid nitrogen tank. Each vial of interest was then associated with a non-specific identifier such as the first letter of their first name and a number for labeling samples during analysis (for example, two patients with last names starting with "A" would be identified as "A1" and "A2"). After I have saved and closed both documents, I disconnect from the VPN network and disconnect my PIV reader. The vial information is then accessed by me or lab personnel trained to handle patient samples and vials retrieved from our liquid nitrogen tank. Once retrieved, vials are packaged on dry ice in a large Styrofoam container which is taped on all sides and shipped my FEDEX to my laboratory in the UK. As these vials could be labeled with identifiers such as an MRN, I transferred these vials to liquid nitrogen by myself.

For sample analysis, I thawed and transferred the contents of each vial to conical of media labeled with the non-specific identifier associated with this vial in the secured document (e.g. "A1"). For all subsequent analysis, the vial was identified only by the assigned letter and number.

3.2.13 Inclusion of Women and Minorities

No patients were excluded on the basis of age, race, or gender. Patients subjects are all adults seen by at the NIB clinic in Bethesda, MD.

Using a private shared document of patient information provided by trained clinical staff, I identified a subset of patients that had contrast-enhancing lesions on the date of their blood draw and were on first-line therapy only (copaxone, Betaseron, or Rebif) or untreated for at least 6 months prior to their visit. Of 11 subjects selected for our initial study, 8 are female and 3 are male, which is reflective of the general gender distribution of our MS patient population. 7 patients identify as African American (5 females, 2 males). While this is not reflective of global racial demographics among MS patients, it is representative of the patient population seen by our clinic at NIH. The average age of this cohort is 38.2 years old. All subjects are over 18 years old. The oldest patient was 64 years old on the date of their blood draw while the youngest patient was 28 years old.

3.3 **Results**

To quantitatively characterize TSPO expression in peripheral blood mononuclear cells (PBMC), human PBMC were isolated from whole blood and aphereses of MS patients with contrast-enhancing lesions (CEL) and age- and gender-matched healthy donors. A schematic of the staining protocol and a representative gating strategy used to identify living single cells are shown in Figure 1. To quantify TSPO in relevant subpopulations of monocytes and lymphocytes, a plot of forward scatter (FSC-A) vs. side scatter (SSC-A) was to identify monocyte and lymphocyte populations as shown in Figure 1. After gating on monocytes and lymphocytes to exclude debris (Figure 1a). The area of the forward scatter peak (FSC-A) was plotted against the height of the forward scatter peak (FSC-H) to visualize single cells, doublets, and cell clumps. After gating on single cells to exclude doublets and cell clumps (Figure 1b), we plotted forward scatter (FSC-A) vs. fixed viability stain 780 and gated on live FVS780- cells to exclude dead and apoptotic cells. After gating on live (FVS-) cells, separate gates were drawn around the monocytes and the lymphocytes in the FSC-A v. SSC-A plot as shown in Figure 1d.

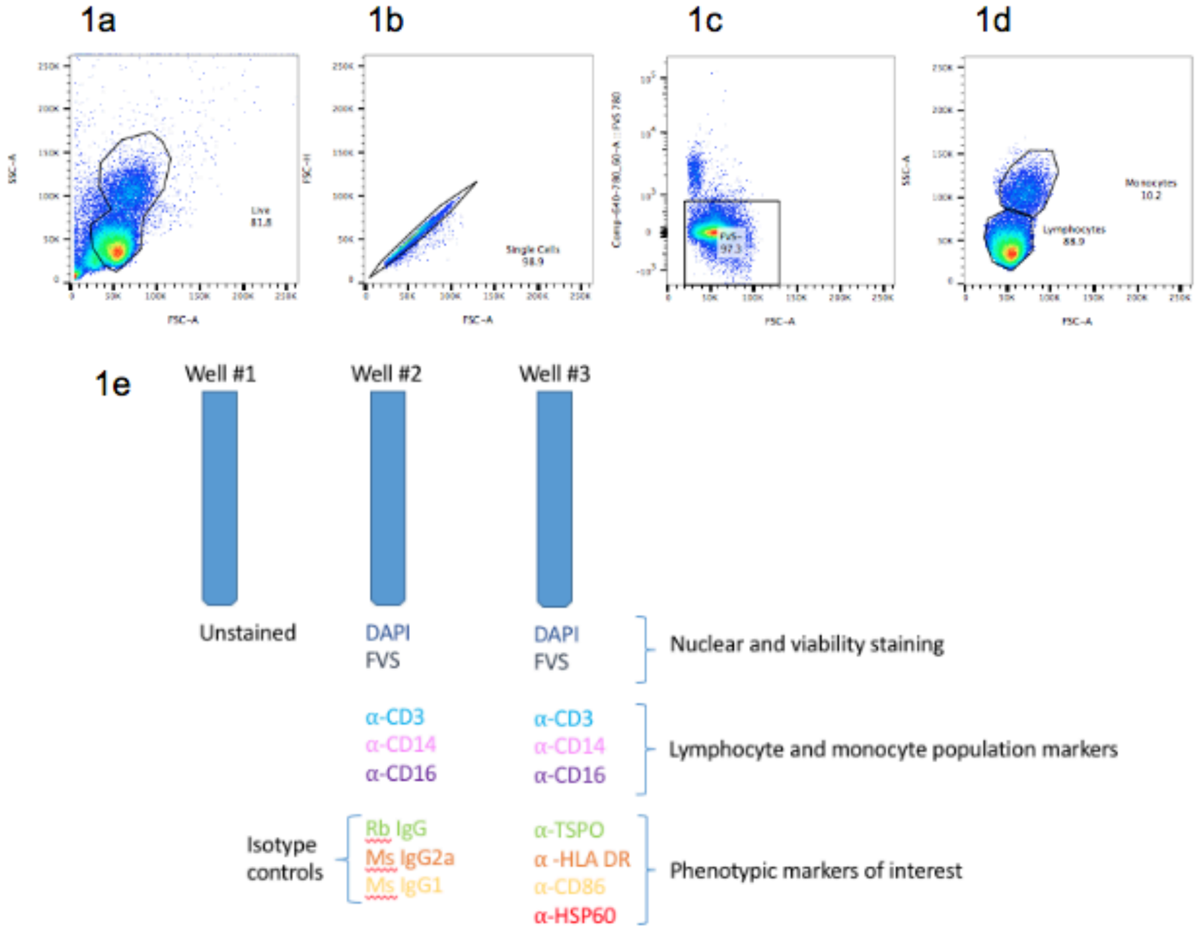

Figure 3-1. *Representative gating of fixed peripheral blood mononuclear cells (PBMC) isolated from an MS patient (n=1).*

3-1a) Representative dot plot of forward scatter signal (FSC-A) vs. side scatter signal (SSC-A) showing gated live cell population.

3-1b) Dot plot of FSC-A signal vs. FSC-H signal in gated live cells from Fig. 1a with gating on single cells to exclude doublets, triplets, and larger cell clusters.

3-1c) Dot plot of FSC-A signal vs. Fixed Vital Stain 780 signal in gated single cells from Fig. 1a with gating on FVS- cells to eliminate apoptotic and dead cells.

3-1d) Representative dot plot of forward scatter signal (FSC-A) v. side scatter signal (SSC-A) showing gating on monocytes and lymphocytes.

3-1e) Schematic showing the stains and antibodies used in each of 3 wells prepared for each donor sample. Cells in well#1 were fixed and permeabilized but remained unstained. Well #3 was stained with DAPI, FVS780 (Fixed Viability Stain), populations markers and antibodies against TSPO, HLA-DR, CD86, and HSP60 to measure the specific staining intensity for each marker of interest in CD3+, CD14+ and CD16+ cells. Well #2 was stained with DAPI, FVS780 (Fixed Viability Stain), populations markers and isotype controls which corresponded in both isotype and fluorophore-conjugate to the antibody against TSPO, HLA-DR, and CD86. This allowed the measurement of the nonspecific staining intensity of the fluorophore-conjugated antibodies used for these markers of interest in CD3+, CD14+, and CD16+ cells.

3.3.1 Quantification of TSPO protein expression in monocytes and lymphocytes

TSPO protein expression in monocytes was quantified by gating upon the monocyte population and gating upon CD3- cells to eliminate contaminating lymphocytes from the monocyte gate. TSPO protein expression in lymphocytes was similarly quantified by gating upon the lymphocyte population as shown in **Figure 3-2a** and subsequently gating on CD14- cells within the lymphocyte gate to eliminate contamination by monocytes as shown in **Figure 3-2b**. To more precisely identify CD3+ lymphocytes and eliminate contamination by CD16+ natural killer cells or CD16+CD3+ NKT-like cells, the fluorescent intensity of CD3 staining was plotted against the intensity of CD16- staining as shown in **Figure 3-2c**, and analysis was limited to lymphocytes (CD3+CD16- cells, blue).

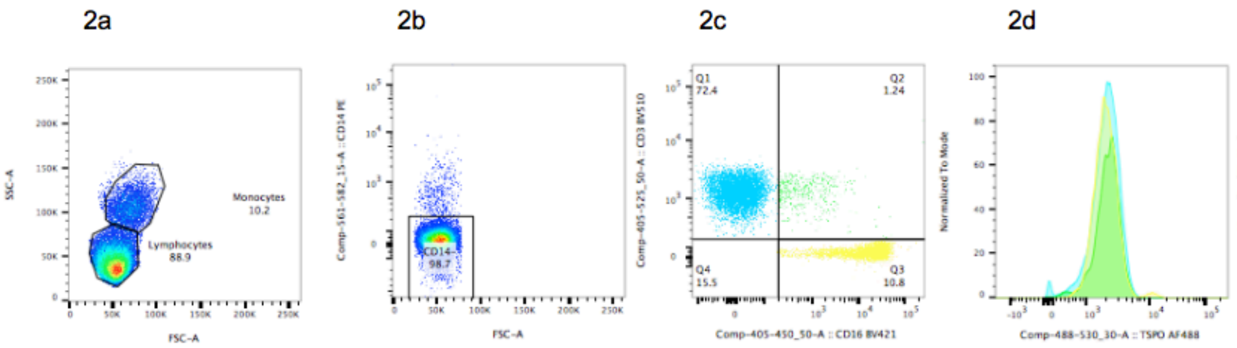

Figure 3-2. *Gating strategy for isolated of CD3+ lymphocytes in human PBMC.*
3-2a) Representative dot plot of forward scatter signal (FSC-A) vs. side scatter signal (SSC-A) showing gated monocyte and lymphocyte populations.
3-2b) A dot plot of FSC-A signal v. CD14 PE signal in cells falling within the lymphocyte gate in Figure 2-2a with gating on CD14- cells to eliminate monocyte contamination of the gated lymphocyte population.
3-2c) A dot plot of CD3 BV510 MFI v. CD16 BV421 MFI in the gated CD14- population in Fig. 2b showing 3 populations: 1) CD13+CD16- lymphocytes (yellow), CD16+CD3- cells (blue), and CD3+CD16+ cells (green).
3-2d) Representative histogram of TSPO AF488 signal intensity in CD3+CD16- lymphocytes (blue), CD16+CD3- cells (yellow), and CD3+CD16+ cells (green).

As shown in **Figure 3-2d**, the median fluorescent intensity (MFI) of TSPO staining in all CD14- cells within the lymphocyte gate was similar in all subsets, including CD3+CD16- lymphocytes (blue), CD16+CD3- cells (yellow, presumed to be natural killer cells), and CD3+CD16+ cells (green, presumed to be NKT cells).

Focusing on lymphocytes alone, we found the average MFI of TSPO staining in the CD3+CD16-CD14- gated lymphocytes (Figure 2c, blue) to be 1918 ± 80.96 in 18 of 20 subjects. Two subjects were omitted due to corruption of data on file transfer, leading to a TSPO MFI in CD3+CD16-CD14- gated lymphocytes of 12.8 in both subjects, which were excluded as outliers. In contrast, the average MFI of TSPO staining in the CD3- gated monocytes in all subjects was 12677 ± 705, which was approximately 6-fold higher than the MFI of TSPO staining in the gated lymphocyte population. This difference is illustrated in Figure 3-3 and is statistically significant (p<0.0001). This is consistent with previously reported measurements of relative TSPO mRNA levels in monocyte and lymphocyte subsets by Harberts et al., 2012, which showed isolated CD14+ monocytes to possess fivefold higher levels of TSPO mRNA when compared to CD4+ and CD8+ lymphocytes.

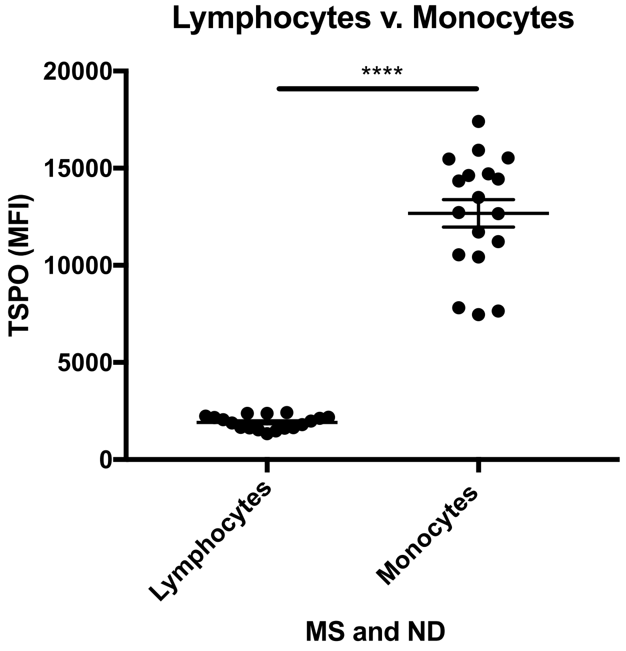

Figure 3-3. *Comparison of MFI of TSPO staining in lymphocytes and monocytes in all donors (inclusive of both MS patients and matched normal donors). **** denotes a p-value <0.0001.*

To more comprehensively characterize TSPO in distinct monocyte subsets, three subpopulations were identified by plotting CD14 v. CD16 signal as shown in Figure 3-5c. These three subsets exhibited a classical pattern of "M1" marker expression (Figure 3-5e-g), with CD14+CD16+ monocytes consistently expressing the highest levels of HLA DR, CD86, and mitochondrial marker HSP60. "Classical" CD14+CD16- monocytes consistently expressed the lowest levels of these phenotypic markers, while "atypical" CD14-CD16+ cells consistently expressed an intermediate level of each.

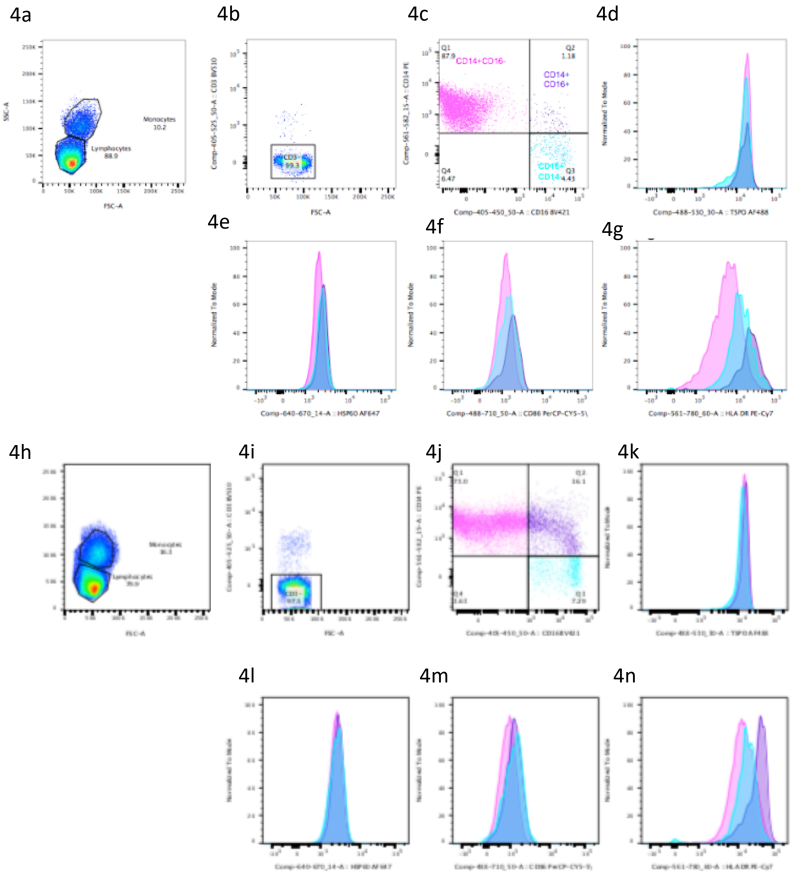

Figure 3-4*. Quantification of TSPO staining intensity in monocyte subsets by flow cytometry.*
4a) Representative dot plot of forward scatter signal (FSC-A) v. side scatter signal (SSC-A) in live FVS- single cells showing gated lymphocyte and monocyte populations from a multiple sclerosis patient.
4b) A dot plot of FSC-A signal v. CD3 BV510 signal from cells falling with the monocyte gate in Fig. 2a with gating on CD3- cells to eliminate lymphocyte contamination of the gated monocyte populations.
4c) Representative dot plot of CD14 PE MFI v. CD16 BV421 MFI in the gated CD3- population in Fig. 2b showing 3 populations: 1) CD14+CD16- or "classical" monocytes (pink), CD16+CD14- or "atypical monocytes (blue), and CD14+CD16+ monocytes (purple).
4d) Representative histogram of TSPO AF488 signal in CD14+CD16- (pink), CD16+CD14- (blue), and CD14+CD16+ monocytes (purple).
4e) Histogram plot of HSP60 AF647 signal in CD14+CD16- (pink), CD16+CD14- (blue), and CD14+CD16+ monocytes (purple).
4f) Histogram plot of CD86 PerCP-Cy5.5 signal in CD14+CD16- (pink), CD16+CD14- (blue), and CD14+CD16+ monocytes (purple).
4g) Histogram plot of HLA DR PE-Cy7 signal in CD14+CD16- (pink), CD16+CD14- (blue), and CD14+CD16+ monocytes (purple).
4h-4n) The same plots described in 5a-5g are shown in 5h-5n for a representative normal donor. All plots for all subjects are shown in the Appendix.

To assess the degree of non-specific fluorescent signal in each cell population, TSPO staining in each subset was compared to baseline autofluorescence in an unstained sample and an isotype-control stained sample from the same donor. Non-specific staining associated with the isotype control was found to be comparable to the autofluorescence of the unstained sample. Stainings from a representative MS patient and normal donor are shown in ***Figure 3-5***.

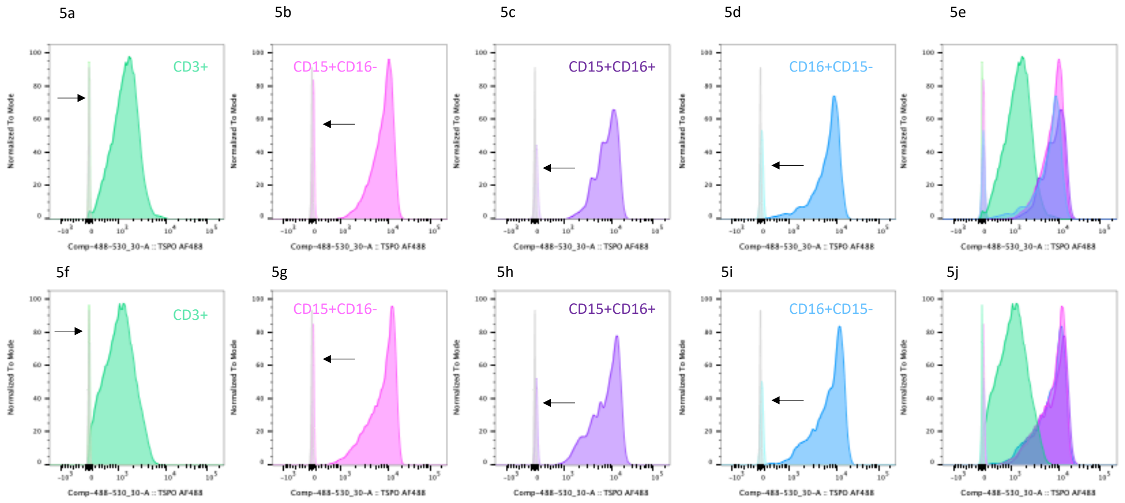

Figure 3-5. *Comparison of specific TSPO staining intensity vs. nonspecific isotype control staining (arrow) vs. signal intensity of unstained cells in CD3+ lymphocytes, CD14+CD16- monocytes, and CD16+CD14- monocytes in a representative MS patient and a representative normal donor. The position of the isotype control peak is indicated by the arrow in 5a-5d and 5f-5i, but in some cases, is completely overlapped by the autofluorescence peak of the unstained cells.*

5a) Comparison of specific TSPO staining (dark green) vs. isotype control (light green) vs. unstained cells (grey) in CD3+ lymphocytes in the representative MS patient.

5b) Comparison of specific TSPO staining (dark pink) vs. isotype control (light pink) vs. unstained cells (grey) in CD14+CD16- monocytes in the representative MS patient.

5c) Comparison of specific TSPO staining (dark purple) vs. isotype control (light purple) vs. unstained cells (grey) in CD16+CD14+ monocytes in the representative MS patient.

5d) Comparison of specific TSPO staining (dark blue) vs. isotype control (light blue) vs. unstained cells (grey) in CD3+ lymphocyte in the representative MS patient s.

5e) Overlay of TSPO staining intensity of gated CD3+ cells (green), CD14+CD16- cells (pink), CD14+CD16+ cells (purple), and CD16+CD14- cells (blue) in the representative MS patient. All monocyte populations exhibit a staining intensity 10-fold higher than the intensity of the CD3+ lymphocyte population.

5f) Comparison of specific TSPO staining (dark green) vs. isotype control (light green) vs. unstained cells (grey) in CD3+ lymphocytes in the representative healthy donor.

5g) Comparison of specific TSPO staining (dark pink) vs. isotype control (light pink) vs. unstained cells (grey) in CD14+CD16- monocytes in the representative healthy donor.

5h) Comparison of specific TSPO staining (dark purple) vs. isotype control (light purple) vs. unstained cells (grey) in CD16+CD14+ monocytes in the representative healthy donor.

5i) Comparison of specific TSPO staining (dark blue) vs. isotype control (light blue) vs. unstained cells (grey) in CD3+ lymphocytes in the representative healthy donor.

5j) Overlay of TSPO staining intensity of gated CD3+ cells (green), CD14+CD16- cells (pink), CD14+CD16+ cells (purple), and CD16+CD14- cells (blue) in the representative healthy donor. All monocyte populations exhibit a staining intensity 10-fold higher than the intensity of the CD3+ lymphocyte population.

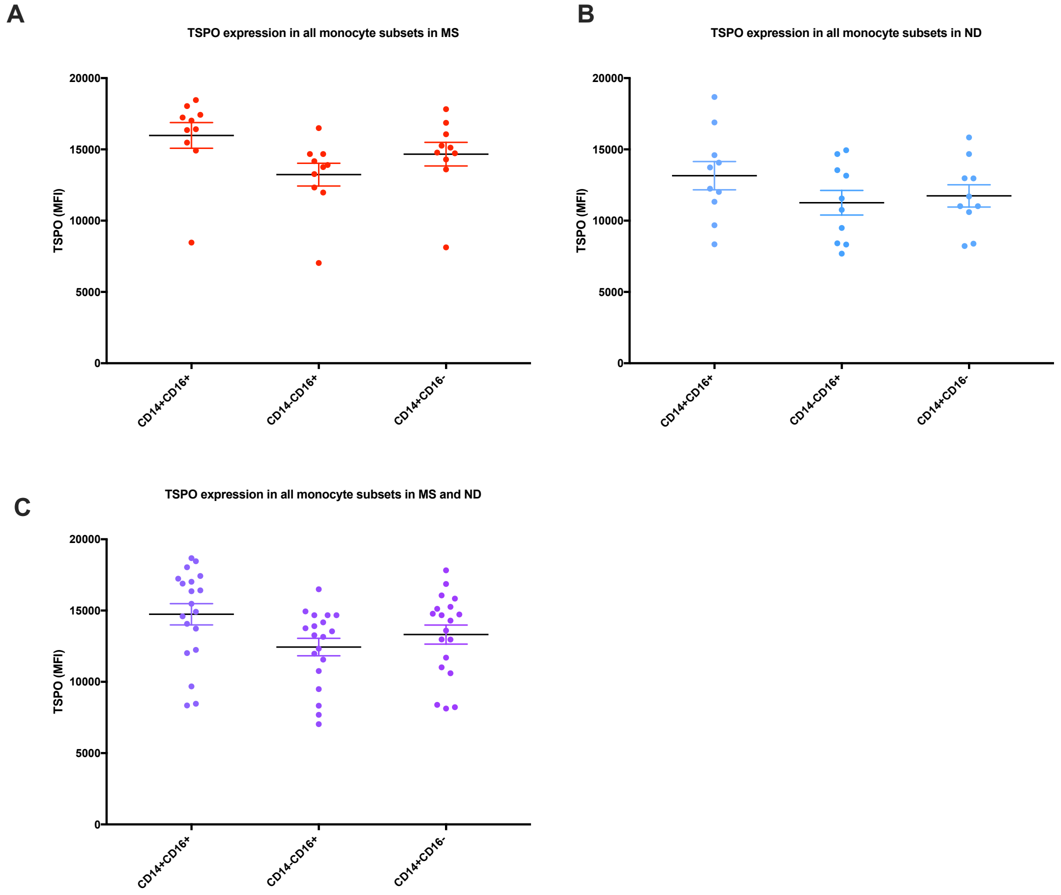

Figure 3-6. *A) Comparison of MFI of TSPO staining in CD14+CD16+, CD14-CD16+, and CD14+CD16- monocytes in all MS patients (n=10, p<0.0001). B) Comparison of MFI of TSPO staining in CD14+CD16+, CD14-CD16+, and CD14+CD16- monocytes in all normal donors (n=10, p<0.0001). C) Comparison of MFI of TSPO staining in all subjects in CD14+CD16+, CD14-CD16+, and CD14+CD16- monocytes in all subjects (n=20, p<0.0001).*

In both MS patients and normal donors, TSPO expression was found to be highest in CD14+CD16+ cells. The overall mean MFI of both patients and donors combined was 14570 ± 728 in CD14+CD16+ monocytes, 12243 ± 615.1 in CD16+CD14- monocytes, and 13203 ± 646.2 in CD14+CD16- monocytes (***Figure 3-6***C). The mean MFI of TSPO in MS patients was 15979 ± 902.5 in CD14+CD16+ monocytes, vs. 14667 ± 825.6 in CD14+CD16- monocytes and 13230 ± 798 in CD14-CD16+ monocytes, as shown in ***Figure 3-6***A, and monocyte subtype was found to be a significant source of variation by repeated measures ANOVA (n=10, p<0.0001). In normal donors, the mean MFI of TSPO was 13160 ± 991.3 in CD14+CD16+ monocytes, vs. 11739 ± 777.9 in CD14+CD16- monocytes and 11256 ± 862.5 in CD14-CD16+ monocytes (***Figure 3-6***, B). This variation was also was also found to be significant (n=10, p<0.0001).

3.3.2 Measuring TSPO expression as a biomarker of active disease in multiple sclerosis

A comparison of TSPO expression in monocytes and lymphocytes found that differences in TSPO expression between MS patients and age-, race-, and gender-matched healthy donors with contrast enhancing lesions (CEL) were predominantly attributable to an increase in TSPO expression in the monocyte gate (**Figure 3-7**). In a comparison of live single cells in fixed PBMC, TSPO expression in MS patients with CEL (2064 ± 115, n=10) was comparable to that of age- and gender-matched healthy donors (2002 ± 163.6, n=10) (p=0.7831). These values predominantly reflect the intensity of TSPO expression in CD3+ lymphocytes, which are the largest subpopulation of PBMC, constituting 60-70% of the live cell population. TSPO staining in lymphocytes from MS patients with CEL (1835 ± 80.14, n=10) was also comparable to that of healthy donors (1666 ± 109.3, n=10) (p=0.2296). The mean MFI of TSPO staining in monocytes, in contrast, was significantly higher (p=0.0227) in MS patients with CEL (14248 ± 825.5, n=10) than in the monocytes of matched healthy donors (11415 ± 782.6, n=10).

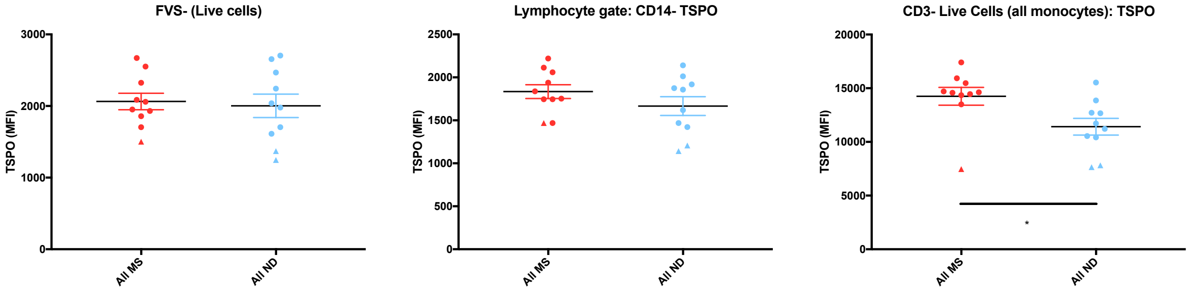

***Figure** 3-7. Comparison of median fluorescent intensity (MFI) of TSPO staining in distinct cell populations in MS patients with CEL and matched healthy donors.*
7a) Comparison of median fluorescent intensity (MFI) of TSPO staining in FVS- (live) single cells in MS patients with CEL and matched healthy donors (p=0.7831)
7b) Comparison of MFI of TSPO staining in gated lymphocytes in MS patients with CEL and matched healthy donors (p=0.02296).
*7c) Comparison of MFI of TSPO staining in FVS- (live) single cells after gating on CD3- monocytes in MS patients with CEL and matched healthy donors (p=0.0227). * indicates a p-value of less than 0.05.*

3.3.3 TSPO expression is significantly elevated in CD14+CD16+ and CD14+CD16- monocytes in MS patients with active disease when compared to matched controls

The differences in TSPO staining intensity in gated monocytes between MS subjects and age-, race-, and gender-matched healthy donors was predominantly reflective of differences expression in classical CD14+CD16- monocytes, which constitute the largest subject of monocytes in all donors. The intensity of staining was significantly higher (p=0.0157) in MS patients with CEL (14667 ± 825.6, n=10) than in age- and gender-matched healthy donors (11681 ± 755.4, n=10). A similar difference was observed in CD14+CD16+ monocytes, where the intensity of staining was significantly higher (p=0.0440) in the MS cohort (15979 ± 902.5, n=10) than in the normal controls (13109 ± 971.1, n=10). However, the mean MFI of TSPO staining in non-classical CD16+CD14- monocytes from MS patients with CEL was not significantly different from that of matched normal donors (p=0.0889). These findings are shown in **Figure 3-8**.

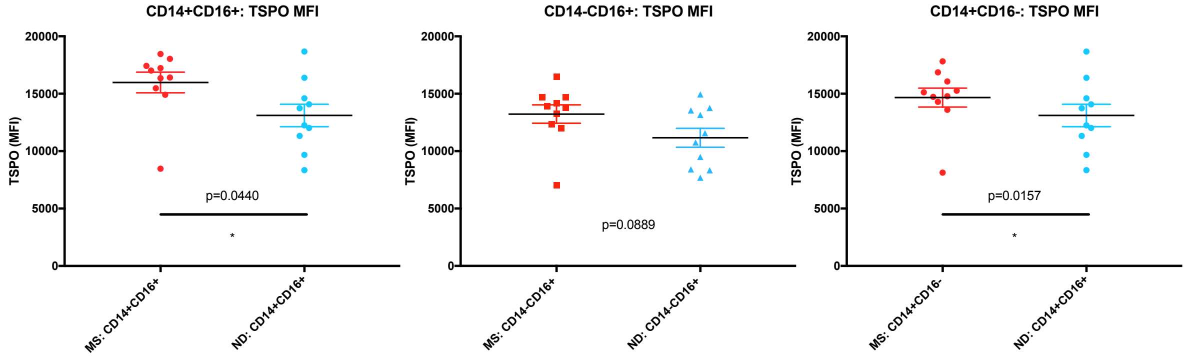

Figure 3-8. *Comparison of MFI of TSPO staining in CD14+CD16+, CD14-16+, and CD14+CD16- monocyte subsets in MS patients (MS, red) and normal donors (ND, blue). * denotes a p-value <0.05.*

Expression levels of HLA DR, CD86 and HSP60 were also compared in MS patients and healthy donors (**Figure 3-9**), but no significant differences were found in any monocyte subsets. Additionally, in contrast to TSPO, which is expressed at an intermediate level in classical CD14+CD16-, these other M1 markers exhibited a more classical pattern of expression, with CD14+CD16- classical cells exhibiting the lowest levels of M1 marker expression.

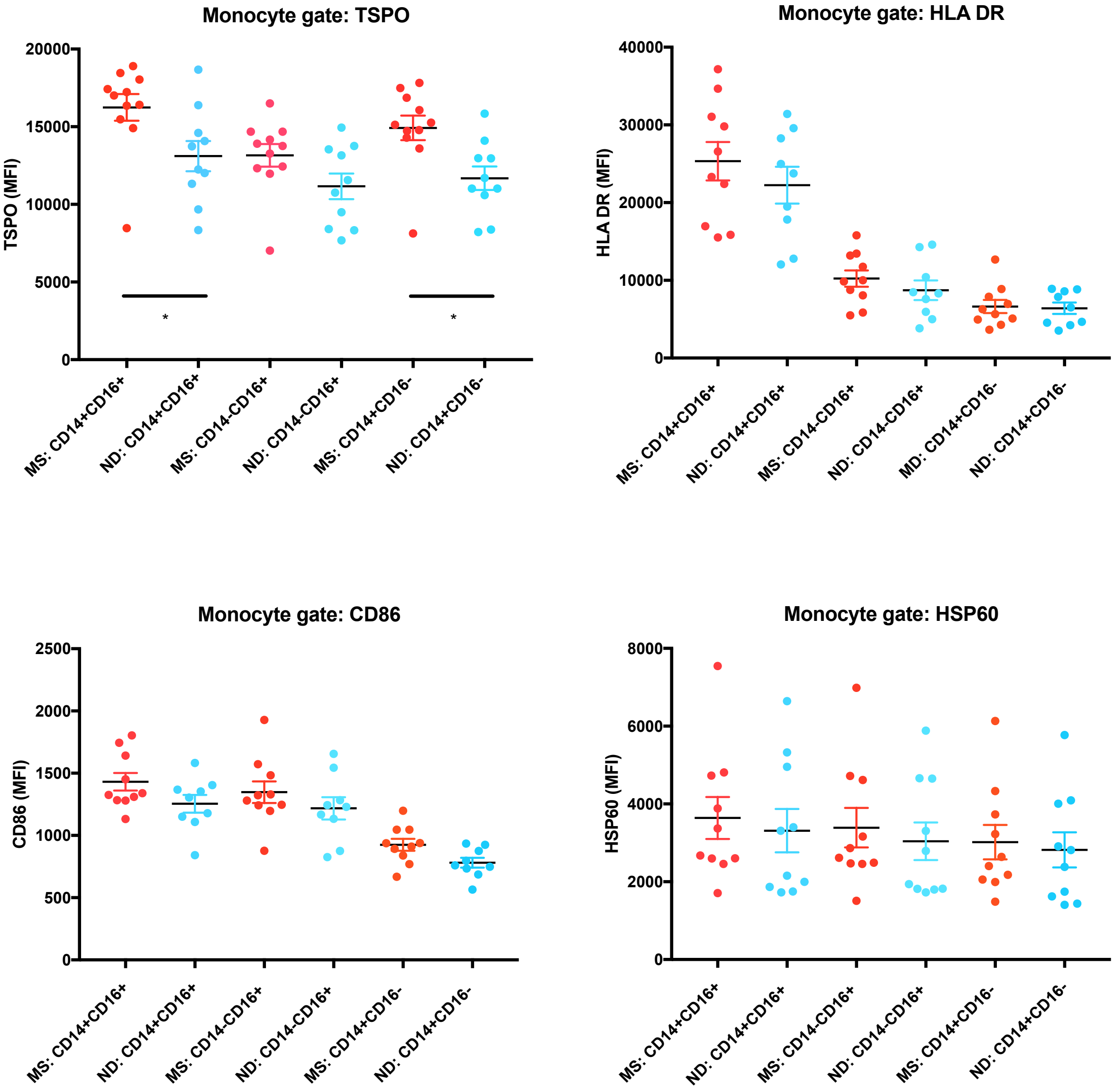

Figure 3-9. *Comparison of MFI of TSPO, HLA DR, CD86, and HSP60 staining in CD14+CD16+, CD14-16+, and CD14+CD16- monocyte subsets in MS patients (MS, red) and normal donors (ND, blue). * denotes a p-value <0.05.*

To further the probe the relationship between TSPO and immunophenotype, the MFI of TSPO staining was plotted against the MFI of HLA DR, CD86, and HSP60 staining as shown in **Figure 3-10**. For the most part, these relationships did not differ significantly between MS patients and controls. HLA DR appears negatively correlated with TSPO expression in CD14+CD16- and CD14+CD16- subsets, but this correlation was not significant. In CD16+CD14- atypical monocytes, HLA DR appears positively correlated with TSPO in MS patients, but this correlation was also not significant. No significant correlation was seen between CD86 and TSPO expression in any monocyte subset, regardless of disease status. A slight difference between patients and controls was seen in the relationship between TSPO expression and HSP60 expression. Controls exhibited a positive relationship between HSP60 and TSPO, in line with expectations that TSPO levels would increase in proportion to mitochondrial volume. In MS patients, in contrast, increases in TSPO expression were not associated with commensurate increases in HSP60 expression, as no significant relationship was observed between the two markers in the MS cohort.

A

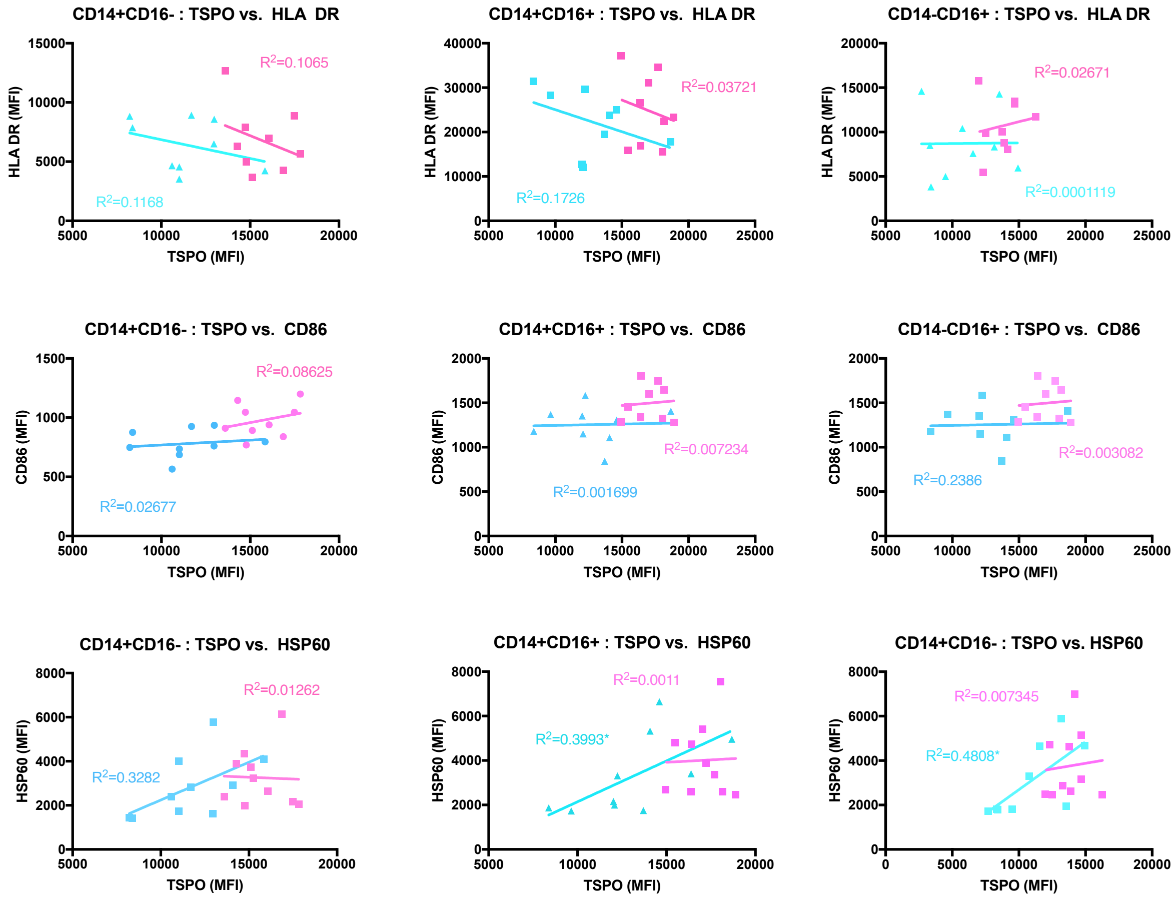

B

	CD14+CD16-	CD14+CD16+	CD14-CD16+
TSPO v. CD86 – MS	0.4431	0.8278	0.8872
TSPO v. CD86 – ND	0.6740	0.9162	0.1840
TSPO v. HLA DR – MS	0.3914	0.6190	0.6744
TSPO v. HLA DR – ND	0.3681	0.2661	0.9784
TSPO v. HSP60 – MS	0.9224	0.9275	0.8139
TSPO v. HSP60 – ND	0.0835	**0.0500***	**0.0383***

Figure 3-10. *TSPO vs. HLA DR, CD86, or HSP60 expression in CD14+CD16- (classical), CD14+CD16+ (intermediate), and CD14-CD16+ (non-classical) monocyte subsets in healthy controls (blue) and MS patients (pink). * denotes a p-value <0.05. B) P-values for TSPO vs. HLA DR, CD86, or HSP60 expression in CD14+CD16- (classical), CD14+CD16+ (intermediate), and CD14-CD16+ (non-classical) monocyte subsets. * denotes a p-value <0.05.*

3.3.4 TSPO expression patterns in marmoset PBMC are comparable to human PBMC

A modified flow panel was applied to two marmoset PBMC samples to measure TSPO expression in CD3+ lymphocytes and CD14+ monocytes. The MFI of TSPO staining in these two animal samples was found to be approximately two-fold higher in monocytes than in lymphocytes. A representative histogram of TSPO staining in monocytes and lymphocytes in shown in *Figure* **3-11**. To quantify TSPO in relevant subpopulations of monocytes and lymphocytes, a plot of forward scatter (FSC-A) vs. side scatter (SSC-A) was used to gate on whole cells ("CW") and exclude debris as shown in **Figure** *3-11***a**. After excluding debris, forward scatter (FSC-A) was plotted against DAPI staining signal in order to gate on DAPI+ whole cells as shown in **Figure** *3-11***b**. CD14-PE signal was then plotted against CD3-APC-Cy7 signal to separate CD3+ lymphocytes from CD14+ monocytes in **Figure** *3-11***c**. **Figure** *3-11***d** shows the intensity of TSPO staining in CD3+ lymphocytes (blue) and CD14+ monocytes (red). **Figure** *3-11***e** shows the intensity of MitoTracker Deep Red in CD3+ lymphocytes (blue) and CD14+ monocytes (red), thus indicating the mitochondrial volume found in each cell type. As seen in human PBMC, marmoset CD14+ monocytes contain higher mitochondrial content and higher levels of TSPO than CD3+ lymphocytes.

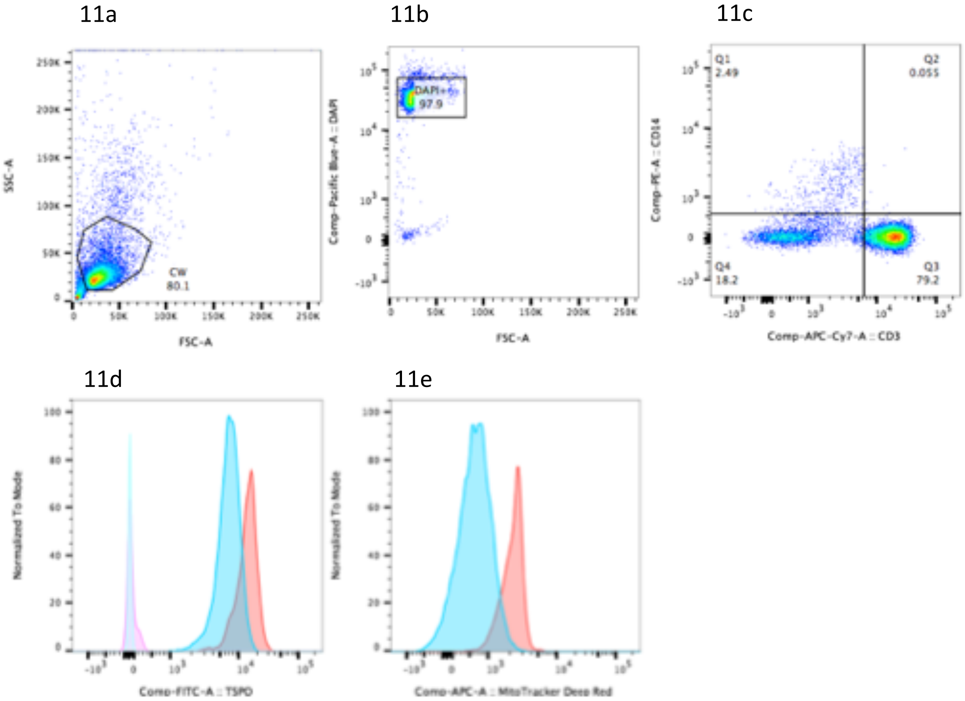

Figure 3-11. *Gating strategy for measuring TSPO and mitochondrial volume inCD3+CD14- lymphocytes and CD14+CD3- monocytes in whole live marmoset PBMC, with representative histograms of the staining intensity of TSPO and MitoTracker Deep Red in monocytes (red) and lymphocytes (blue).*
11a) Representative dot plot of forward scatter signal (FSC-A) vs. side scatter signal (SSC-A) with gating on "CW" population to exclude debris.
11b) Dot plot of FSC-A signal vs. DAPI in gated whole cells from Figure 11a with gating on DAPI+ nucleated cells to further exclude debris.
11c) Dot plot of CD14 PE signal vs. CD3 APC-Cy7 signal in whole nucleated from 11b) with quadrants drawn to define a CD3+CD14- lymphocyte population and a CD14+CD3- monocyte population.
11d) Comparison of intensity of TSPO staining intensity in CD3+CD14- lymphocytes (blue) vs. CD14+CD3- monocytes in a representative marmoset sample.
11e). Comparison of intensity of MitoTracker Deep Red staining intensity for the quantification of mitochondrial volume per cell in CD3+CD14- lymphocytes (blue) and CD14+CD3- monocytes in a representative marmoset sample.

3.4 **Discussion**

Not only did we detect significant differences in monocytic TSPO expression between MS patients with active disease and controls, but these differences were observed in both intermediate CD14+CD16+ and classical CD14+CD16- monocytes. There were no differences in the expression of HLA DR or CD86 in these subsets. The observation that these differences in TSPO expression were ultimately more pronounced and statistically more robust than differences detected in other markers suggests that TSPO expression in monocytes may be a superior marker of disease status than CD86 or HLA DR. However, the absence of any statistically significant relationship between TSPO and HLA DR or CD86 in any monocyte subset runs contrary to our hypothesis that TSPO would be associated with increased expression of M1 phenotypic markers. Ultimately, the only M1 marker that was found to correlate with TSPO was heat shock protein HSP60. Surprisingly, while a statistically significant positive relationship was detected between TSPO and HSP60 in CD14+CD16+ and CD14-CD16+ monocytes in normal donors, no relationship was found in MS patients with CEL. This discrepancy implies TSPO should increase in proportion to increases in mitochondrial volume in physiologic states yet fails to increase in multiple sclerosis. This is especially surprising given the significant increase in TSPO expression in the CD14+CD16+ subpopulation in MS patients and may indicate deficiency of TSPO relative to mitochondrial volume, despite the overall increase in TSPO expression.

Moreover, TSPO levels were observed to be highest in intermediate and classical monocytes, which are monocytes that express CD14 and possess a phagocytic phenotype [263,266,269]. Atypical monocytes, which express CD16 without CD14, expressed the lowest levels of TSPO relative to the other subsets. The observation that TSPO is highest in monocytes expressing a marker associated with phagocytosis may indicate that TSPO plays a role in a compensatory anti-inflammatory phagocytic response.

These findings are especially interesting in light of conflicting evidence in the literature regarding whether TSPO is marker of M1 or M2 phenotype in neuroinflammation and whether it is would be expected to increase or decrease in conditions of neuroinflammation. Studies of microglia in mice have found TSPO levels to increase with M1 stimulation [205], while studies of human macrophages have found TSPO to increase with M1 stimulation [204]. *Ex vivo* studies have observed TSPO in both M1 and M2 microglia in MS and animal models of CNS injury. As discussed previously, a 2012 study by Harberts et al. showed that PBR28 binding in PBMC is significantly lower in MS patients [213]. While this reduction may be attributed to a reduction in the size of the monocyte populations that exhibit the highest increases in TSPO relative to controls, my experiments found the size of the monocyte population was not significantly reduced in MS patients. The total TSPO expression of the PBMC sample is ultimately also determined by the CD3+ lymphocyte population, which is not significantly different in MS patients and expressed comparable levels of TSPO. Thus, changes in the relative sizes of these distinct subpopulations of PBMC would not explain the reduced levels of binding observed in Harberts's experiments.

On the basis of this study, we conclude that TSPO is significantly elevated in classical and intermediate monocytes in MS and that the detection and monitoring of TSPO expression in isolated PBMC may have potential utility as a peripheral biomarker of central neuroinflammation. We further conclude that isolated PBMC may provide a useful context to probe this seemingly paradoxical relationship between protein expression and binding. Preliminary studies of marmoset PBMC, while limited by tissue availability, suggest similar relationships may be observed and studied in the common marmoset.

3.4.1 Future directions

Many questions remain regarding the relationship between TSPO expression, disease status, and disease progression in this study: Is the elevation of TSPO in PBMC in MS patients with contrast-enhancing lesions a reflection of their current exacerbation or an intrinsic component of their disease status? Is the expression of TSPO in these subjects influenced by treatment? The patients included in this study were untreated or on first-line therapies, such as interferon- β or glatiramer acetate. Patients on second-line immunosuppressive therapies and patients who had received steroid therapies for acute exacerbations within the six months prior to their visit were excluded.

Due to subject availability, this study did not seek to compare TSPO expression between untreated patients and patients on first-line therapies. Within the cohort selected for this study, there was no evident difference in TSPO expression between untreated patients and patients on first-line therapies. However, we do not know whether these first-line therapies may influence TSPO expression in patients who received them therapies. Therefore, we cannot exclude the possibility that a difference would be seen between untreated and first-line-treated patients with a higher number of subjects. Moreover, we have not probed the effect of second-line immunosuppressive therapies. In future studies, it would be ideal to include higher numbers of untreated, first-line-treated, and second-line-treated patients. Alternatively, we may seek to monitor patients longitudinally and measure TSPO expression at multiple points in the course of treatment e.g. before and at multiple time points after steroid treatment for acute exacerbations. Specifically, I would select 10 patients with active CEL who are untreated at the time of lesion detection, and 10 patients without clinical or radiological evidence of active disease. I would then compare TSPO levels, mitochondrial volume, and immunophenotype in classical, non-classical, and intermediate monocytes in these subjects using the same antibody panel described in this chapter (CD14, CD16, CD3, TSPO, CD86, HLA DR, HSP60).

Another limitation of this chapter is that it includes only a preliminary investigation of the potential use of TSPO as a peripheral biomarker in marmoset EAE. Due to extremely limited sample availability, the intensity of TSPO staining and mitochondrial volume was measured in CD14+ monocytes and CD3+ lymphocytes in only two healthy common marmosets. We were not able to detect CD16+ monocytes or measure immunophenotypic markers such as CD86 and HLA DR due to the absence of commercially available antibodies capable of cross-reacting with these epitopes in marmoset tissue. Future experiments would ideally investigate the differences in TSPO expression in CD14+ monocytes in larger numbers of healthy and EAE-affected marmoset and would give insight into the significance of TSPO expression in an induced experimental autoimmune disease.

Specifically, I would propose to collect and isolate PBMC from 1 ml of blood from 6 healthy marmosets prior to EAE induction. I would then propose to collect and isolate PBMC from the same marmosets at one-month intervals after EAE induction. Our MRI protocol of biweekly scanning would likely facilitate the detection of animals with active contrast-enhancing lesions, allowing the comparison of TSPO in PBMC in animals with CEL to TSPO in animals without active lesions. However, as IRB protocols limit the volume of blood to drawn from a single marmoset in a one-month period, drawing blood from an animal at fixed time-points would likely preclude drawing additional samples in response to clinical or radiological changes. I would then thaw samples from the same animal before and after EAE induction and run same-day cytometric analyses of TSPO expression in CD14+ monocytes and CD3+ lymphocytes. I would then perform a paired T-test to determine if TSPO levels are significantly different before and after EAE induction.

Finally, while using flow cytometry allows the direct measurement of TSPO protein levels with antibody-conjugated probes, it does not necessarily give insight into the utility of

TSPO as a PET imaging target. Further studies are needed to determine if TSPO protein levels correlate directly to ligand-binding levels. This challenge is explored further in Chapter 4.

4 Comparison of TSPO protein expression and TSPO radioligand-binding in peripheral blood mononuclear cells in multiple sclerosis

4.1 Introduction

The detection and monitoring of biomarkers of neuroinflammation in the central nervous system may offer a means of both diagnosing neurological disease and determining disease prognosis and treatment [62–66]. The imaging of PET radioligands offers the possibility of detecting such biomarkers in vivo in health and disease and monitoring changes in expression over time as disease symptoms progress or regress [62–66]. However, there are both cost limitations and health considerations that may restrict the utilization of this technology in a clinical context. The process of PET scanning itself requires significant infrastructure and clinical resources and would ultimately subject the patient to radiation exposure [257]. Serial monitoring of a chronic disease such as MS would dramatically increase this exposure over time [257].. Moreover, it is not always possible to ascertain how accurately ligand-binding reflects protein expression *in vivo*. The requirement of an invasive procedure for the procurement of brain tissue and CSF limits the detection of TSPO protein in living subjects to patients with medical conditions where surgical procedures are medically justified, such as tissue resection for epilepsy or tumor resection. The correlation of PET signal to pathology in MS is especially limited, as biopsies in MS subjects are relatively rare – studies of pathology in MS may be obtained from autopsy in patients with advanced disease or patients who died of other causes, but biopsies from earlier stages of disease are generally obtained due to an atypical presentation, in tissue sampling is necessary to assess for infection or malignancy [81,237].

Whole blood, in contrast to brain tissue, is a source of tissue that is easily accessible in a clinical setting and may be procured regularly during clinical visits at various stages of treatment and disease progression. Isolated peripheral blood mononuclear cells (PBMC) may be readily cryopreserved for different applications and assay types without requiring the methods of fixation that result in the modification of ligand-binding epitopes.

Isolated PBMC, in this sense, constitute an ideal tissue source to probe the relationship between TSPO expression in the periphery and radioligand binding, which has been called into question by previous studies. Multiple studies have found decreased TSPO mRNA levels in neuropsychiatric disorders such as anxiety [201,214,215,217,218,270,271]. For example, a 1996 study by Gavish et al. found decreased PK11195 binding in platelets harvested from patients with anxiety disorders[271]. An 1998 study found reduced TSPO protein density in the platelets of patients with generalized anxiety disorders [215], while a later 2008 study of protein levels indicated reduced protein density in the platelets of patients with depression and adult separation anxiety [214]. It was believed that the apparent reduction in TSPO levels in diverse psychiatric conditions may constitute a biomarker of disease status and that TSPO expression might rise with treatment. However, a recent study of TSPO protein expression in the platelets of patients treated for depression and anxiety challenged the hypothesis that TSPO expression would increase with treatment [218]. Instead, TSPO levels were found to decrease after therapy in all treated subjects [218]. Thus, further studies are needed to understand changes in TSPO protein expression in disease, as well the relationship between protein expression and ligand-binding.

A 2012 study of TSPO in the peripheral blood of MS patients surprisingly found a significant reduction in TSPO binding with second-generation ligand PBR28 in isolated PBMC [228]. While this decrease was presumed to reflect a decrease in TSPO expression in the peripheral blood, the study did not directly measure TSPO protein expression in the same PBMC samples [228], and therefore, it is unknown whether TSPO radioligand-binding directly reflects TSPO protein levels in peripheral blood and therefore, it is not certain that TSPO protein levels are truly decreased in MS patients.

Moreover, the comparison of TSPO radioligand-binding and TSPO protein expression in humans is further complicated by the existence of the rs6971 polymorphism, a single-nucleotide polymorphism that results in the substitution of a nonpolar alanine residue in the TSPO molecule with a polar threonine residue [9,77,270,272,273]. This substitution abrogates TSPO binding by second-generation ligands, such as PBR28, such that homozygous carriers of the allele will express exclusively low-affinity binding sites while heterozygous carriers will express a combination of high-affinity and low-binding sites in equal proportions, resulting in intermediate binding activity on binding [77,274]. To account for the effect of this polymorphism on ligand-binding in diverse human subjects, it is necessary to ensure patients and healthy subjects are matched on the basis of rs6971 genotype. Therefore, we seek to determine if a protein expression and TSPO-radioligand binding may be correlated in isolated PBMC from genotype-matched patients and healthy donors. My aim is to compare patterns of TSPO expression determined by flow cytometry with trends in ligand-binding by second-generation ligand ^{3}H-PBR28 in cell suspensions of thawed PBMC. The ability to detect TSPO ligand binding with PET radioligands in the peripheral blood represents a npotential non-invasive method of monitoring inflammatory activity related to disease progression. The opportunity to measure both protein expression and radioligand-binding in the same blood sample with our collaborators in the UK gives us a crucial opportunity to directly compare the accuracy with which different radioligands reflect TSPO expression.

Summary of Aim 3

Question: Do changes in TSPO expression in PBMC in MS correlate directly to changes in ligand-binding with second-generation TSPO ligands?

Specific Aim: I aim to measure TSPO-ligand binding with second-generation ligand PBR28 in MS patients and matched healthy donors and compare levels of TSPO-radioligand-binding with levels of TSPO protein expression measured in Aim 2.

Specifically, I will measure and compare ligand-binding with second-generation TSPO radioligand PBR28 in isolated cell membranes and whole PBMC in MS patients with contrast-enhancing lesions and age-, race-, and gender-matched normal donors.

Hypothesis: I hypothesize that TSPO expression is correlated directly to ligand-binding in human PBMC from MS patients and matched healthy controls.

4.2 **Methodology**

4.2.1 Division of responsibility

Blood draws were performed by clinical staff as described in Chapter 3. I performed mRNA extraction, cDNA synthesis, and primer design for genotyping. KASP genotyping was performed by LGC Genomics (Teddington, Middlesex, UK). I performed all radioligand-binding experiments and data analyses.

4.2.2 PBMC isolation

Whole blood or lymphocyte aphereses were obtained from the NIH Blood Bank. All subjects provided informed written consent under a National Institutes of Health Clinical Center Institutional Review Board-approved research protocol. The peripheral blood mononuclear cells (PBMC) were collected after separation on a Ficoll gradient using lymphocyte separation medium (BioWhittaker, Walkersville, MD) and cryofrozen in RPMI-1640 containing 10% fetal bovine serum and 10% dimethyl sulfoxide (DMSO) for storage in liquid nitrogen as described previously. Samples from healthy donors (HD) (*n*=7) and MS patients (*n*=7) were of similar demographics, which are described in Sections 3.2.10-3.2-17. Subject demographics are shown in **Table 4-1** and **Table 4-2**.

Genotype	Subject	Gender	Ethnicity	Age	MS subtype	CEL	Treatment
HAB	1	F	White	40	RRMS	present	None
HAB	2	F	AA	45	RRMS	present	Tecfidera
HAB	3	M	Latino	42	RRMS	present	None
HAB	4	F	white	29	RRMS	present	Copaxone
MAB	1	F	white	26	RRMS	present	None
MAB	2	F	AA	42	RRMS	present	None
MAB	3	F	AA	44	*RRMS*	present	Copaxone

Table 4-1. *Genotype, demographics (gender, ethnicity, age), MS subtype, presence of contrast-enhancing lesions (CEL) and treatment status of MS patients included in this study.*

Genotype	Subject	Gender	Ethnicity	Age
HAB	1	F	AA	50
HAB	2	F	AA	45
HAB	3	M	Latino	42
HAB	4	F	white	32
MAB	1	F	white	22
MAB	2	F	white	51
MAB	3	F	white	44

Table 4-2. *Genotype, demographics (gender, ethnicity, and age) of normal donor included in this study.*

4.2.3 TSPO genotyping

De-identified patient and normal donor PBMC samples from 25 patients and 25 normal donors were assigned alphanumerical IDs and genotyped to detect the rs6971 polymorphism. 1 x 10^6 thawed PBMC were washed in PBS and reserved for mRNA extraction and cDNA synthesis. Subjects were categorized as high-, low-, or non-binders on the basis of genotype, so that patients and normal donors could be matched in terms of genotype, as well as gender, and age were possible.

4.2.4 mRNA extraction

mRNA extraction was performed using a Qiagen RNAeasy Kit (Qiagen, Germantown, PA). 1 x 10^6 thawed PBMC were washed in FACS buffer (1% heat-inactivated fetal bovine serum, 0.1% sodium azide in PBS) and lysed in 350 µl RLT buffer (Qiagen, Germantown, PA). The lysate was centrifuged at 20835 x G for 3 minutes, and the supernatant was collected and combined with an equal volume of 70% molecular-biology grade ethanol. The combined volume was transferred to an RNA microcentrifuge column, which was centrifuged at 8000 x G for 30 seconds, after which the flow-through was discarded and the column was rinsed with 350 µl RW1 buffer (Qiagen, Germantown, PA). After the first wash, 80 µl DNAse I in RDD buffer (Qiagen, Germantown, PA) was added to the column and incubated for 15 minutes at room temperature. The column was washed twice with 500 µl RPE buffer (Qiagen, Germantown, PA) and centrifuged at 8000 x G for 30 seconds on the first wash and 2 minutes on the second wash. The column membrane was dried by centrifuging for 1 minute in an empty collection tube. mRNA was eluted in 40 µl Rnase-free water into a collection tube by centrifugation at 8000 x G for 1 minute. The mRNA concentration of the resulting eluent was quantified using a Nanodrop 2000c spectrophotometer (Thermo Scientific, Waltham, MA). Isolated mRNA samples were stored at -80C for subsequent cDNA synthesis.

4.2.5 cDNA synthesis

To reduce mRNA secondary structures and facilitate primer annealing, 75 or 150 µg of purified mRNA was incubated with an equivalent quantity of RT Random Primer mix (Promega, Madison, WI) and RNase-free water in a total reaction volume of 15 µl at 70^{o}C for 10 minutes, after which the samples were immediately cooled on ice. The following were added to the annealed sample: 5 µl 5x Reaction Buffer (250mM Tris-HCl, pH 8.3 at 25°C), 375mM KCl, 15mM $MgCl_2$, 50mM DTT), 1 µl Reverse Transcriptase, and 1 µl dNTP. RNase-free water was added to bring the total reaction volume to 40 µl. The samples were incubated for 1 hour at 37C in a C1000 Touch ThermoCycler (Bio-Rad, Deeside, UK). The resulting cDNA was stored at -20^{o}C for subsequent KASP genotyping assays.

4.2.6 KASP™ Genotyping Assays

A patented proprietary genotyping assay was provided by LGC Genomics (Teddington, Middlesex, UK). Briefly, mRNA was extracted from thawed PBMC and used for cDNA synthesis, as described in previously. The resulting cDNA was processed by LGC genomics to detect the rs6971 polymorphism.

KASP™ genotyping assays use competitive allele-specific PCR to enable bi-allelic scoring of single nucleotide polymorphisms (SNPs). In this assay, allele-specific primers are combined with a KASP Master mix containing two universal fluorescence resonant energy transfer (FRET) cassettes consisting of oligonucleotide sequences conjugated to fluorescent dyes FAM and HEX. Initially, these dyes are quenched by the binding of complementary strand conjugated to a quenching molecule. In addition, the master mix contains a passive reference dye (ROX), Taq polymerase, free nucleotides, and $MgCl_2$ in an optimised buffer solution (LGC Genomics, Teddington, Middlesex, UK).

The gene-specific primers used in each assay are non-labelled oligonucleotides consisting of two allele-specific forward primers—each binding one of two alleles of interest— and one common reverse primer. The allele-specific forward primers each contain a unique 5’ tail sequence that that is also contained in either the universal FAM-conjugated FRET cassette or the HEX-conjugated FRET cassette. During thermal cycling, the relevant allele-specific forward primers bind to the template and elongated. In subsequent cycles, the newly synthesized strands generated from the elongation of these forward primers are bound by the common reverse primer. The elongation of the reverse primer generates a sequence complementary to the forward primer, including the allele-specific 5’ tail sequences on the forward primer. This complementary sequence of the generated from the dye-conjugated oligonucleotide in the FRET cassette, displacing the sequence conjugated to the quenching molecule. The displacement of the quenching element results in the emission of fluorescence.

If the patient is homozygous for the allele bound by the allele-specific forward primer corresponding to the HEX-conjugated cassette, only the HEX dye will fluoresce. If the patient is homozygous for the allele bound by forward primer corresponding to the FAM-conjugated cassette, only the FAM dye will fluoresce. If the patient is heterozygous and expresses both alleles, a mixed fluorescent signal will be detected. By assaying at the site of the rs6971 polymorphism, patients were categorized as high-affinity binders (C:C), medium-affinity binders (C:T), or low-affinity binders (T:T).

The following primers were used to assay for the TSPO rs6971 polymorphism:
Forward: 5’-GCGGCCTGGCTAACTCCTGC-3’
Reverse: 5’-AAAGCGGGAGCCCACGAAGC-3’

4.2.7 PBMC Membrane Isolation

PBMC frozen in FACS buffer at a concentration of 20 million cells per ml were thawed at room temperature, resuspended, and diluted 1:10 in Buffer 1 (0.32mM Sucrose, 5mM Tris Base, 1mM $MgCl_2$, pH 7.4). These diluted cell suspensions were homogenized using a Polytron PT1200 (Kinematic, Bohemia, NY) on speed setting 4 for 4 cycles consisting of 30 seconds of homogenization followed by 15 seconds of cooling on ice. The resulting homogenate was centrifuged at 32,000 x G for 20 minutes at 4^oC to pellet cell membrane components. The supernatant was removed, and the pellet was washed twice by resuspension in 5 ml of Buffer 2 (50mM Tris HCL, $MgCl_2$, pH 7.4), followed by centrifugation at 32,000 x G for 20 minutes at 4°C. Following the second wash, the pellet was reconstituted in 5 ml of Buffer 2. The protein concentration of the resulting suspension was quantified using a Bicinchoninic acid assay (Sigma-Aldrich, UK).

4.2.8 Bichinchoic Acid Assay

Homogenates prepared from PBMC cell suspensions were quantified using a BCA kit from Sigma Aldrich (UK) according to manufacturer's provided protocol. Briefly, diluted albumin standards ranging from 20-2000 µg/ml were prepared in Buffer 2 using a provided bovine serum albumin (BSA) stock solution. 25 µl of each standard and sample were aliquoted in triplicate in a 96-well microplate. To prepare the working reagent, 4% cupric acid (Reagent B) was diluted 1:50 in Reagent A, a solution containing sodium carbonate, sodium bicarbonate, bicinchoninic acid and sodium tartrate in 0.1M sodium hydroxide. 200 µl of the working reagent was added to each well using a multichannel pipette. The plate was agitated gently for 30 seconds and incubated for 30 minutes at 37°C. The plate was then allowed to cool for 5 minutes and a GloMax Discover System Microplate Reader (Promega, Madison, WI) was used to measure the absorbance of each well at 560 nm.

4.2.9 Radioligand binding assay

Thawed PBMC from healthy donors and patients classified as high-affinity, medium-affinity, or low-affinity PBR28 binders were pelleted by centrifugation at 400 x G to remove DMSO used in their cryopreservation, re-suspended in RPMI containing 10% heat-inactivated fetal bovine serum, and counted in Trypan Blue using a TC20 Automated Cell Counter (Bio-Rad, Hertfordshire, UK) to determine cell number and viability. Following cell counting, PBMC were re-suspending in FACS buffer to a concentration of 20 million cells per ml. Aliquots of 10 or 20 million cells were frozen for subsequent ligand binding studies. Prior to each ligand binding study, aliquots were thawed on ice and re-suspended in cold RPMI-1640 to a final concentration of 500,000 cells per ml. Stock concentrations of ^{3}H-PBR28 were prepared in Buffer 3 (50mM Tris Base, 140mM NaCl, 1.5mM $MgCl_2$, 5mM KCl, 1.5 $CaCl_2$, pH 7.4).

To measure total ligand binding in medium-affinity binders, 200,000 cells were incubated, in triplicate, for 60 min at room temperature, with ^{3}H-PBR28 alone at the following concentrations: 100 nM, 50 nM, 30 nM, 10 nM, 3 nM, 1 nM, 0.3 nM, and 0.1 nM. To measure nonspecific ligand binding, 200,000 cells were incubated in triplicate with 10 nM "cold" ^{1}H-PBR28 and ^{3}H- PBR28 at the concentrations listed previously.

To measure total and nonspecific ligand binding in high-affinity binders, 50,000 cells were incubated, in triplicate, for 60 min at room temperature, with either ^{3}H-PBR28 alone or 10 nM "cold" ^{1}H-PBR28 and ^{3}H-PBR28 at the previously listed concentrations.

After incubation, the cells were harvested using a TomTec Harvester 96 Mach III M over a glass fibre filter paper (PerkinElmer) in Buffer 4 (50mM Tris Base, 1.4mM $MgCl_2$). The harvested cells from each well were retained in the filter paper, which was then placed in 2 ml scintillation fluid (PerkinElmer, Waltham, MA) and allowed to incubate for 4 hours at room temperature before counting. Radioactivity per well was counted using a 1450 MicroBeta TriLux Plate Reader (PerkinElmer, Waltham, MA). The mean specific binding was calculated by subtracting the mean nonspecific binding from the mean total binding at each concentration of ^{3}H-PBR28.

To account for experimental error in the preparation of ^{3}H-PBR28 stock solutions and more precisely quantify the concentration of ^{3}H-PBR28 in each well, the radioactivity of each stock concentration was measured by diluting 5 µl of the stock solution in 2 ml scintillation fluid. These dilutions were prepared in triplicate and the radioactivity of each dilution was measuring using a 1450 MicroBeta TriLux Plate Reader. The mean radioactivity counts of each stock solution was plotted against the specific binding of cells incubated with that stock solution in GraphPad (Prism 7). A two-site and one-site binding curve was fitted to each plot and a comparison of fits was performed.

4.2.10 Statistical Analysis

Data are expressed as a mean ± SEM of (n) independent experiments. Two-tailed students t-tests were used to assess significance. A p-value of less than or equal to 0.05 was considered significant.

4.3 **Results**

4.3.1 Assay Optimization

To determine the best method of isolating TSPO for binding studies, ^{3}H-PBR28 binding in isolated PBMC was compared to ^{3}H-PBR28 binding in membranous organelles isolated from homogenized PBMC. PBMC were isolated from whole blood using a ficoll-separation protocol. Membrane isolation was performed on homogenized PBMC using ultracentrifugation. ^{3}H-PBR28 binding for a given quantity of cells in suspension was compared to ^{3}H-PBR28 binding in a suspension of protein extracted from the same quantity of cells. For example, as membrane isolation from 1 million cells yielded 20 μg of protein, ^{3}H-PBR28 binding in suspensions of 1 million cells, 500,000 cells, 250,000 cells, and 125,000 cells were compared to ^{3}H-PBR28 binding in suspensions of 20 μg, 10 μg, 5 μg, and 2.5 μg of protein, respectively.

As shown in **Figure 4-1,** total specific binding of ^{3}H-PBR28 in homogenized PBMC after membrane isolation ranged from 250 DPM per 5 μg of protein to 2500 DPM per 20 μg of protein. Total specific binding of ^{3}H-PBR28 in isolated PBMC ranged from 2500 DPM per 125,000 cells to 21,000 DPM per 1 million cells. Measurement of radioligand binding in whole isolated PBMC was determined to provide a much higher signal-to-noise ratio than measurement of binding in isolated membrane-bound proteins and subsequent radioligand binding assays were performed on whole isolated PBMC.

Subsequently, total, nonspecific and specific binding curves were generated for ^{3}H-PBR28 binding in whole PMBC cell suspensions containing 200,000 cells per well. Total ^{3}H-PBR28 binding was quantified in triplicate at 0.1, 0.3, 1, 3, 10, 30, 100 and 100 nM concentrations of ^{3}H-PBR28. Nonspecific ^{3}H-PBR28 binding was quantified in triplicate at 0.1, 0.3, 1, 3, 10, 30, 100 and 100 nM ^{3}H-PBR28 in the presence of 10 μM non-tritiated ^{1}H-PBR28. Mean nonspecific binding was subtracted from mean total binding to calculate specific binding at each concentration. The resulting curves are shown in **Figure 4-2**.

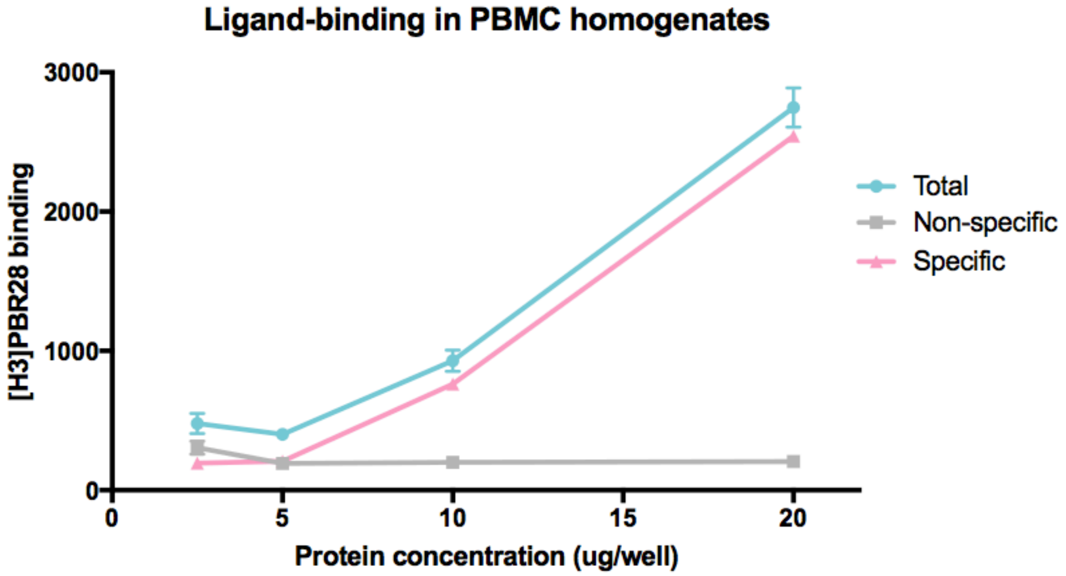

A

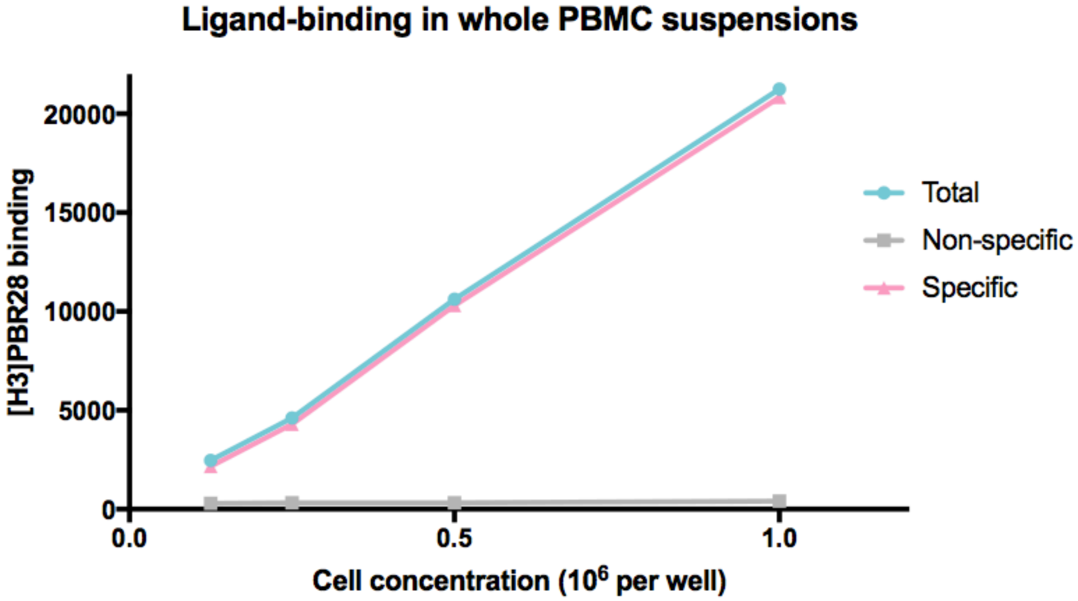

B

Figure 4-1. *Comparison of total, non-specific, and specific ^{3}H- PBR28 binding in protein homogenates isolated from PBMC and whole PBMC.*

a) *Comparison of total (blue), nonspecific (gray), and calculated specific ^{3}H- PBR28 binding (pink) in PBMC homogenate at protein concentrations ranging from 5-20 µg per well.*
b) *Comparison of total (blue), nonspecific (gray), and calculated specific binding (pink) in suspension of whole cells at concentrations ranging from 250,000 to 1 million cells per well.*

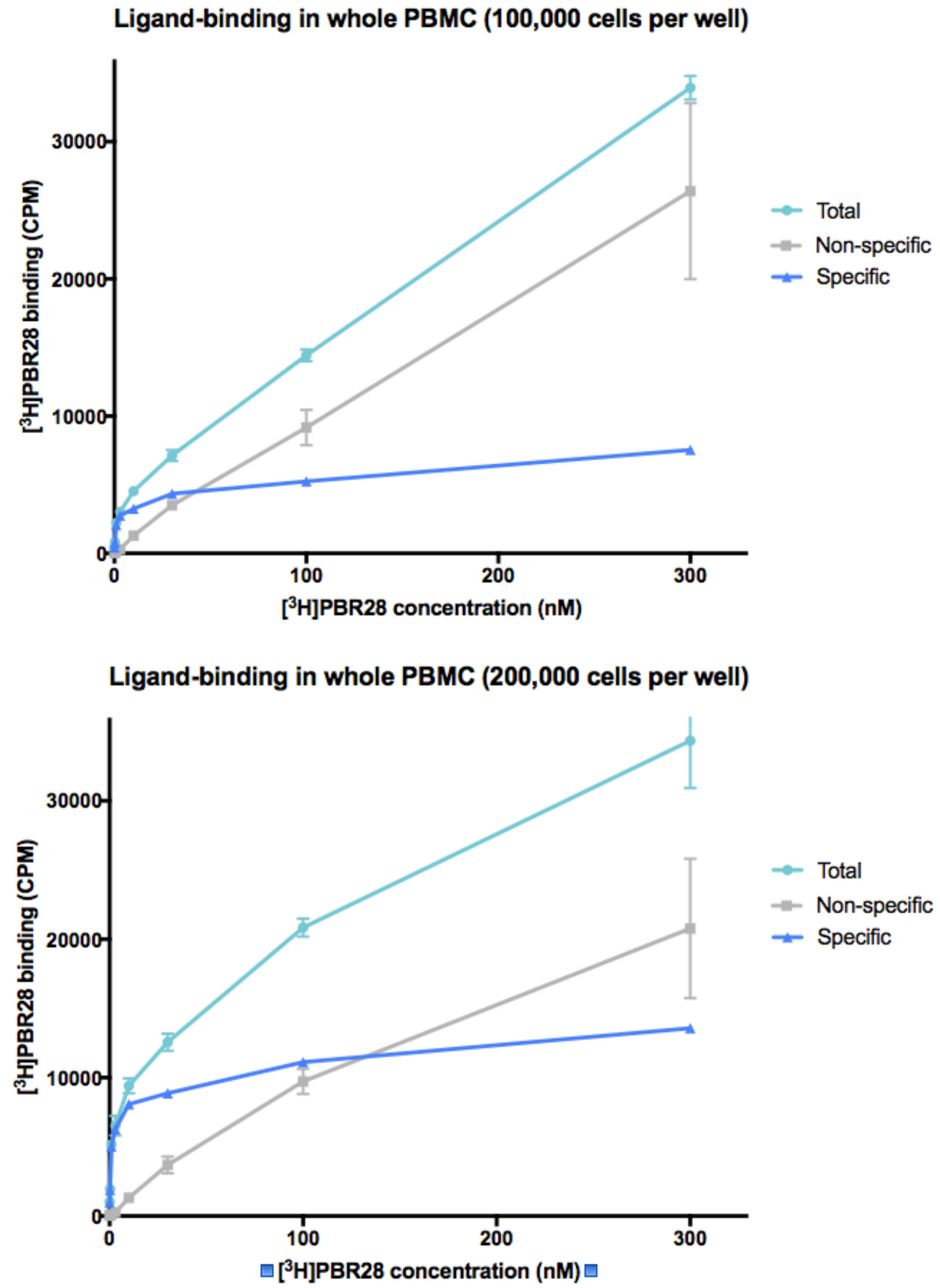

Figure 4-2. *A) Comparison of total (light blue), nonspecific (gray), and calculated specific binding (dark blue) in suspensions of whole PBMC (100,000 cells per well) at ^{3}H-PBR28 concentrations of 0.1, 0.3, 1, 3, 10, 30, 100, and 300 nm. B) Comparison of total (light blue), nonspecific (gray), and calculated specific binding (dark blue) in suspensions of whole PBMC (200,000 cells per well) at ^{3}H-PBR28 concentrations of 0.1, 0.3, 1, 3, 10, 30, 100, and 300 nm.*

Subsequently, binding curves were generated for known MABs and HABS at different cell concentrations to determine the optimal cell number. To determine the cell numbers necessary to measure specific binding in medium-affinity binders, two ^{3}H-PBR28 binding curves were generated using either 100,000 cells or 200,000 cells per well. Curves generated using 200,000 cells per well were found to have less variation and subsequent experiments with MAB donors used 200,000 cells per well. As shown in **Figure 4-3**, a comparison-of-fits was performed comparing one-site and two-site binding curves. A two-site curve was found to provide the best fit, as indicated by an R^2 value of 0.9965 and an absolute sum-of-squares of 12,465,824. Moreover, the calculated percentage of binding sites with high-affinity binding characteristics was determined to be 46.12%, which is consistent with studies in vitro which show high- and low-affinity binding sites exist at a 1:1 ratio in medium-affinity binders, each constituting approximately 50% of available binding sites [8,274].

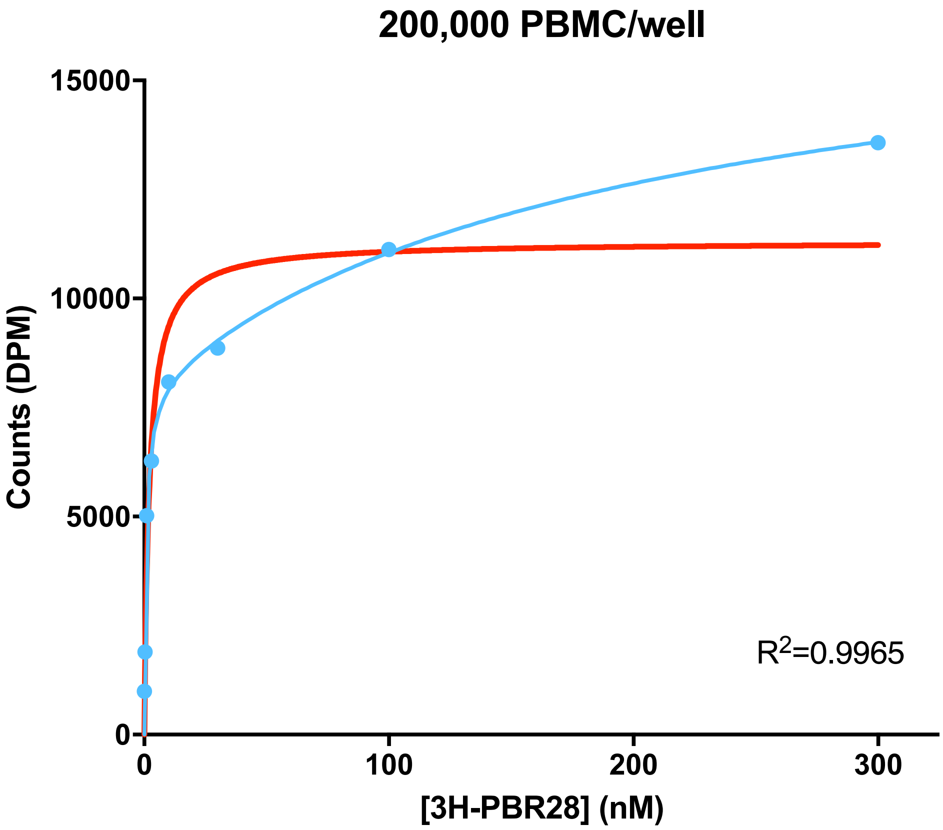

Figure 4-3. *Comparison-of-fits for one-site (red) and two-site (blue) binding curves fitted to specific binding values generated for PBMC (200,000 cells per well) from a known MAB healthy donor.*

To determine the cell numbers necessary to measure specific binding in high-affinity binders, two ^{3}H-PBR28 binding curves were generated using either 50,000 cells or 25,000 cells per well. In high affinity binders, it was determined that at least 50,000 cells per well was necessary to generate an accurate binding curve (R^2=0.9956). Experiments with fewer cells yielded results with much higher variation (R^2=0.9893) (**Figure 4-4**).

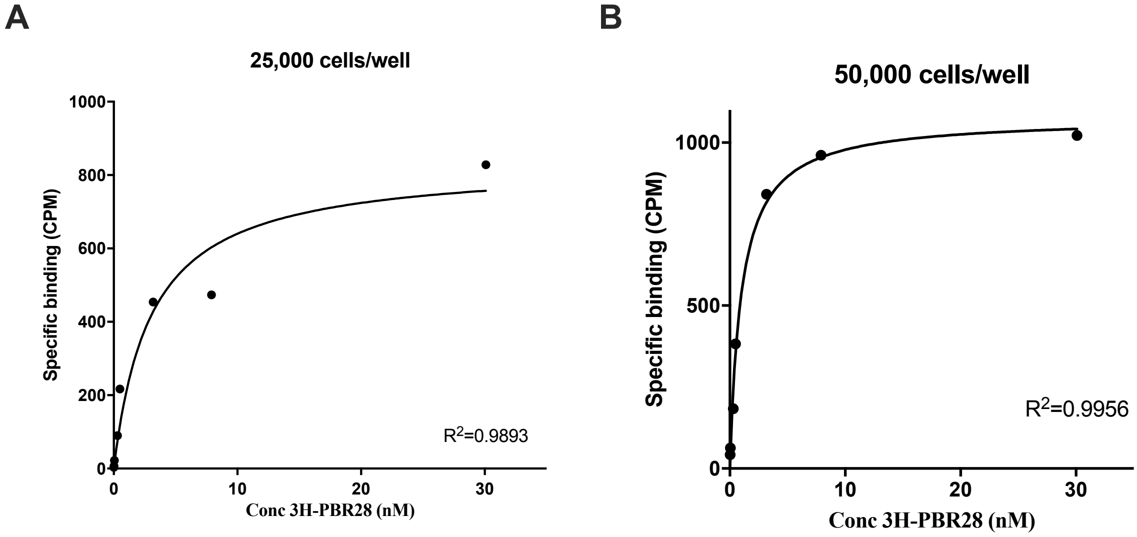

Figure 4-4. Comparison of one-site binding curves fitted to calculated specific binding values generated for a known HAB donor in wells containing A) 25,000 or B) 50,000 cells per well.

4.3.2 TSPO-^{3}H-PBR28 binding is lower in MS patients than in genotype-matched healthy donors

Following assay optimization, three MS patient MABs were compared with three normal donor MABs. Each patient was paired to a normal donor and the pairs were thawed and assayed concurrently on the same day. Despite finding no significant difference in TSPO expression between these subsets of MS subjects and normal donors, the MS subjects displayed much lower levels of signal intensity at 300 nM [^{3}H-PBR28] (1432.78±239.3, n=3) when compared to the normal donors (2845.00±217.6, n=3) as demonstrated in **Figure 4-5**. This difference was statistically significant (p=0.0112).

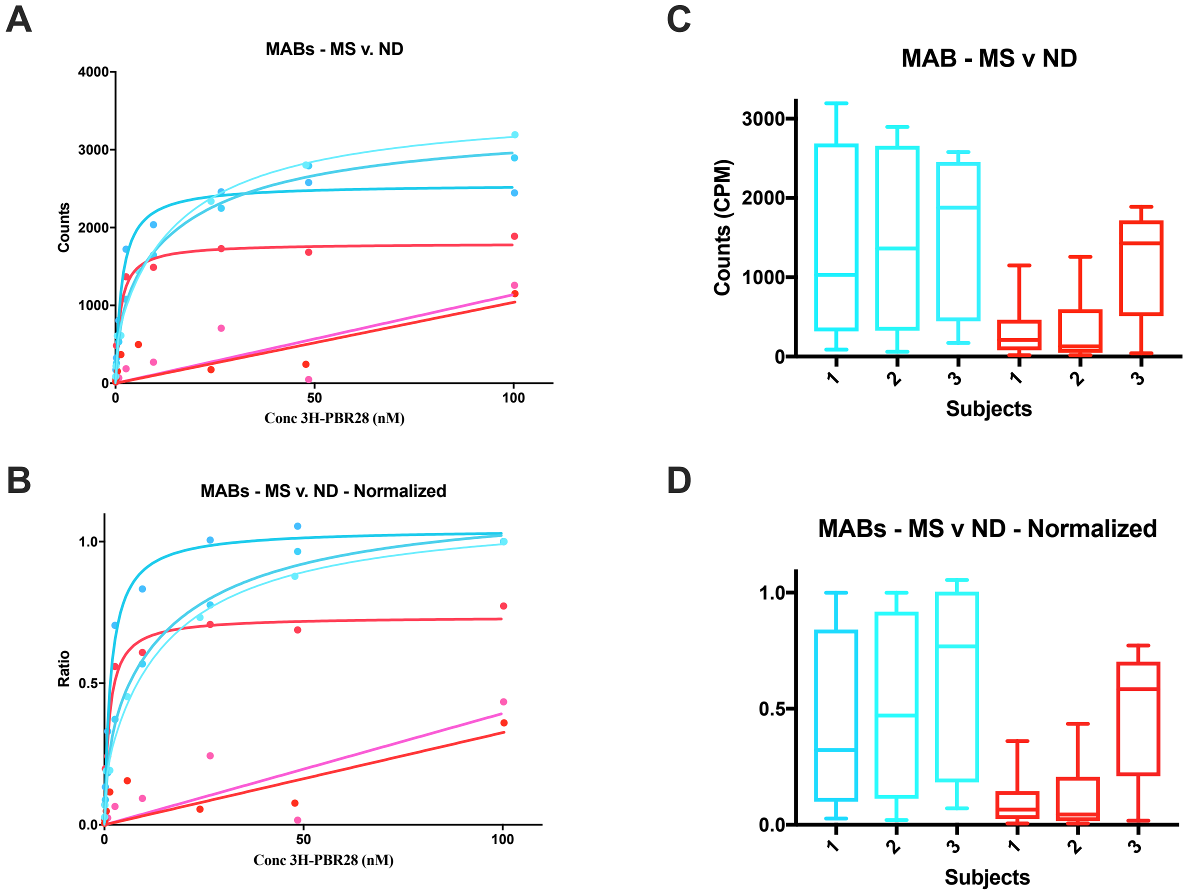

Figure 4-5. *A) Comparison of ^{3}H-PBR28 specific binding curves in 4 MABS with multiple sclerosis (red) and 4 MAB normal donors (blue). B) Comparison of ^{3}H-PBR28 specific binding curves in 4 MABS with multiple sclerosis (red) normalized to one of 4 MAB normal donors (blue). C) Box plots of ^{3}H-PBR28 specific-binding values in 4 MABS with multiple sclerosis (red) and 4 MAB normal donors (blue). D) Box plots of ^{3}H-PBR28 specific-binding values in 4 MABS with multiple sclerosis (red) normalized to one of 4 MAB normal donors (blue). Curves for MS subjects were normalized to curves for normal donor subjects run on the same day.*

The MS HAB subjects also had a higher mean level of TSPO protein expression but a markedly lower level of signal intensity at 300 nM [^{3}H-PBR28] (1299.37±770.4, n=4) when compared to normal donors (2940.13±2410.33, n=4) as shown in **Figure 4-6**. However, this difference was not significant (p=0.2423).

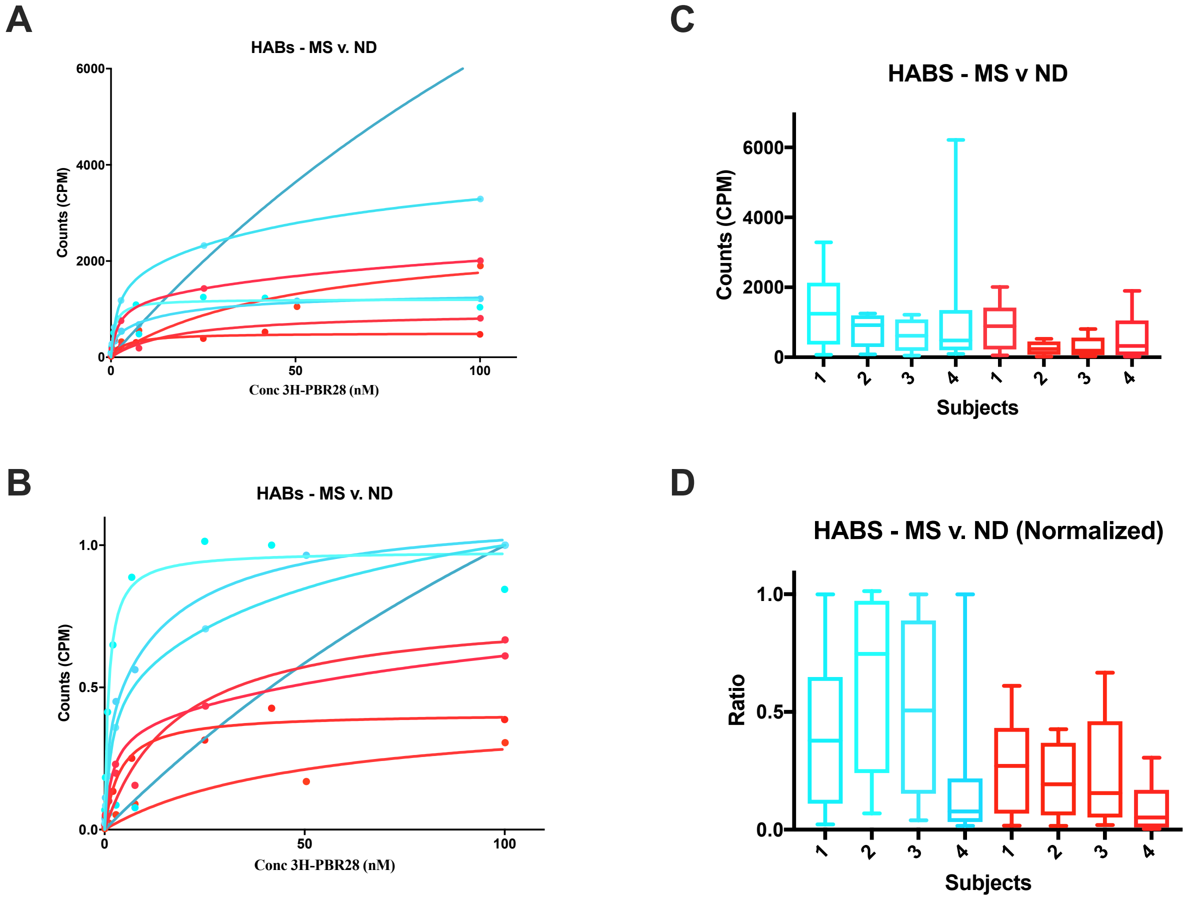

Figure 4-6. *A) Comparison of* ^{3}*H-PBR28 specific-binding curves in 4 HABS with multiple sclerosis (red) and 4 HAB normal donors (blue). B) Comparison of* ^{3}*H-PBR28 specific-binding curves in 4 HABS with multiple sclerosis (red) normalized to one of 4 HAB normal donors (blue). C) Box plots of* ^{3}*H-PBR28 specific-binding values in 4 HABS with multiple sclerosis (red) and 4 HAB normal donors (blue). D) Box plots of* ^{3}*H-PBR28 specific-binding values in 4 HABS with multiple sclerosis (red) normalized to one of 4 HAB normal donors (blue). Curves for MS subjects were normalized to values for normal donor subjects run on the same day.*

4.4 **Discussion**

Our results suggest a discordance between TSPO protein expression and second-generation ligand-binding in the peripheral blood, which has significant implications for the clinical use of second-generation ligands to detect neuroinflammation. While PBMC samples showed globally elevated TSPO protein expression in MS patients, radioligand-binding by second-generation ligand PBR28 was significantly decreased in those same MS patient samples. This paradoxical discordance between protein expression and protein-radioligand binding suggests that MS patients, despite exhibiting moderately elevated TSPO protein expression, may have an impairment in the ability of TSPO to bind second-generation ligands. This may indicate a conformational change in the protein structure or an external element altering the availability of the radioligand binding site.

Previous studies have indicated that TSPO exists in both monomeric and multimeric forms [245,275]. For example, TSPO is known to form a heteromultimeric complex with 32kDA voltage-dependent anion channel (VDAC) and 30 kDa adenine nucleotide carrier (ANT) that is thought to facilitate the transport of cholesterol through the outer mitochondrial membrane [275]. Alternatively, TSPO may exist in monomeric or homomultimeric forms that are hypothesized to mediate ROS metabolism in conditions of oxidative stress [245,275]. Western blots of testicular Leydig and breast cancer cells probed with TSPO-reactive antisera have consistently identified immunoreactive protein bands of 18, 40, and 56 kDa [275]. Larger bands of 72, 90, and 110 kDa are also occasionally detected in some conditions [275]. These higher molecular weight bands are thought to contain dimers and oligomers of TSPO, and conditions that induced the production of ROS also resulted in the detection of larger TSPO polymers [275].

X-ray crystallography and NMR studies in bacteria and rodents have since visualized the 3D structure of TSPO, as well as its ligand binding sites [26,246,276–278]. These structural studies of TSPO homodimers in bacteria and mice have found that dimer structure varies in the presence and absence of PK11195 as a stabilizing ligand, suggesting that ligand-binding may alter the dimer structure and implying that, conversely, conformational changes induced by dimerization may modify or block ligand-binding sites [26,246,276–278].

TSPO ligands vary in their ability to bind TSPO in different populations. For example, 7-chloro-5-(4-chlorophenyl)-1-methyl-1,3-dihydrobenzo[e][1,4] diazepin-2-one (Ro5-4864) is a benzodiazepine that binds variably with TSPO across species. Isoquinoline carboxamide derivative PK11195, in contrast, is a non-benzodiazepine observed to bind TSPO with high affinity in all species [40,66,197,279–285]. The differential binding pattern between these two ligands is thought to indicate that they bind different sites within the TSPO molecule [66,279–285]. Likewise, PBR28 and other second-generation ligands are known to be a sensitive to a specific TSPO polymorphism called rs6971, in which a single-nucleotide substitution results in the conversion of a nonpolar alanine residue near the C-terminus of the molecule into a polar threonine residue [8,77,286–289]. This polymorphism is observed to abrogate the binding of PBR28, such that heterozygotes carrying one copy of the rs6971 allele show reduced binding affinity in all tissues, and homozygotes carrying two copies of rs6971 allele show virtually no binding at all [8,77,286–289]. It is therefore hypothesized that the PBR28 binding site is sensitive to conformational changes induced by the amino-acid substitution [8,77].

Moreover, radioligand-binding assays detected significantly less [3H]PBR28-binding in healthy human peripheral blood MDM stimulated with LPS and IFN-γ than in unstimulated MDM [204]. It is therefore hypothesized that LPS stimulation may conformationally alter the binding site of PBR28 and further diminish binding of PBR28 in medium- and high-affinity binders. Our finding of reduced PBR28 binding in MS patients with increased levels of TSPO corroborates this hypothesis, suggesting that increases in pro-inflammatory activation in peripheral blood immune cells leads to conformational changes that reduce or abrogate TSPO-PBR28 binding. This would suggest that PBR28 ligand-binding signal may underestimate the true extent of TSPO protein expression in both blood and inflammatory lesions, which has significant implications for the clinical application of second-generation ligands in MS PET imaging. This may warrant caution in the interpretation of brain PET scans using PBR28 and similar second-generation ligands for the imaging of inflammation in the brain and may also serve to explain the difficulty of detecting significantly elevations of PBR28 binding in the brain, even in active disease.

4.4.1 Future directions

While we hypothesize that the decreased TSPO radioligand-binding observed with PBR28 in MS patients is the result of conformational changes induced by inflammatory stimuli associated with their disease state, we have not directly measured TSPO radioligand-binding with PBR28 in PBMC isolated from MS patients after exposure to inflammatory stimuli *in vitro*. While studies by Narayan et al. have demonstrated a decrease in PBR28-binding by human macrophages exposed to LPS and IFN-γ *in vitro*, these human macrophages were derived from monocytes isolated from the blood of healthy subjects and synovial fluid drawn from subjects with rheumatoid arthritis [204]. Whether a similar decrease in PBR28-binding upon exposure to pro-inflammatory stimuli would be seen in macrophages cultured from the blood of MS patients has not yet been tested. To probe this relation, I would propose to culture monocyte-derived macrophages from isolated MS and ND PBMC and measure TSPO protein levels in response to M1 (LPS and IFN-γ) and M2 (IL-4) treatment using flow cytometry and Western blotting. I would attempt to preserve and refreeze as many cells as possible for subsequent radioligand-binding assays.

Additionally, as discussed in the previous chapter, due to subject availability, this study compared a cohort of normal donors with an MS patient cohort that included both untreated MS patients and MS patients on first-line therapies, such as interferon-β or glatiramer acetate. Ideally, to identify changes in TSPO expression in active neuroinflammatory disease, we would compare TSPO levels in healthy donors to TSPO levels specifically in untreated MS patients with active disease. However, patients are unlikely to remain off treatment in this clinical context and we did not have sufficient numbers of untreated patients to make this comparison. Within the cohort selected for this study, there was no difference in TSPO expression in PBMC between untreated patients and patients on first-line therapies, but we cannot exclude the possibility that first-line immunomodulatory therapies may exert some influence on TSPO expression. Moreover, patients on second-line immunosuppressive therapies and patients who had received steroid therapies for acute exacerbations within the six months prior to their visit were excluded from this study. The effect of these second-line therapies on TSPO expression and radioligand binding has not been studied. In future studies, it would be ideal to include higher numbers of untreated, first-line-treated, and second-line-treated patients and compare the effect of both first-line and second-line therapies on TSPO radioligand-binding. Specifically, I would select 10 untreated, 10 first-line-treated, and 10 second-line-treated patients. I would then compare TSPO levels, mitochondrial volume, and immunophenotype in classical, non-classical, and intermediate monocytes in these subjects using the same antibody panel described in this chapter (CD14, CD16, CD3, TSPO, CD86, HLA DR, HSP60). From each sample, I would retain 10 million cells at -80C for subsequent ligand-binding experiments using PBR28. This would enable me to measure total PBR28-binding and non-specific binding in triplicate at 8 different concentrations and generate a binding curve to robustly determine the level of TSPO-PBR28 binding in each subject and compare radioligand binding with TSPO protein expression measured by flow cytometry.

Another limitation of this study is that we were not able to measure TSPO radioligand binding with a first-generation ligand. Due to the high quantity of cells required for each ligand-binding assay, this limitation would likely persist even with access to larger patient cohort. To generate a full binding-curve with total and non-specific binding in triplicate at eight different radioligand concentration currently requires 2.4 x 10^6 cells in high-affinity binders (50,000 cells per well) and 9.6 x 10^6 cells in medium-affinity binders (200,000 cells per well). As first- and second-generation ligand are thought to be bind different sites with the TSPO protein [66,279–285], detecting a difference between first- and second-generation ligand-binding in the same tissue sample could provide significant mechanistic insight but is unfortunately unlikely to be feasible with PBMC. An alternative method of probing this question would be to measure PK-11195 and PBR28 binding in frozen tissue by autoradiography and compare with TSPO immunostaining in a contiguous section.

Lastly, again due to the high quantity of isolated PBMC required for radioligand-binding experiments and extremely limited sample availability, we were unable to directly compare TSPO protein expression with second-generation ligand-binding in marmoset PBMC. With sufficient sample availability, it would be ideal to measure TSPO expression and PBR28-binding in isolated marmoset PBMC before and after EAE induction. Specifically, I would propose to collect and isolate PBMC from 1 ml of blood from 6 healthy marmosets prior to EAE induction. I would then propose to collect and isolate PBMC from the same marmosets at one-month intervals after EAE induction. I would thaw samples from the same animal on the same day and run same-day comparisons of TSPO expression in CD14+ monocytes and CD3+ lymphocytes as described in Chapter 3. Where possible, I would attempt to retain 1.2 million cells at -80C for subsequent ligand-binding experiments using PBR28. This would enable me to measure total PBR28-binding and non-specific binding in triplicate at a single PBR28 concentration.

5 Conclusions

5.1 Overview

The studies described in this thesis affirm the clinical utility of TSPO as potential PET imaging target for the detection of activated microglia and macrophages and the monitoring of CNS disease in both MS and a relevant nonhuman primate model of autoimmune neuroinflammatory disease. Moreover, they indicate TSPO to be a potential peripheral biomarker of neuroinflammation in multiple sclerosis, one that can be measured in the peripheral to non-invasively monitor disease and in the long term may potentially be useful for patient prognosis and stratification. The ability to monitor TSPO levels in the peripheral blood may also enable the comparison of patterns of protein expression with patterns of ligand-binding, which may be necessary for the development and validation of TSPO radioligands in the future.

5.2 TSPO is expressed in both glia and neurons in marmoset EAE and is expressed predominantly by CD74+ microglia/macrophages in acute disease

From the histopathological characterization of TSPO expression in postmortem marmoset EAE tissue, we conclude that the common marmoset is an extremely relevant model for the study of TSPO in human neurological disease. In characterizing the cellular localization and temporal pattern of TSPO expression in healthy and inflamed marmoset CNS tissues, this study is the first to establish the expression of TSPO by microglia/macrophages, astrocytes, and neurons in marmoset EAE, confirming the model to recapitulate both the glial and neuronal expression of TSPO observed in multiple sclerosis and thus rendering it a valuable proxy for the modeling of human neuroinflammatory disease. Furthermore, this study is the first to our knowledge to characterize the time course of TSPO expression in marmoset EAE, which was found to peak in the first month of lesion development and appears to decline gradually over a course of several months. Analysis using a linear mixed effects model of TSPO expression over time demonstrated a statistically significant decrease in TSPO at 4-5 months after lesion onset. We have also detected temporal patterns in the cellular association of TSPO in lesion development, with early TSPO expression occurring principally in Iba1+ microglia/macrophages, and later TSPO expression occurring in both microglia/macrophages and hypertrophic astrocytes. Specifically, marmoset EAE exhibits the pattern of astrocytic expression of TSPO in older lesions with significant astrogliosis that is seen in human disease, in which TSPO expression is observed in hypertrophic GFAP+ reactive astrocytes. The expression of TSPO by hypertrophic astrocytes in gliotic lesions further distinguishes marmoset EAE from many rodent models of EAE, where astrocytic TSPO expression is frequently absent. Furthermore, the finding of decreasing microglial TSPO expression and increasing astrocytic TSPO expression over time is consistent with temporal patterns of TSPO expression observed in MS.

Additionally, this study has confirmed neuronal TSPO expression in marmoset EAE. While TSPO expression was observed in less than 1% of neurons detected by NeuN staining in control primate brain tissue, distinct cytoplasmic TSPO expression was observed in 1-45% of NeuN+ neurons in multiple areas of normal-appearing gray matter in EAE marmoset brain tissue. Multiplex immunofluorescence imaging of TSPO in conjunction with markers of neuronal phenotype localized TSPO expression to excitatory glutaminergic neurons expressing GLS2, a finding that is consistent with recent RNAseq studies profiling TSPO in single cells obtained from human brain homogenates, which found neuronal TSPO to be moderately expressed in pyramidal neurons [254–256]. While phenotyping studies were limited to a single animal, the ability to detect neuronal TSPO in this disease model may enable further study of the neuronal phenotype associated with TSPO expression in other animals. The ability to monitor changes in neuronal TSPO expression in response to disease progression or therapeutic intervention may give further insight into its prognostic and therapeutic value.

In addition to establishing marmoset EAE as a suitable proxy for multiple sclerosis in the study of TSPO in neuroinflammation, this study has also observed potential disease-specific changes in the immunophenotype of TSPO+ microglia and macrophages in neuroinflammatory disease. Whereas TSPO in the healthy primate brain is more frequently expressed by Arg1+Iba1+ microglia and macrophages than by CD74+ or MRP14+ microglia/macrophages, TSPO in acute lesions is expressed predominantly by CD74+ microglia/ macrophages. The finding that TSPO is predominantly associated with Arg1+/"M2" phagocytes in healthy brain tissue but becomes more associated with a "M1"-like phenotype in diseased brain tissue suggests that TSPO expression may become dysregulated in inflammatory states.

The greatest limitation of this study is that we were only able to access one control animal. While the patterns described here may ultimately yield some insight into the dynamics of TSPO expression in EAE and MS, it is difficult to assess the statistical significance of differences between EAE and control tissue with a single control.

Nonethelss, the commonalities between marmoset EAE and multiple sclerosis identified in this study demonstrate marmoset EAE to be a suitable model for the study of TSPO expression in human neuroinflammatory disease. We may therefore envision informative PET imaging experiments in EAE marmosets comparing TSPO-radioligand binding by first- and second-generation ligands with clinical and pathological parameters of disease progression, such as MRI lesion burden and disability. Moreover, such studies would also facilitate the direct the spatial comparison of changes in TSPO-radioligand binding on PET imaging with changes in T2W hyperintensity on MRI. Finally, these experiments would facilitate the comparison of terminal PET imaging studies with postmortem pathology. Limitations would include the lack of control tissue (as in this study), high cost and the small size of the animal, which may preclude the use of an arterial line to administer PET radioligands.

5.3 TSPO expression is significantly elevated in multiple subsets of monocytes in the peripheral blood of MS patients and may function as a peripheral biomarker of CNS inflammation

We conclude that TSPO expression in peripheral blood mononuclear cells may be a useful peripheral biomarker of CNS inflammation in active neuroinflammatory disease. When compared to age- and race-matched controls, monocytic TSPO expression was significantly increased in the peripheral blood of MS patients with active disease who were untreated or on first-line treatments, and these differences were detected in both typical CD14+CD16- and atypical CD16+CD14- monocytes. Moreover, elevations in TSPO were more statistically robust than elevations detected in other markers of activation, such as HLA DR and CD86, suggesting that TSPO expression in monocytes may be a more sensitive marker of disease status than these conventional activation markers. Finally, the ability to measure TSPO expression in isolated PBMC renders the peripheral blood a useful model system in which to probe the relationship between protein expression and binding, as discussed in Section 5.4. However, we did not probe TSPO levels in the PBMC of patients on second-line disease-modifying agents, nor did we longitudinally monitor TSPO levels in patients over the course of treatment, so the influence of therapy and disease progression on peripheral TSPO expression is not yet known.

The analysis of TSPO expression in marmoset PBMC was unfortunately limited by the low blood volume available for flow cytometry, but preliminary studies confirmed the expression of TSPO in marmoset lymphocytes and monocytes. Monocytic TSPO expression in marmoset blood was found to be 5-fold higher than lymphocytic TSPO expression, a finding that is consistent with the trends observed in human PBMC in both this thesis and literature on the subject [213]. The ability to measure TSPO protein expression in marmoset monocytes and lymphocytes may ultimately facilitate the monitoring of TSPO levels in marmoset blood before and after EAE induction, providing the opportunity to directly measure the effect of neuroinflammation on peripheral TSPO expression. Future experiments would ideally compare TSPO expression by flow cytometry in CD14+ monocytes and CD3+ lymphocytes from healthy animals before EAE induction with TSPO expression in the same animal at precise time points after EAE induction e.g. 1 month after induction, 2 months after induction, etc. It would also be valuable to draw blood from animals during clinical exacerbations and compare TSPO levels in PBMC during exacerbation with TSPO levels during remission. Our MRI protocol would facilitate the detection of animals with active contrast-enhancing lesions, allowing the comparison of TSPO in PBMC in animals with CEL to TSPO in animals without active lesions. Furthermore, the ability to measure TSPO protein expression in marmoset PBMC could facilitate the comparison of protein expression with radioligand-binding in both healthy marmosets and EAE marmosets.

5.4 PBR28-binding is decreased in the peripheral blood of MS patients with active disease, despite increases in protein expression

To probe the correlation between TSPO expression and TSPO ligand-binding, I compared TSPO protein expression measured by flow cytometry in normal donors and MS patients with active disease to TSPO-radioligand binding by second-generation ligand PBR28 in the same cohorts. Whereas TSPO was elevated in both monocytes and lymphocytes in MS patients when compared to matched controls, radioligand-binding by second-generation ligand PBR28 was significantly decreased in PBMC samples from those same MS patients. The results of this study suggest a discordance between TSPO protein expression and second-generation ligand-binding in the peripheral blood, which implies that second-generation ligands may be of limited clinical utility for the detection and quantification of TSPO expression in neuroinflammation. It is therefore hypothesized that TSPO proteins in MS patients may be impaired in their ability to bind second-generation ligands, despite elevated expression relative to matched controls. This is possibly due to a conformational change in the protein structure occurring in inflammatory disease that alters the availability of the binding site for second-generation radioligands.

Studies of purified TSPO isolated from bacteria have found to protein to form dimers and oligomers [245,275], and structural studies of TSPO homodimers in bacteria and mice have found that the TSPO homodimer structure appears to vary in the presence and absence of stabilizing ligand such as PK11195, suggesting that ligand-binding may directly alter the dimer structure. This implies that conversely, conformational changes induced by dimerization may modify or block the ligand-binding site [26,276,277,290,291]. More recent radioligand-binding assays have detected a decrease in ^{3}H-PBR28-binding in healthy human peripheral blood monocyte-derived macrophages stimulated with LPS and IFN-γ [204], suggesting that LPS stimulation may specifically inhibit PBR28-binding by conformationally altering its binding site. Our finding of reduced PBR28 binding in MS patients, despite increased levels of TSPO, aligns with this hypothesis. If pro-inflammatory activation in peripheral blood immune cells leads to conformational changes that reduce or abrogate TSPO-PBR28 binding, then it is likely that PBR28 ligand-binding signal in inflamed tissues may underestimate the true extent of TSPO protein expression in both blood and CNS lesions, which has significant implications for the clinical application of second-generation ligands in MS PET imaging. This may also explain the difficulty of detecting significant elevations of PBR28 binding in the brain, even in active inflammatory disease, where TSPO expression is expected to be highly elevated.

However, a major limitation of this study is that I was not able to measure TSPO-PET radioligand binding with a first-generation ligand. Measuring binding with both a first- and second-generation ligand could provide potential mechanistic insight, as these ligand categories are thought to be bind different sites with the TSPO protein. Detecting a difference between first- and second-generation ligand-binding in the same tissue sample would corroborate this hypothesis, but unfortunately, would require a much higher quantity of tissue.

6 Concluding Summary

This thesis examines the immunophenotype of TSPO-expressing cells in the CNS and peripheral blood in MS and EAE and the relationship between TSPO expression and ligand-binding in conditions of neuroinflammation. Collectively, these results allow us to better understand the pathological significance of TSPO expression and TSPO-ligand binding in the central nervous system and peripheral blood in neuroinflammatory disease, providing a framework through which to further probe the clinical utility of TSPO as a marker of inflammation.

Through our pathological studies of marmoset EAE, we have established that TSPO in marmoset EAE is predominantly expressed by microglia and macrophages and is expressed by virtually all microglia and macrophages in acute lesions. TSPO expression in microglia in healthy marmoset brain tissue is more closely associated with markers of "M2"-like immunophenotype, whereas TSPO expression in microglia/macrophages in inflamed brain tissue is more closely associated with an "M1"-like immunogenic phenotype. We have further observed that TSPO expression by microglia/macrophages persists in chronic lesions. However, the intensity of TSPO expression decreases with lesion age. The study of TSPO expression in peripheral blood mononuclear cells indicates that TSPO expression in the periphery is also altered in neuroinflammatory conditions and may be used as a peripheral biomarker of inflammation. However, TSPO-binding by second-generation PET radioligand PBR28 is decreased in the peripheral blood of MS patients. This paradoxical decrease in ligand-binding is hypothesized to arise from conformational changes in the second-generation ligand-binding site and likely limits the utility of the ligand as a marker of TSPO expression in inflammatory disease.

From these studies, we conclude that marmoset EAE is a suitable experimental model for the use of TSPO radioligands to detect activated microglia and macrophages in acute and chronic lesions *in vivo*. Given its demonstrated association with "M1" activation marker CD74 in diseased brain tissue, the visualization of TSPO expression in marmoset EAE may provide further insight into the extent of pro-inflammatory activation in acute and chronic lesions. Subsequent decreases in TSPO expression in EAE lesions may be useful as a marker of chronicity. However, studies of second-generation TSPO radioligand-binding should be interpreted with caution, as our studies indicate a discrepancy between TSPO expression and second-generation radioligand-binding in inflammatory disease.

7 Appendix

7.1 Antibodies

Secondary antibodies used for immunohistochemistry

Goat anti-Mouse IgG (H+L) Cross-Adsorbed Secondary Antibody, HRP (Invitrogen, # G-21040)
Goat anti-Rabbit IgG (H+L) Secondary Antibody, HRP (Invitrogen, # 65-6120)
Goat anti-Mouse IgG (H+L) Secondary Antibody, AP (Invitrogen, # 31320)

7.2 Tables

Target	**Clone**	**Host**	**Isotype**	**Company**	**Cat. No.**	**Dilution**	**[mg/ml]**
PLP	Plpc1	Mouse	IgG2a	Bio-Rad	MAC839G	1:200	1
TSPO	EPR5384	Rabbit	IgG	Abcam	ab109497	1:100	0.92
Iba1	Polyclonal	Guinea Pig	IgG	Synaptic Systems	234004	1:100	1
Arg1	ARG1	Mouse	IgG3	NSJ Biologicals	V2652	1:200	0.2
CD74	Polyclonal	Sheep	IgG	R&D Systems	AF3590	1:100	1
MRP14	MAC387	Mouse	IgG1	DAKO	M074701	1:100	0.227
CD163	6E10.1G6	Mouse	IgG2b	Novus Biologicals	NBP2-36494	1:100	1

***Table 7-1**. A complete list of validated primary antibodies used for the phenotyping of microglia and macrophages expressing TSPO in inflammatory lesions in the marmoset CNS. A rabbit monoclonal antibody was used to detect TSPO, while guinea pig anti-Iba1 was used to detect activated microglia and macrophages. A mouse anti-PLP antibody was used to stain myelin and define areas of demyelinating inflammation. Anti-CD74 was used to identify microglia and macrophages with functional capacity for antigen presentation, while anti-MRP14 was used to detect phagocytes in a stage early activation. Anti-CD163 and anti-Arginase 1 were used to detect microglia and macrophages with a tolerogenic function.*

Fluorophore	**Secondary host**	**Target Host**	**Target Isotype**	**Company**	**Cat. No.**	**Dilution**	**Conc. [mg/ml]**
DY395XL	Goat	Mouse	IgG2a	Li-Cor Biosciences	CSQ-0007-3	1:100	2
Alexa Fluor 488	Goat	Rabbit	IgG	ThermoFisher	A21131	1:200	2
Alexa Fluor 546	Goat	Guinea Pig	IgG	ThermoFisher	A11035	1:200	2
Alexa Fluor 594	Goat	Mouse	IgG3	ThermoFisher	A21125	1:200	2
Alexa Fluor 647	Goat	Sheep	IgG	R&D Systems	A21450	1:200	2
IRDye 680LT	Goat	Mouse	IgG1	DAKO	016-120-084	1:200	1
IRDye 800CW	Goat	Mouse	IgG2b	Li-Cor Biosciences	926-32352	1:100	1

Table 7-2*. A complete list of secondary antibodies used for the phenotyping of microglia and macrophages expressing TSPO in inflammatory lesions in the marmoset CNS. Primary antibodies are described in* ***Table 7-1****.*

Target	**Clone**	**Host**	**Isotype**	**Company**	**Cat. No.**	**Dilution**	**[mg/ml]**
PCNA	PC8	Mouse	IgG3	GeneTex	GTX40237	1:200	0.5
Collagen IV	Polyclonal	Rabbit	IgG	Abcam	ab6586	1:200	1
NeuN	Polyclonal	Guinea Pig	IgG	Millipore	ABN90	1:500	1
S100	15E2E2	Mouse	IgG2a	Millipore	MAB079-1	1:200	1
CNPase	11-5B	Mouse	IgG1	Millipore	MAB326	1:200	1
NFH	Polyclonal	Chicken	IgY	Millipore	AB5539	1:500	1
Lectin*	LEL	N/A	N/A	Vector Labs	B-1175	1:200	2
MBP	82-87	Rat	IgG2a	Millipore	MAB386	1:200	1
GFAP	Polyclonal	Mouse	IgG2b	BD Biosciences	55630	1:200	0.5

Table 7-3*. A complete list of validated primary antibodies used for the phenotyping of neurons and astrocytes expressing TSPO in inflammatory lesions in the marmoset CNS. A rabbit monoclonal antibody was used to detect TSPO, while guinea pig anti-NeuN and chicken anti-NFH were used to detect neuronal nuclei and axons, respectively. Mouse anti-CNPase, anti-GFP and anti-S100A antibodies were used to detect astrocyte cell bodies and processes. A rat anti-MBP antibody was used to stain myelin and define areas of demyelinating inflammation. Mouse IgG3 anti-PCNA was used to detect proliferating cells. Antibodies to lectin and collagen IV were used to detect endothelial cells and the subendothelial basement membrane, respectively.*

Fluorophore	**Secondary host**	**Target Host**	**Target Isotype**	**Company**	**Cat. No.**	**Dilution**	**Conc. [mg/ml]**
DyLight 405	Goat	Mouse	IgG3	Li-Cor Biosciences	CSQ-0007-3	1:100	1
Alexa Fluor 430	Goat	Rabbit	IgG	ThermoFisher	A11064	1:100	2
Alexa Fluor 488	Goat	Guinea Pig	IgG	ThermoFisher	A21151	1:100	2
Alexa Fluor 546	Goat	Mouse	IgG2a	ThermoFisher	A21133	1:200	2
Alexa Fluor 594	Goat	Mouse	IgG1	ThermoFisher	A21125	1:200	2
Alexa Fluor 647	Goat	Chicken	IgY	ThermoFisher	Z21449	1:200	2
StreptAvidin-PerCP	N/A	N/A	N/A	Jackson ImmunoResearch	016-120-084	1:200	0.2
IRDye 680LT	Goat	Rat	IgG2a	Li-Cor Biosciences	926-68051	1:200	1
IRDye 800CW	Goat	Mouse	IgG2b	Li-Cor Biosciences	926-32219	1:100	1

***Table 7-4**. A complete list of secondary antibodies used for the phenotyping of neurons and astrocytes expressing TSPO in inflammatory lesions in the marmoset CNS. Primary antibodies are described in **Table 7-3**.*

Target	Name	Functional association or target	Clone	Host isotype
TSPO	18 kDa translocator protein	Activated macrophages/microglia; reactive astrocytes	EPR5384	Rabbit
Iba-1	Ionized calcium binding adaptor molecule 1	Activated macrophages/microglia	Polyclonal	Guinea Pig
MRP14	S100 calcium-binding protein A9 (S100A9); migration inhibitory factor-related protein 14 (MRP14)	Early activated macrophages/microglia	MACS387	Mouse IgG1, κ
CD74	Invariant chain of HLA-DR	Antigen presentation	Polyclonal	Sheep IgG
Arg-1	Arginase 1	Canonical "M2" marker	ARG1/1126	Mouse IgG3
CD163	Cluster of Differentiation 163; hemoglobin-haptoglobin scavenger receptor	Phagocytosis of hemoglobin/haptoglobin	6E10.1G6	Mouse IgG2b
PLP	Proteolipid protein	Myelin debris	plpc1	Mouse IgG2a
DAPI	-	Cell nuclei	-	-

***Table 7-5**. A summary of the markers used to identify and determine the immunophenotype of microglia and macrophages in healthy and EAE marmoset brain in this study, including target name, functional association, and the clone and host isotype of the antibody used to the detect the marker.*

Antibody	**Isotype**	**Clone**	**Provider**	**[mg/ml]**	**Quantity**
Anti-CD14 PE	Mouse IgG_{2a}	M5E2	BD Biosciences	0.05	1 µl
Anti CD16 PE-eFluor 610	Mouse IgG_1	CB16	ThermoFisher	0.025	2 µl
Anti-CD3 BV510	Mouse IgG_{2a}	OKT3	BioLegend	0.25	1 µl
Anti-CD86 PerCP-Cy5.5	Mouse IgG_1	2331 (FUN-1)	BD Biosciences	0.5	1 µl
Anti-HLA PE-Cy7	Mouse IgG_{2a}	G46-6	BD Biosciences	0.5	0.5 µl
Anti-TSPO AlexaFluor488	Rabbit IgG	EPR5384	AbCam	0.92	1 µl
Anti-HSP60 AlexaFluor647	Rabbit polyclonal	-	Novus	1	1 µl

***Table 7-6**. Antibodies used for the measurement of specific TSPO-antibody staining, CD86-antibody staining, HLA-antibody staining and HSP60-antibody staining in CD3+, CD14+, and CD16+ PBMC.*

Antibody	**Isotype**	**Clone**	**Provider**	**[mg/ml]**	**Quantity**
Anti-CD14 PE	Mouse IgG_{2a}	M5E2	BD Biosciences	0.05	1 µl
Anti CD16 PE-eFluor 610	Mouse IgG_1	CB16	ThermoFisher	0.025	2 µl
Anti-CD3 BV510	Mouse IgG_{2a}	OKT3	BioLegend	0.25	1 µl
Isotype control (PerCP-Cy5.5-conjugate)	Mouse IgG_1	MOPC-21	BD Biosciences	0.5	1 µl
Isotype control (PE-Cy7-conjugate)	Mouse IgG_{2a}	G155-178	BD Biosciences	0.5	0.5 µl
Isotype control (AlexaFluor 488-conjugate)	Rabbit IgG	N/A	Cell Signaling Technologies	0.1	1 µl

***Table 7-7**. Antibodies used for the measurement of nonspecific staining associated with isotypes of antibodies used to detect TSPO, CD86, HLA, and HSP60 in CD3+, CD14+, and CD16+ PBMC.*

7.3 Flow cytometry gating: Normal donors and MS subjects

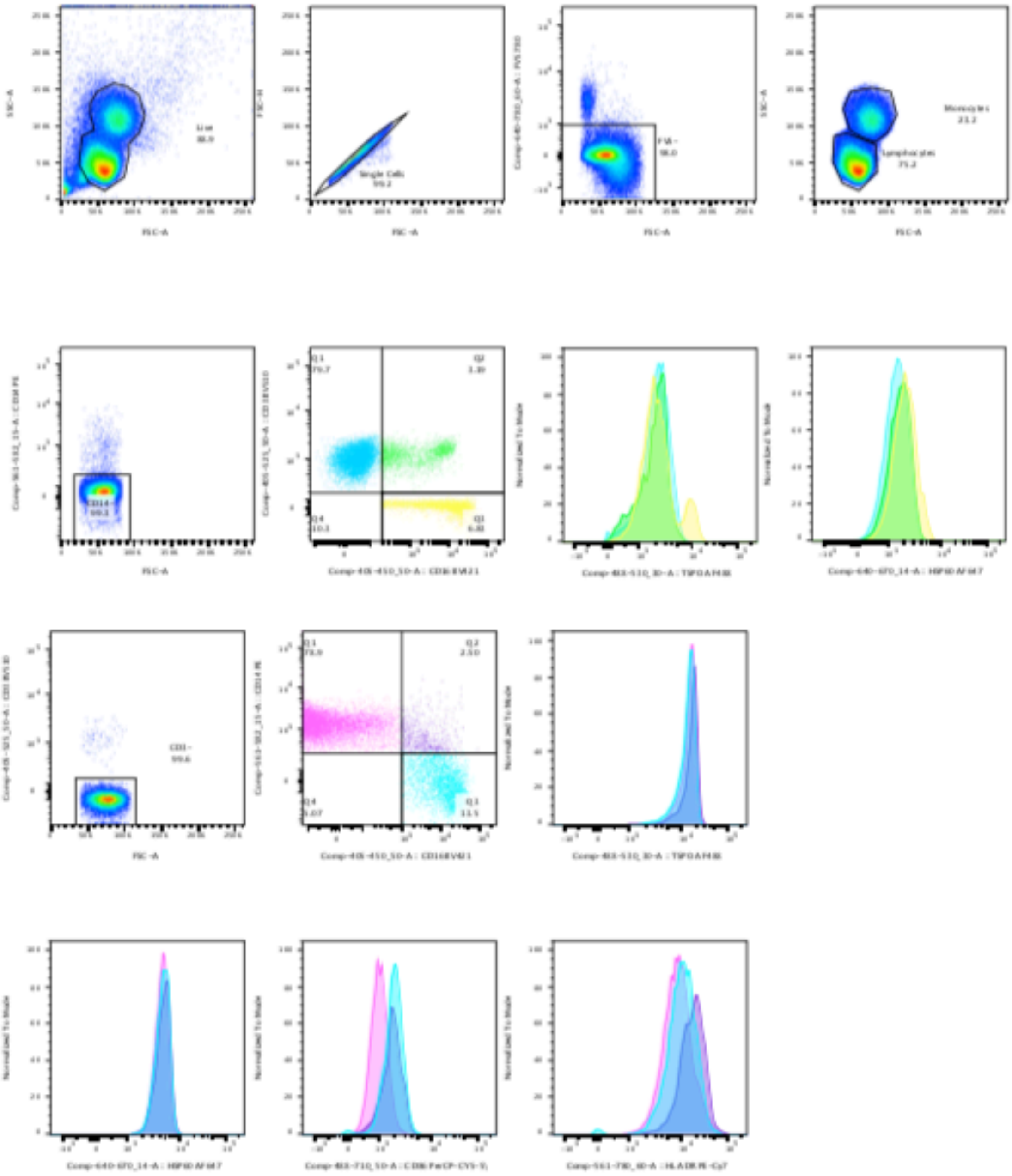

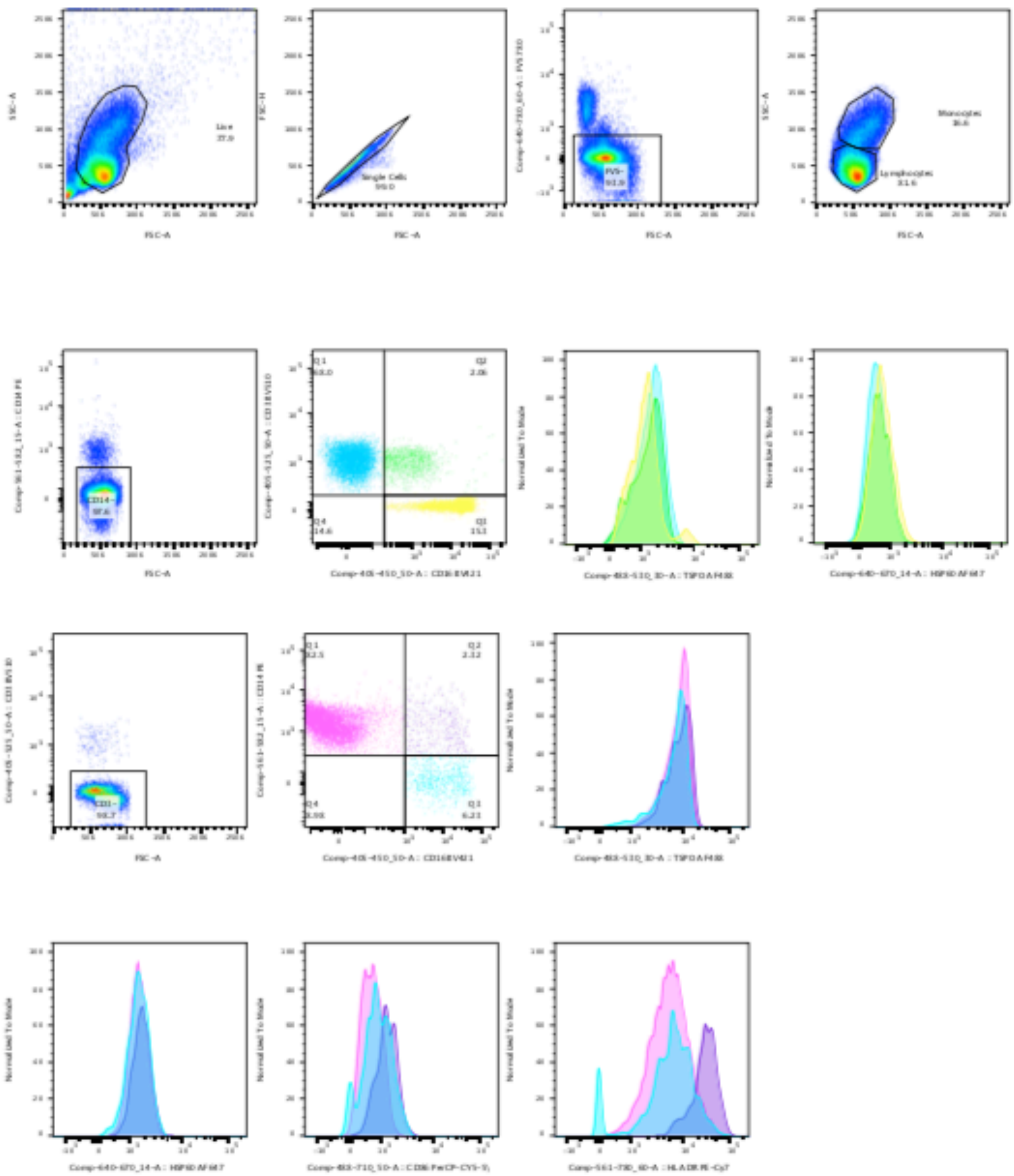
SSC-A
FSC-A
Live
37.9
FSC-H
Single Cells
99.0
Comp-640-780_60-A :: FVS780
FVS-
93.9
Monocytes
16.6
Lymphocytes
31.6
Comp-561-582_15-A :: CD14 PE
CD14-
97.6
Comp-405-525_50-A :: CD1 BV510
Q1
83.0
Q2
2.06
Q3
15.1
Q4
14.6
Comp-405-450_50-A :: CD16 BV421
Normalized To Mode
Comp-488-530_30-A :: TSPO AF488
Comp-640-670_14-A :: HSP60 AF647
CD1-
98.7
Q1
92.5
Q2
2.32
Q3
6.21
Comp-488-710_50-A :: CD86 PerCP-CY5-5
Comp-561-780_60-A :: HLA DR PE-Cy7

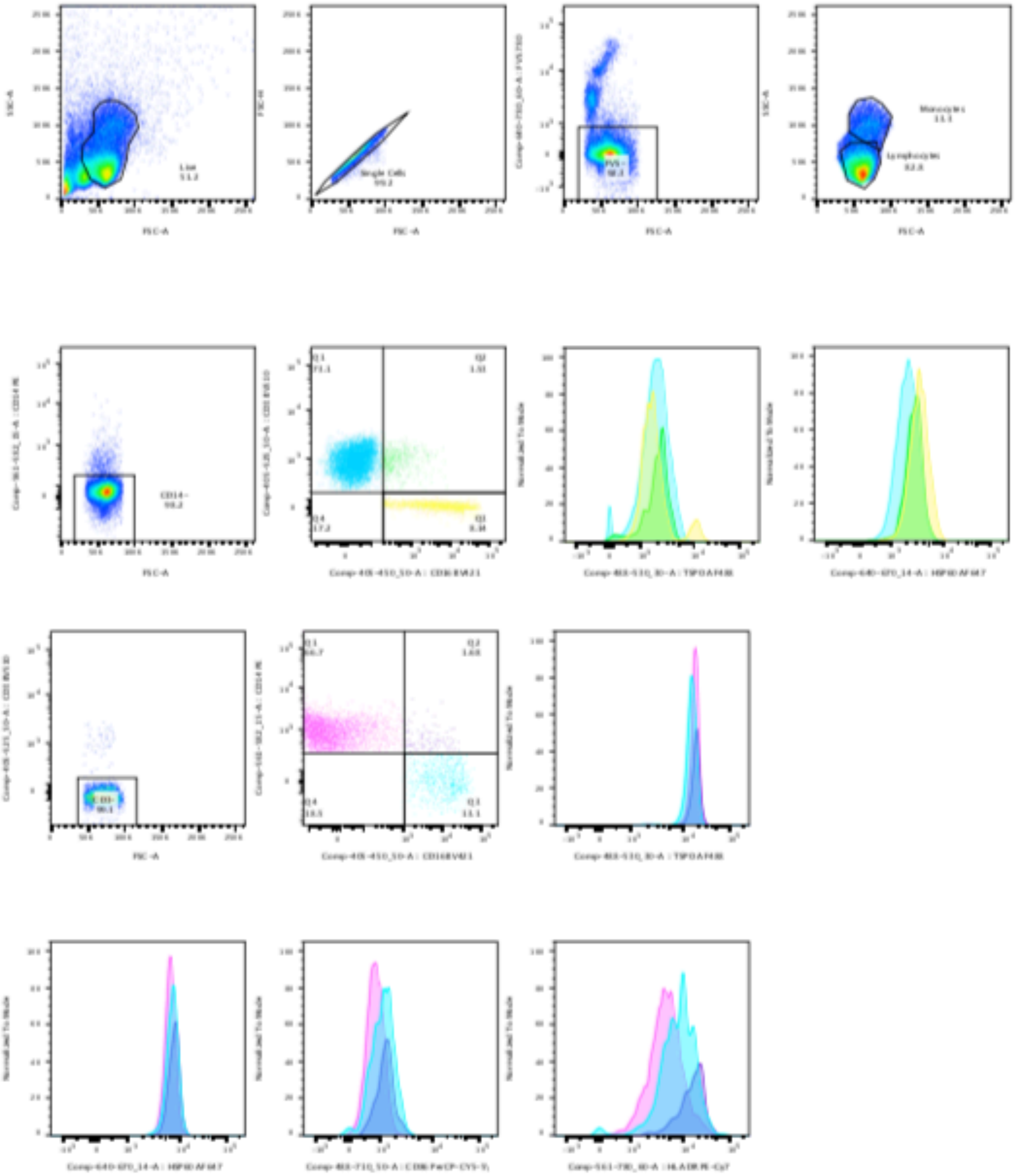
SSC-A
FSC-A
Live
FSC-H
Single Cells
FVS-
Monocytes
Lymphocytes
CD14-
Q1
Q2
Q3
Q4
Normalized To Mode
CD3-

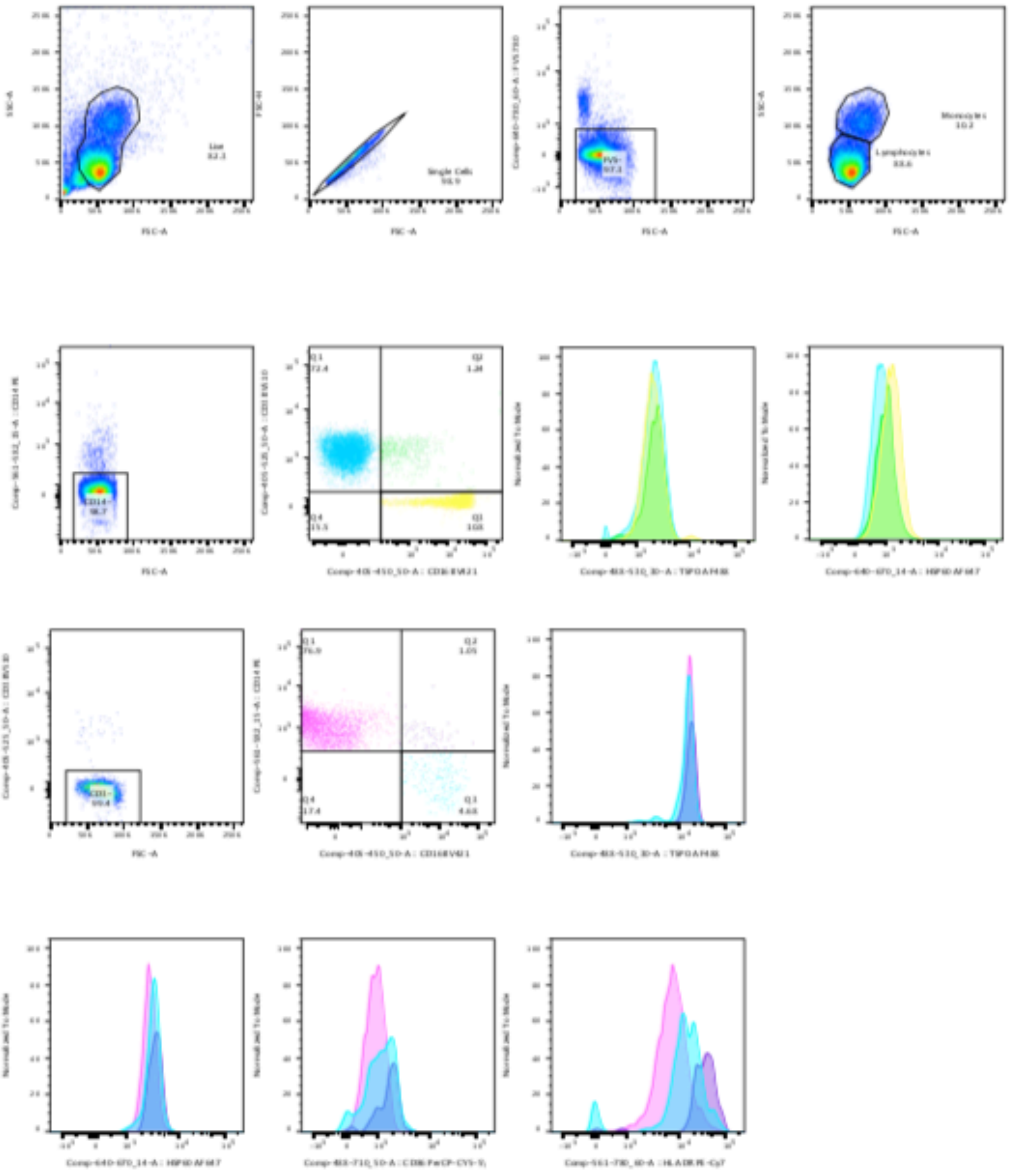
SSC-A
FSC-A
Live
82.1
FSC-H
Single Cells
98.9
FVS-
97.3
Monocytes
10.2
Lymphocytes
83.6
CD14-
98.7
Q1
72.4
Q2
1.24
Q4
15.5
Q3
10.8
Comp-405-450_50-A :: CD16 BV421
Normalized To Mode
Comp-488-530_30-A :: TSPO AF488
Comp-640-670_14-A :: HSP60 AF647
CD3-
99.4
Q1
76.9
Q2
1.05
Q4
17.4
Q3
4.68
Comp-488-710_50-A :: CD86 PerCP-CY5-5
Comp-561-780_60-A :: HLA DR PE-Cy7

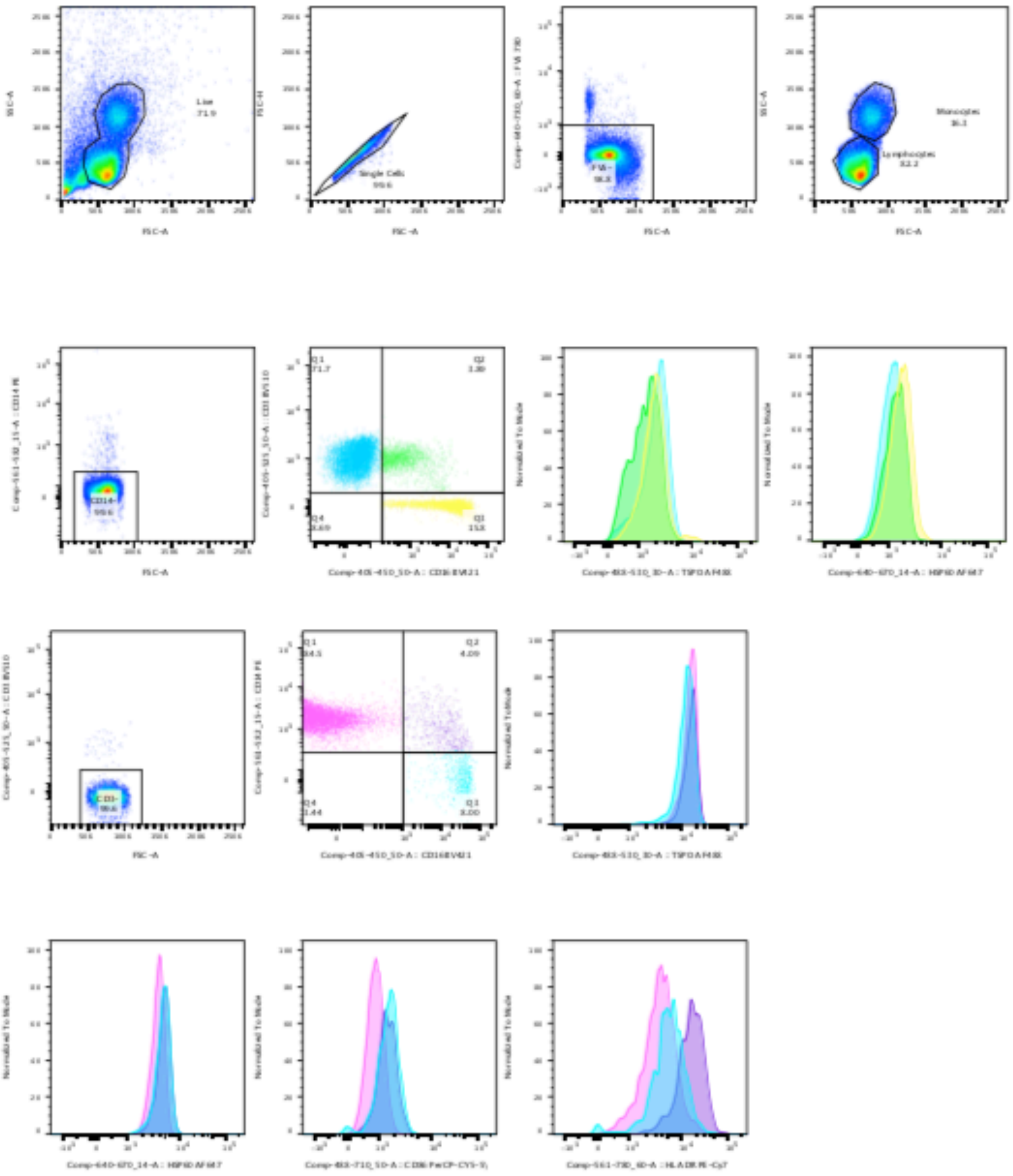
SSC-A
FSC-A
Live
71.9
FSC-H
Single Cells
99.6
Comp-640-780_60-A :: FVS 780
FVS-
98.8
Monocytes
16.3
Lymphocytes
82.2
Comp-561-582_15-A :: CD14 PE
CD14-
99.6
Comp-405-525_50-A :: CD3 BV510
Q1
71.7
Q2
3.89
Q4
8.69
Q3
15.8
Comp-405-450_50-A :: CD16 BV421
Normalized To Mode
Comp-488-530_30-A :: TSPO AF488
Comp-640-670_14-A :: HSP60 AF647
CD3-
99.6
Q1
84.5
Q2
4.09
Q4
3.44
Q3
8.00
Comp-488-710_50-A :: CD86 PerCP-CY5-5
Comp-561-780_60-A :: HLA DR PE-Cy7

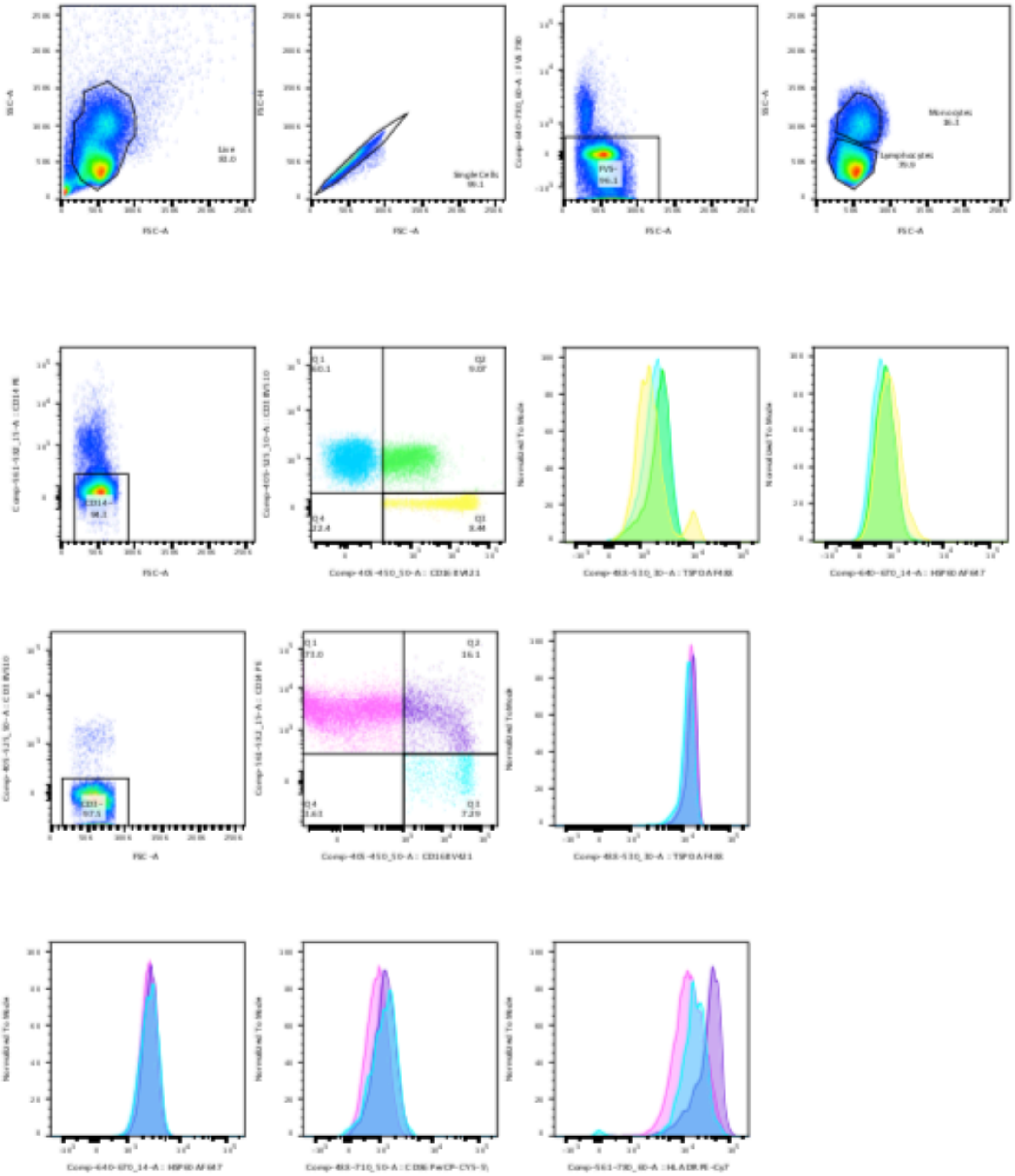
SSC-A
FSC-A
Live
82.0
FSC-H
Single Cells
99.1
Comp-640-730_60-A :: FVS 780
FVS-
96.1
Monocytes
16.3
Lymphocytes
79.9
Comp-561-582_15-A :: CD14 PE
CD14-
98.3
Comp-405-525_50-A :: CD3 BV510
Comp-405-450_50-A :: CD16 BV421
Q1
60.1
Q2
9.07
Q3
8.44
Q4
22.4
Normalized To Mode
Comp-488-530_30-A :: TSPO AF488
Comp-640-670_14-A :: HSP60 AF647
CD3-
97.5
Comp-561-582_15-A :: CD14 PE
Q1
73.0
Q2
16.1
Q3
7.29
Q4
3.63
Comp-488-710_50-A :: CD86 PerCP-CY5-5
Comp-561-780_60-A :: HLA DR PE-Cy7

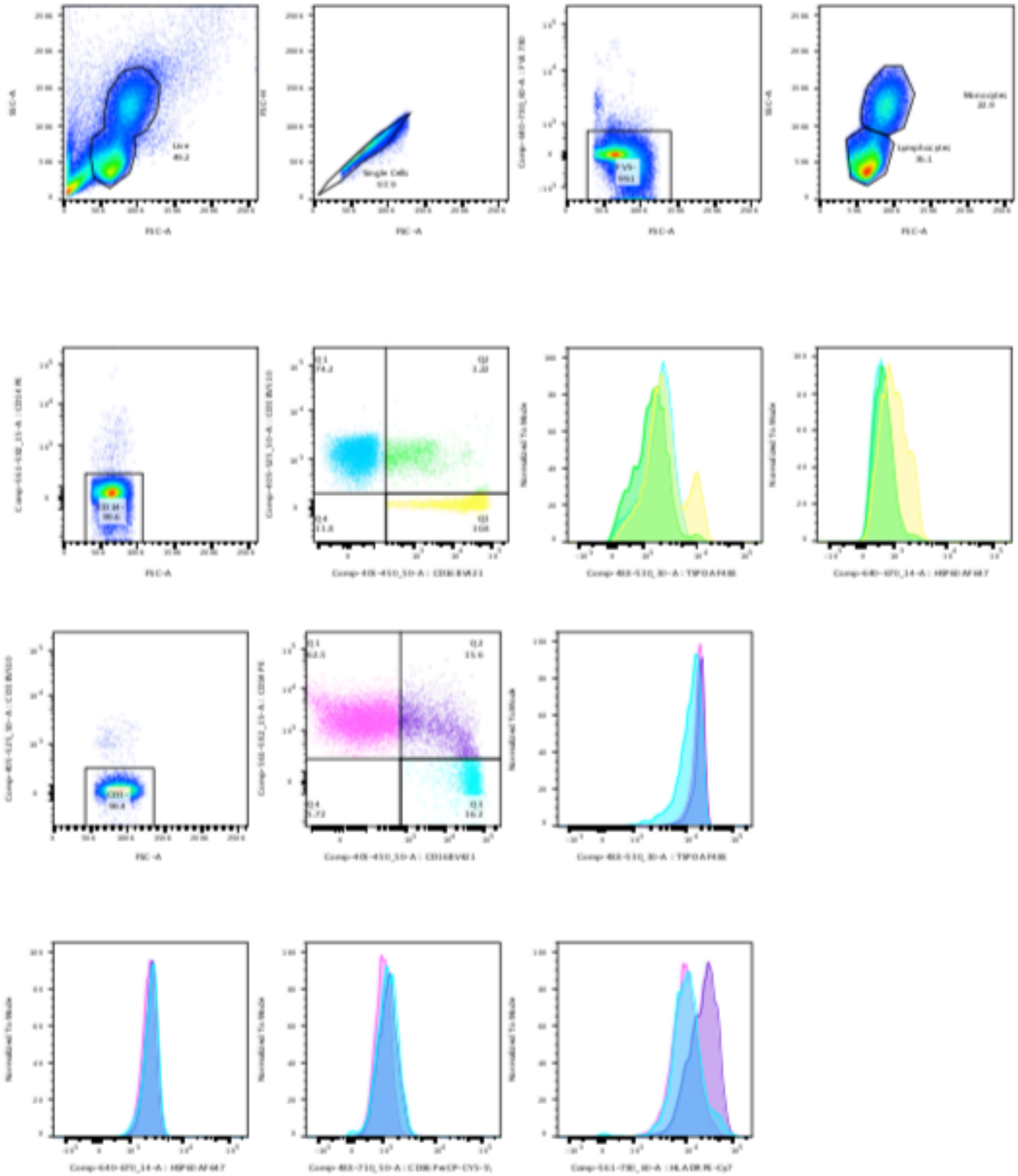
SSC-A
FSC-A
Live
49.2
FSC-H
Single Cells
97.9
FVS-
99.1
Monocytes
22.9
Lymphocytes
35.1
Q1
Q2
Q3
Q4
Normalized To Mode
Comp-405-450_50-A : CD16 BV421
Comp-488-530_30-A : TSPO AF488
Comp-640-670_14-A : HSP60 AF647
Comp-488-710_50-A : CD86 PerCP-CY5-5
Comp-561-780_60-A : HLA DR PE-Cy7

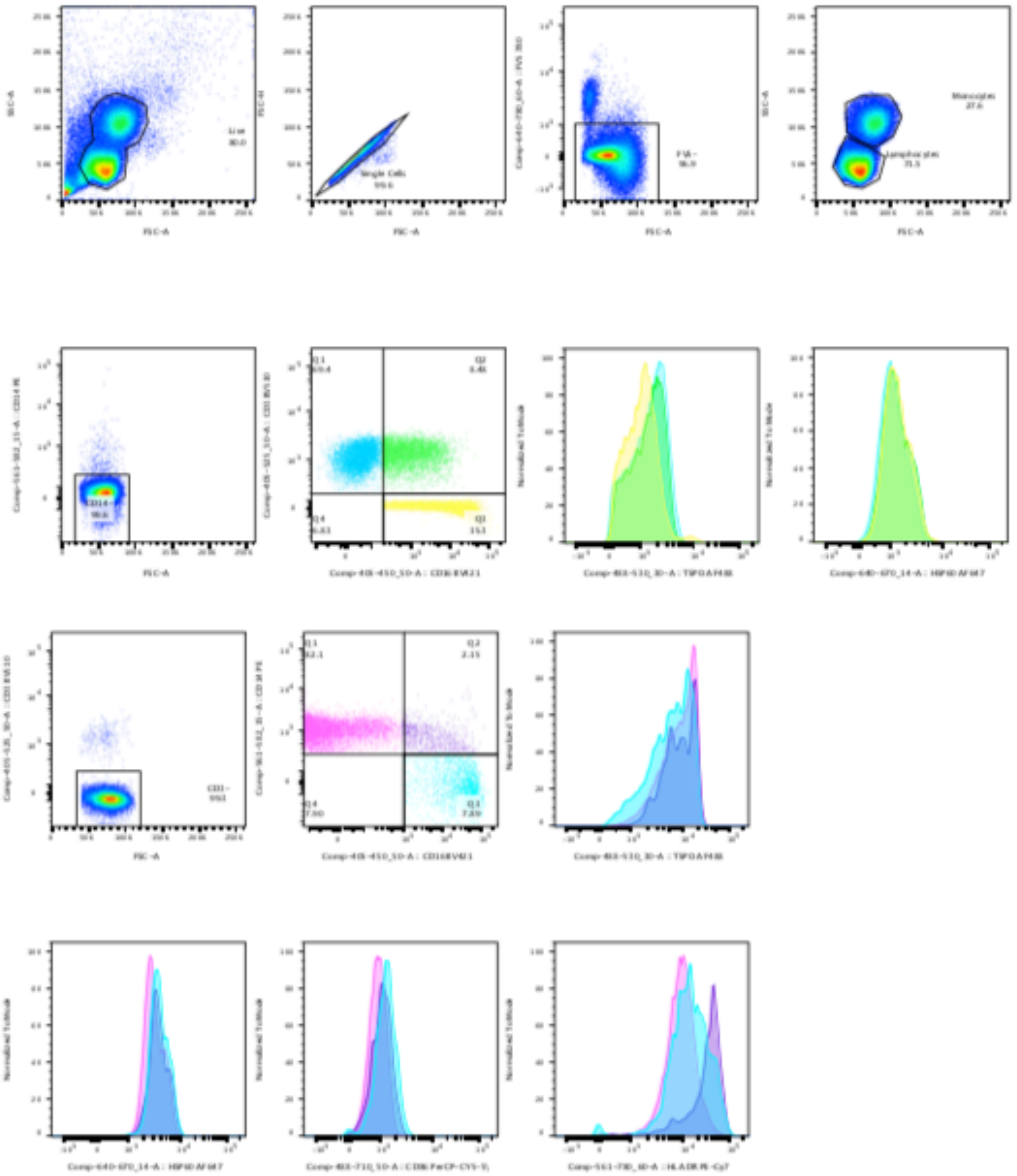
SSC-A
FSC-A
Live
80.0
SSC-H
Single Cells
99.6
FVS-
96.9
Monocytes
27.6
Lymphocytes
71.5
CD14-
98.6
Q1
59.4
Q2
3.46
Q3
15.3
Q4
0.83
Normalized To Mode
Comp-405-450_50-A :: CD16 BV421
Comp-488-530_30-A :: TSPO AF488
Comp-640-670_14-A :: HSP60 AF647
CD3-
95.1
Q1
82.1
Q2
2.15
Q3
7.83
Q4
7.90
Comp-488-710_50-A :: CD86 PerCP-CY5-5
Comp-561-780_60-A :: HLA DR PE-Cy7

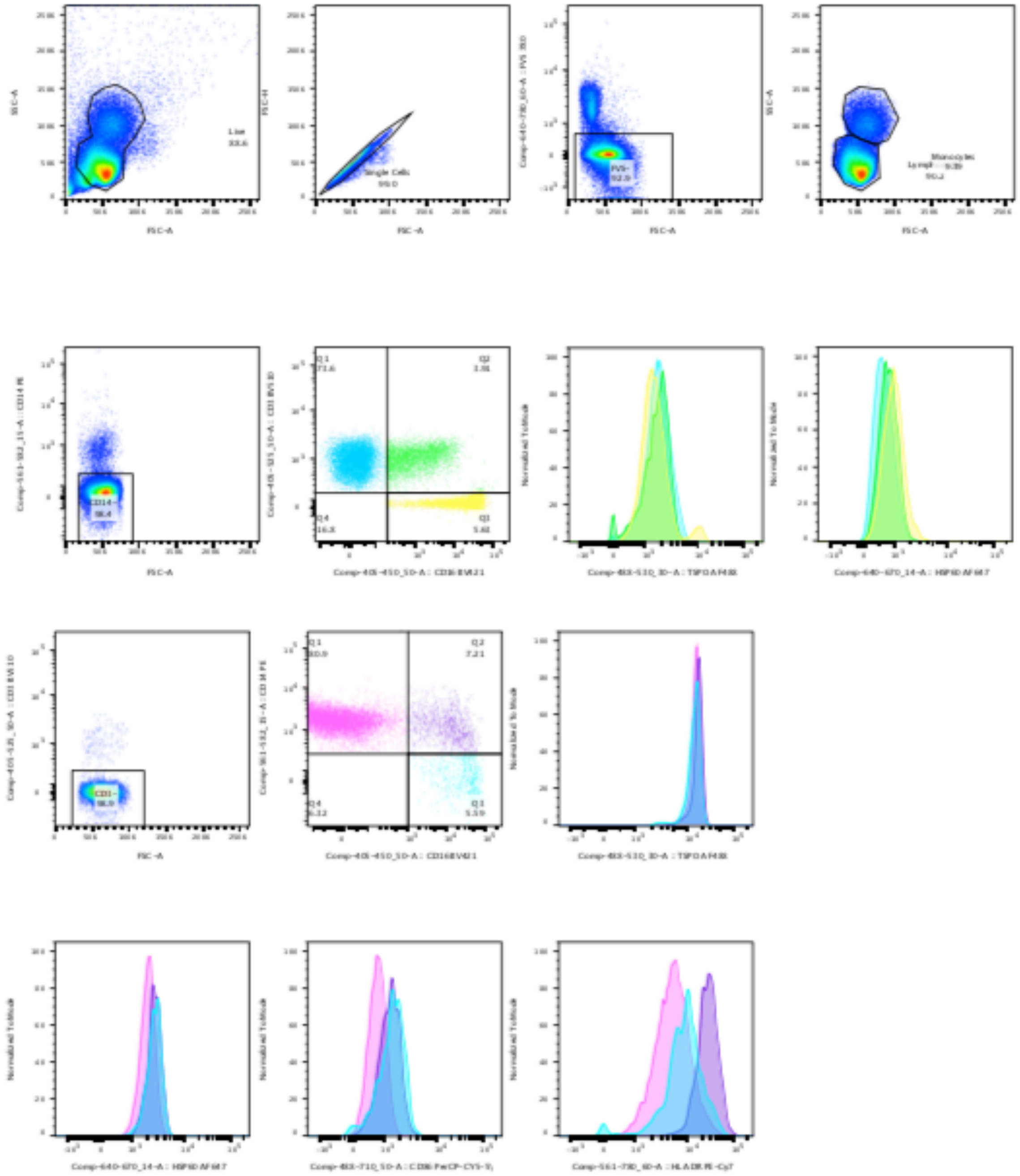
SSC-A
FSC-A
Live
33.6
FSC-H
Single Cells
99.0
Comp-640-780_60-A :: FVS 780
FVS-
92.9
Monocytes
9.39
Lymph
90.2
Comp-561-582_15-A :: CD14 PE
CD14-
98.4
Comp-405-525_50-A :: CD3 BV510
Q1
73.6
Q2
3.91
Q3
5.63
Q4
16.8
Comp-405-450_50-A :: CD16 BV421
Normalized To Mode
Comp-488-530_30-A :: TSPO AF488
Comp-640-670_14-A :: HSP60 AF647
CD3-
98.9
Q1
80.9
Q2
7.21
Q3
5.59
Q4
6.32
Comp-488-710_50-A :: CD86 PerCP-CY5-5
Comp-561-780_60-A :: HLA DR PE-Cy7

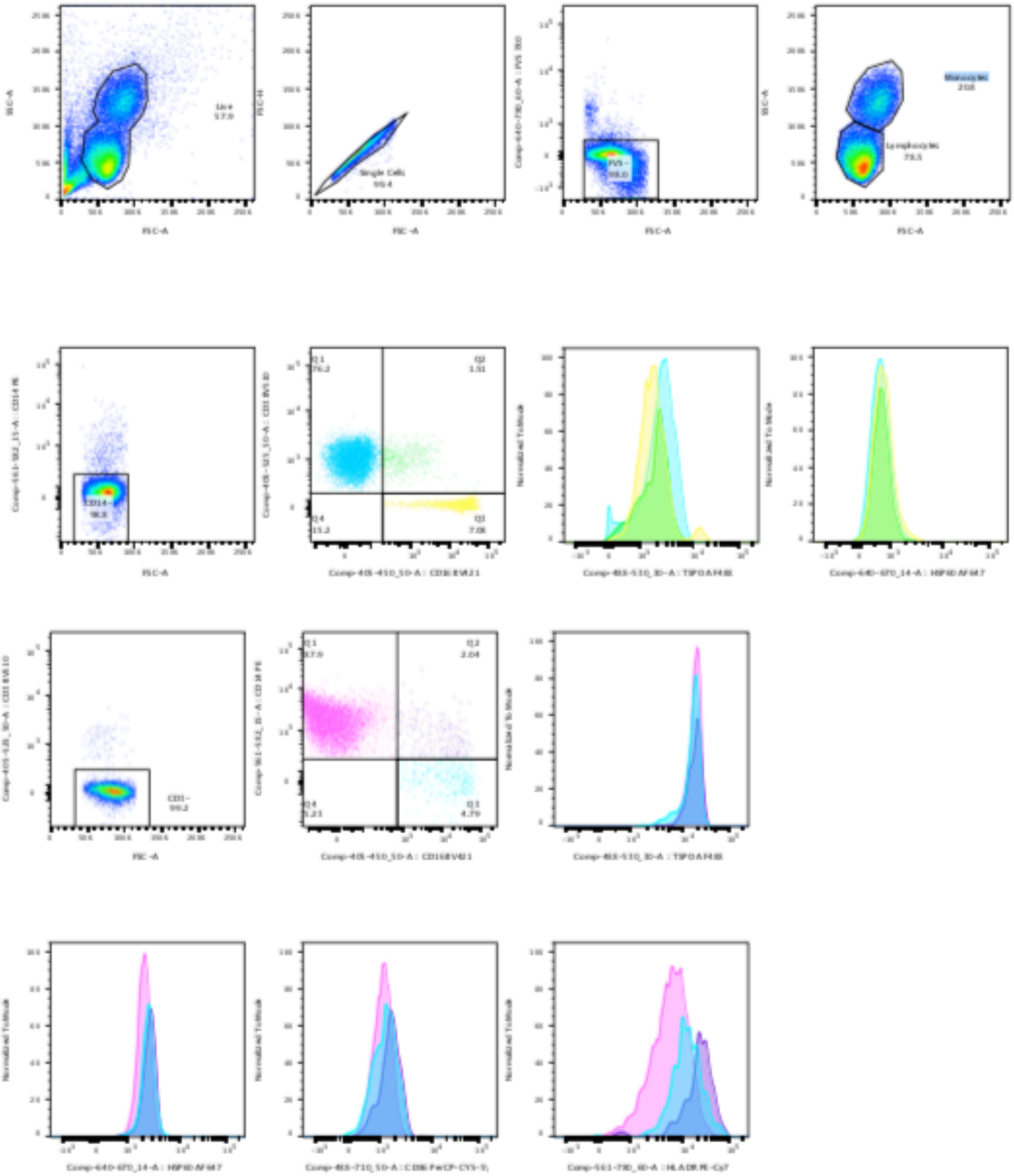
SSC-A
FSC-A
Live
57.9
FSC-H
Single Cells
99.4
Comp-640-780_60-A :: FVS 780
FVS-
98.0
Monocytes
20.8
Lymphocytes
73.5
Comp-561-582_15-A :: CD14 PE
CD14-
98.8
Comp-405-525_50-A :: CD3 BV510
Q1
76.2
Q2
1.51
Q3
7.08
Q4
15.2
Comp-405-450_50-A :: CD16 BV421
Normalized To Mode
Comp-488-530_30-A :: TSPO AF488
Comp-640-670_14-A :: HSP60 AF647
CD3-
99.2
Q1
87.9
Q2
2.04
Q3
4.79
Q4
5.21
Comp-488-710_50-A :: CD86 PerCP-CY5-5
Comp-561-780_60-A :: HLA DR PE-Cy7

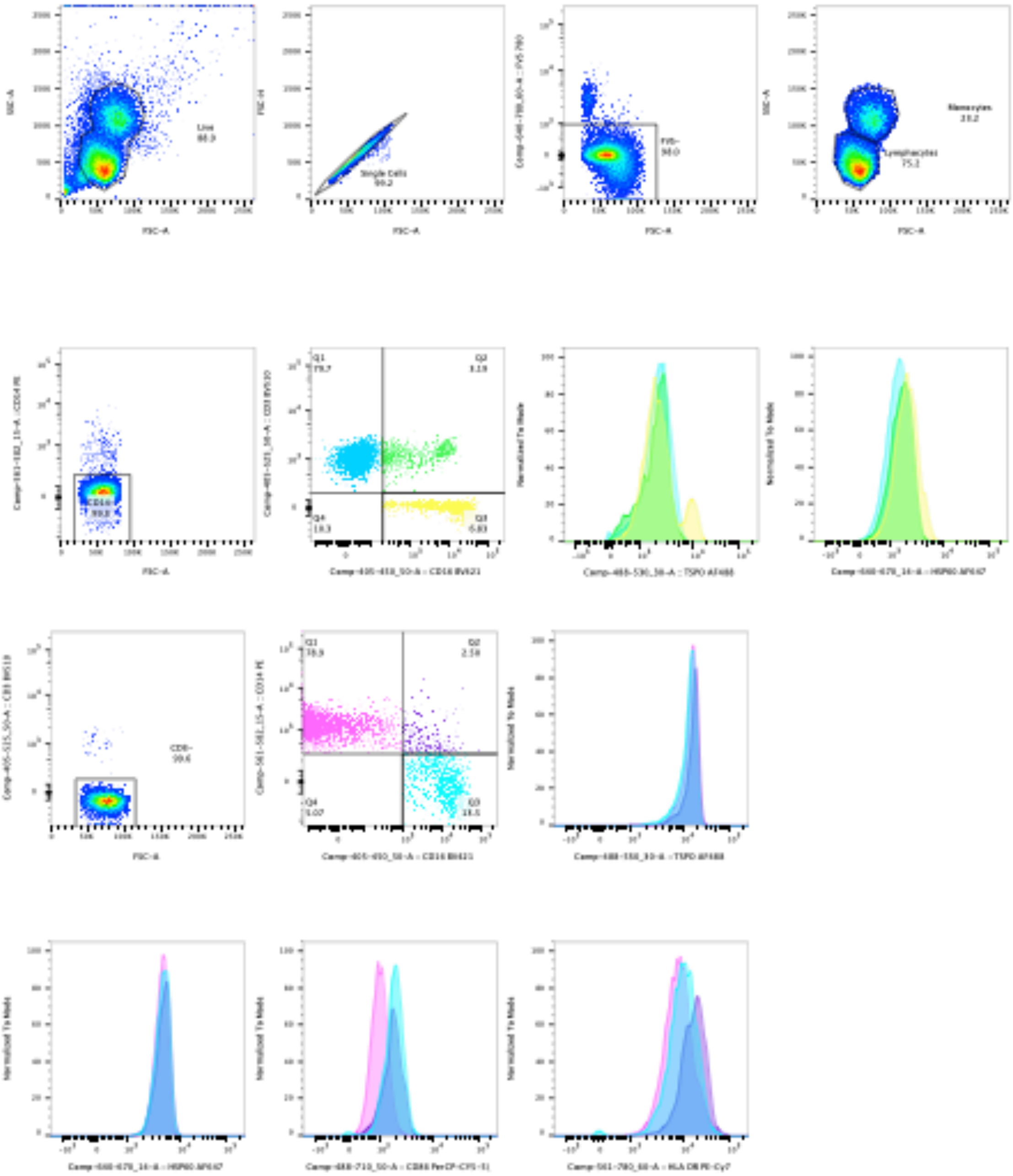
SSC-A
FSC-A
Live
88.3
FSC-H
Single Cells
99.2
Comp-Grd-780_60-A :: FVS 780
FVS-
98.0
Monocytes
23.2
Lymphocytes
75.2
Comp-561-582_15-A :: CD14 PE
CD14-
99.8
Q1
79.7
Q2
3.19
Q3
6.83
Q4
10.3
Comp-405-450_50-A :: CD16 BV421
Normalized To Mode
Comp-488-530_30-A :: TSPO AF488
Comp-640-670_14-A :: HSP60 AF647
Comp-405-515_50-A :: CD3 BV510
CD3-
99.6
Q1
78.9
Q2
2.58
Q3
18.5
Q4
0.07
Comp-561-582_15-A :: CD14 PE
Comp-488-710_50-A :: CD86 PerCP-CY5-5
Comp-561-780_60-A :: HLA DR PE-Cy7

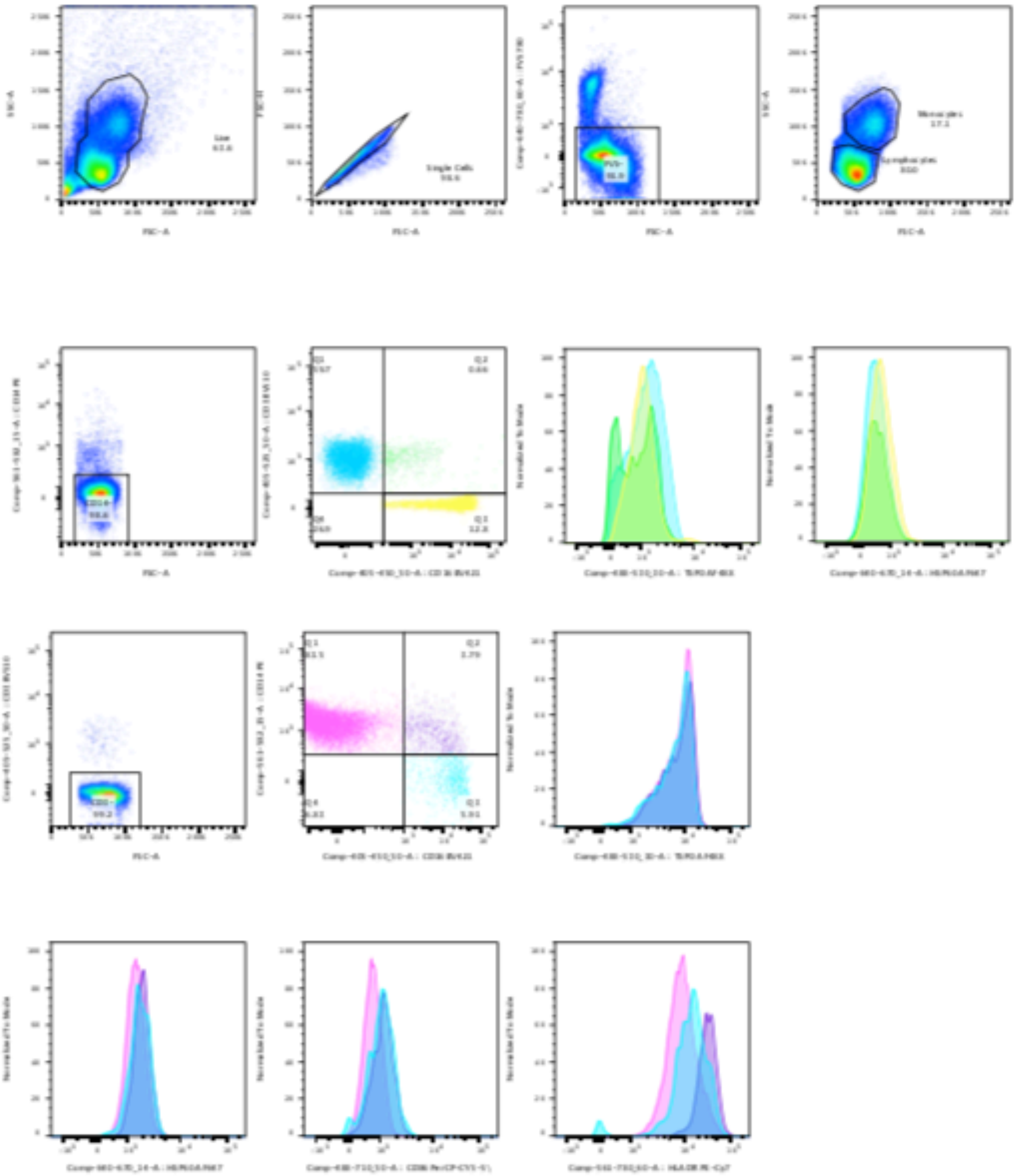
SSC-A
FSC-A
Live
FSC-H
Single Cells
Monocytes
17.1
Lymphocytes
FSC-A
Q1
Q2
Q3
Q4
Comp-405-450_50-A :: CD16 BV421
Normalized To Mode
Comp-488-530_30-A :: TSPO AF488
Comp-660-670_14-A :: HSP60A PAB7
Q1
Q2
Q3
Q4
Comp-405-450_50-A :: CD16 BV421
Normalized To Mode
Comp-660-670_14-A :: HSP60A PAB7
Comp-488-710_50-A :: CD86 PerCP-CY5-5
Comp-561-780_60-A :: HLA-DR PE-Cy7

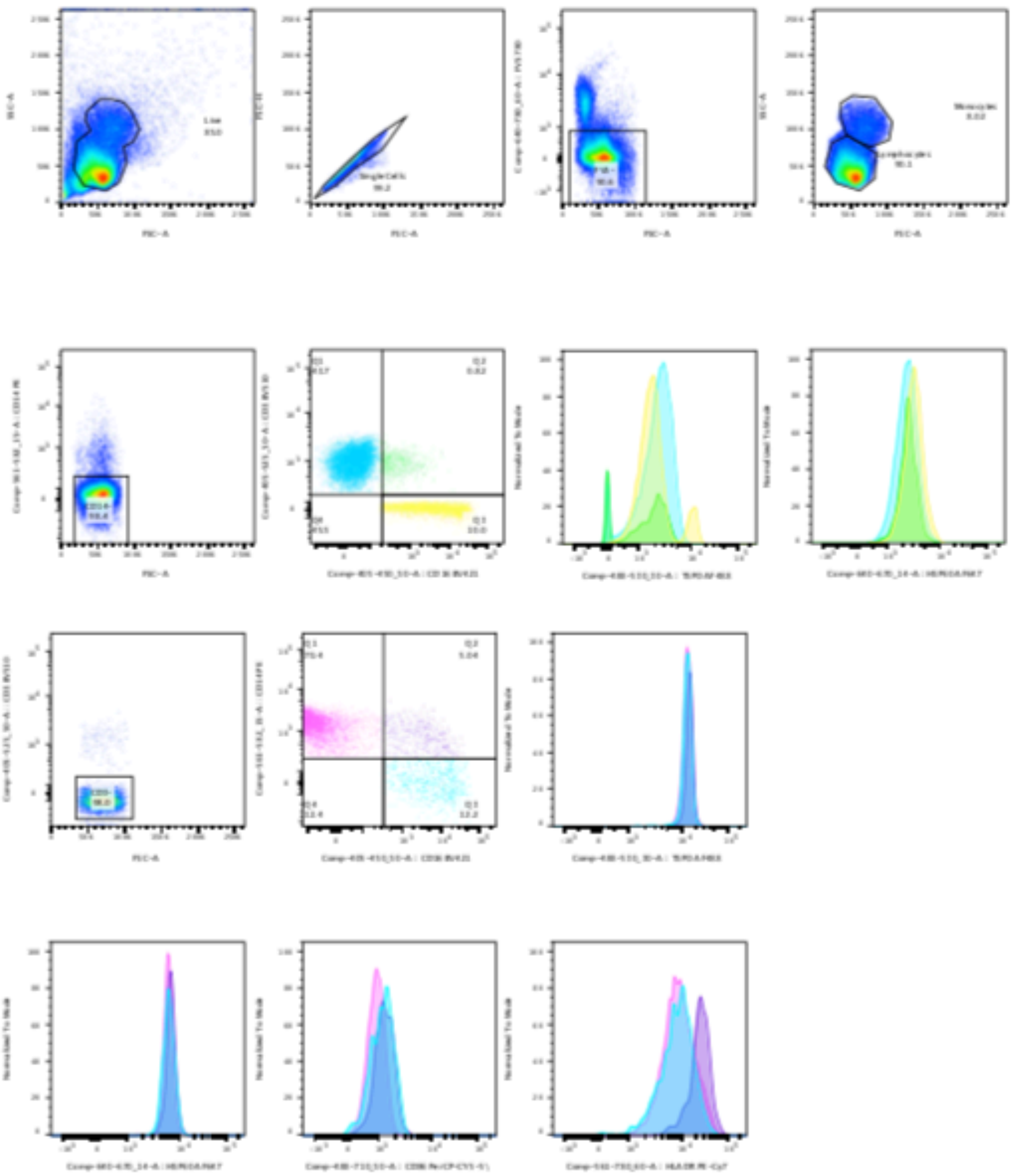
SSC-A
FSC-A
Live
Single Cells
Monocytes
Lymphocytes
Normalized To Mode

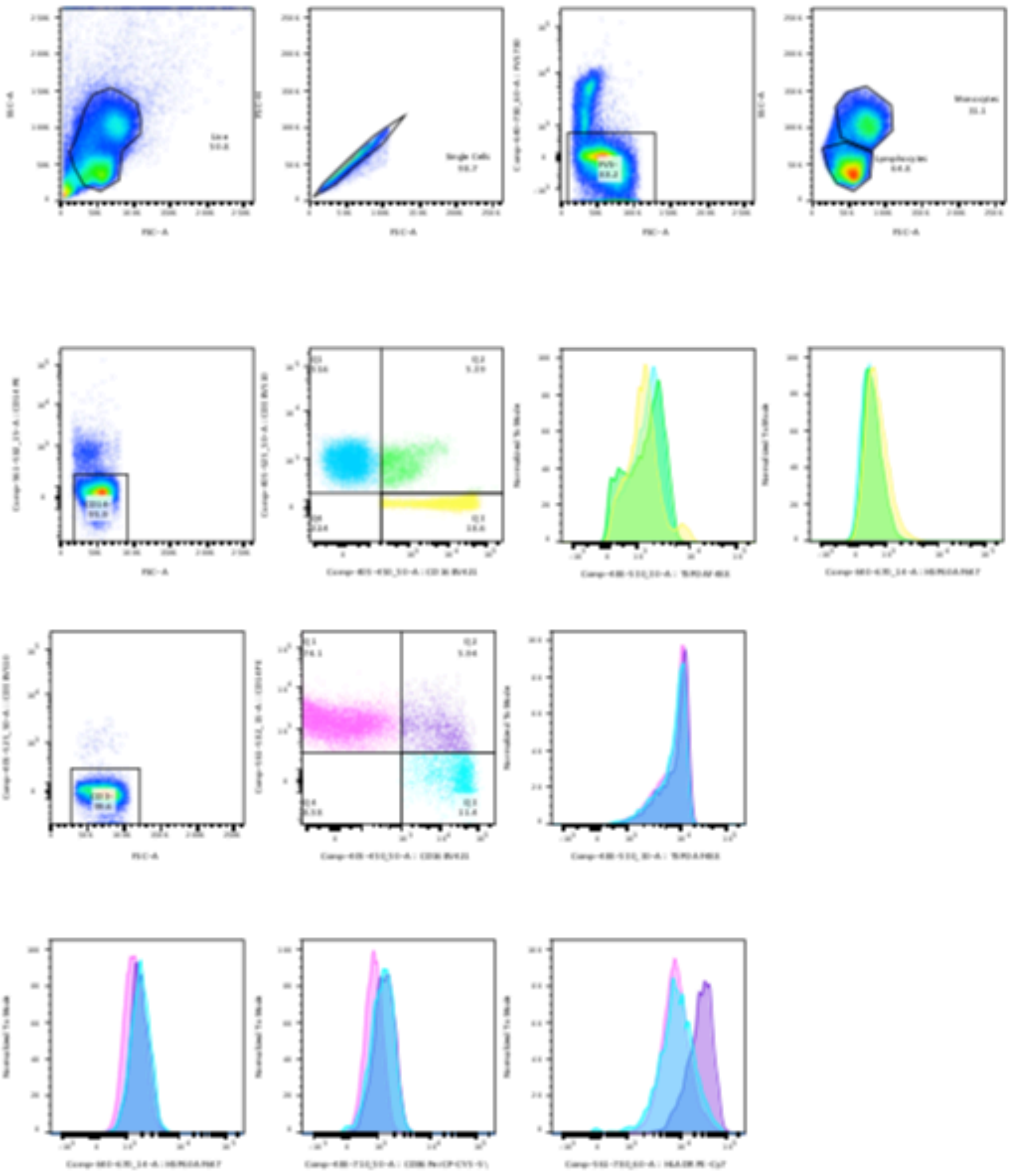
SSC-A
FSC-A
Single Cells
Monocytes
Lymphocytes
Normalized To Mode

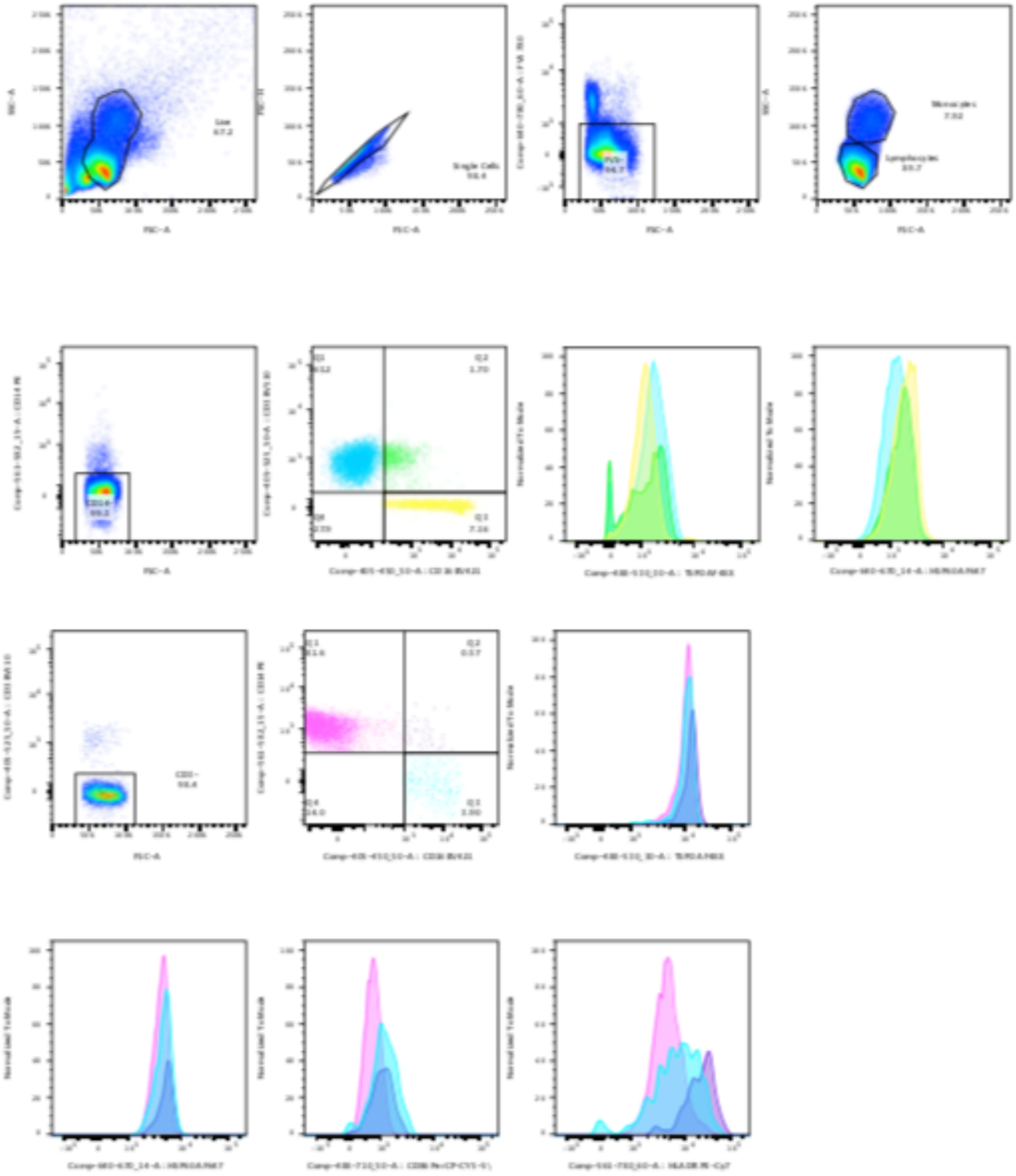
SSC-A
FSC-A
Live
Single Cells
Monocytes
Lymphocytes
Normalized To Mode

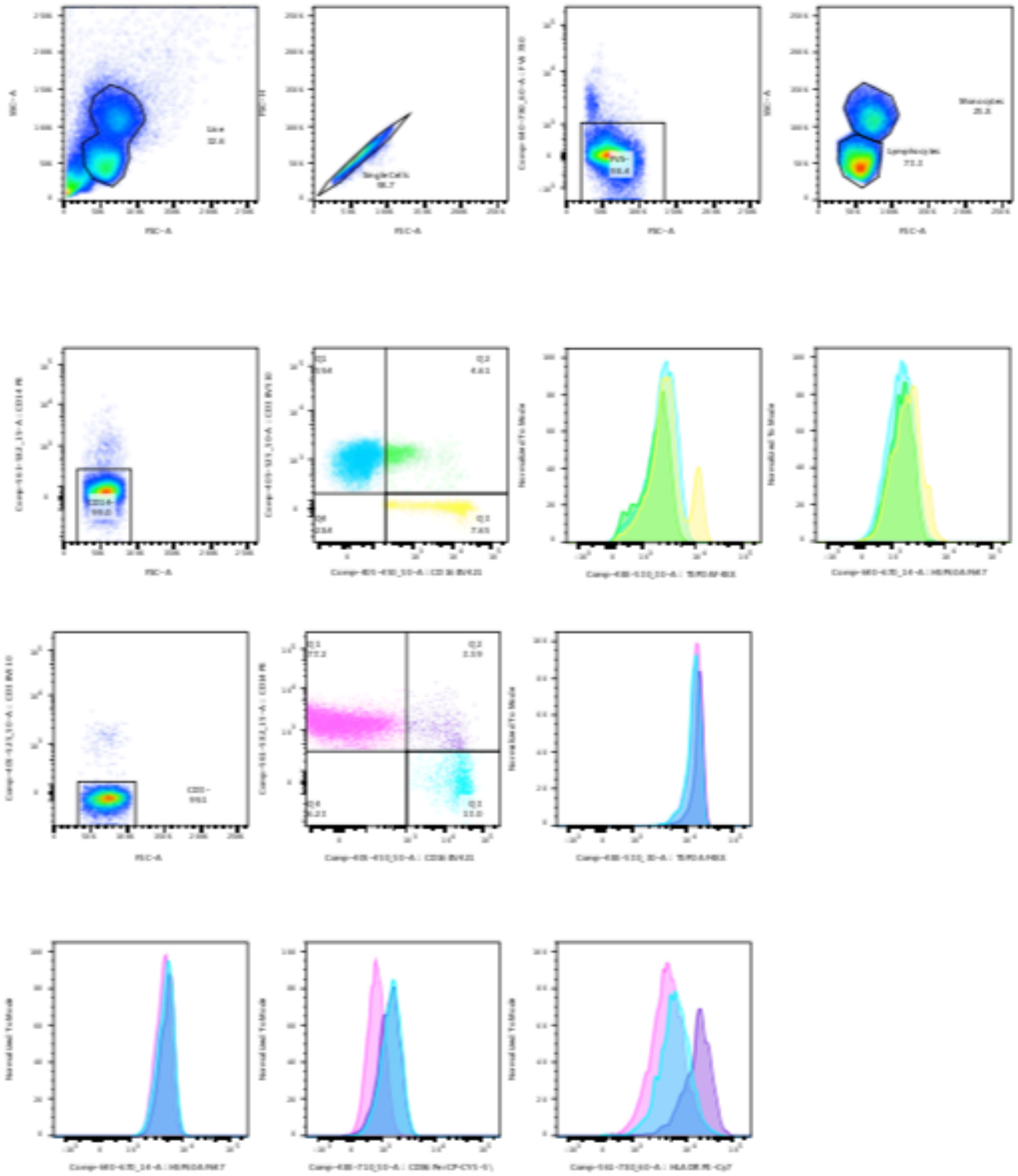
SSC-A
FSC-A
Live
Single Cells
FVS-
Monocytes
Lymphocytes
CD14-
CD3-
Q1
Q2
Q3
Q4
Normalized To Mode

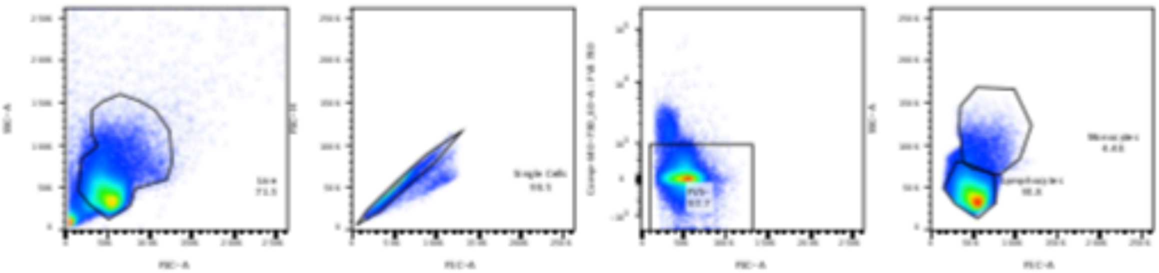
SSC-A
FSC-A
Single Cells
Lymphocytes
Monocytes

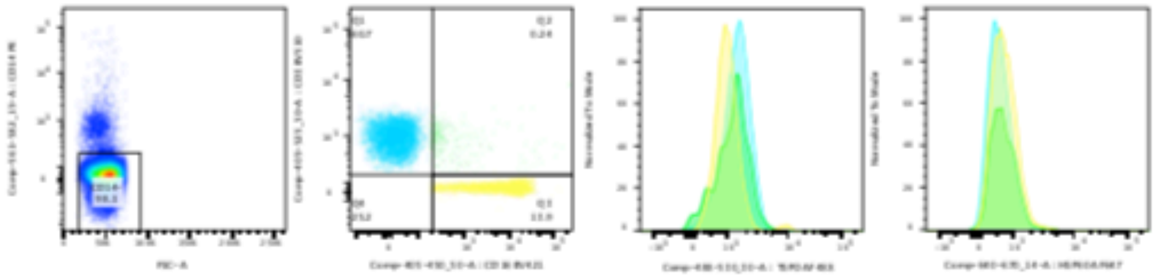

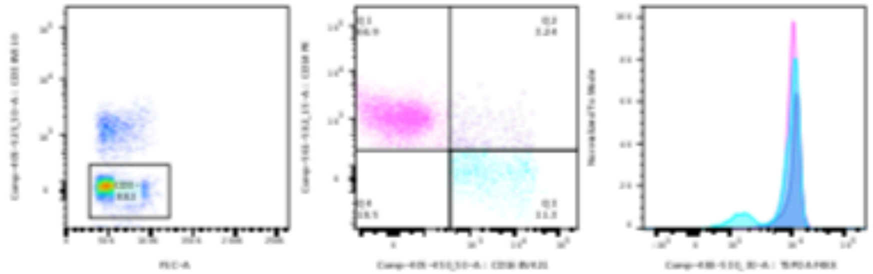

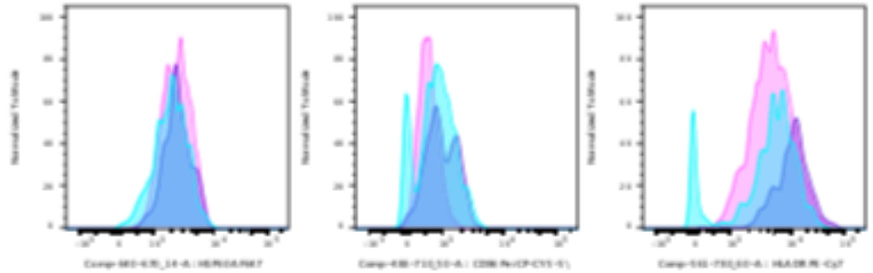

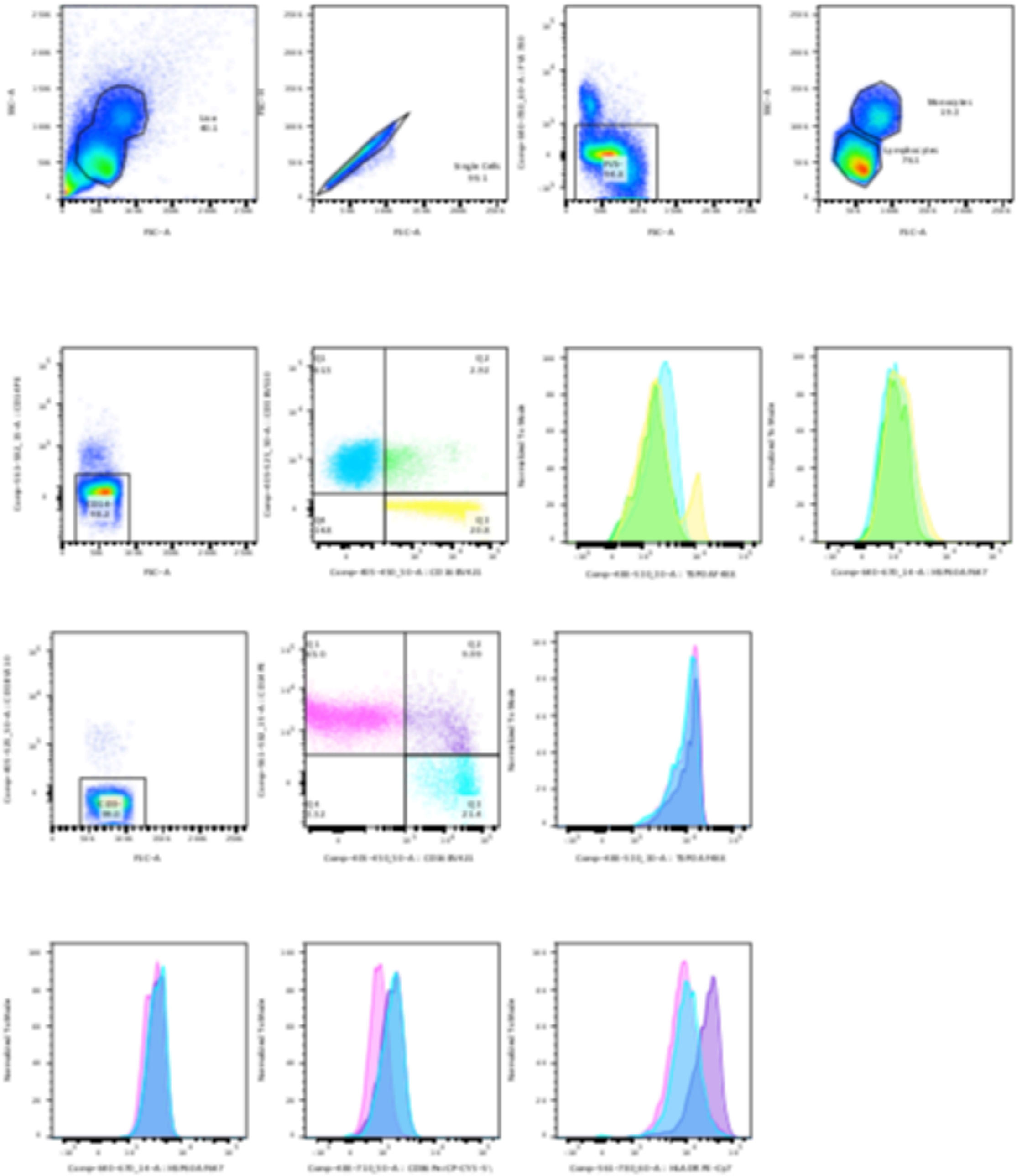
SSC-A
FSC-A
Single Cells
Monocytes
Lymphocytes
Normalized To Mode

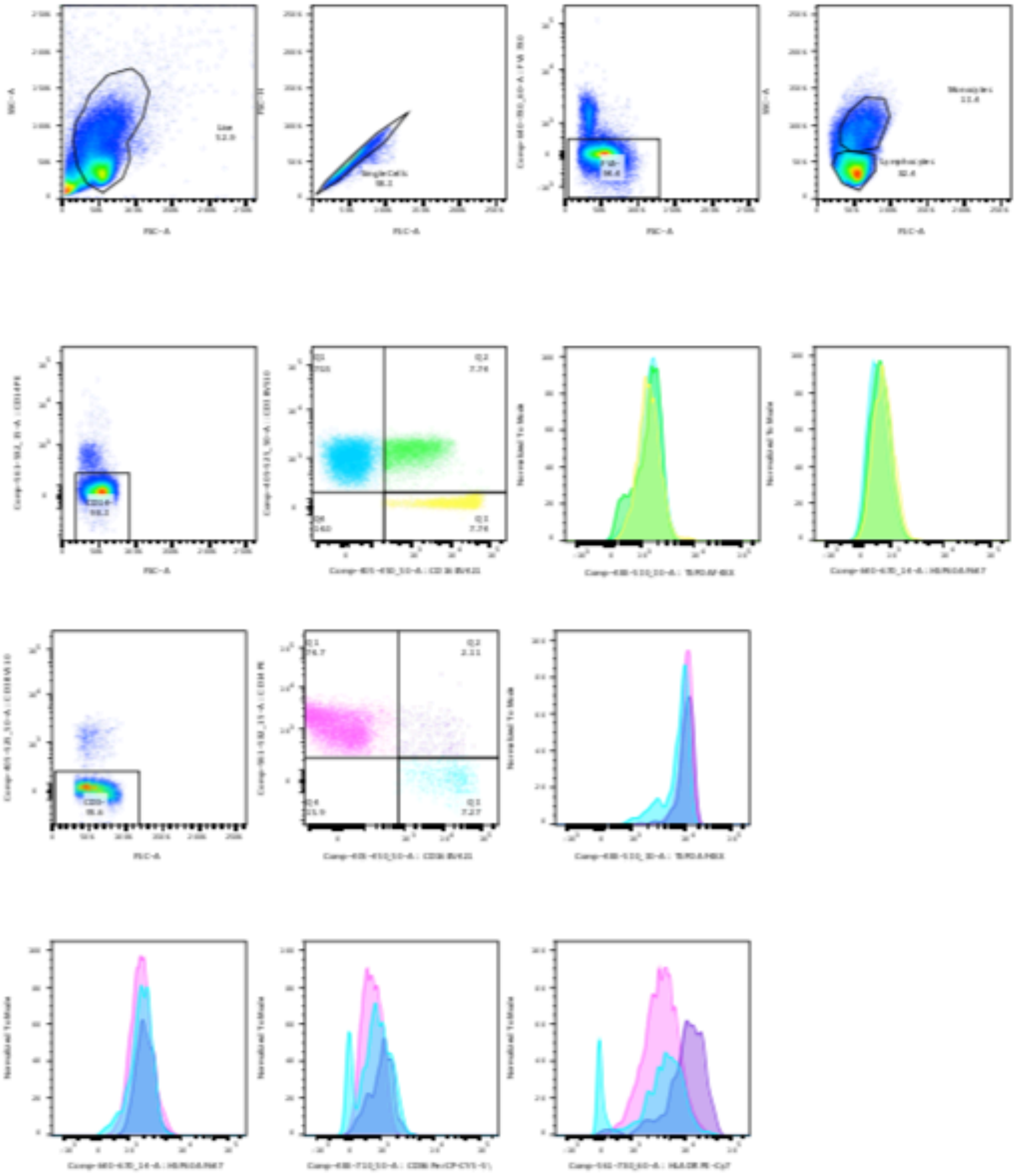
SSC-A
FSC-A
Live
Single Cells
Monocytes
Lymphocytes
Q1
Q2
Q3
Q4
Normalized To Mode

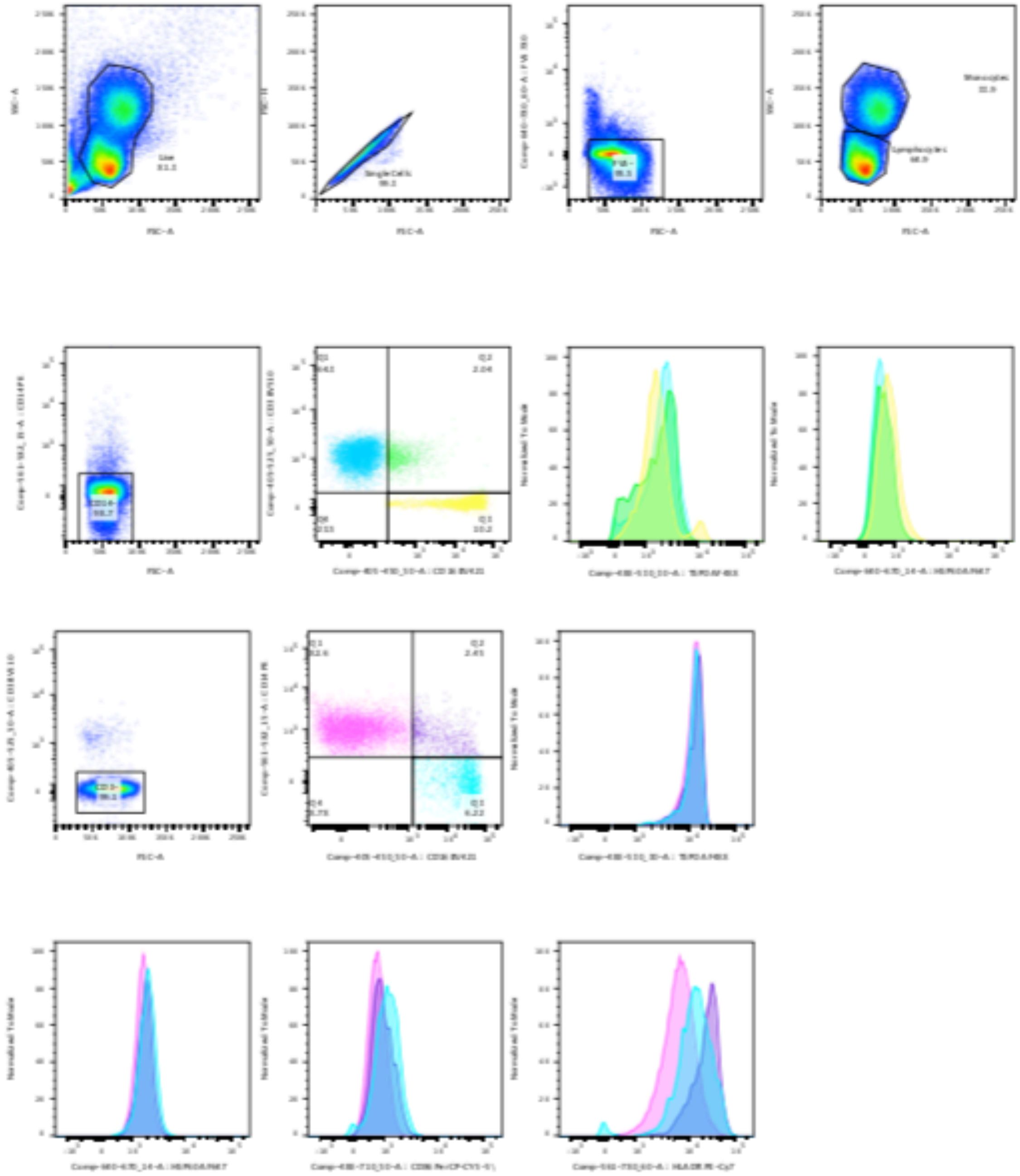
SSC-A
FSC-A
Live
FSC-H
Single Cells
FVS-
Monocytes
Lymphocytes
CD14-
Q1
Q2
Q3
Q4
Normalized To Mode
CD3-

7.4 R code for linear mixed effects modeling

```
install.packages(c("lme4","lmerTest","pbkrtest","ordinal")
library(lme4)            ## Access that version for current session
library(lmerTest)        ## Access that version for current session
library(pbkrtest)        ## Access that version for current session
library(ordinal)         ## Access that version for current session

MonkeyRatioData.model.Stop2 <- lmer( ## -MonthStop sets min=0 as reference value
       Ratio ~ Treatment + factor(-MonthStop) + (1|Monkey),
       data=MonkeyRatioData)
summary(MonkeyRatioData.model.Stop2)

plot(MonkeyRatioData.model.Stop2)           ## Residual versus Fitted Values
title(main="Residual versus Fitted Values") ## Title will not save with plot !!

anova(MonkeyRatioData.model.Stop2)
Type III Analysis of Variance Table with Satterthwaite's method
                     Sum Sq  Mean Sq NumDF  DenDF F value  Pr(>F)
Treatment          0.004168 0.004168     1 3.1515  1.6814 0.28152
factor(-MonthStop) 0.164179 0.023454     7 5.3091  9.4616 0.01041 *
```

```
## Compare change-point model for time: deviations from progressive average
attach(MonkeyRatioData)
rev.MonthStop <- factor(-MonthStop,ordered=TRUE)
MonkeyRatioData.ChangePoint.Stop2 <- lmer(
       Ratio ~ Treatment + rev.MonthStop + (1|Monkey),
       contrasts=list(rev.MonthStop=contr.helmert),
       data=MonkeyRatioData)
summary(MonkeyRatioData.ChangePoint.Stop2)
coef(summary(MonkeyRatioData.ChangePoint.Stop2))

anova(MonkeyRatioData.ChangePoint.Stop2)
Type III Analysis of Variance Table with Satterthwaite's method
                Sum Sq   Mean Sq NumDF  DenDF F value  Pr(>F)
Treatment     0.004168 0.0041679     1 3.1513  1.6814 0.28152
rev.MonthStop 0.164179 0.0234541     7 5.3089  9.4617 0.01041 *

## p-values should be tested against a Bonferroni limit:
## 0.05/7=0.007142857  0.01/7=0.00142857
```

```
################################################################################
colors6 <- c("red","orange","brown","green","blue","purple")

## Plot: TSPO Ratio versus Months before Sacrifice
plot(  type="n",y=range(c(0,1)),
       x=range(as.vector(MonkeyRatioData[,c("MonthStop","MonthStart")])),
       xlab="Months before Sacrifice",ylab="TSPO Ratio")
title(main="TSPO Ratio versus Months before Sacrifice")

points(y=MonkeyRatioData[,"Ratio"],x=MonkeyRatioData[,"MonthStop"],
        type="p",cex=0.75,pch=MonkeyRatioData[,"Monkey"],  ## col=”black”)
        col=colors6[as.factor(MonkeyRatioData[,"Monkey"])])

points(y=MonkeyRatioData[,"Ratio"],x=MonkeyRatioData[,"MonthStart"],
        type="p",cex=0.75,pch=MonkeyRatioData[,"Monkey"],
        col=colors6[as.factor(MonkeyRatioData[,"Monkey"])])

segments(y0=MonkeyRatioData[,"Ratio"],x0=MonkeyRatioData[,"MonthStart"],
          y1=MonkeyRatioData[,"Ratio"],x1=MonkeyRatioData[,"MonthStop"],
          col=colors6[as.factor(MonkeyRatioData[,"Monkey"])],lty=2)

segments(
       y0=MonkeyRatioData[MonkeyRatioData[,"Treatment"]=="Steroid","Ratio"],
      x0=MonkeyRatioData[MonkeyRatioData[,"Treatment"]=="Steroid","MonthStart"],
       y1=MonkeyRatioData[MonkeyRatioData[,"Treatment"]=="Steroid","Ratio"],
       x1=MonkeyRatioData[MonkeyRatioData[,"Treatment"]=="Steroid","MonthStop"])
## Exporting this graphic as a MetaFile loses the dotted lines found in the BitMap
```

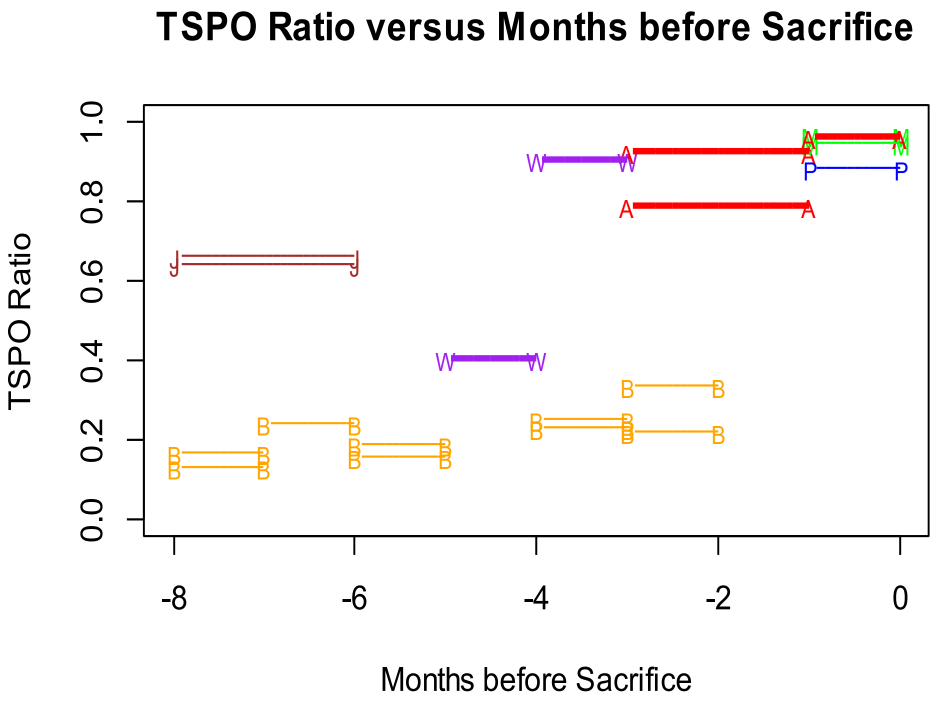

```
plot(MonkeyRatioData.model.Stop) ## Residual versus Fitted Values
```

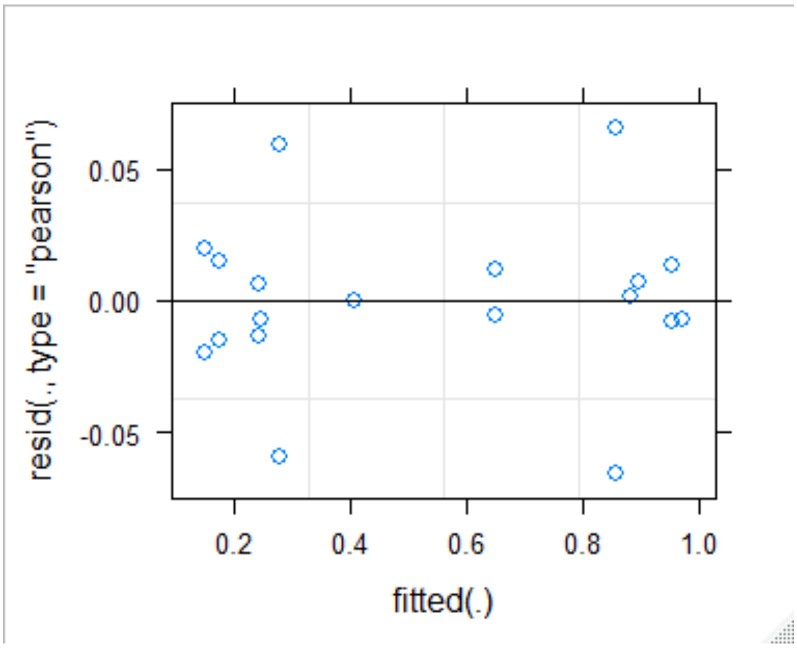

```
MonkeyRatioData.model.Stop2.summary.data <-
cbind(MonkeyRatioData[,c(2,3,7,6,4,5,8)],
       Fitted=predict(MonkeyRatioData.model.Stop2),
      Resid=resid(MonkeyRatioData.model.Stop2,type="pearson"))
MonkeyRatioData.model.Stop2.summary.data
Row             ID  Monkey Lesion Treatment Start  Stop    Ratio    Fitted   Residual
01    <1 mo. - M       M      1      None    -1     0 0.945000 0.9528262 -0.0078262
02    <1 mo. - M       M      2      None    -1     0 0.966000 0.9528262  0.0131738
03    <1 mo. - P       P      1      None    -1     0 0.882804 0.8811997  0.0016043
04   2-3 mo. - B       B      1      None    -3    -2 0.220000 0.2790000 -0.0590000
05   2-3 mo. - B       B      2      None    -3    -2 0.338000 0.2790000  0.0590000
06   3-4 mo. - B       B      3      None    -4    -3 0.250000 0.2434760  0.0065240
07   3-4 mo. - B       B      4      None    -4    -3 0.230000 0.2434760 -0.0134760
08   5-6 mo. - B       B      5      None    -6    -5 0.190000 0.1750000  0.0150000
09   5-6 mo. - B       B      6      None    -6    -5 0.160000 0.1750000 -0.0150000
10   6-7 mo. - B       B      7      None    -7    -6 0.240000 0.2470123 -0.0070123
11   7-8 mo. - B       B      8      None    -8    -7 0.130000 0.1500000 -0.0200000
12   7-8 mo. - B       B      9      None    -8    -7 0.170000 0.1500000  0.0200000
13   6-8 mo. - J       J      1      None    -8    -6 0.660571 0.6483833  0.0121877
14   6-8 mo. - J       J      2      None    -8    -6 0.643208 0.6483833 -0.0051753
15    <1 mo. - A       A      1   Steroid    -1     0 0.961887 0.9688389 -0.0069519
16    >1 mo. - A       A      2   Steroid    -3    -1 0.791196 0.8570595 -0.0658635
17    >1 mo. - A       A      3   Steroid    -3    -1 0.922923 0.8570595  0.0658635
18   3-4 mo. - M2      W      1   Steroid    -4    -3 0.902000 0.8950481  0.0069519
19   4-5 mo. - M2      W      1   Steroid    -5    -4 0.404400 0.4044000  0.0000000

## Notice the highlighted rows with extreme residual values; notice that they are
## balanced with respect to fitted values and not both on the Steroid treatment
## Also, the highlighted Monkey label "M2" is converted to a single character "W"
## Also, the bottom right value of -5.55e-17 was manually converted to 0.00000000
```

```
Transformations.within.Excel <- function(){
TSPO_MRP14 <- cbind(TSPO_MRP14
               ,TSPO=TSPO_MRP14[,4]+TSPO_MRP14[,5]
               ,CD74=TSPO_MRP14[,4]+TSPO_MRP14[,6]
               )
TSPO_MRP14 <- cbind(TSPO_MRP14, OddsRatio=

(TSPO_MRP14[,4]*TSPO_MRP14[,7])/(TSPO_MRP14[,5]*TSPO_MRP14[,6])
               )
TSPO_MRP14 <- cbind(TSPO_MRP14
               ,log10(OR)=log10(TSPO_MRP14[,10])
               )

TSPO_CD74 <- cbind(TSPO_CD74
               ,TSPO=TSPO_CD74[,4]+TSPO_CD74[,5]
               ,CD74=TSPO_CD74[,4]+TSPO_CD74[,6]
               )
TSPO_CD74 <- cbind(TSPO_CD74,  OddsRatio=
                     (TSPO_CD74[,4]*TSPO_CD74[,7])/(TSPO_CD74[,5]*TSPO_CD74[,6])
               )
TSPO_CD74 <- cbind(TSPO_CD74
               ,log10(OR)=log10(TSPO_CD74[,10])
               )
} ## Transformations.within.Excel()


## !! Critical conversion !! ##
TSPO_CD74    <- as.data.frame(TSPO_CD74)
TSPO_MRP14   <- as.data.frame(TSPO_MRP14)

dimnames(TSPO_CD74)[[2]]
dimnames(TSPO_MRP14)[[2]]

TSPO_CD74[13,"Monkey"]  <- "Q"  ## for "P0"
TSPO_MRP14[13,"Monkey"] <- "Q"  ## for "P0"

dimnames(TSPO_CD74)[[2]]
 [1] "Row"              "Monkey"           "Lesion"           "Months"
 [5] "MonthStart"       "MonthStop"        "TSPO+CD74+"       "TSPO+CD74-"
 [9] "TSPO-CD74+"       "TSPO-CD74-"       "TSPO+"            "CD74+"
[13] "OddsRatio"        "log10OR"     ## log10(OR) automatically converted ##
dimnames(TSPO_MRP14)[[2]]
 [1] "Row"              "Monkey"           "Lesion"           "Months"
 [5] "MonthStart"       "MonthStop"        "TSPO+MRP14+"      "TSPO+MRP14-"
 [9] "TSPO-MRP14+"      "TSPO-MRP14-"      "TSPO+"            "MRP14+"
[13] "OddsRatio"        "log10OR"     ## log10(OR) automatically converted ##
dimnames(TSPO_PLP)[[2]]
 [1] "Row"        "Monkey"     "Lesion"     "Months"
 [5] "MonthStart" "MonthStop"  "TSPO+PLP+"  "TSPO+PLP-"
 [9] "TSPO-PLP+"  "TSPO-PLP-"  "TSPO+"      "PLP+"
[13] "OddsRatio"        "log10OR"     ## log10(OR) automatically converted ##
```

```
## Plot:  TSPO.v.MRP14 OddsRatio versus Months before Sacrifice
colors6 <- c("red","orange","brown","green","blue","purple")

plot(  type="n",
       y=range(c(0,as.vector(TSPO_MRP14[,c("OddsRatio")]))),
       x=range(as.vector(TSPO_MRP14[,c("MonthStop","MonthStart")])),
       xlab="Months before Sacrifice",ylab="TSPO.v.MRP14 OddsRatio")
title(main="TSPO.v.MRP14 OddsRatio versus Months before Sacrifice")

points(y=TSPO_MRP14[,"OddsRatio"],x=TSPO_MRP14[,"MonthStop"],
        type="p",cex=0.75,pch=TSPO_MRP14[,"Monkey"],  ## col="black")
        col=colors6[as.factor(TSPO_MRP14[,"Monkey"])])

points(y=TSPO_MRP14[,"OddsRatio"],x=TSPO_MRP14[,"MonthStart"],
        type="p",cex=0.75,pch=TSPO_MRP14[,"Monkey"],
        col=colors6[as.factor(TSPO_MRP14[,"Monkey"])])

segments(y0=TSPO_MRP14[,"OddsRatio"],x0=TSPO_MRP14[,"MonthStart"],
                       y1=TSPO_MRP14[,"OddsRatio"],x1=TSPO_MRP14[,"MonthStop"],
          col=colors6[as.factor(TSPO_MRP14[,"Monkey"])],lty=2)

## Exporting this graphic as a MetaFile loses the dotted lines found in the BitMap
```

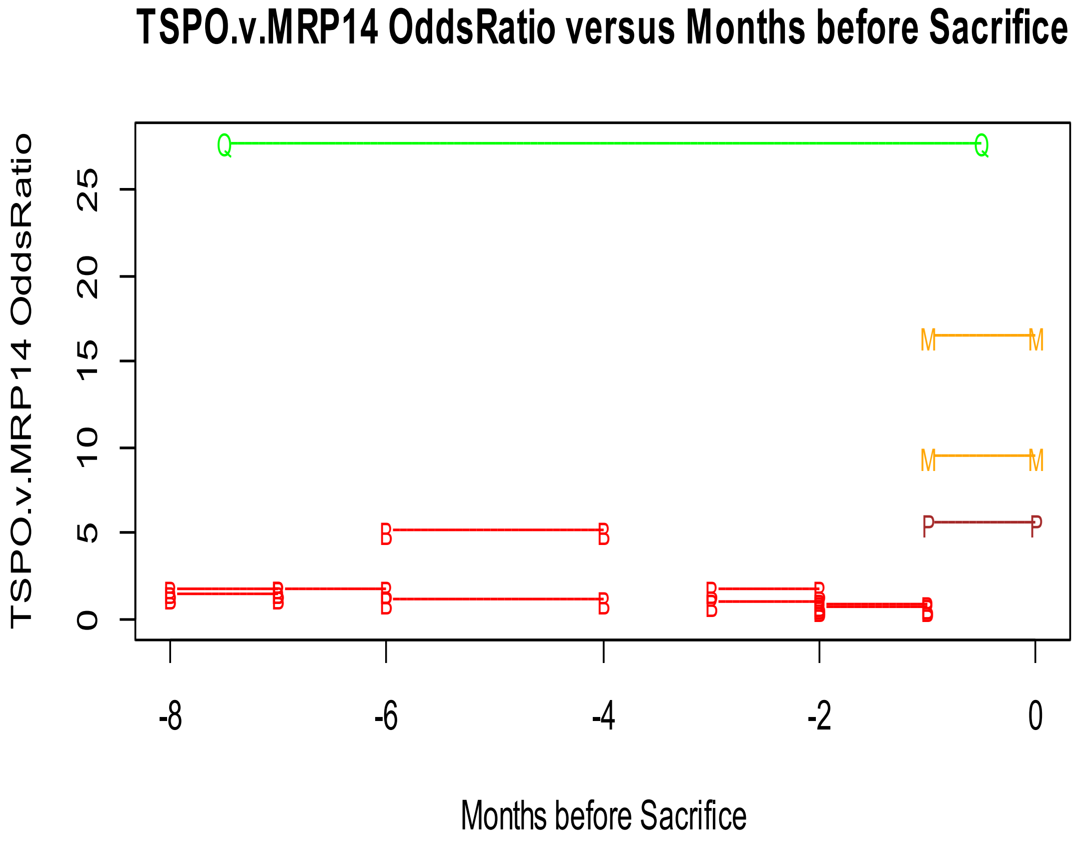

```
## Plot:  TSPO.v.MCD74 OddsRatio versus Months before Sacrifice
plot( type="n",
      y=range(c(0,as.vector(TSPO_CD74[,c("OddsRatio")]))),
      x=range(as.vector(TSPO_CD74[,c("MonthStop","MonthStart")])),
      xlab="Months before Sacrifice",ylab="TSPO.v.CD74 OddsRatio")
title(main="TSPO.v.CD74 OddsRatio versus Months before Sacrifice")

points(y=TSPO_CD74[,"OddsRatio"],x=TSPO_CD74[,"MonthStop"],
       type="p",cex=0.75,pch=TSPO_CD74[,"Monkey"],  ## col="black")
       col=colors6[as.factor(TSPO_CD74[,"Monkey"])])

points(y=TSPO_CD74[,"OddsRatio"],x=TSPO_CD74[,"MonthStart"],
       type="p",cex=0.75,pch=TSPO_CD74[,"Monkey"],
       col=colors6[as.factor(TSPO_CD74[,"Monkey"])])

segments(y0=TSPO_CD74[,"OddsRatio"],x0=TSPO_CD74[,"MonthStart"],
                y1=TSPO_CD74[,"OddsRatio"],x1=TSPO_CD74[,"MonthStop"],
         col=colors6[as.factor(TSPO_CD74[,"Monkey"])],lty=2)
```

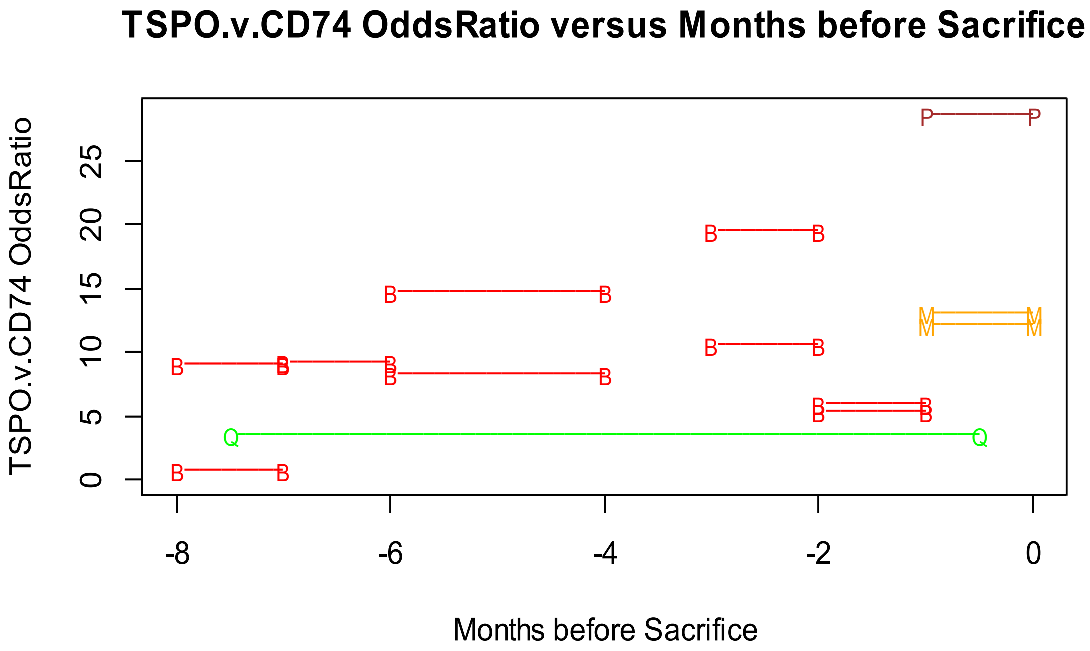

```
## Compare change-point model for time: deviations from progressive average
attach(TSPO_MRP14[-13,])
rev.MonthStop <- factor(-MonthStop,ordered=TRUE)
table(rev.MonthStop)
TSPO_MRP14.ChangePoint.OddsRatio <- lmer(
       OddsRatio ~ rev.MonthStop + (1|Monkey),
       contrasts=list(rev.MonthStop=contr.helmert),
       data=TSPO_MRP14[-13,])
summary(TSPO_MRP14.ChangePoint.OddsRatio)
coef(summary(TSPO_MRP14.ChangePoint.OddsRatio))
```

```
Random effects:
 Groups   Name        Variance Std.Dev.
 Monkey   (Intercept) 22.201   4.712
 Residual              6.643   2.577
Number of obs: 12, groups:  Monkey, 3

Fixed effects:
Parameter        Estimate  Std.Error  ~df       t-stat     Pr(>|t|)
(Intercept)     3.0912720  4.0431817 0.7173073  0.7645642 0.6211879
rev.MonthStop1 -4.3769928  3.1250592 0.9150781 -1.4006112 0.4098770
rev.MonthStop2 -1.2558214  1.2058910 1.6182328 -1.0414054 0.4282392
rev.MonthStop4 -0.1821393  0.7084784 2.8015076 -0.2570852 0.8148255
rev.MonthStop6 -0.3775046  0.6164355 5.5822282 -0.6123991 0.5643660
rev.MonthStop7 -0.2910788  0.3878563 5.3048922 -0.7504810 0.4849038

~df: Satterthwaite approximate degrees of freedom employed in t-tests.
```

For the single healthy monkey (Proton, with symbol “P0”, or “Q” in the displays), the observed OddsRatio=27.70907 may be tested against the independent sample estimate. For model parameterizations representing Months-before-Sacrifice as contrasts, the overall mean is estimated as the Intercept=3.0912720 of the model, with SEM=4.0431817 and Satterthwaite degrees of freedom~0.7173073. That individual OddsRatio=27.70907 approaches statistical significance at the level 0.169282 two-sided.

```
For Monkey P0~Q: OddsRatio=27.70907 Intercept=3.0912720 SEM=4.0431817 df~0.7173073
             t(0.7173073)=(27.70907-3.0912720)/4.0431817=6.088719 2p=0.169282
```

```
## Compare change-point model for time: deviations from progressive average
attach(TSPO_CD74[-13,])
rev.MonthStop <- factor(-MonthStop,ordered=TRUE)
table(rev.MonthStop)
TSPO_CD74.ChangePoint.OddsRatio <- lmer(
       OddsRatio ~ rev.MonthStop + (1|Monkey),
       contrasts=list(rev.MonthStop=contr.helmert),
       data=TSPO_CD74[-13,])
summary(TSPO_CD74.ChangePoint.OddsRatio)
coef(summary(TSPO_CD74.ChangePoint.OddsRatio))
```

```
Random effects:
 Groups   Name        Variance Std.Dev.
 Monkey   (Intercept) 114.36   10.69
 Residual              18.92    4.35
Number of obs: 12, groups:  Monkey, 3


Fixed effects:
Parameter        Estimate   Std.Error  ~df         t-stat   Pr(>|t|)
(Intercept)     11.1781634  9.0981264 0.8249590  1.2286226 0.4657772
rev.MonthStop1  -7.3360534  6.8558380 0.9496699 -1.0700447 0.4857644
rev.MonthStop2   0.6705094  2.5047677 1.3627491  0.2676932 0.8237703
rev.MonthStop4  -0.5568007  1.4009730 2.0574047 -0.3974386 0.7284996
rev.MonthStop6  -0.7871332  1.1288558 4.5351741 -0.6972841 0.5197318
rev.MonthStop7  -1.2548523  0.7167945 4.1325469 -1.7506444 0.1525968

~df: Satterthwaite approximate degrees of freedom employed in t-tests.
```

```
summary(TSPO_MRP14[-13,c(7:10)])
summary(TSPO_MRP14[-13,c(11:14)])

rbind(
Mean    =     apply(TSPO_MRP14[-13,c(7:10)],2,"mean"),
Std.Dev =sqrt(apply(TSPO_MRP14[-13,c(7:10)],2,"var")),
SEM     =sqrt(apply(TSPO_MRP14[-13,c(7:10)],2,"var")
             /apply(TSPO_MRP14[-13,c(7:10)],2,"length")),
N       =     apply(TSPO_MRP14[-13,c(7:10)],2,"length")  )

rbind(
Mean    =     apply(TSPO_MRP14[-13,c(11:14)],2,"mean"),
Std.Dev =sqrt(apply(TSPO_MRP14[-13,c(11:14)],2,"var")),
SEM     =sqrt(apply(TSPO_MRP14[-13,c(11:14)],2,"var")
             /apply(TSPO_MRP14[-13,c(11:14)],2,"length")),
N       =     apply(TSPO_MRP14[-13,c(11:14)],2,"length")  )
```

```
  TSPO+MRP14+        TSPO+MRP14-       TSPO-MRP14+         TSPO-MRP14-
 Min.   :0.003811   Min.   :0.08087   Min.   :0.0004704   Min.   :0.03233
 1st Qu.:0.031533   1st Qu.:0.14646   1st Qu.:0.0129143   1st Qu.:0.30385
 Median :0.050005   Median :0.19768   Median :0.0481938   Median :0.59173
 Mean   :0.093196   Mean   :0.30251   Mean   :0.0979045   Mean   :0.50639
 3rd Qu.:0.119896   3rd Qu.:0.35022   3rd Qu.:0.1018028   3rd Qu.:0.72296
 Max.   :0.387733   Max.   :0.81468   Max.   :0.4349112   Max.   :0.84359

     TSPO+            MRP14+          OddsRatio          Log10OR
 Min.   :0.1334   Min.   :0.01677   Min.   : 0.7224   Min.   :-0.14121
 1st Qu.:0.1882   1st Qu.:0.09094   1st Qu.: 1.1563   1st Qu.: 0.06229
 Median :0.2419   Median :0.13980   Median : 1.8240   Median : 0.26103
 Mean   :0.3957   Mean   :0.19110   Mean   : 3.9840   Mean   : 0.37833
 3rd Qu.:0.4757   3rd Qu.:0.25326   3rd Qu.: 5.3391   3rd Qu.: 0.72721
 Max.   :0.9667   Max.   :0.54832   Max.   :16.5486   Max.   : 1.21876


Parameter   TSPO+MRP14+ TSPO+MRP14- TSPO-MRP14+ TSPO-MRP14-
Mean         0.09319630  0.30250550  0.09790455  0.50639366
Std.Dev      0.11193598  0.24804697  0.13510060  0.30233381
SEM          0.03231314  0.07160499  0.03900018  0.08727625
N           12.00000000 12.00000000 12.00000000 12.00000000

Parameter    TSPO+      MRP14+      OddsRatio      Log10OR
Mean         0.3957018  0.19110084    3.984050     0.3783338
Std.Dev      0.3298303  0.16549971    4.763926     0.4341112
SEM          0.0952138  0.04777565    1.375227     0.1253171
N           12.0000000 12.00000000   12.000000    12.0000000
```

```
summary(TSPO_CD74[-13,c(7:10)])
summary(TSPO_CD74[-13,c(11:14)])

rbind(
Mean    =     apply(TSPO_CD74[-13,c(7:10)],2,"mean"),
Std.Dev =sqrt(apply(TSPO_CD74[-13,c(7:10)],2,"var")),
SEM     =sqrt(apply(TSPO_CD74[-13,c(7:10)],2,"var")
             /apply(TSPO_CD74[-13,c(7:10)],2,"length")),
N       =     apply(TSPO_CD74[-13,c(7:10)],2,"length")  )

rbind(
Mean    =     apply(TSPO_CD74[-13,c(11:14)],2,"mean"),
Std.Dev =sqrt(apply(TSPO_CD74[-13,c(11:14)],2,"var")),
SEM     =sqrt(apply(TSPO_CD74[-13,c(11:14)],2,"var")
             /apply(TSPO_CD74[-13,c(11:14)],2,"length")),
N       =     apply(TSPO_CD74[-13,c(11:14)],2,"length")  )
```

```
   TSPO+CD74+         TSPO+CD74-         TSPO-CD74+          TSPO-CD74-
 Min.   :0.05107   Min.   :0.01085   Min.   :0.003528   Min.   :0.02848
 1st Qu.:0.16634   1st Qu.:0.02471   1st Qu.:0.142327   1st Qu.:0.22572
 Median :0.21481   Median :0.04120   Median :0.243567   Median :0.46468
 Mean   :0.28272   Mean   :0.11298   Mean   :0.232705   Mean   :0.37159
 3rd Qu.:0.31480   3rd Qu.:0.13682   3rd Qu.:0.296083   3rd Qu.:0.53061
 Max.   :0.69222   Max.   :0.45520   Max.   :0.539448   Max.   :0.65571

     TSPO+             CD74+            OddsRatio           Log10OR
 Min.   :0.1334   Min.   :0.3005   Min.   : 0.7546   Min.   :-0.1223
 1st Qu.:0.1882   1st Qu.:0.4306   1st Qu.: 7.7781   1st Qu.: 0.8870
 Median :0.2419   Median :0.4808   Median : 9.9920   Median : 0.9986
 Mean   :0.3957   Mean   :0.5154   Mean   :11.5137   Mean   : 0.9501
 3rd Qu.:0.4757   3rd Qu.:0.6612   3rd Qu.:13.5782   3rd Qu.: 1.1323
 Max.   :0.9667   Max.   :0.7229   Max.   :28.7548   Max.   : 1.4587


Parameter   TSPO+CD74+  TSPO+CD74-    TSPO-CD74+  TSPO-CD74-
Mean        0.28272411  0.11297769    0.23270533  0.37159288
Std.Dev     0.21251028  0.14017069    0.17142297  0.21678877
SEM         0.06134643  0.04046379    0.04948555  0.06258153
N          12.00000000 12.00000000   12.00000000 12.00000000

Parameter        TSPO+        CD74+    OddsRatio      Log10OR
Mean        0.3957018   0.51542943    11.513659   0.9500996
Std.Dev     0.3298303   0.14120731     7.255675   0.3932375
SEM         0.0952138   0.04076304     2.094533   0.1135179
N          12.0000000  12.00000000    12.000000  12.0000000
```

8 References

1. Rupprecht R, Papadopoulos V, Rammes G, et al. Translocator protein (18 kDa) (TSPO) as a therapeutic target for neurological and psychiatric disorders. *Nat Rev Drug Discov*. 2010;9(12):971-988. doi:10.1038/nrd3295
2. Chen M-K, Guilarte TR. Translocator Protein 18kDA (TSPO): Molecular Sensor of Brain Injury & Repair. 2009;118(1):1-17. doi:10.1016/j.pharmthera.2007.12.004.Translocator
3. Poutiainen P, Jaronen M, Quintana FJ, Brownell A-L. Precision Medicine in Multiple Sclerosis: Future of PET Imaging of Inflammation and Reactive Astrocytes. *Front Mol Neurosci*. 2016;9(September):1-23. doi:10.3389/fnmol.2016.00085
4. Nutma E, Stephenson JA, Gorter RP, et al. A quantitative neuropathological assessment of translocator protein expression in multiple sclerosis. *Brain*. 2019:3440-3455. doi:10.1093/brain/awz287
5. Airas L, Rissanen E, Rinne JO. Imaging neuroinflammation in multiple sclerosis using TSPO-PET. *Clin Transl Imaging*. 2015;3(6):461-473. doi:10.1007/s40336-015-0147-6
6. Largeau B, Dupont AC, Guilloteau D, Santiago-Ribeiro MJ, Arlicot N. TSPO PET imaging: From microglial activation to peripheral sterile inflammatory diseases? *Contrast Media Mol Imaging*. 2017;2017. doi:10.1155/2017/6592139
7. Tronel C, Largeau B, Ribeiro MJS, Guilloteau D, Dupont AC, Arlicot N. Molecular targets for PET imaging of activated microglia: The current situation and future expectations. *Int J Mol Sci*. 2017. doi:10.3390/ijms18040802
8. Owen DR, Howell OW, Tang S-P, et al. Two binding sites for [3H]PBR28 in human brain: implications for TSPO PET imaging of neuroinflammation. *J Cereb Blood Flow Metab*. 2010;30(9):1608-1618. doi:10.1038/jcbfm.2010.63
9. Mizrahi R, Rusjan PM, Kennedy J, et al. Translocator protein (18 kDa) polymorphism (rs6971) explains in-vivo brain binding affinity of the PET radioligand [18F]-FEPPA. *J Cereb Blood Flow Metab*. 2012. doi:10.1038/jcbfm.2012.46
10. Papadopoulos V, Lecanu L. Translocator protein (18 kDa) TSPO: an emerging therapeutic target in neurotrauma. *Changes*. 2009;29(6):997-1003. doi:10.1016/j.biotechadv.2011.08.021.Secreted
11. Kim E-J, Yu SS-W. Translocator protein 18 kDa (TSPO): old dogma, new mice, new structure, and new questions for neuroprotection. *Neural Regen Res*. 2015;10(6):2015-2017. doi:10.4103/1673-5374.158338
12. Da Pozzo E, Giacomelli C, Costa B, et al. TSPO PIGA Ligands Promote Neurosteroidogenesis and Human Astrocyte Well-Being. *Int J Mol Sci*. 2016;17(7). doi:10.3390/ijms17071028
13. Li HD, Li M, Shi E, et al. A translocator protein 18 kDa agonist protects against cerebral ischemia/reperfusion injury. *J Neuroinflammation*. 2017;14:151. doi:10.1186/s12974-017-0921-7
14. Colasanti A, Guo Q, Giannetti P, et al. Hippocampal neuroinflammation, functional connectivity, and depressive symptoms in multiple sclerosis. *Biol Psychiatry*. 2016;80(1):62-72. doi:10.1016/j.biopsych.2015.11.022

15. Datta G, Colasanti A, Kalk N, et al. (11)C-PBR28 and (18)F-PBR111 Detect White Matter Inflammatory Heterogeneity in Multiple Sclerosis. *J Nucl Med*. 2017. doi:10.2967/jnumed.116.187161

16. Vogel DY, Vereyken EJ, Glim JE, et al. Macrophages in inflammatory multiple sclerosis lesions have an intermediate activation status. *J Neuroinflammation*. 2013;10(1):35. doi:10.1186/1742-2094-10-35

17. Mattner F, Staykova M, Berghofer P, et al. Central nervous system expression and PET imaging of the translocator protein in relapsing-remitting experimental autoimmune encephalomyelitis. *J Nucl Med*. 2013;54:291-298. doi:10.2967/jnumed.112.108894

18. Daugherty DJ, Selvaraj V, Chechneva O V., Liu X-B, Pleasure DE, Deng W. A TSPO ligand is protective in a mouse model of multiple sclerosis. *EMBO Mol Med*. 2013;5(6):891-903. doi:10.1002/emmm.201202124

19. ’t Hart B a, Vogels J, Bauer J, Brok HPM, Blezer E. Non-invasive measurement of brain damage in a primate model of multiple sclerosis. *Trends Mol Med*. 2004;10(2):85-91. doi:10.1016/j.molmed.2003.12.008

20. ’t Hart B a, Hintzen RQ, Laman JD. Multiple sclerosis - a response-to-damage model. *Trends Mol Med*. 2009;15(6):235-244. doi:10.1016/j.molmed.2009.04.001

21. ’t Hart B a, Laman JD, Bauer J, Blezer E, van Kooyk Y, Hintzen RQ. Modelling of multiple sclerosis: lessons learned in a non-human primate. *Lancet Neurol*. 2004;3(10):588-597. doi:10.1016/S1474-4422(04)00879-8

22. Gaitan MI, Maggi P, Wohler J, et al. Perivenular brain lesions in a primate multiple sclerosis model at 7-tesla magnetic resonance imaging. *Mult Scler*. 2014;20(1):64-71. doi:10.1177/1352458513492244

23. Stassart RM, Helms G, Garea-Rodríguez E, et al. A New Targeted Model of Experimental Autoimmune Encephalomyelitis in the Common Marmoset. *Brain Pathol*. 2016;26(4):452-464. doi:10.1111/bpa.12292

24. Leibovitch E, Wohler JE, Cummings Macri SM, et al. Novel marmoset (Callithrix jacchus) model of human Herpesvirus 6A and 6B infections: immunologic, virologic and radiologic characterization. *PLoS Pathog*. 2013;9(1):e1003138. doi:10.1371/journal.ppat.1003138

25. Maggi P, Sati P, Massacesi L. Magnetic resonance imaging of experimental autoimmune encephalomyelitis in the common marmoset. *J Neuroimmunol*. 2017;304:86-92. doi:10.1016/j.jneuroim.2016.09.016

26. Jaremko Ł, Jaremko M, Giller K, Becker S, Zweckstetter M. Structure of the mitochondrial translocator protein in complex with a diagnostic ligand. *Science (80-)*. 2014. doi:10.1126/science.1248725

27. Gut P, Zweckstetter M, Banati RB. Lost in translocation: the functions of the 18-kD translocator protein. *Trends Endocrinol Metab*. 2015;26(7):349-356. doi:10.1016/j.tem.2015.04.001

28. Tu LN, Morohaku K, Manna PR, et al. Peripheral Benzodiazepine Receptor/Translocator Protein Global Knockout Mice are Viable with no Effects on Steroid Hormone Biosynthesis. *J Biol Chem*. 2014;289(40):27444-27454. doi:10.1074/jbc.M114.578286

29. Banati RB, Middleton RJ, Chan R, et al. Positron emission tomography and functional

characterization of a complete PBR/TSPO knockout. *Nat Commun*. 2014;5:5452. doi:10.1038/ncomms6452

30. Liu GJ, Middleton RJ, Hatty CR, et al. The 18 kDa translocator protein, microglia and neuroinflammation. *Brain Pathol*. 2014;24(8):631-653. doi:10.1111/bpa.12196

31. Selvaraj V, Stocco DM. The changing landscape in translocator protein (TSPO) function. *Trends Endocrinol Metab*. 2015;26(7):341-348. doi:10.1016/j.tem.2015.02.007

32. Batarseh A, Barlow KD, Martinez-Arguelles DB, Papadopoulos Vassilios. Functional Characterization of the Human Translocator Protein (18 kDa) Gene Promoter in Human Breast Cancer Cell Lines. *Biochim Biophys Acta*. 2012;1819(1):38-56. doi:10.1038/nature13314.A

33. Li J, Papadopoulos V. Translocator protein (18 kDa) as a pharmacological target in adipocytes to regulate glucose homeostasis. *Biochem Pharmacol*. 2015;97(1):99-110. doi:10.1016/j.bcp.2015.06.020

34. Parmar A, Szabo AM, Kam W, et al. Molecular imaging of altered 18 KD translocator protein (TSPO) expression in the adipose tissue of diet-induced obese mice using inveon PET/CT scanner. *Intern Med J*. 2014;44:13. doi:10.1111/imj.12418

35. Parmar A, Szabo AM, Kam W, et al. In vivo PET imaging shows impaired 18 kDa translocator protein (TSPO) expression in the adipose tissue of diet-induced obese mice. *Mol Imaging Biol*. 2015. doi:10.1007/s11307-014-0809-1

36. Thompson MM, Manning HC, Ellacott KLJ. Translocator protein 18 kDa (TSPO) is regulated in white and brown adipose tissue by obesity. *PLoS One*. 2013;8(11):e79980. doi:10.1371/journal.pone.0079980

37. Barron AM, Tokunaga M, Zhang MR, Ji B, Suhara T, Higuchi M. Assessment of neuroinflammation in a mouse model of obesity and β-amyloidosis using PET. *J Neuroinflammation*. 2016;13(1):221. doi:10.1186/s12974-016-0700-x

38. Ran C, Albrecht DS, Bredella MA, et al. PET Imaging of Human Brown Adipose Tissue with the TSPO Tracer [11C]PBR28. *Mol Imaging Biol*. 2018;20(3):188-193. doi:10.1007/s11307-017-1129-z

39. Oh HR. In vivo monitoring of brown fat using F-18-CB251 PET/CT targeting translocator protein: A comparative study with F-18-FDG PET/CT. *Mol Imaging Biol*. 2017. doi:10.1007/s11307-01-017-1138-y

40. Bird JLE, Izquierdo-Garcia D, Davies JR, et al. Evaluation of translocator protein quantification as a tool for characterising macrophage burden in human carotid atherosclerosis. *Atherosclerosis*. 2010. doi:10.1016/j.atherosclerosis.2009.11.047

41. Zheng J, Boisgard R, Siquier-Pernet K, Decaudin D, Dollé F, Tavitian B. Differential expression of the 18 kDa translocator protein (TSPO) by neoplastic and inflammatory cells in mouse tumors of breast cancer. *Mol Pharm*. 2011;8(3):823-832. doi:10.1021/mp100433c

42. Lavisse S, Guillermier M, Herard A-S, et al. Reactive Astrocytes Overexpress TSPO and Are Detected by TSPO Positron Emission Tomography Imaging. *J Neurosci*. 2012;32(32):10809-10818. doi:10.1523/JNEUROSCI.1487-12.2012

43. Chechneva O V., Deng W. Mitochondrial translocator protein (TSPO), astrocytes and neuroinflammation. *Neural Regen Res*. 2016;11(7):1056-1057. doi:10.4103/1673-5374.187027

44. Maeda J, Higuchi M, Inaji M, et al. Phase-dependent roles of reactive microglia and astrocytes in nervous system injury as delineated by imaging of peripheral benzodiazepine receptor. *Brain Res*. 2007;1157(1):100-111. doi:10.1016/j.brainres.2007.04.054

45. De Rosa A, Zappavigna S, Villa MR, et al. Prognostic role of translocator protein and oxidative stress markers in chronic lymphocytic leukemia patients treated with bendamustine plus rituximab. *Oncol Lett*. 2015;9(3):1327-1332. doi:10.3892/ol.2014.2817

46. Zhang J. Mapping neuroinflammation in frontotemporal dementia with molecular PET imaging. *J Neuroinflammation*. 2015;12(108). doi:10.1186/s12974-015-0236-5

47. Janssen B, Vugts DJ, Funke U, et al. Imaging of neuroinflammation in Alzheimer's disease, multiple sclerosis and stroke: Recent developments in positron emission tomography. *Biochim Biophys Acta - Mol Basis Dis*. 2016;1862(3):425-441. doi:10.1016/j.bbadis.2015.11.011

48. Hommet C, Mondon K, Camus V, et al. Neuroinflammation and β amyloid deposition in alzheimer's disease: In vivo quantification with molecular imaging. *Dement Geriatr Cogn Disord*. 2014;37(1-2):1-18. doi:10.1159/000354363

49. Schain M, Kreisl WC. Neuroinflammation in Neurodegenerative Disorders—a Review. *Curr Neurol Neurosci Rep*. 2017;17(3):25. doi:10.1007/s11910-017-0733-2

50. Tyler P, Butt S. Basic principles of MRI. In: *Radionuclide and Hybrid Bone Imaging*. ; 2012. doi:10.1007/978-3-642-02400-9_7

51. van Horssen J, Singh S, van der Pol S, et al. Clusters of activated microglia in normal-appearing white matter show signs of innate immune activation. *J Neuroinflammation*. 2012;9(156). doi:10.1186/1742-2094-9-156

52. Schmitz RE, Alessio AM, Kinahan PE. 1 The Physics of PET/CT Scanners. *PET PET/CT*. 2019:1-16. doi:10.1055/b-0039-166611

53. Cherry SR, Sorenson JA, Phelps ME. in NUCLEAR MEDICINE.

54. Wernick MN, Aarsvold JN. *Emission Tomography: The Fundamentals of PET and SPECT*.; 2004. doi:10.1097/00024382-200504000-00016

55. Alessio AM, Kinahan PE, Cheng PM, Vesselle H, Karp JS. PET/CT scanner instrumentation, challenges, and solutions. *Radiol Clin North Am*. 2004;42(6):1017-1032. doi:10.1016/j.rcl.2004.08.001

56. Van Waarde A. Introduction on PET: Description of basics and principles. In: *Trends on the Role of PET in Drug Development*. ; 2012. doi:10.1142/9789814317740_0001

57. N. Kuzhuppilly Ramakrishnan, A.A. R, A.K.D. V, et al. Sigma-1 receptors in healthy aging: Brain receptor density in young and aged rats assessed with 11C-SA4503 and microPET. *Eur J Nucl Med Mol Imaging*. 2010.

58. Shukla A, Kumar U. Positron emission tomography: An overview. *J Med Phys*. 2006;31(1):13-21. doi:10.4103/0971-6203.25665

59. Trapani A, Palazzo C, De Candia M, Lasorsa FM, Trapani G. Targeting of the translocator protein 18 kDa (TSPO): A valuable approach for nuclear and optical imaging of activated microglia. *Bioconjug Chem*. 2013;24(9):1415-1428. doi:10.1021/bc300666f

60. Cagnin A, Brooks DJ, Kennedy AM, et al. In-vivo measurement of activated microglia

in dementia. *Lancet*. 2001;358(9280):461-467. doi:10.1016/S0140-6736(01)05625-2

61. Chauveau F, Boutin H, Van Camp N, Dollé F, Tavitian B. Nuclear imaging of neuroinflammation: A comprehensive review of [11C]PK11195 challengers. *Eur J Nucl Med Mol Imaging*. 2008;35(12):2304-2319. doi:10.1007/s00259-008-0908-9

62. Cerami C, Iaccarino L, Perani D. Molecular imaging of neuroinflammation in neurodegenerative dementias: The role of in vivo PET imaging. *Int J Mol Sci*. 2017;18(5). doi:10.3390/ijms18050993

63. Chauveau F, Van Camp N, Dollé F, et al. Comparative evaluation of the translocator protein radioligands 11C-DPA-713, 18F-DPA-714, and 11C-PK11195 in a rat model of acute neuroinflammation. *J Nucl Med*. 2009. doi:10.2967/jnumed.108.058669

64. Paul J. PET and MRI as Yardstick for Neuro-Inflammation, a Pathological Trademark of Multiple Sclerosis (MS). *J Clin Rev Case Reports*. 2018;3(4):1-2. doi:10.33140/jcrc/03/04/00001

65. Rissanen E, Tuisku J, Rokka J, et al. In vivo detection of diffuse inflammation in secondary progressive multiple sclerosis using PET imaging and the radioligand11C-PK11195. *J Nucl Med*. 2014;55(6):939-944. doi:10.2967/jnumed.113.131698

66. Giannetti P, Politis M, Su P, et al. Increased PK11195-PET binding in normal-appearing white matter in clinically isolated syndrome. *Brain*. 2015;38(1):110-119. doi:10.1093/brain/awu331

67. Wu C, Wang C, Popescu DC, et al. A novel PET marker for in vivo quantification of myelination. *Bioorganic Med Chem*. 2010. doi:10.1016/j.bmc.2010.10.018

68. Tran L, Huitema ADR, Van Rijswijk MH, et al. CD20 antigen imaging with124I-rituximab PET/CT in patients with rheumatoid arthritis. *Hum Antibodies*. 2011;20(1-2):29-35. doi:10.3233/HAB-2011-0239

69. Di Gialleonardo V, Signore A, Glaudemans AWJM, Dierckx RAJO, De Vries EFJ. N-(4- 18F-fluorobenzoyl)interleukin-2 for PET of human-activated T lymphocytes. *J Nucl Med*. 2012;53(5):679-686. doi:10.2967/jnumed.111.091306

70. Uddin MJ, Crews BC, Blobaum AL, et al. Selective visualization of cyclooxygenase-2 in inflammation and cancer by targeted fluorescent imaging agents. *Cancer Res*. 2010. doi:10.1158/0008-5472.CAN-09-2664

71. Uddin MJ, Crews BC, Ghebreselasie K, et al. Fluorinated COX-2 inhibitors as agents in PET imaging of inflammation and cancer. *Cancer Prev Res*. 2011. doi:10.1158/1940-6207.CAPR-11-0120

72. Hartung D, Schäfers M, Fujimoto S, et al. Targeting of matrix metalloproteinase activation for noninvasive detection of vulnerable atherosclerotic lesions. *Eur J Nucl Med Mol Imaging*. 2007;34(1 SUPPL.):1-8. doi:10.1007/s00259-007-0435-0

73. Nahrendorf M, Keliher E, Panizzi P, et al. 18F-4V for PET-CT Imaging of VCAM-1 Expression in Atherosclerosis. *JACC Cardiovasc Imaging*. 2009;2(10):1213-1222. doi:10.1016/j.jcmg.2009.04.016

74. Brosnan CF, Raine CS. The astrocyte in multiple sclerosis revisited. *Glia*. 2013;61(4):453-465. doi:10.1002/glia.22443

75. Lavisse S, Inoue K, Jan C, et al. [18F]DPA-714 PET imaging of translocator protein TSPO (18 kDa) in the normal and excitotoxically-lesioned nonhuman primate brain. *Eur J Nucl Med Mol Imaging*. 2015;42(3):478-494. doi:10.1007/s00259-014-2962-9

76. Dupont AC, Largeau B, Ribeiro MJS, Guilloteau D, Tronel C, Arlicot N. Translocator protein-18 kDa (TSPO) positron emission tomography (PET) imaging and its clinical impact in neurodegenerative diseases. *Int J Mol Sci*. 2017;18(4):1-37. doi:10.3390/ijms18040785

77. Owen DR, Yeo AJ, Gunn RN, et al. An 18-kDa translocator protein (TSPO) polymorphism explains differences in binding affinity of the PET radioligand PBR28. *J Cereb Blood Flow Metab*. 2012;32(1):1-5. doi:10.1038/jcbfm.2011.147

78. Park E, Gallezot JD, Delgadillo A, et al. ^{11}C-PBR28 imaging in multiple sclerosis patients and healthy controls: test-retest reproducibility and focal visualization of active white matter areas. *Eur J Nucl Med Mol Imaging*. 2015;42(7):1081-1092. doi:10.1007/s00259-015-3043-4

79. Dendrou CA, Fugger L, Friese MA. Immunopathology of multiple sclerosis. *Nat Rev Immunol*. 2015. doi:10.1038/nri3871

80. Korn T. Pathophysiology of multiple sclerosis. *J Neurol*. 2008. doi:10.1007/s00415-008-6001-2

81. Filippi M, Rocca MA, Barkhof F, et al. Association between pathological and MRI findings in multiple sclerosis. *Lancet Neurol*. 2012. doi:10.1016/S1474-4422(12)70003-0

82. Noseworthy J, Lucchinetti C, Rodriquez M, Weinshenker B. Multiple sclerosis. *N Engl J Med*. 2000;343(13):938-952. doi:10.1056/NEJM200009283431307

83. Ramagopalan S V, Sadovnick a D. Epidemiology of multiple sclerosis. *Neurol Clin*. 2011;29(2):207-217. doi:10.1016/j.ncl.2010.12.010

84. Jacobson DL, Gange SJ, Rose NR, Graham NMH. Epidemiology and Estimated Population Burden of Selected Autoimmune Diseases in the United States. 1997;84(3):223-243.

85. Simpson S, Blizzard L, Otahal P, Van der Mei I, Taylor B. Latitude is significantly associated with the prevalence of multiple sclerosis: a meta-analysis. *J Neurol Neurosurg Psychiatry*. 2011;82(10):1132-1141. doi:10.1136/jnnp.2011.240432

86. Kappos L, De Stefano N, Freedman MS, et al. Inclusion of brain volume loss in a revised measure of "no evidence of disease activity" (NEDA-4) in relapsing-remitting multiple sclerosis. *Mult Scler*. 2016;22(10):1297-1305. doi:10.1177/1352458515616701

87. Bomprezzi R. Dimethyl fumarate in the treatment of relapsing-remitting multiple sclerosis: An overview. *Ther Adv Neurol Disord*. 2015;8(1):20-30. doi:10.1177/1756285614564152

88. Antel J, Antel S, Caramanos Z, Arnold DL, Kuhlmann T. Primary progressive multiple sclerosis: part of the MS disease spectrum or separate disease entity? *Acta Neuropathol*. 2012;123(5):627-638. doi:10.1007/s00401-012-0953-0

89. Compston A, Coles A. Multiple sclerosis. *Lancet*. 2008;372(9648):1502-1517. doi:10.1016/S0140-6736(08)61620-7

90. Loma I, Heyman R. Multiple Sclerosis: Pathogenesis and Treatment. *Curr Neuropharmacol*. 2011. doi:10.2174/157015911796557911

91. Weissbart SJ, Pechersky D, Malykhina A, et al. The impact of pontine disease on lower urinary tract symptoms in patients with multiple sclerosis. *Neurourol Urodyn*.

2017;36:453–456. doi:10.1002/nau.22953

92. Winder K, Linker RA, Seifert F, et al. Neuroanatomic Correlates of Female Sexual Dysfunction in Multiple Sclerosis. *Ann Neurol*. 2016;80(4):490-498. doi:10.1002/ana.24746

93. Kutzelnigg A, Lassmann H. *Pathology of Multiple Sclerosis and Related Inflammatory Demyelinating Diseases*. Vol 122. 1st ed. Elsevier B.V.; 2014. doi:10.1016/B978-0-444-52001-2.00002-9

94. Krupp LB, Serain DJ. Multiple sclerosis-associated fatigue. In: *Multiple Sclerosis Therapeutics, Fourth Edition*. ; 2011. doi:10.1017/CBO9781139023986.059

95. Induruwa I, Constantinescu CS, Gran B. Fatigue in multiple sclerosis - A brief review. *J Neurol Sci*. 2012. doi:10.1016/j.jns.2012.08.007

96. Braley TJ, Chervin RD. Fatigue in multiple sclerosis: Mechanisms, evaluation, and treatment. *Sleep*. 2010;33(8):1061-1067. doi:10.1093/sleep/33.8.1061

97. Kos D, Kerckhofs E, Nagels G, D'hooghe MB, Ilsbroukx S. Origin of fatigue in multiple sclerosis: Review of the literature. *Neurorehabil Neural Repair*. 2008;22(1):91-100. doi:10.1177/1545968306298934

98. Feinstein A. Multiple sclerosis and depression. *Mult Scler J*. 2011. doi:10.1177/1352458511417835

99. Tedeschi G, Docimo R, Bisecco A, Gallo A. Neuroimaging in multiple sclerosis. In: *Neuropsychiatric Dysfunction in Multiple Sclerosis*. ; 2014. doi:10.1007/978-88-470-2676-6_8

100. Politi LS, Bacigaluppi M, Brambilla E, et al. Magnetic-resonance-based tracking and quantification of intravenously injected neural stem cell accumulation in the brains of mice with experimental multiple sclerosis. *Stem Cells*. 2007;25(10):2583-2592. doi:10.1634/stemcells.2007-0037

101. Csépány T. Diagnosis of multiple sclerosis: A review of the 2017 revisions of the McDonald criteria. *Ideggyogy Sz*. 2018;71(9-10):321-329. doi:10.18071/isz.71.0321

102. Kamphorst W, Ravid R. Histopathologic correlate of hypointense lesions on Tl-weighted spin-echo MRI in multiple sclerosis. *Neurology*. 1998;(95):1282-1288.

103. Laule C, Vavasour I, Kolind S. Magnetic resonance imaging of myelin. *Neurother J Am Soc Exp Neurother Magn*. 2007;4(July):460-484. http://www.sciencedirect.com/science/article/pii/S1933721307000888. Accessed November 13, 2014.

104. Paolillo A, Pozzilli C, Gasperini C, et al. Brain atrophy in relapsing-remitting multiple sclerosis: relationship with 'black holes', disease duration and clinical disability. *J Neurol Sci*. 2000;174(2):85-91. doi:10.1016/S0022-510X(00)00259-8

105. Zivadinov R. Can imaging techniques measure neuroprotection and remyelination in multiple sclerosis? *Neurology*. 2007;68(22 Suppl 3):S72-82; discussion S91-6. doi:10.1212/01.wnl.0000275236.51129.d2

106. Alonso A, Hernan MA. Temporal trends in the incidence of multiple sclerosis. *Neurology*. 2008;71:129-135.

107. Barcellos LF, Sawcer S, Ramsay PP, et al. Heterogeneity at the HLA-DRB1 locus and risk for multiple sclerosis. *Hum Mol Genet*. 2006. doi:10.1093/hmg/ddl223

108. Marrosu MG, Muntoni F, Murru MR, et al. HLA-DQB1 genotype in Sardinian multiple sclerosis: evidence for a key role of DQB1 *0201 and *0302 alleles. *Neurology*. 1992. doi:10.1212/WNL.42.4.883

109. Okuda DT, Srinivasan R, Oksenberg JR, et al. Genotype–Phenotype correlations in multiple sclerosis: HLA genes influence disease severity inferred by 1HMR spectroscopy and MRI measures. *Brain*. 2009. doi:10.1093/brain/awn301

110. Stickler M, Valdes a M, Gebel W, et al. The HLA-DR2 haplotype is associated with an increased proliferative response to the immunodominant CD4(+) T-cell epitope in human interferon-beta. *Genes Immun*. 2004. doi:10.1038/sj.gene.6364027

111. Dyment DA, Herrera BM, Cader MZ, et al. Complex interactions among MHC haplotypes in multiple sclerosis: Susceptibility and resistance. *Hum Mol Genet*. 2005. doi:10.1093/hmg/ddi206

112. Rich C, Link JM, Zamora A, et al. Myelin oligodendrocyte glycoprotein-35-55 peptide induces severe chronic experimental autoimmune encephalomyelitis in HLA-DR2-transgenic mice. *Eur J Immunol*. 2004;34(5):1251-1261. doi:10.1002/eji.200324354

113. ’t Hart B, Massacesi L. Clinical, Pathological, and Immunologic Aspects of the Multiple Sclerosis Model in Common Marmosets. *Exp Neurol*. 2009.

114. Agliardi C, Guerini FR, Saresella M, et al. Vitamin D receptor (VDR) gene SNPs influence VDR expression and modulate protection from multiple sclerosis in HLA-DRB1*15-positive individuals. *Brain Behav Immun*. 2011. doi:10.1016/j.bbi.2011.05.015

115. Lonergan R, Kinsella K, Fitzpatrick P, et al. Multiple sclerosis prevalence in Ireland: Relationship to vitamin D status and HLA genotype. *J Neurol Neurosurg Psychiatry*. 2011. doi:10.1136/jnnp.2010.220988

116. Holick MF. Sunlight and vitamin D for bone health and prevention of autoimmune diseases , cancers , and cardiovascular disease 1 – 4. 2004;80:1678-1688.

117. Harp C, Lee J, Lambracht-Washington D, et al. Cerebrospinal fluid B cells from multiple sclerosis patients are subject to normal germinal center selection. *J Neuroimmunol*. 2007;183(1-2):189-199. doi:10.1016/j.jneuroim.2006.10.020

118. Qin Y, Duquette P, Zhang Y, Talbot P, Poole R, Antel J. Clonal expansion and somatic hypermutation of V(H) genes of B cells from cerebrospinal fluid in multiple sclerosis. *J Clin Invest*. 1998;102(5):1045-1050. doi:10.1172/JCI3568

119. Ascherio A, Munger KL. Epstein-barr virus infection and multiple sclerosis: a review. *J Neuroimmune Pharmacol*. 2010;5(3):271-277. doi:10.1007/s11481-010-9201-3

120. Levin L, Munger K, O’Reilly E. Primary Infection with the Epstein-Barr Virus and Risk of Multiple Sclerosis. *Ann Neurol*. 2010;67(6):824-830. doi:10.1002/ana.21978.Primary

121. Sundqvist E, Sundström P, Lindén M, et al. Epstein-Barr virus and multiple sclerosis: Interaction with HLA. *Genes Immun*. 2012. doi:10.1038/gene.2011.42

122. Kawakami N, Bartholomäus I, Pesic M, Mues M. An autoimmunity odyssey: how autoreactive T cells infiltrate into the CNS. *Immunol Rev*. 2012;248(1):140-155. doi:10.1111/j.1600-065X.2012.01133.x

123. Ifergan I, Kébir H, Bernard M, et al. The blood-brain barrier induces differentiation of migrating monocytes into Th17-polarizing dendritic cells. *Brain*. 2008;131(3):785-

799. doi:10.1093/brain/awm295

124. Pashenkov M, Huang YM, Kostulas V, Haglund M, Söderström M, Link H. Two subsets of dendritic cells are present in human cerebrospinal fluid. *Brain*. 2001;124(3):480-492. doi:10.1093/brain/124.3.480

125. Durelli L, Conti L, Clerico M, et al. T-helper 17 cells expand in multiple sclerosis and are inhibited by interferon-β. *Ann Neurol*. 2009. doi:10.1002/ana.21652

126. Brucklacher-Waldert V, Stuerner K, Kolster M, Wolthausen J, Tolosa E. Phenotypical and functional characterization of T helper 17 cells in multiple sclerosis. *Brain*. 2009. doi:10.1093/brain/awp289

127. Haider L, Simeonidou C, Steinberger G, et al. Multiple sclerosis deep grey matter: The relation between demyelination, neurodegeneration, inflammation and iron. *J Neurol Neurosurg Psychiatry*. 2014. doi:10.1136/jnnp-2014-307712

128. Davis SL, Wilson TE, White AT, Frohman EM. Thermoregulation in multiple sclerosis. *J Appl Physiol*. 2010. doi:10.1152/japplphysiol.00460.2010

129. Craner MJ, Newcombe J, Black JA, Hartle C, Cuzner ML, Waxman SG. Molecular changes in neurons in multiple sclerosis: Altered axonal expression of Nav1.2 and Nav1.6 sodium channels and Na+/Ca2+ exchanger. *Proc Natl Acad Sci U S A*. 2004;101(21):8168-8173. doi:10.1073/pnas.0402765101

130. Witte ME, Bø L, Rodenburg RJ, et al. Enhanced number and activity of mitochondria in multiple sclerosis lesions. *J Pathol*. 2009;219:193-204. doi:10.1002/path

131. Trapp BD, Stys PK. Virtual hypoxia and chronic necrosis of demyelinated axons in multiple sclerosis. *Lancet Neurol*. 2009. doi:10.1016/S1474-4422(09)70043-2

132. Sedel F, Bernard D, Mock DM, Tourbah A. Targeting demyelination and virtual hypoxia with high-dose biotin as a treatment for progressive multiple sclerosis. *Neuropharmacology*. 2016;110:644-653. doi:10.1016/j.neuropharm.2015.08.028

133. Bodini B, Branzoli F, Poirion E, et al. Dysregulation of energy metabolism in multiple sclerosis measured in vivo with diffusion-weighted spectroscopy. *Mult Scler J*. 2018;24(3):313-321. doi:10.1177/1352458517698249

134. Bjartmar C, Wujek JR, Trapp BD. Axonal loss in the pathology of MS: Consequences for understanding the progressive phase of the disease. *J Neurol Sci*. 2003;206(2):165-171. doi:10.1016/S0022-510X(02)00069-2

135. Trapp BD, Ransohoff R, Rudick R. Axonal pathology in multiple sclerosis: Relationship to neurologic disability. *Curr Opin Neurol*. 1999;12(3):295-302. doi:10.1097/00019052-199906000-00008

136. Berard JL, Wolak K, Fournier S, David S. Characterization of relapsing-remitting and chronic forms of experimental autoimmune encephalomyelitis in C57BL/6 mice. *Glia*. 2010;58(4):434-445. doi:10.1002/glia.20935

137. Bennett ML, Bennett FC, Liddelow SA, et al. New tools for studying microglia in the mouse and human CNS. *Proc Natl Acad Sci*. 2016. doi:10.1073/pnas.1525528113

138. Lefeuvre JA, Guy J, Leibovitch E, et al. Characterization of spinal cord lesions by MRI in marmoset EAE. *Mult Scler*. 2017;23(1):52.

139. Booss J, Esiri MM, Tourtellotte WW, Mason DY. Immunohistological analysis of T lymphocyte subsets in the central nervous system in chronic progressive multiple sclerosis. *J Neurol Sci*. 1983;62(1-3):219-232. doi:10.1016/0022-510X(83)90201-0

140. Lassmann H, Ransohoff RM. The CD4-Th1 model for multiple sclerosis: A crucial re-appraisal. *Trends Immunol*. 2004;25(3):132-137. doi:10.1016/j.it.2004.01.007

141. Diem R, Demmer I, Boretius S, et al. Autoimmune optic neuritis in the common marmoset monkey: comparison of visual evoked potentials with MRI and histopathology. *Invest Ophthalmol Vis Sci*. 2008;49(8):3707-3714. doi:10.1167/iovs.08-1896

142. Imaizumi M, Briard E, Zoghbi SS, et al. Brain and whole-body imaging in nonhuman primates of [11C]PBR28, a promising PET radioligand for peripheral benzodiazepine receptors. *Neuroimage*. 2008. doi:10.1016/j.neuroimage.2007.09.063

143. Hannestad J, Gallezot JD, Schafbauer T, et al. Endotoxin-induced systemic inflammation activates microglia: [11C]PBR28 positron emission tomography in nonhuman primates. *Neuroimage*. 2012. doi:10.1016/j.neuroimage.2012.06.055

144. Daneman R, Prat A. The Blood–Brain Barrier. *Cold Spring Harb Perspect Biol*. 2015;7:a020412. doi:10.1016/b978-0-12-802381-5.00010-5

145. Tilling T, Korte D, Hoheisel D, Galla H-J. Basement Membrane Proteins Influence Brain Capillary Endothelial Barrier Function In Vitro. *J Neurochem*. 2002;71(3):1151-1157. doi:10.1046/j.1471-4159.1998.71031151.x

146. Kebir H, Ifergan I, Alvarez JI, et al. Preferential recruitment of interferon-γ-expressing TH17 cells in multiple sclerosis. *Ann Neurol*. 2009;66:390–402. doi:10.1002/ana.21748

147. Kebir H, Kreymborg K, Ifergan I, et al. Human TH17 lymphocytes promote blood-brain barrier disruption and central nervous system inflammation. 2016;13(10):1173-1175. doi:10.1038/nm1651.Human

148. Jadidi-Niaragh F, Mirshafiey A. Th17 cell, the new player of neuroinflammatory process in multiple sclerosis. *Scand J Immunol*. 2011;74(1):1-13. doi:10.1111/j.1365-3083.2011.02536.x

149. Zozulya AL, Wiendl H. The role of regulatory T cells in multiple sclerosis. *Nat Clin Pract Neurol*. 2008;4(7):384-398. doi:10.1038/ncpneuro0832

150. Haas J, Hug A, Viehöver A, et al. Reduced suppressive effect of CD4+CD25high regulatory T cells on the T cell immune response against myelin oligodendrocyte glycoprotein in patients with multiple sclerosis. *Eur J Immunol*. 2005;35(11):3343-3352. doi:10.1002/eji.200526065

151. Borsellino G, Kleinewietfeld M, Di Mitri D, et al. Expression of ectonucleotidase CD39 by Foxp3+ Treg cells: Hydrolysis of extracellular ATP and immune suppression. *Blood*. 2007;110:1225-1232. doi:10.1182/blood-2006-12-064527

152. Viglietta V, Baecher-Allan C, Weiner HL, Hafler DA. Loss of functional suppression by CD4+CD25+ regulatory T cells in patients with multiple sclerosis. *J Exp Med*. 2004;199:971-979. doi:10.1084/jem.20031579\rjem.20031579 [pii]

153. Kouwenhoven M, Teleshova N, Özenci V, Press R, Link H. Monocytes in multiple sclerosis: Phenotype and cytokine profile. *J Neuroimmunol*. 2001;112(1-2):197-205. doi:10.1016/S0165-5728(00)00396-9

154. Mishra MK, Wee Yong V. Myeloid cells-targets of medication in multiple sclerosis. *Nat Rev Neurol*. 2016;12(9):539-551. doi:10.1038/nrneurol.2016.110

155. Grigoriadis N, van Pesch V. A basic overview of multiple sclerosis immunopathology.

Eur J Neurol. 2015;22:3-13. doi:10.1111/ene.12798

156. Vogel DYS, Heijnen PDAM, Breur M, et al. Macrophages migrate in an activation-dependent manner to chemokines involved in neuroinflammation. *J Neuroinflammation*. 2014;11(1):23. doi:10.1186/1742-2094-11-23

157. Popescu BFG, Pirko I, Lucchinetti CF. Pathology of multiple sclerosis: where do we stand? *Continuum (Minneap Minn)*. 2013;19(4 Multiple Sclerosis):901-921. doi:10.1212/01.CON.0000433291.23091.65

158. Miron VE, Boyd A, Zhao J-W, et al. M2 microglia and macrophages drive oligodendrocyte differentiation during CNS remyelination. *Nat Neurosci*. 2013;16:1211-1218. doi:10.1038/nn.3469

159. Nathan CF, Murray HW, Wlebe IE, Rubin BY. Identification of interferon-γ, as the lymphokine that activates human macrophage oxidative metabolism and antimicrobial activity. *J Exp Med*. 1983;158(3):670-689. doi:10.1084/jem.158.3.670

160. Fleetwood AJ, Lawrence T, Hamilton JA, Cook AD. Granulocyte-Macrophage Colony-Stimulating Factor (CSF) and Macrophage CSF-Dependent Macrophage Phenotypes Display Differences in Cytokine Profiles and Transcription Factor Activities: Implications for CSF Blockade in Inflammation. *J Immunol*. 2007;178(8):5245-5252. doi:10.4049/jimmunol.178.8.5245

161. Arnold CE, Whyte CS, Gordon P, Barker RN, Rees AJ, Wilson HM. A critical role for suppressor of cytokine signalling 3 in promoting M1 macrophage activation and function in vitro and in vivo. *Immunology*. 2014. doi:10.1111/imm.12173

162. Chávez-Galán L, Olleros ML, Vesin D, Garcia I. Much more than M1 and M2 macrophages, there are also CD169+ and TCR+ macrophages. *Front Immunol*. 2015;6(MAY):1-15. doi:10.3389/fimmu.2015.00263

163. Martinez FO, Gordon S. The M1 and M2 paradigm of macrophage activation: time for reassessment. *F1000Prime Rep*. 2014;6(March):13. doi:10.12703/P6-13

164. Kou PM, Babensee JE. Macrophage and dendritic cell phenotypic diversity in the context of biomaterials. *J Biomed Mater Res A*. 2011;96(1):239-260. doi:10.1002/jbm.a.32971

165. Mantovani A, Sica A, Sozzani S, Allavena P, Vecchi A, Locati M. The chemokine system in diverse forms of macrophage activation and polarization. *Trends Immunol*. 2004. doi:10.1016/j.it.2004.09.015

166. Tamas R. Understanding the Mysterious M2 Macrophage through Activation Markers and Effector Mechanisms. *Mediators Inflamm*. 2015;2015:16-18.

167. Huang X, Li Y, Fu M, Xin HB. Polarizing macrophages in vitro. In: *Methods in Molecular Biology*. ; 2018. doi:10.1007/978-1-4939-7837-3_12

168. Peferoen L a N, Vogel DYS, Ummenthum K, et al. Activation status of human microglia is dependent on lesion formation stage and remyelination in multiple sclerosis. *J Neuropathol Exp Neurol*. 2015;74(1):48-63. doi:10.1097/NEN.0000000000000149

169. Ginhoux F, Lim S, Hoeffel G, Low D, Huber T. Origin and differentiation of microglia. *Front Cell Neurosci*. 2013;7(April):1-14. doi:10.3389/fncel.2013.00045

170. Perry VH, Teeling J. Microglia and macrophages of the central nervous system: The contribution of microglia priming and systemic inflammation to chronic

neurodegeneration. *Semin Immunopathol*. 2013;35(5):601-612. doi:10.1007/s00281-013-0382-8

171. Block ML, Zecca L, Hong JS. Microglia-mediated neurotoxicity: Uncovering the molecular mechanisms. *Nat Rev Neurosci*. 2007. doi:10.1038/nrn2038

172. Biber K, Owens T, Boddeke E. What is microglia neurotoxicity (Not)? *Glia*. 2014:841-854. doi:10.1002/glia.22654

173. Hanisch UK, Kettenmann H. Microglia: Active sensor and versatile effector cells in the normal and pathologic brain. *Nat Neurosci*. 2007. doi:10.1038/nn1997

174. Ransohoff RM, Perry VH. Microglial Physiology: Unique Stimuli, Specialized Responses. *Annu Rev Immunol*. 2009;27:119-145. doi:10.1146/annurev.immunol.021908.132528

175. Ransohoff RM. A polarizing question: Do M1 and M2 microglia exist. *Nat Neurosci*. 2016;19:987-991. doi:10.1038/nn.4338

176. Ransohoff RM. How neuroinflammation contributes to neurodegeneration. *Science (80-)*. 2016. doi:10.1126/science.aag2590

177. Crawford AH, Stockley JH, Tripathi RB, Richardson WD, Franklin RJ. Oligodendrocyte progenitors: Adult stem cells of the central nervous system? *Exp Neurol*. 2014. doi:10.1016/j.expneurol.2014.04.027

178. Franklin RJ, Gallo V. The translational biology of remyelination: Past, present, and future. *Glia*. 2014. doi:10.1002/glia.22622

179. Ruckh JM, Zhao JW, Shadrach JL, et al. Rejuvenation of regeneration in the aging central nervous system. *Cell Stem Cell*. 2012;10(1):96-103. doi:10.1016/j.stem.2011.11.019

180. Miron VE, Franklin RJ. Macrophages and CNS remyelination. *J Neurochem*. 2014;130(2):165-171. doi:10.1111/jnc.12705

181. Goldmann T, Prinz M. Role of microglia in CNS autoimmunity. *Clin Dev Immunol*. 2013;2013(88). doi:10.1155/2013/208093

182. Sofroniew M V., Vinters H V. Astrocytes: Biology and pathology. *Acta Neuropathol*. 2010;119(1):7-35. doi:10.1007/s00401-009-0619-8

183. Araque A, Carmignoto G, Haydon PG, Oliet SHR, Robitaille R, Volterra A. Gliotransmitters travel in time and space. *Neuron*. 2014. doi:10.1016/j.neuron.2014.02.007

184. Ponath G, Lincoln MR, Levine-Ritterman M, et al. Enhanced astrocyte responses are driven by a genetic risk allele associated with multiple sclerosis. *Nat Commun*. 2018;9(1):1-9. doi:10.1038/s41467-018-07785-8

185. Voskuhl RR, Peterson RS, Song B, et al. Reactive astrocytes form scar-like perivascular barriers to leukocytes during adaptive immune inflammation of the CNS. *J Neurosci*. 2009;29(37):11511-11522. doi:10.1523/JNEUROSCI.1514-09.2009

186. Frischer JM, Weigand SD, Guo Y, et al. Clinical and pathological insights into the dynamic nature of the white matter multiple sclerosis plaque. *Ann Neurol*. 2015;78(5):710-721. doi:10.1002/ana.24497

187. Brück W. The pathology of multiple sclerosis is the result of focal inflammatory demyelination with axonal damage. *J Neurol*. 2005;252(SUPPL. 5):3-9.

doi:10.1007/s00415-005-5002-7

188. Kuhlmann T, Lingfeld G, Bitsch A, Schuchardt J, Brück W. Acute axonal damage in multiple sclerosis is most extensive in early disease stages and decreases over time. *Brain*. 2002;125(10):2202-2212. doi:10.1093/brain/awf235

189. Trapp BD, Peterson J, Ransohoff RM, Rudick R, Mörk S, Bö L. Axonal transection in the lesions of multiple sclerosis. *N Engl J Med*. 1998;338(5):278-285. doi:10.1056/NEJM199801293380502

190. Kuhlmann T, Ludwin S, Prat A, Antel J, Brück W, Lassmann H. An updated histological classification system for multiple sclerosis lesions. *Acta Neuropathol*. 2017;133(1):13-24. doi:10.1007/s00401-016-1653-y

191. Lucchinetti C, Brück W, Parisi J, Scheithauer B, Rodriguez M, Lassmann H. Heterogeneity of multiple sclerosis lesions: Implications for the pathogenesis of demyelination. *Ann Neurol*. 2000. doi:10.1002/1531-8249(200006)47:6<707::AID-ANA3>3.0.CO;2-Q

192. Brownell B, Hughes J. The distribution of plaques in the cerebrum in multiple sclerosis. *J Neurol neurosurgery, …*. 1962;265(25):315-320. http://www.ncbi.nlm.nih.gov/pmc/articles/PMC495470/. Accessed December 8, 2014.

193. Cifelli A, Arridge M, Jezzard P, Esiri MM, Palace J, Matthews PM. Thalamic neurodegeneration in multiple sclerosis. *Ann Neurol*. 2002;52(5):650-653. doi:10.1002/ana.10326

194. Pirko I, Lucchinetti C, Sriram S, Bakshi R. Gray matter involvement in multiple sclerosis. *Neurology*. 2007;68:634-642. http://www.neurology.org/content/68/9/634.short. Accessed December 8, 2014.

195. Peterson JW, Bö L, Mörk S, Chang A, Trapp BD. Transected neurites, apoptotic neurons, and reduced inflammation in cortical multiple sclerosis lesions. *Ann Neurol*. 2001;50:389-400. doi:10.1002/ana.1123

196. Banati RB, Newcombe J, Gunn RN, et al. The peripheral benzodiazepine binding site in the brain in multiple sclerosis Quantitative in vivo imaging of microglia as a measure of disease activity. *Brain*. 2000;123:2321-2337. doi:10.1093/brain/123.11.2321

197. Debruyne JC, Versijpt J, Van Laere KJ, et al. Pet visualization of microglia in multiple sclerosis patients using [11C]PK11195. *Eur J Neurol*. 2003;10(3):257-264. doi:10.1046/j.1468-1331.2003.00571.x

198. Datta G, Colasanti A, Rabiner EA, et al. Neuroinflammation and its relationship to changes in brain volume and white matter lesions in multiple sclerosis. *Brain*. 2017;140(11):2927-2938. doi:10.1093/brain/awx228

199. Wang M, Wang X, Zhao L, et al. Macroglia-microglia interactions via TSPO signaling regulates microglial activation in the mouse retina. *J Neurosci*. 2014;34(10):3793-3806. doi:10.1523/JNEUROSCI.3153-13.2014

200. Bae K-R, Shim H-J, Balu D, Kim SR, Yu S-W. Translocator Protein 18 kDa Negatively Regulates Inflammation in Microglia. *J Neuroimmune Pharmacol*. 2014;9(3):424-437. doi:10.1007/s11481-014-9540-6

201. Nudmamud S, Siripurkpong P, Chindaduangratana C, et al. Stress, anxiety and peripheral benzodiazepine receptor mRNA levels in human lymphocytes. *Life Sci*. 2000;67:2221–2231. doi:10.1016/S0024-3205(00)00806-7

202. Rupprecht R, Ranimes G, Eser D, et al. Translocator protein (18 kD) as target for anxiolytics without benzodiazepine-like side effects. *Science (80-)*. 2009;325:490-493. doi:10.1126/science.1175055

203. Hamon A, Morel A, Hue B, Verleye M, Gillardin JM. The modulatory effects of the anxiolytic etifoxine on GABAA receptors are mediated by the β subunit. *Neuropharmacology*. 2003;(45):293-303. doi:10.1016/S0028-3908(03)00187-4

204. Narayan N, Mandhair H, Smyth E, et al. The macrophage marker translocator protein (TSPO) is down-regulated on pro-inflammatory 'M1' human macrophages. *PLoS One*. 2017;12(10):1-19. doi:10.1371/journal.pone.0185767

205. Beckers L, Ory D, Geric I, et al. Increased Expression of Translocator Protein (TSPO) Marks Pro-inflammatory Microglia but Does Not Predict Neurodegeneration. *Mol Imaging Biol*. 2018;20(1):94-102. doi:10.1007/s11307-017-1099-1

206. Betlazar C, Harrison-Brown M, Middleton RJ, Banati R, Liu GJ. Cellular sources and regional variations in the expression of the neuroinflammatory marker translocator protein (TSPO) in the normal brain. *Int J Mol Sci*. 2018;19(9). doi:10.3390/ijms19092707

207. Ji B, Maeda J, Sawada M, et al. Imaging of Peripheral Benzodiazepine Receptor Expression as Biomarkers of Detrimental versus Beneficial Glial Responses in Mouse Models of Alzheimer's and Other CNS Pathologies. *J Neurosci*. 2008;28(47):12255-12267. doi:10.1523/JNEUROSCI.2312-08.2008

208. Praet J, Guglielmetti C, Berneman Z, Van der Linden A, Ponsaerts P. Cellular and molecular neuropathology of the cuprizone mouse model: Clinical relevance for multiple sclerosis. *Neurosci Biobehav Rev*. 2014;47:485-505. doi:10.1016/j.neubiorev.2014.10.004

209. Varga B, Markó K, Hádinger N, et al. Translocator protein (TSPO 18 kDa) is expressed by neural stem and neuronal precursor cells. *Neurosci Lett*. 2009;462(3):257-262. doi:10.1016/j.neulet.2009.06.051

210. Zeno S, Zaaroor M, Leschiner S, Veenman L, Gavish M. CoCl2 induces apoptosis via the 18 kDa translocator protein in U118MG human glioblastoma cells. *Biochemistry*. 2009. doi:10.1021/bi900064t

211. Tárnok K, Kiss E, Luiten PGM, et al. Effects of Vinpocetine on mitochondrial function and neuroprotection in primary cortical neurons. *Neurochem Int*. 2008;31(1):13-21. doi:10.1016/j.neuint.2008.08.003

212. Ferzaz B, Brault E, Bourliaud G, et al. SSR180575 (7-chloro-N,N,5-trimethyl-4-oxo-3-phenyl-3,5-dihydro-4H-pyridazino[4,5-b] indole-1-acetamide), a peripheral benzodiazepine receptor ligand, promotes neuronal survival and repair. *J Pharmacol Exp Ther*. 2002;301(3):1067-1078. doi:10.1124/jpet.301.3.1067

213. Harberts E, Datta D, Chen S, Wohler JE, Oh U, Jacobson S. Translocator protein 18 kDa (TSPO) expression in multiple sclerosis patients. *J Neuroimmune Pharmacol*. 2013;8(1):51-57. doi:10.1007/s11481-012-9397-5

214. Chelli B, Pini S, Abelli M, et al. Platelet 18 kDa Translocator Protein density is reduced in depressed patients with adult separation anxiety. *Eur Neuropsychopharmacol*. 2008. doi:10.1016/j.euroneuro.2007.10.003

215. Johnson MR, Marazziti D, Brawman-Mintzer O, et al. Abnormal peripheral benzodiazepine receptor density associated with generalized social phobia. *Biol*

Psychiatry. 1998. doi:10.1016/S0006-3223(97)00390-9

216. Soreni N, Apter A, Weizman A, et al. Decreased platelet peripheral-type benzodiazepine receptors in adolescent inpatients with repeated suicide attempts. *Biol Psychiatry*. 1999. doi:10.1016/S0006-3223(98)00342-4

217. Gavish M, Laor N, Bidder M, et al. Altered platelet peripheral-type benzodiazepine receptor in posttraumatic stress disorder. *Neuropsychopharmacology*. 1996. doi:10.1016/0893-133X(95)00078-R

218. Sarubin N, Baghai TC, Lima-Ojeda JM, et al. Translocator Protein (TSPO) Expression in Platelets of Depressed Patients Decreases during Antidepressant Therapy. *Pharmacopsychiatry*. 2016;49(5):204-209. doi:10.1055/s-0042-107795

219. Coles A, Compston A, Selmay K, et al. Alemtuzumab versus interferon beta-1a in early multiple sclerosis. *N Engl J Med*. 2008;359(17):1786-1801. http://www.ncbi.nlm.nih.gov/pubmed/21397567.

220. Bourdette D, Yadav V. B-cell depletion with rituximab in relapsing-remitting multiple sclerosis. *Curr Neurol Neurosci Rep*. 2008;8(5):417-418. http://www.ncbi.nlm.nih.gov/pubmed/18713578.

221. Goodin DS. Glucocorticoid treatment of multiple sclerosis. *Handb Clin Neurol*. 2014;122:455-464. doi:10.1016/B978-0-444-52001-2.00020-0

222. Shaikh S, Verma H, Yadav N, Jauhari M, Bullangowda J. Applications of Steroid in Clinical Practice: A Review. *ISRN Anesthesiol*. 2012;2012:1-11. doi:10.5402/2012/985495

223. Constantinescu CS, Farooqi N, O'Brien K, Gran B. Experimental autoimmune encephalomyelitis (EAE) as a model for multiple sclerosis (MS). *Br J Pharmacol*. 2011;164(4):1079-1106. doi:10.1111/j.1476-5381.2011.01302.x

224. D. F, K. C, A. E, et al. 1099: Progressive multifocal leukoencephalopathy following Rituximab therapy in HIV negative patients: A report of 56 cases from the research on adverse drug event and reports (RADAR) project. *Haematologica*. 2009;94(20):445. doi:10.1182/blood-2008-10-186999.Presented

225. Filippini G, Munari L, Incorvaia B, et al. Interferons in relapsing remitting multiple sclerosis: A systematic review. *Lancet*. 2003;361:545-552. doi:10.1016/S0140-6736(03)12512-3

226. Shirani A, Zhao Y, Karim M, et al. Association Between Use of Interferon Beta and Progression of Disability in Patients With Relapsing-RemittingMultiple Sclerosis. *J Am Med Assoc*. 2014;308(3):247-256.

227. Aharoni R, Sasson E, Blumenfeld-Katzir T. Magnetic resonance imaging characterization of different experimental autoimmune encephalomyelitis models and the therapeutic effect of glatiramer acetate. *Exp …*. 2013;240:130-144. doi:10.1016/j.expneurol.2012.11.004

228. Wolinsky JS, Narayana PA, O'Connor P, et al. Glatiramer acetate in primary progressive multiple sclerosis: Results of a multinational, multicenter, double-blind, placebo-controlled trial. *Ann Neurol*. 2007;61:14-24. doi:10.1002/ana.21079

229. Winkelmann A, Loebermann M, Reisinger EC, Zettl UK. Multiple sclerosis treatment and infectious issues: Update 2013. *Clin Exp Immunol*. 2014;175(3):425-438. doi:10.1111/cei.12226

230. Nandoskar A, Raffel J, Scalfari AS, Friede T, Nicholas RS. Pharmacological Approaches to the Management of Secondary Progressive Multiple Sclerosis. *Drugs*. 2017;77(8):885-910. doi:10.1007/s40265-017-0726-0

231. Karlstetter M, Nothdurfter C, Aslanidis A, et al. Translocator protein (18 kDa) (TSPO) is expressed in reactive retinal microglia and modulates microglial inflammation and phagocytosis. *J Neuroinflammation*. 2014;11:3. doi:10.1186/1742-2094-11-3

232. Wang D, Tian Z, Guo Y, et al. Anxiolytic-like effects of translocator protein (TSPO) ligand ZBD-2 in an animal model of chronic pain. *Mol Pain*. 2015;11(1):1-10. doi:10.1186/s12990-015-0013-6

233. Kumar A, Muzik O, Shandal V, Chugani D, Chakraborty P, Chugani HT. Evaluation of age-related changes in translocator protein (TSPO) in human brain using 11C-[R]-PK11195 PET. *J Neuroinflammation*. 2012;9. doi:10.1186/1742-2094-9-232

234. Venneti S, Lopresti BJ, Wiley CA. Molecular imaging of microglia/macrophages in the brain. *Glia*. 2013;61(1):10-23. doi:10.1002/glia.22357

235. Ji B, Maeda J, Sawada M, et al. Imaging of peripheral benzodiazepine receptor expression as biomarkers of detrimental versus beneficial glial responses in mouse models of Alzheimer's and other CNS pathologies. *J Neurosci*. 2008;28(47):12255–12267. doi:10.1523/JNEUROSCI.2312-08.2008

236. Notter T, Meyer U, Beckers L, et al. Letter to the Editor re: Increased Expression of Translocator Protein (TSPO) Marks Pro-inflammatory Microglia but Does Not Predict Neurodegeneration. *Mol Imaging Biol*. 2018;20(3):352-353. doi:10.1007/s11307-018-1172-4

237. Fritzsching B, Haas J, König F, et al. Intracerebral human regulatory T cells: analysis of CD4+ CD25+ FOXP3+ T cells in brain lesions and cerebrospinal fluid of multiple sclerosis patients. *PLoS One*. 2011;6(3):e17988. doi:10.1371/journal.pone.0017988

238. Yokoyama C, Mawatari A, Kawasaki A, et al. Marmoset serotonin 5-HT1areceptor mapping with a biased agonist PET probe18F-F13714: Comparison with an antagonist tracer18F-MPPF in awake and anesthetized states. *Int J Neuropsychopharmacol*. 2016;19(12):1-12. doi:10.1093/ijnp/pyw079

239. Maggi P, Macri SMC, Gaitán MI, et al. The formation of inflammatory demyelinated lesions in cerebral white matter. *Ann Neurol*. 2014;76(4):594-608. doi:10.1002/ana.24242

240. Giannetti P, Politis M, Su P, et al. Microglia activation in multiple sclerosis black holes predicts outcome in progressive patients: An in vivo [(11)C](R)-PK11195-PET pilot study. *Neurobiol Dis*. 2014;65:203-210. doi:10.1016/j.nbd.2014.01.018

241. Guy JR, Sati P, Leibovitch E, Jacobson S, Silva AC, Reich DS. Custom fit 3D-printed brain holders for comparison of histology with MRI in marmosets. *J Neurosci Methods*. 2015:1-9. doi:10.1016/j.jneumeth.2015.09.002

242. Winter B. Linear models and linear mixed effects models in R with linguistic applications. 2013;(Tutorial 2):1-22. http://arxiv.org/abs/1308.5499.

243. Kuznetsova A, Brockhoff PB, Christensen RHB. lmerTest Package: Tests in Linear Mixed Effects Models . *J Stat Softw*. 2017;82(13). doi:10.18637/jss.v082.i13

244. R Core Team. *R: A Language and Environment for Statistical Computing*. Vienna, Austria doi:10.1108/eb003648

245. McNeela AM, Bernick C, Hines RM, Hines DJ. TSPO regulation in reactive gliotic diseases. *J Neurosci Res*. 2018. doi:10.1002/jnr.24212

246. Li F, Liu J, Garavito RM, Ferguson-Miller S. Evolving understanding of translocator protein 18kDa (TSPO). *Pharmacol Res*. 2015;99:404-409. doi:10.1016/j.phrs.2015.03.022

247. Bonsack F, Sukumari-Ramesh S. TSPO: An evolutionarily conserved protein with elusive functions. *Int J Mol Sci*. 2018. doi:10.3390/ijms19061694

248. Bonsack F, Alleyne CH, Sukumari-Ramesh S. Augmented expression of TSPO after intracerebral hemorrhage: A role in inflammation? *J Neuroinflammation*. 2016. doi:10.1186/s12974-016-0619-2

249. Satoh J ichi, Kino Y, Asahina N, et al. TMEM119 marks a subset of microglia in the human brain. *Neuropathology*. 2016;36(1):39-49. doi:10.1111/neup.12235

250. Lee N. SPATIOTEMPORAL EVOLUTION OF INFLAMMATORY DEMYELINATING LESIONS IN CEREBRAL WHITE MATTER. 2019. doi:1037//0033-2909.I26.1.78

251. Martin A, Boisgard R, Theze B, et al. Evaluation of the PBR/TSPO radioligand [(18)F]DPA-714 in a rat model of focal cerebral ischemia. *J Cereb Blood Flow Metab*. 2010;30(1):230-241. doi:10.1038/jcbfm.2009.205

252. Anholt RRH, Murphy KMM, Mack GE, Snyder SH. Peripheral-type benzodiazepine receptors in the central nervous system: Localization to olfactory nerves. *J Neurosci*. 1984;4(2):593-603. doi:10.1523/jneurosci.04-02-00593.1984

253. Karchewski LA, Bloechlinger S, Woolf CJ. Axonal injury-dependent induction of the peripheral benzodiazepine receptor in small-diameter adult rat primary sensory neurons. *Eur J Neurosci*. 2004;20(3):671-683. doi:10.1111/j.1460-9568.2004.03530.x

254. Tasic B, Menon V, Nguyen TN, et al. Adult mouse cortical cell taxonomy revealed by single cell transcriptomics. *Nat Neurosci*. 2016. doi:10.1038/nn.4216

255. Darmanis S, Sloan SA, Zhang Y, et al. A survey of human brain transcriptome diversity at the single cell level. *Proc Natl Acad Sci*. 2015. doi:10.1073/pnas.1507125112

256. Zeisel A, M͡oz-Manchado AB, Codeluppi S, et al. Cell types in the mouse cortex and hippocampus revealed by single-cell RNA-seq. *Science (80-)*. 2015. doi:10.1126/science.aaa1934

257. Huang B, Law MWM, Khong PL. Whole-body PET/CT scanning: Estimation of radiation dose and cancer risk. *Radiology*. 2009;251(1):166-174. doi:10.1148/radiol.2511081300

258. Fairweather DL, Coronado MJ, Garton AE, et al. Sex differences in translocator protein 18 kDa (TSPO) in the heart: Implications for imaging myocardial inflammation. *J Cardiovasc Transl Res*. 2014;7(2):192-202. doi:10.1007/s12265-013-9538-0

259. Roncaroli F, Su Z, Herholz K, Gerhard A, Turkheimer FE. TSPO expression in brain tumours: is TSPO a target for brain tumour imaging? *Clin Transl Imaging*. 2016;4(2):145-156. doi:10.1007/s40336-016-0168-9

260. Vembadi A, Menachery A, Qasaimeh MA. Cell Cytometry: Review and Perspective on Biotechnological Advances. *Front Bioeng Biotechnol*. 2019;7(JUN).

doi:10.3389/fbioe.2019.00147

261. Shapiro HM. Multistation multiparameter flow cytometry: A critical review and rationale. *Cytometry*. 1983;3(4):227-243. doi:10.1002/cyto.990030402

262. Enose-Akahata Y, Azodi S, Smith BR, et al. Immunophenotypic characterization of CSF B cells in virus-associated neuroinflammatory diseases. *PLoS Pathog*. 2018;14(4):1-20. doi:10.1371/journal.ppat.1007042

263. Ziegler-Heitbrock L, Hofer TPJ. Toward a refined definition of monocyte subsets. *Front Immunol*. 2013;4(23). doi:10.3389/fimmu.2013.00023

264. Ziegler-Heitbrock L, Ancuta P, Crowe S, et al. Nomenclature of monocytes and dendritic cells in blood. *Blood*. 2010;116:e74-80. doi:10.1182/blood-2010-02-258558

265. Schlitt A, Heine GH, Blankenberg S, et al. CD14+CD16+ monocytes in coronary artery disease and their relationship to serum TNF-α levels. *Thromb Haemost*. 2004;92(2):419-424. doi:10.1160/th04-02-0095

266. Mukherjee R, Kanti Barman P, Kumar Thatoi P, Tripathy R, Kumar Das B, Ravindran B. Non-Classical monocytes display inflammatory features: Validation in Sepsis and Systemic Lupus Erythematous. *Sci Rep*. 2015;5(May):1-14. doi:10.1038/srep13886

267. Prosperini L, Giannì C, Leonardi L, et al. Escalation to natalizumab or switching among immunomodulators in relapsing multiple sclerosis. *Mult Scler J*. 2012;18(1):64-71. doi:10.1177/1352458511417481

268. Gajofatto A, Bacchetti P, Grimes B, High A, Waubant E. Switching first-line disease-modifying therapy after failure: Impact on the course of relapsing-remitting multiple sclerosis. *Mult Scler*. 2009;15(1):50-58. doi:10.1177/1352458508096687

269. Wildgruber M, Aschenbrenner T, Wendorff H, et al. The “intermediate” CD14++ CD16+ monocyte subset increases in severe peripheral artery disease in humans. *Sci Rep*. 2016;6(December):1-8. doi:10.1038/srep39483

270. Costa B, Pini S, Abelli M, et al. Role of translocator protein (18 kDa) in adult separation anxiety and attachment style in patients with depression. *Curr Mol Med*. 2012. doi:10.2174/1566524011207040483

271. Gavish M, Laor N, Bidder M, et al. Altered platelet peripheral-type benzodiazepine receptor in posttraumatic stress disorder. *Neuropsychopharmacology*. 1996;14(3):181-186. doi:10.1016/0893-133X(95)00078-R

272. Costa B, Pini S, Gabelloni P, et al. The spontaneous Ala147Thr amino acid substitution within the translocator protein influences pregnenolone production in lymphomonocytes of healthy individuals. *Endocrinology*. 2009;150(12):5438-5445. doi:10.1210/en.2009-0752

273. Loggia ML, Chonde DB, Akeju O, et al. Evidence for brain glial activation in chronic pain patients. *Brain*. 2015. doi:10.1093/brain/awu377

274. Owen DR, Guo Q, Kalk NJ, et al. Determination of [11C]PBR28 binding potential in vivo: A first human TSPO blocking study. *J Cereb Blood Flow Metab*. 2014. doi:10.1038/jcbfm.2014.46

275. Delavoie F, Li H, Hardwick M, et al. In vivo and in vitro peripheral-type benzodiazepine receptor polymerization: Functional significance in drug ligand and cholesterol binding. *Biochemistry*. 2003. doi:10.1021/bi0267487

276. Jaremko Ł, Jaremko M, Giller K, Becker S, Zweckstetter M. Conformational

Flexibility in the Transmembrane Protein TSPO. *Chem - A Eur J*. 2015. doi:10.1002/chem.201502314

277. Korkhov VM, Sachse C, Short JM, Tate CG. Three-Dimensional Structure of TspO by Electron Cryomicroscopy of Helical Crystals. *Structure*. 2010. doi:10.1016/j.str.2010.03.001

278. Li F, Xia Y, Meiler J, Ferguson-Miller S. Characterization and modeling of the oligomeric state and ligand binding behavior of purified translocator protein 18 kDa from Rhodobacter sphaeroides. *Biochemistry*. 2013. doi:10.1021/bi400431t

279. Guilarte TR, Loth MK, Guariglia SR. TSPO Finds NOX2 in Microglia for Redox Homeostasis. *Trends Pharmacol Sci*. 2016. doi:10.1016/j.tips.2016.02.008

280. Pugliese F, Gaemperli O, Kinderlerer AR, et al. Imaging of vascular inflammation with [11C]-PK11195 and positron emission tomography/computed tomography angiography. *J Am Coll Cardiol*. 2010;56(8):653-661. doi:10.1016/j.jacc.2010.02.063

281. Politis M, Giannetti P, Su P, et al. Increased PK11195 PET binding in the cortex of patients with MS correlates with disability. *Neurology*. 2012;79(6):523-530. doi:10.1212/WNL.0b013e3182635645

282. Gerhard A, Schwarz J, Myers R, Wise R, Banati RB. Evolution of microglial activation in patients after ischemic stroke: A [11C](R)-PK11195 PET study. *Neuroimage*. 2005;24(2):591-595. doi:10.1016/j.neuroimage.2004.09.034

283. Schuitemaker A, Kropholler MA, Boellaard R, et al. Microglial activation in Alzheimer’s disease: An (R)-[11C]PK11195 positron emission tomography study. *Neurobiol Aging*. 2013;34(1):128-136. doi:10.1016/j.neurobiolaging.2012.04.021

284. Turner MR, Cagnin A, Turkheimer FE, et al. Evidence of widespread cerebral microglial activation in amyotrophic lateral sclerosis: An [11C](R)-PK11195 positron emission tomography study. *Neurobiol Dis*. 2004;15(3):601-609. doi:10.1016/j.nbd.2003.12.012

285. Rojas S, Martín A, Arranz MJ, et al. Imaging brain inflammation with [11C]PK11195 by PET and induction of the peripheral-type benzodiazepine receptor after transient focal ischemia in rats. *J Cereb Blood Flow Metab*. 2007;27(12):1975-1986. doi:10.1038/sj.jcbfm.9600500

286. Yoder KK, Nho K, Risacher SL, Kim S, Shen L, Saykin AJ. Influence of TSPO Genotype on 11C-PBR28 Standardized Uptake Values. *J Nucl Med*. 2013;54(8):1320. doi:10.2967/jnumed.112.118885

287. Kreisl WC, Jenko KJ, Hines CS, et al. A genetic polymorphism for translocator protein 18 kDa affects both in vitro and in vivo radioligand binding in human brain to this putative biomarker of neuroinflammation. *J Cereb Blood Flow Metab*. 2013;33(1):53-58. doi:10.1038/jcbfm.2012.131

288. Guo Q, Colasanti A, Owen DR, et al. Quantification of the Specific Translocator Protein Signal of 18F-PBR111 in Healthy Humans: A Genetic Polymorphism Effect on In Vivo Binding. *J Nucl Med*. 2013;54(11):1915-1923. doi:10.2967/jnumed.113.121020

289. Suridjan I, Rusjan PM, Voineskos AN, et al. Neuroinflammation in healthy aging: A PET study using a novel Translocator Protein 18kDa (TSPO) radioligand, [18F]-FEPPA. *Neuroimage*. 2014;84:868-875. doi:10.1016/j.neuroimage.2013.09.021

290. Jaremko M, Jaremko Ł, Giller K, Becker S, Zweckstetter M. Structural Integrity of the

A147T Polymorph of Mammalian TSPO. *ChemBioChem*. 2015. doi:10.1002/cbic.201500217

291. Jaremko Ł, Jaremko M, Becker S, Zweckstetter M. Toward the functional oligomerization state of tryptophan-rich sensory proteins. *Protein Sci*. 2014. doi:10.1002/pro.2487